

Emission-oriented management of land-based freight transportation

Inaugural-Dissertation
zur Erlangung des akademischen Grades eines Doktors
der Wirtschafts- und Sozialwissenschaften
der Wirtschafts- und Sozialwissenschaftlichen Fakultät
der Christian-Albrechts-Universität zu Kiel

vorgelegt von
M.Sc. Arne Heinold
aus Henstedt-Ulzburg

Kiel, 2022

My work has been funded for 4.5 years by project 268276815 of the Deutsche Forschungsgemeinschaft (DFG, German Research Foundation). The thesis would not have been possible without this support.

Printed with the kind courtesy of the department and university (Wirtschafts- und Sozialwissenschaftliche Fakultät, Christian-Albrechts-Universität, Kiel).

Erstbegutachtung

Zweitbegutachtung

Drittbegutachtung

Day of oral examination

Prof. Dr. Frank Meisel

Prof. Dr. Catherine Cleophas

Prof. Dr. Kathrin Firscher

17.06.2022

Table of Contents

List of Figures	VI
List of Tables	X
1 Synopsis	1
1.1 Introduction	1
1.2 Research agenda	4
1.3 State-of-the-art research and thesis contributions	6
1.3.1 Assessing emissions	7
1.3.2 Communicating emissions	9
1.3.3 Managing emissions	10
1.4 Future research	12
Bibliography	14
2 Emission Rates of Intermodal Rail/Road and Road-only Transportation in Europe: A Comprehensive Simulation Study	17
2.1 Introduction	18
2.2 Modelling the European Rail/Road Network	20
2.2.1 Multilayer Network Structure for Intermodal Transportation	20
2.2.2 Network Data for the European Rail and Road Network	21
2.3 Emission Estimation for Road and Rail Transportation	23
2.3.1 Literature Review	23
2.3.2 Estimating Emissions from Road Transportation	26
2.3.3 Estimating Emissions from Rail Transportation	29
2.4 Simulation Settings	30
2.4.1 Generation of Shipments and Routing	30
2.4.2 Specification of Emission Model Parameters	32

2.4.3	Definition of Simulation Configurations	34
2.5	Results	36
2.5.1	General Findings	36
2.5.2	Emission Model Analysis	40
2.5.3	Further Configurations	41
2.6	Conclusion	45
2.7	Appendix A. Supplementary data	46
	Bibliography	47
3	Emission-oriented vs. Time-oriented Routing in the European Inter-	
	modal Rail/Road Freight Transportation Network	53
3.1	Introduction	54
3.2	Literature review	54
3.3	Problem description	56
3.4	Methodology and data	57
3.4.1	Terminal-and-service selection problem (TSSP)	57
3.4.2	European road and rail network data	60
3.5	Simulation	62
3.5.1	Generation of orders	62
3.5.2	Results	63
3.6	Conclusion	66
	Bibliography	68
4	Comparing Emission Estimation Models for Rail Freight Transporta-	
	tion	72
4.1	Introduction	73
4.2	Principles of estimating emissions from rail freight transportation	74
4.3	Emission estimation models	75
4.3.1	MEET	76
4.3.2	ARTEMIS	78
4.3.3	EcoTransIT World	81
4.3.4	Mesoscopic model	82
4.4	Experiments	85
4.4.1	Model and simulation parameters	85
4.4.2	Number of wagons	87
4.4.3	Payload per wagon	88

4.4.4	Speed	89
4.4.5	Distance	89
4.4.6	Number of stops	90
4.4.7	Altitude difference	91
4.5	Selecting an appropriate model	91
4.6	Conclusion	93
4.7	Appendix A. Python scripts	95
	Bibliography	96
5	Emission Limits and Emission Allocation Schemes in Intermodal Freight Transportation	99
5.1	Introduction	100
5.2	Literature review	101
5.3	The SSP-TALE model	106
5.3.1	Problem description and notation	106
5.3.2	Optimization model	109
5.4	Experiments with real-world data	112
5.4.1	Data	112
5.4.2	Computation time	115
5.4.3	Customers eco-friendliness (p-value)	117
5.4.4	Emission limits and order emissions	118
5.4.5	Allocation schemes and order size	120
5.4.6	Allocation schemes and default load	122
5.4.7	Overall results for five and eight orders and both country pairs . .	123
5.4.8	Network results	125
5.5	Conclusion	126
5.6	Appendix A. Illustrative example of the SSP-TALE	127
5.7	Appendix B. Implementation of the SSP-TALE	130
5.8	Appendix C. Rail network data	133
	Bibliography	134
6	Eco-Labeling of Freight Transport Services: Design, Evaluation and Research Directions	138
6.1	Introduction	139
6.2	Emission reporting standard EN 16258	140
6.3	Communication structure	142

6.4	Eco-labeling system design	145
6.4.1	General requirements	145
6.4.2	Reference base for transport emissions	147
6.4.3	Grading eco-performance of transport services	148
6.5	Evaluation of eco-labeling systems	150
6.5.1	Transport order data and transport services	150
6.5.2	FTL road transportation	151
6.5.3	LTL road transportation	153
6.5.4	Multimodal rail-road transportation without intermediate storage of goods (intermodal)	154
6.5.5	Multimodal rail-road transportation with intermediate storage of goods	156
6.5.6	Evaluation summary	157
6.6	Research directions	158
6.7	Conclusion	160
6.8	Appendix A. Figures and Tables	162
	Bibliography	164
7	Primal-Dual Value Function Approximation for Stochastic Dynamic Intermodal Transportation with Eco-labels	168
7.1	Introduction	169
7.2	Related literature	172
7.2.1	Multimodal transportation	172
7.2.2	Improved value function approximation	175
7.3	Stochastic dynamic intermodal transportation with eco-labels	177
7.3.1	Problem description	178
7.3.2	Illustrative example	180
7.3.3	Sequential decision process	181
7.4	Solution approach	187
7.4.1	Motivation	187
7.4.2	VFA with basis functions	189
7.4.3	Learning in primal-dual VFA	191
7.4.4	Feature selection	194
7.5	Experimental study	197
7.5.1	Test data and experimental design	197
7.5.2	The value of objective specific feature sets	200

7.5.3	The value of primal-dual VFA	203
7.5.4	Eco-label fulfillment under varied transport emission rates	205
7.6	Conclusion and outlook	207
7.7	Appendix A. Rail corridor data	209
7.8	Appendix B. Analyzing the fit of the feature sets	209
	Bibliography	211
Appendix		217
A A Tutorial on Value Function Approximation for Stochastic Dynamic Transportation Problems		218
A.1	Introduction	219
A.2	Solving stochastic and dynamic problems (in transportation)	221
A.3	The taxicab problem	224
A.4	Modeling and optimal policy	225
	A.4.1 Markov Decision Process	225
	A.4.2 Bellman equation	227
	A.4.3 Optimal policy for the taxicab problem	228
A.5	Value Function Approximation	229
	A.5.1 Motivation and VFA's main principles	230
	A.5.2 Basic VFA algorithm	230
	A.5.3 Post-decision states	232
	A.5.4 Step-by-step application	233
A.6	More about VFA	237
	A.6.1 Harmonic stepsize	237
	A.6.2 Exploration strategy	239
	A.6.3 Parameter tuning and runtime analysis	241
A.7	Conclusion	242
A.8	Appendix A. Python scripts	243
A.9	Appendix B. Additional algorithms	243
A.10	Appendix C. Optimal policy in a small-scale example	246
	Bibliography	249
Authors' Contribution Statements		252
Erklärung zum selbstständigen Verfassen der Arbeit		257

List of Figures

1.1	Freight transport volume and modal split within the EU (European Environment Agency; 2021, Figure 3).	2
1.2	Research agenda of the thesis.	5
2.1	Exemplary routings through an intermodal multilayer network.	20
2.2	Railway network and customer nodes.	23
2.3	Two routes with different slope profiles.	27
2.4	Example of an intermodal and a road-only routing from Portugal to France.	31
2.5	Convergence of emission rates for country pairs (<i>POL, PRT</i>) and (<i>FRA, FRA</i>).	34
2.6	Relative frequency of emission rates.	37
2.7	Top 5 and bottom 5 emission rates for RO and IM heavy shipments.	38
2.8	Emission rates from fixed shipment sizes (grey bars) and random sizes (black bars).	40
2.9	Composition of the energy demand of heavy shipments.	41
2.10	Exemplary emission rates of heavy goods from configuration IV.	42
2.11	<i>IM-share</i> depending on the emission rate per transshipment operation.	43
2.12	Change of IM emissions rates for transshipment emissions of 25 kgCO ₂ e/TU.	44
3.1	Representation of rail services as multiple time-sensitive arcs.	57
3.2	Randomly created locations (left) and TEN-T railway corridors (right) for continental Europe.	60
3.3	Convergence of the average emission rate and transit time.	63
3.4	Example of an emission oriented and a time oriented routing from France to Germany.	65
3.5	Relation between emission rates (left), transit times (right) and (<i>o, d</i>)-airline distance.	65

3.6	Cumulative distribution function of emission rates (left) and transit times (right) for both routing options.	66
4.1	Structure of estimating energy and emissions from rail transportation. . .	75
4.2	Spatial distribution of speed-acceleration combinations of train GP7523 between Glostrup (DK) and Fredericia (DK) (Lindgreen and Sorenson; 2005b).	80
4.3	WTW emission rate r for a varying number of wagons n_w	87
4.4	Emission rate and energy consumption for a varying payload per wagon m_{wt} (diesel train).	88
4.5	WTW emission rate r for a varying average speed v and a varying distance d (diesel train).	89
4.6	WTW emission rate r for a varying number of stops n_s and a varying altitude difference h (diesel train).	90
4.7	Impact of varying train and truck parameters (rows) on each model's WTW emission rate (columns).	92
5.1	Structure of the service selection problem with transshipment processes, allocation schemes per service and limits on order emissions in an emission-oriented setting (SSP-TALE).	105
5.2	Considered rail network and exemplary routing through the road network.	113
5.3	Average computation time for a varying number of orders and varying values of p	115
5.4	Number of green orders for varying values of p	117
5.5	Emissions per order under primary objectives F1 to F4 (instance 17, PT-NL).	119
5.6	Emissions per instance under primary objectives F1 to F4 (five orders, PT-NL).	120
5.7	Emissions per instance for three emission allocation cases (five orders, PT-NL).	121
5.8	Used rail services for three emission allocation policies (instance 10, five orders, PT-NL).	122
5.9	Average emissions over all instances for varying values of default load (five orders, PT-NL).	123
5.10	Average results for performance measure "network emissions" (PT-NL). .	126
5.11	Results for an example with one order of different sizes.	128

5.12	Solutions for all routing-allocation possibilities in the example with two orders.	129
5.13	Emissions per order from sets of powerset $P(\mathcal{O})$	131
6.1	Communication protocol of an eco-labeling process.	142
6.2	Frequency and cumulative frequency of emissions rates in European land-based container transportation (Heinold and Meisel; 2018).	147
6.3	Three eco-labeling systems for freight transport services.	149
6.4	Vehicle routes for all transport services along with energy demand rates .	152
6.5	Transport-related CO ₂ e emissions worldwide, 2000-2018. Source: International Energy Agency (2020)	162
7.1	Considered eco-labeling scheme (a) and load-dependent emissions rates (b).170	
7.2	Illustration of an order's possible routings.	179
7.3	Illustration of the stochastic dynamic intermodal transportation problem with eco-labels.	181
7.4	Illustration of the primal-dual VFA.	192
7.5	Rail service network considered in our experimental study.	198
7.6	Results for objective eco-label violations and costs.	200
7.7	Results for the VFA feature sets for different weights of the two objectives. 202	
7.8	Learning curves with different settings of the primal-dual learning parameter β for <i>VFA EL</i> under objective eco-labels and for <i>VFA CO</i> under objective costs.	203
7.9	Results for varying the primal-dual parameter β and the eco-label stochasticity parameter γ	205
7.10	Eco-label violations and intermodal shares for varied emission rates of the transport modes (both under the eco-label objective).	206
A.1	Policy classes in Approximate Dynamic Programming (based on Powell and Meisel; 2015; Soeffker et al.; 2021).	222
A.2	Illustration of the taxicab problem with five locations and three periods. .	224
A.3	Generic decision tree for the transition from state S_0 to next period's states S_1 . Squares are decision nodes, circles are outcome nodes, solid lines are decisions, and dashed lines are (uncertain) outcomes.	226
A.4	Illustrative example and algorithm for calculating the expected value of the optimal policy.	228
A.5	Results for three instances using the basic VFA algorithm.	237

A.6	Results using different stepsizes and a greedy exploration strategy (instance $V = T = 10$).	238
A.7	Analyzing states' downstream values under backward dynamic programming and VFA with a harmonic stepsize (instance $V = 10, T = 10$).	239
A.8	Analyzing states' downstream values using an exploration strategy (instance $V = 10, T = 10$).	240
A.9	Tuning VFA parameters and analyzing computation time savings.	241
A.10	Decision tree for the example problem. Values atop of the arcs are the demand and its probability and the values atop of the decision nodes are the discounted downstream value following an optimal policy.	248

List of Tables

1.1	Overview of the essays belonging to this thesis.	3
2.1	Descriptive network data for 27 European countries.	22
2.2	Some emission rates per ton-km for road, rail and intermodal transportation.	24
2.3	Notation of the mesoscopic model for road transportation.	26
2.4	Adjusted gradients i^α (in %) for the paths from Figure 2.3.	28
2.5	Notation of the mesoscopic model for rail transportation.	29
2.6	Traffic conditions for road and rail transportation.	33
2.7	Configurations of simulation parameters.	35
2.8	Aggregated results for simulation configurations I to VIII.	36
3.1	Selected relevant literature for this study.	55
3.2	Sets, parameters and decision variables in the TSSP.	58
3.3	Parameter values for the emission estimation.	61
3.4	Results obtained from the simulation experiments.	64
4.1	Consistent notation of common trip and train parameters.	76
4.2	Train and trip parameters that are varied in the experiments.	84
5.1	Overview of selected relevant literature.	102
5.2	Sets, parameters and decision variables in the SSP-TALE.	107
5.3	Emission rates from truck and train freight transportation.	114
5.4	Average results from a hierarchical optimization over 25 instances.	124
5.5	Emissions for the default load and the orders under both allocation schemes.	130
6.1	Emission declarations and eco-labels under FTL road transportation.	153
6.2	Emission declaration, allocation and eco-labels under LTL road transportation (values in CO ₂ e).	154

6.3	Emission declaration, allocation and eco-labels under intermodal rail-road transportation (values in CO ₂ e).	155
6.4	Emissions declaration, allocation and eco-labels under multimodal transportation.	157
6.5	Comparison of allocation measures compliant with EN 16258: A van moves two orders $j = 1, 2$ on transport leg $i = 1$. Its total emission is $e_1 = 60$ kg CO ₂ e.	162
6.6	Transport order data and utilization rates for individual carriage by a heavy truck.	163
6.7	Vehicle data for transport modes used in section 6.5.	163
6.8	Emission allocation (in kg CO ₂ e) for pre/post-carriage (road) and main carriage (rail).	163
6.9	Ranges of allocated emissions (in kg CO ₂ e) and associated labels achieved by four transport services. Eco-labels are recorderd as obtained form the order of payload-based, pallet-based and egalitarian allocation.	163
7.1	Overview of multimodal studies related to our problem.	173
7.2	Overview of the notation used in the sequential decision process.	182
7.3	Feature sets used in our study.	195
7.4	Relative performance (in %) of feature sets VFA EL and VFA CO.	201
7.5	Rail corridor data used in the experiments.	209
7.6	Coefficient of determination (R^2) of the solution approaches under both objectives.	210
A.1	Relevant notation used in this study.	226
A.2	Probability and demand of the example.	233
A.3	Sample realizations (random numbers) used in the first two VFA iterations.	234
A.4	Approximation of the states' downstream values \bar{V}_t^n	235

Chapter 1

Synopsis

1.1 Introduction

Freight and passenger transportation is one of the largest contributors to climate change and global warming. In the United States, the transportation sector was responsible for 29% of anthropogenic greenhouse gas emissions in 2019, followed by the economic sectors electricity, industry, commercial and residential, and agriculture with 25%, 23%, 13%, and 10%, respectively (U.S. Environmental Protection Agency; 2021b). In this regard, greenhouse gas emissions (GHG emissions or, simply, emissions) subsume those gases that are known to be responsible for causing global warming. The most important GHG is carbon dioxide (CO_2), followed by methane (CH_4), nitrous oxide (N_2O), and fluorinated gases (U.S. Environmental Protection Agency; 2021a). Regarding transportation, those gases are primarily emitted by vehicles like trucks or trains through the combustion of fossil fuels (e.g., Demir et al.; 2015; Piecyk et al.; 2012). Inside the transportation sector, the transport of freight plays an important role and, here, trucks are the dominant mode of transportation. For example, 51.7% of freight's total tonne-kilometer were transported via road in the European Union (EU) in 2017, followed by transportation via maritime waterways, rail, inland waterways, and air with 32.5%, 11.6%, 4.1%, and 0.1%, respectively (European Environment Agency; 2021). Figure 1.1 illustrates this so-called modal split in the EU between the years 1995 and 2017. The figure shows the billion tonne-kilometers for each of the modes in each of the considered years.

Three notable conclusions can be drawn from the figure. First, total freight volume increases yearly except for the years following the economic recession that started in 2007/08. This demonstrates that emission-oriented policies are needed to enforce a greening of the transportation sector. Second, the relative modal split is somehow constant

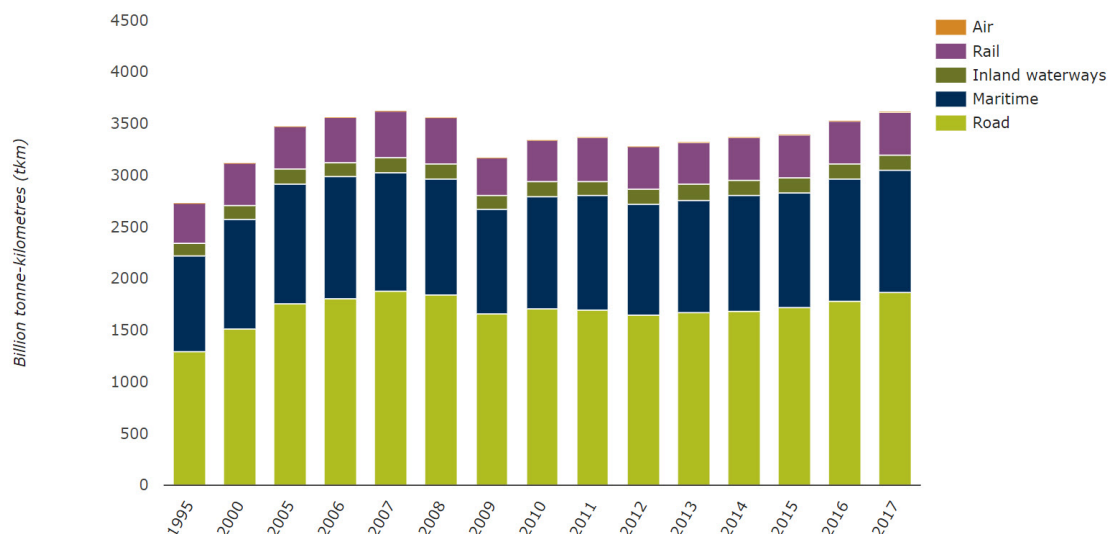


Figure 1.1: Freight transport volume and modal split within the EU (European Environment Agency; 2021, Figure 3).

over the years. This is surprising as shifting freight from trucks to more environmentally friendly modes like trains is widely considered as a way to reduce transport-related emissions (e.g., SteadieSeifi et al.; 2014). In this context, transport solutions that rely on multiple modes for transporting a shipment are of vital importance as a limited network coverage makes a complete shift of door-to-door shipments from road to rail usually not practical. Thus, multimodal networks can work as a means to reduce the prominence of trucks and, eventually, this can lead to more sustainable transport solutions. To this end, a special case of multimodal transportation is the so-called intermodal transportation in which the same unit (e.g., a container) is used for the transportation of freight shipments throughout an entire transport chain (Crainic and Kim; 2007). Third, land-based transport modes (i.e., trucks and trains) generate a large share of freight-related tonne-kilometres. One reason for this is that water-based transportation via maritime and inland waterways depends on the geographical infrastructure that limits their applicability. In contrast, rail networks are relatively well-developed and dense, especially in Europe, which is why they play an important role in multimodal transportation.

It is for those reasons that this thesis comprises seven essays contributing to research on emission-oriented freight transportation that takes place in land-based intermodal or multimodal networks. Table 1.1 provides an overview of the essays, their titles, their author(s), their year, and information about their publication status. The first six essays form the main body of the thesis. Essay 7 is a methodological tutorial for the algorithm

Table 1.1: Overview of the essays belonging to this thesis.

	Title	Author(s)	Year	Publication
Essay 1 (Chapter 2)	Emission Rates of Intermodal Rail/Road and Road-only Transportation in Europe: A Comprehensive Simulation Study	Heinold, A. Meisel, F.	2018	<i>Transportation Research Part D: Transport and Environment</i> , 65: 421–437.
Essay 2 (Chapter 3)	Emission-oriented vs. Time-oriented Routing in the European Intermodal Rail/Road Freight Transportation Network	Heinold, A. Meisel, F.	2019	Logistics Management (LM19). <i>Lecture Notes in Logistics</i> . Springer, Cham, pp. 188–202.
Essay 3 (Chapter 4)	Comparing Emission Estimation Models for Rail Freight Transportation	Heinold, A.	2020	<i>Transportation Research Part D: Transport and Environment</i> , 86: 102468.
Essay 4 (Chapter 5)	Emission Limits and Emission Allocation Schemes in Intermodal Freight Transportation	Heinold, A. Meisel, F.	2020	<i>Transportation Research Part E: Logistics and Transportation Review</i> , 141: 101963.
Essay 5 (Chapter 6)	Eco-Labeling of Freight Transport Services: Design, Evaluation and Research Direction	Kirschstein, T. Heinold, A. Behnke, M. Meisel, F. Bierwirth, C.	2021	<i>Journal of Industrial Ecology</i> , under review (2 nd round after major revision).
Essay 6 (Chapter 7)	Primal-Dual Value Function Approximation for Stochastic Dynamic Intermodal Transportation with Eco-labels	Heinold, A. Meisel, F. Ulmer, M. W.	2021	<i>Transportation Science</i> , under review (1 st round).
Essay 7 (Appendix A)	A Tutorial on Value Function Approximation for Stochastic Dynamic Transportation Problems	Heinold, A.	2021	<i>4OR - A Quarterly Journal of Operations Research</i> , under review (1 st round).

used in Essay 6. The tutorial appears in the appendix of the thesis as it does not represent a direct contribution to its main topic.

The journals in which the essays are published or to which they have been submitted for possible publication are generally associated to the fields of logistics management and operations research. According to VHB-JOURQUAL3 (2021), the ranking of the

journals to which Essays 5 and 6 are submitted is ‘A’, the ranking of the journals in which Essays 1, 3, and 4 are published is ‘B’, and the ranking of the journal to which Essay 7 is submitted is ‘C’. Essay 2 is published in the proceedings series *Lecture Notes in Logistics*, which does not appear in the VHB-ranking.

The rest of the thesis is structured as follows. The following three subsections complete the synopsis: Section 1.2 describes the research agenda of the thesis, Section 1.3 reports about the state-of-the-art research and the thesis’ contributions to it, and Section 1.4 outlines future research opportunities. After the synopsis, a distinct chapter is devoted to each of the essays. Thereby, the tutorial on value function approximation is part of the appendix. The thesis concludes with a detailed statement of the author’s contribution to each essay and a declaration on the originality and novelty of the work.

1.2 Research agenda

This section outlines the thesis’ research agenda by depicting the main research questions that are addressed by the essays. For this, each essay’s research focus is assigned to one of the following three emission-oriented research fields: assessing emissions, communicating emissions, and managing emissions. Figure 1.2 illustrates each essay’s assignment to one of these fields, names each essay’s research topic, and indicates how the essays relate to each other. The figure is further explained in the following by shortly outlining the thesis’ research questions regarding the assessment, communication, and management of emissions. Detailed descriptions of the relevant state-of-the-art research, the gaps that are closed by the essays, and a concise description of how the essays address the research questions are provided afterwards in Section 1.3.

Assessing emissions: This field spans around research regarding the accurate assessment of emissions for a specific transport process. For this, the following research questions are addressed (the related essays are named in parenthesis at the end of each question):

1. What are realistic emission rates for intermodal rail/road transportation in Europe? (Essay 1)
2. What is the trade-off between an emission-oriented routing and a time-oriented routing in a large-scale intermodal network in Europe? (Essay 2)
3. Which models can be used to obtain realistic emission estimates from rail freight transportation? (Essay 3)

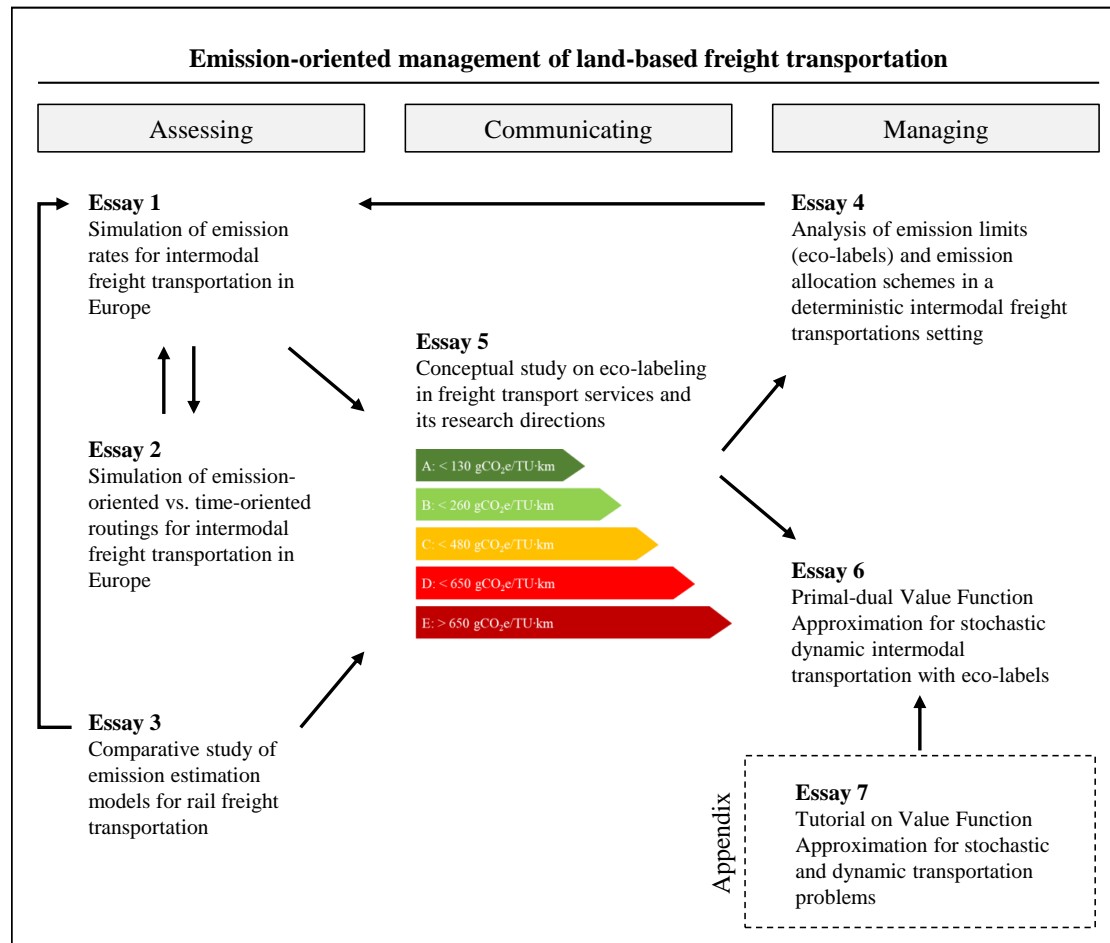


Figure 1.2: Research agenda of the thesis.

Communicating emissions: This field deals with the communication of emissions between customers and transport companies. Here, the thesis' main contribution is the proposition of using so-called eco-labels as a way to evaluate (and communicate) a shipment's environmental impact. To this end, eco-labels refer to a (colored) grading-system reflecting the relative amount of emissions for transporting a shipment. The middle panel of Figure 1.2 shows an exemplary eco-labeling system. In this context, the thesis addresses the following research questions (the related essays are named in parenthesis at the end of each question):

1. What are realistic values in an eco-labeling system for freight transportation in Europe? (Essays 1, 3, and 5)

2. What research directions arise from using an eco-labeling system in the transportation sector? (Essay 5)
3. How can transport companies measure the eco-label of an individual customer shipment in different transportation settings? (Essay 5)

Managing emissions: This field considers the management of emissions in transportation. To this end, the term management refers in this thesis to the decision making in operational settings to achieve a more sustainable and environmentally friendly transportation. That is, the goal is to find transport solutions for shipments in order to reduce total emissions in the network. This thesis evaluates how eco-labels can be used as a way to manage emissions. For this, it addresses the following research questions (the related essays are named in parenthesis at the end of each question):

1. What is the impact of emission allocation schemes in the context of intermodal transportation? (Essay 4)
2. How do eco-labels interact with ‘traditional’ objectives like costs or transit time? (Essays 4 and 6)
3. What are ways to circumvent the additional (mathematical) challenges of solving transportation problems that arise from considering eco-labels? (Essays 4 and 6)
4. How to create an efficient solution approach to deal with eco-labels in a stochastic and dynamic setting? (Essay 6)

Regarding the fourth research question, it is noted that a shipment’s eco-label might not be known with certainty at the time when an acceptance-decision is made for a shipment because the actual emissions are determined by the mode of transport being chosen, the routing of other (not yet known) shipments, and the allocation of emissions among the jointly served shipments. To deal with this, Essay 6 makes a methodological contribution to the field of reinforcement learning by enhancing the learning process of value function approximation, an important solution class of approximate dynamic programming (Powell; 2011). Essay 7 provides an introductory tutorial on value function approximation and is included in the appendix.

1.3 State-of-the-art research and thesis contributions

This section describes the state-of-the-art research and the thesis’ contributions for the introduced three fields of emission-oriented management of land-based freight transporta-

tion: assessing emissions, communicating emissions, and managing emissions. For this, the following subsections cover each of these fields in more detail and elaborate on how the essays address the research questions that have been outlined in the previous section. Still, this is no in-depth review of the essays' contributions nor of the related literature, as those can be found in the respective sections of each corresponding essay.

1.3.1 Assessing emissions

Assessing emissions of a shipment or a vehicle is typically seen as a multistage process. This results from the fact that many freight transportation processes involve multiple transportation legs (potentially performed by different modes of transportation) that each require an environmental assessment on their own before aggregating the results for the overall transportation process. The European norm EN 16258 (2012) describes a practical approach in which transports are principally analyzed 'leg by leg'. Thereby, a leg refers to the smallest distinct section of a transport for which emissions can be determined, and total emissions of a shipment or vehicle are then calculated by aggregating over all applicable legs. There are two aspects in this process to which this thesis contributes: (i) the estimation of emissions for a vehicle on a leg (Essay 3), and (ii) the allocation of a vehicle's emissions to shipments (Essay 4).

The first aspect (estimating a vehicle's emissions while driving) has received considerable attention in the literature. This is mainly motivated by two reasons: first, estimates are a prerequisite for considering the environmental impact in transportation planning and, second, an exact calculation ex-post is often not practicable due to lack of data. Consequently, several energy estimation models have been proposed in which the energy estimate is then converted into an emission estimate. However, slightly different emission estimates are obtained from them as these models rely on different levels of granularity for the input data and on different computation schemes. Demir et al. (2011) provide a comparative analysis of such models for trucks transporting freight but there had been no such study for rail transportation, which is an important mode in freight transportation too. Essay 3 (Heinold; 2020) has filled this gap by comparing five emission estimation models for rail freight transportation. The study also includes a detailed experimental section showing the impact of several relevant input factors, such as speed or slope profile, on the estimated emissions per model. The essay's electronic appendix provides Python implementations of the considered models, allowing researchers and practitioners to use the models on their own and to apply them to specific transportation settings.

The second aspect (allocation of a vehicle's emissions to shipments using the vehicle)

occurs after a vehicle's emissions are estimated. There is rich literature on allocation schemes for products using the same vehicle (or machine) or for companies in collaborative settings but these schemes usually focus on allocating costs (e.g., Guajardo and Rönnqvist; 2016). Some studies have also analyzed aspects specific to the allocation of emissions (e.g., Kellner and Otto; 2012; Kellner and Schneiderbauer; 2019) but none of the studies have considered the possibility of a company to select the 'optimal' allocation model for each vehicle in transportation planning. However, the freedom of selecting a scheme for each vehicle is generally permitted by the European norm. Essay 4 (Heinold and Meisel; 2020) addresses this issue by providing a multi-objective mixed-integer linear program to select transport services as well as allocation schemes per service. The study considers the case of a company operating in an intermodal network in which emissions of each vehicle can either be allocated equally among the shipments or in relation to each shipment's payload. Experiments with artificial shipments in a real-world infrastructural network demonstrate how the selection of allocation schemes can help to improve emission-related service levels. The freedom of choosing an allocation scheme also raises questions of fairness and validity regarding a shipment's emissions, which are discussed in the essay as well.

Following this, the thesis also comprises two simulation studies for assessing realistic emission rates of intermodal transportation in Europe (Essays 1 and 2). Both essays use the mesoscopic model to estimate emissions (Kirschstein and Meisel; 2015) and a payload-based scheme to allocate emissions. Essay 1 (Heinold and Meisel; 2018) is a comprehensive simulation study for emission rates from intermodal rail/road and road-only transportation in Europe. Detailed infrastructural and geographical data is used to create large data sets of realistic emission rates for shipping freight between 27 European countries. With this, it is the first study to provide such comprehensive data of emission-rates for a large-scale transportation network like the European rail/road network. The results generally facilitate the emission-oriented research, for example, by using simulated emission rates to benchmark a company's performance or as inputs in macroscopic analyses like the conceptual eco-labeling study in Essay 5 (which is explained in the next section). Essay 2 (Heinold and Meisel; 2019) follows up on the simulation study performed in Essay 1 by additionally measuring the transit time of the shipments. It then provides an analysis comparing a shipment's emission-oriented routing with its time-oriented routing. The results show that routings of least emissions have a substantially longer transit time compared to routings of least transit time. With this, the study is among the first to quantify the trade-off between the two objectives (emissions vs. transit time) for large freight shipments in Europe.

1.3.2 Communicating emissions

Communicating emissions regarding the transportation of a freight shipment can generally go into one out of two directions. First, a customer can communicate to the transport company the preference regarding a shipment's emissions when the shipment order is placed (ex-ante). Then, these preferences work as a kind of service level for the company who has to ensure that preferences are met for transporting the shipment. Second, the transport company can communicate a shipment's emissions to the customer after the shipment is completed (ex-post). Here, the information might work as a way to gain a competitive advantage or as a way to provide the customer with the possibility to offset the emissions caused by the shipment. So far, studies on emission-oriented transportation usually communicate emissions either as an absolute value (e.g., kilogram CO₂) or as a distance-weighted rate (e.g., gram CO₂ per ton per km). A major contribution of this thesis is the design, conceptualization, and application of using eco-labels for communicating emissions in freight transportation.

Eco-labels generally refer to a standard way of communicating the ecological footprint of products, services, or facilities. For example, eco-labels might be awarded to products that meet certain ecological criteria like the consumption of water. In this thesis, an eco-label refers to one particular class in a system evaluating the relative environmental impact for transporting a shipment. An intuitive traffic light-coloring is used to visualize an eco-label's relative performance. Such eco-labels have received considerable attention in the industry of white goods (e.g., Lorenzo-Toja et al.; 2016) and there are also some studies on eco-labeling in the maritime industry and in airline passenger transportation (Poulsen et al.; 2017; Baumeister and Onkila; 2017; Baumeister et al.; 2020). However, so far, no such labels have been implemented in real-world freight transport operations nor have they been discussed in the respective emission-oriented research. Essay 5 (Kirschstein et al.; 2021) addresses this issue by providing the conceptual framework for using eco-labels in transportation. Essays 4 and 6 provide studies on how to apply such labels in realistic transport settings and are subject of the next section on managing emissions.

Essay 5 elaborates on the design, evaluation, and future research directions of eco-labels in transportation. It also is the first study to design an applicable eco-labeling system for freight shipments. The system is based on the large-scale simulation study of artificial freight shipments across Europe presented in Essays 1 and 2. An example of such system is provided in the middle panel of Figure 1.2. Here, five labels (A to E) with decreasing levels of strictness are proposed: eco-label 'A' is awarded to shipments

whose transportation causes less than 130 gram CO₂e per transport unit and per km (gCO₂e/TU·km) and eco-label ‘E’ is awarded to shipments whose transportation causes more than 650 gCO₂e/TU·km, where a transport unit (TU) refers to a 20-foot equivalent container and CO₂e subsumes all relevant GHG in the single measure of carbon dioxide equivalents. The essay also discusses issues regarding the interplay of the awarded eco-label and the applied emission allocation scheme. Finally, the study compares the awarded eco-labels of a heavy and a voluminous shipment using readily accessible intermodal transportation settings.

1.3.3 Managing emissions

This section describes the thesis’ contribution to the abundant literature on managing emissions in transportation planning. Different ways have been considered to achieve more sustainable transport solutions. One straight possibility is to convert emissions resulting from transportation into costs, which, for example, can be done by using its price determined by an emission trading system like the one of the European Union (e.g., Demailly and Quirion; 2008). It might also be the case that governmental regulations directly impact the set of feasible routing options, for example, by establishing low-emission zones for heavy vehicles (e.g., Fensterer et al.; 2014) or precise emission reduction targets (e.g., Chen et al.; 2014). This thesis considers emissions from a customer-oriented perspective by taking up upon the eco-labeling concept described in the previous section. Essays 4 and 6 are among the first to consider such perspective in the context of intermodal transportation. In particular, they examine settings in which eco-labels are applied to a deterministic (Essay 4) and a stochastic and dynamic (Essay 6) transportation problem.

Essay 4 (Heinold and Meisel; 2020) uses emission limits to indicate the amount of emissions that shall not be exceeded by a shipment. Such limits relate to eco-labels in terms of that they describe the upper bound emissions of a corresponding eco-label. In order to ensure that a routing plan complies with each shipment’s emission limit, it is necessary to estimate emissions caused by the used transport services and to allocate relevant emissions to the shipments. These two issues have already been discussed in Section 1.3.1 on the assessment of emissions. Essay 4 analyzes the impact of emission limits under objectives costs, emissions, and service level for a deterministic transportation problem. A mixed-integer linear program is formulated, several efficient cuts and pre-calculated boundary values are described, and the problem is then solved to optimality using IBM’s CPLEX solver. Experiments with artificial shipments in real-world intermodal networks

demonstrate the interrelated impact of emission limits, emission allocation schemes, and routing decisions. In particular, solutions that maximize the number of shipments that are routed with emissions below their requested limit usually differ from solutions that minimize total emissions. Following these results, the essay then critically discusses the pros and cons of using emission limits per shipment in transportation planning.

Essay 6 (Heinold et al.; 2021) uses eco-labels in a stochastic and dynamic transportation problem. Here, a train operates on a known schedule whereas shipments appear spontaneously over time between the train’s stops. The problem is modelled as a sequential decision process and solved via value function approximation (VFA) with basis functions, a solution class from approximate dynamic programming belonging to the broad field of reinforcement learning. Essay 7 (Heinold; 2021) provides a hands-on introductory tutorial to VFA that is included in this thesis’ appendix. This tutorial uses the taxicab problem, a well-studied and easy-to-understand problem from transportation planning, and shows step-by-step how VFA approaches this problem. The tutorial also explains how more advanced VFA methods can be integrated in the basic version of the algorithm. Overall, the tutorial aims at providing readers with an intuition on VFA in order to apply it to their own transport-related problems. With this, it addresses a broad audience of researchers, lecturers, students, and practitioners from various disciplines including business administration, computer science, and engineering.

Coming back to Essay 6, it is not only among the first studies to consider the idea of eco-labels in a stochastic and dynamic setting but it also makes two major methodological contributions to the literature on VFA. First, the problem is solved under two objectives using feature sets specific to each of the objectives. Computational experiments for a real-world network show that such a careful design increases the average solution quality. Second, a novel ‘primal-dual’ VFA learning approach is introduced to enhance the VFA algorithm. While the classical VFA algorithm learns iteratively from observations resulting from a combination of forward decisions and simulation (primal observation), the proposed extension additionally learns from observations resulting from re-solving the problem ex-post after each iteration (dual observation). The experiments show the improved learning of the primal-dual VFA (in speed and solution quality) that, ultimately, results in an improved real-time decision making. This is a general contribution to the literature on approximate dynamic programming and likely to improve the performance of VFA in other problem classes as well.

1.4 Future research

The synopsis is concluded by briefly describing four promising research directions resulting from the author's work on emission-oriented management of land-based freight transportation: (i) applying eco-labels to collaborative transport settings, (ii) comparing emission reduction strategies in transportation, (iii) analyzing eco-labels in the presence of dynamic pricing, and (iv) applying primal-dual VFA to other problem domains. Further topics of future research are stated in the concluding sections of each of the essays.

The first direction for future research concerns the application of eco-labels in collaborative transport settings. Collaboration in transportation is done for many reasons, such as cost benefits resulting from economies of scale or competitive advantages resulting from an improved network coverage. Eco-labels describe yet another way of differentiating shipments as they refer to the relative environmental performance for transporting a shipment. Essays 4 and 6 have shown that intermodal transportation can be a means to route more shipments in accordance with their requested eco-labels. More generally, emission-oriented routing benefits from diverse and large networks, which might be achieved by a horizontal collaboration among companies operating with different modes of transportation. For example, a trucking company whose fleet consists of road vehicles and a rail company that operates freight trains might collaborate to route more shipments in accordance with their eco-label. A joint research project with Yimeng Zhang, Bilge Atasoy, and Rudy Negenborn from the Technical University Delft (The Netherlands) and Frank Meisel and Arne Heinold from Kiel University is currently investigating settings in which eco-labels work as an incentive to collaborate. Several additional topics follow from this research direction like the stability of collaborations or operational issues regarding information sharing.

The second direction for future research takes up upon the various approaches described in the literature to reduce emissions in transportation: emission taxation, low-emission zones, emission limits, emission reduction target, eco-labels, and others. It seems worth an investigation to identify settings in which these strategies work particularly well and to provide some guidance to decision makers and politics on each strategy's relative performance. This direction might be combined with a general review on the fast emerging research about emission-oriented transportation.

The third direction for future research aims at analyzing pricing schemes in the presence of eco-labels. The results of Essays 4 and 6 have shown that routing as many shipments as possible in accordance with their eco-label comes along with higher overall costs. Furthermore, Essay 2 has described the trade-off between routing a shipment un-

der the objectives of minimizing emissions and minimizing transit time. Some of these issues might be addressed by implementing a (dynamic) pricing scheme considering the requested eco-labels. In this way, a transport company could receive a financial compensation for the effort of routing a shipment according to its eco-label. In this context, it might also be interesting to consider eco-labels in a more ‘flexible’ way, e.g., by considering not only whether or not an eco-label is met but also by considering of how much emissions fall below or exceed a certain eco-label.

Finally, the fourth direction of future research addresses the primal-dual VFA, the most significant methodological contribution of this thesis. Essay 6 has demonstrated the benefits of this approach in an intermodal transportation setting with eco-labels. It could be interesting to analyze the performance of the primal-dual VFA in other problem domains. First preliminary results from a research group at the Analytics & Optimization department at Augsburg University (Germany) already confirm the faster learning for a complex machine scheduling problem. The overall benefits of the primal-dual VFA might also become more apparent by using well-studied operational research problems like the traveling salesman or the vehicle routing problem. More generally, it might be interesting to analyze the impact of considering different observations of the same iteration in the learning of a VFA algorithm.

Bibliography

- Baumeister, S. and Onkila, T. (2017). An eco-label for the airline industry?, *Journal of Cleaner Production* **142**: 1368–1376.
- Baumeister, S., Zeng, C. and Hoffendahl, A. (2020). The effect of an eco-label on the booking decisions of air passengers, *Transport Policy* (In Press).
- Chen, K., Yang, Z. and Notteboom, T. (2014). The design of coastal shipping services subject to carbon emission reduction targets and state subsidy levels, *Transportation Research Part E: Logistics and Transportation Review* **61**: 192–211.
- Crainic, T. G. and Kim, K. H. (2007). Chapter 8 intermodal transportation, in C. Barnhart and G. Laporte (eds), *Transportation*, Vol. 14 of *Handbooks in Operations Research and Management Science*, Elsevier, pp. 467–537.
- Demaily, D. and Quirion, P. (2008). European emission trading scheme and competitiveness: A case study on the iron and steel industry, *Energy Economics* **30**(4): 2009–2027.
- Demir, E., Bektaş, T. and Laporte, G. (2011). A comparative analysis of several vehicle emission models for road freight transportation, *Transportation Research Part D: Transport and Environment* **16**(5): 347–357.
- Demir, E., Huang, Y., Scholts, S. and Van Woensel, T. (2015). A selected review on the negative externalities of the freight transportation: Modeling and pricing, *Transportation Research Part E: Logistics and Transportation Review* **77**: 95–114.
- EN 16258 (2012). *Methodology for calculation and declaration of energy consumption and GHG emissions of transport services (freight and passengers)*, European Committee for Standardization.
- European Environment Agency (2021). Passenger and freight transport demand in Europe. <https://www.eea.europa.eu/data-and-maps/indicators/passenger-and-freight-transport-demand/assessment-1> (visited on 22.11.2021).
- Fensterer, V., Küchenhoff, H., Maier, V., Wichmann, H.-E., Breitner, S., Peters, A., Gu, J. and Cyrus, J. (2014). Evaluation of the impact of low emission zone and heavy traffic ban in Munich (Germany) on the reduction of PM10 in ambient air, *International Journal of Environmental Research and Public Health* **11**(5): 5094–5112.

- Guajardo, M. and Rönnqvist, M. (2016). A review on cost allocation methods in collaborative transportation, *International Transactions in Operational Research* **23**(3): 371–392.
- Heinold, A. (2020). Comparing emission estimation models for rail freight transportation, *Transportation Research Part D: Transport and Environment* **86**: 102468.
- Heinold, A. (2021). A tutorial on value function approximation for stochastic dynamic transportation problems, *Working paper (submitted)*, Kiel. URL: <https://www.scm.bwl.uni-kiel.de/de/team/arne-heinold/data/heinold-vfa-tutorial.pdf> (visited on 22.11.2021).
- Heinold, A. and Meisel, F. (2018). Emission rates of intermodal rail/road and road-only transportation in Europe: A comprehensive simulation study, *Transportation Research Part D: Transport and Environment* **65**: 421–437.
- Heinold, A. and Meisel, F. (2019). Emission oriented vs. time oriented routing in the European intermodal rail/road freight transportation network, in C. Bierwirth, T. Kirschstein and D. Sackmann (eds), *Logistics Management*, Springer International Publishing, Cham, pp. 188–202.
- Heinold, A. and Meisel, F. (2020). Emission limits and emission allocation schemes in intermodal freight transportation, *Transportation Research Part E: Logistics and Transportation Review* **141**: 101963.
- Heinold, A., Ulmer, M. and Meisel, F. (2021). Primal-dual value function approximation for stochastic dynamic intermodal transportation with eco-labels, *Working paper (submitted)*, Kiel. URL: <https://www.scm.bwl.uni-kiel.de/de/team/arne-heinold/data/heinold-meisel-ulmer-primal-dual-vfa.pdf> (visited on 22.11.2021).
- Kellner, F. and Otto, A. (2012). Allocating co 2 emissions to shipments in road freight transportation, *Journal of Management Control* **22**(4): 451–479.
- Kellner, F. and Schneiderbauer, M. (2019). Further insights into the allocation of greenhouse gas emissions to shipments in road freight transportation: the pollution routing game, *European Journal of Operational Research* **278**(1): 296–313.
- Kirschstein, T., Heinold, A., Behnke, M., Meisel, F. and Bierwirth, C. (2021). Eco-labeling of freight transport services: Design, evaluation and research directions, *Working paper (submitted)*, Kiel. URL: <https://www.scm.bwl.uni-kiel.de/de/team/arne-heinold/data/kirschstein-et-al-eco-labeling.pdf> (visited on 22.11.2021).

- Kirschstein, T. and Meisel, F. (2015). GHG-emission models for assessing the eco-friendliness of road and rail freight transports, *Transportation Research Part B: Methodological* **73**: 13–33.
- Lorenzo-Toja, Y., Vázquez-Rowe, I., Amores, M. J., Termes-Rifé, M., Marín-Navarro, D., Moreira, M. T. and Feijoo, G. (2016). Benchmarking wastewater treatment plants under an eco-efficiency perspective, *Science of the Total Environment* **566**: 468–479.
- Piecyk, M., Cullinane, S. and Edwards, J. (2012). Assessing the external impacts of freight transport, in A. McKinnon, M. Browne and A. Whiteing (eds), *Green logistics: Improving the Environmental Sustainability of Logistics*, 2 edn, Kogan Page Limited London, New York, chapter 2, pp. 31–50.
- Poulsen, R. T., Hermann, R. R. and Smink, C. K. (2017). Do ecolabels lead to better environmental outcomes in the international shipping industry? Paper presented at 24th NFF Conference, Bodø, Norway.
- Powell, W. B. (2011). *Approximate Dynamic Programming: Solving the Curses of Dimensionality*, 2nd edn, John Wiley & Sons.
- StadieSeifi, M., Dellaert, N., Nuijten, W., Van Woensel, T. and Raoufi, R. (2014). Multimodal freight transportation planning: A literature review, *European Journal of Operational Research* **233**(1): 1–15.
- U.S. Environmental Protection Agency (2021a). Overview of Greenhouse Gases. <https://www.epa.gov/ghgemissions/overview-greenhouse-gases> (visited on 22.11.2021).
- U.S. Environmental Protection Agency (2021b). Sources of Greenhouse Gas Emissions. <https://www.epa.gov/ghgemissions/sources-greenhouse-gas-emissions> (visited on 22.11.2021).
- VHB-JOURQUAL3 (2021). Liste der Fachzeitschriften in VHB-JOURQUAL3. <https://vhbonline.org/vhb4you/vhb-jourqual/vhb-jourqual-3/gesamtlste> (visited on 22.11.2021).

Chapter 2

Emission Rates of Intermodal Rail/Road and Road-only Transportation in Europe: A Comprehensive Simulation Study

Publication status Published in 2018: *Transportation Research Part D: Transport and Environment* 65: 421–437.

Arne Heinold and Frank Meisel

School of Economics and Business, Kiel University, Kiel, Germany

Abstract Intermodal rail/road transportation combines advantages of both modes of transport and is often seen as an effective approach for reducing the environmental impact of freight transportation. This is because it is often expected that rail transportation emits less greenhouse gases than road transportation. However, the actual emissions of both modes of transport depend on various factors like vehicle type, traction type, fuel emission factors, payload utilization, slope profile or traffic conditions. Still, comprehensive experimental results for estimating emission rates from heavy and voluminous goods in large-scale transportation systems are hardly available so far. This study describes an intermodal rail/road network model that covers the majority of European countries. Using this network model, we estimate emission rates with a mesoscopic model within and between the considered countries by conducting a large scale simulation of road-only

transports and intermodal transports. We show that there are high variations of emission rates for both road-only transportation and intermodal rail/road transportation over the different transport relations in Europe. We found that intermodal routing is more eco-friendly than road-only routing for more than 90% of the simulated shipments. Again, this value varies strongly among country pairs.

Keywords Emission Rates, European Rail/Road Network, Intermodal Transportation, Simulation, Mesoscopic Model

2.1 Introduction

In 2015, a total of 4,452 million tons of anthropogenic CO₂ equivalent greenhouse gases were emitted in the European Union (EU), see Eurostat (2018b). Around 20% of these emissions resulted from transportation (Eurostat; 2018b), where road transportation is the dominant mode in the freight sector. For example, 75.3% of the total inland freight ton-kilometers (ton-km) in the EU were transported by truck, 18.3% by train and 6.4% by inland waterways in 2015 (Eurostat; 2018a). Recent research and political initiatives that seek for a reduction of the human-made environmental impact therefore also focus on emissions from transportation, see e.g. McKinnon et al. (2012), Psaraftis and Kontovas (2016), or DIN EN 16258 (2012). The amount of greenhouse gases (GHG) emitted per ton-km are used as a typical measure for the environmental impact of freight transportation. Although greenhouse gases subsume various substances like carbon dioxide, methane, nitrous oxide, hydrofluorocarbons, perfluorocarbons and sulphur hexafluoride, their global warming potential can be expressed as carbon dioxide equivalents (CO₂e) and, therefore, the amount of CO₂e per ton-km is considered a valid indicator of the environmental performance of freight transportation. Shifting freight from road to rail is often seen as an effective option to improve this measure (e.g. Dekker et al.; 2012, McKinnon et al.; 2012). Thereby, an objective comparison of transport options requires to consider well-to-wheel emissions that include not just the actual emissions of the transport operation (so called tank-to-wheel emissions) but also the emissions caused by producing and providing the fuel or energy to the vehicle (so called well-to-tank emissions), see Hoffrichter et al. (2012), Moro and Lonza (2018).

Research in the field of environmental transportation focusses on the development of eco-oriented routing and transport flow models (e.g. Bauer et al.; 2010; Behnke and Kirschstein; 2017; Bektaş and Laporte; 2011; Ehmke et al.; 2016; Rudi et al.; 2016). Such

studies usually consider emission rates obtained from emission estimation models or they use aggregated empirical rates reported in the literature. Experimental results in such papers typically refer to artificial networks or to relatively small real networks that cover a specific region. A comprehensive overview of emission rates that are observed in large-scale transportation systems like the European rail/road system is not provided by these studies. With our paper, we fill this gap and provide a systematic and broad overview of emission rates from intermodal rail/road and road-only transportation in Europe. More precisely, we analyze intra- and inter-country freight shipments for 27 European countries. We conduct a comprehensive simulation study that respects country specific attributes like the electrification and density of the rail network and geographical characteristics. To this end, we (i) collect data of an intermodal rail network across the considered countries, based on the corridors from the Trans-European Transport Network policy (TEN-T), see European Commission (2018), (ii) adapt a suitable emission estimation model for rail and road transportation and (iii) present results from an extensive simulation study that covers numerous experimental settings. We focus on relatively large shipments of several truck loads of heavy and voluminous goods, as these are candidates for rail transportation. Next to the differentiation between heavy and voluminous goods, we analyze the impact of further vehicle characteristics, shipment characteristics, and route characteristics such as traction type, electric emission factors, cargo size, gradient or traffic conditions. To estimate emissions, we adapt the mesoscopic model from Kirschstein and Meisel (2015). This model can capture both road and rail transportation and allows us to test the relevance of the previously mentioned parameters for the European transport system. We also contribute to the improvement of this estimation model by presenting an alternative way of approximating the gradient of a route. With these contributions, we present a broad and holistic overview of intermodal rail/road emission rates for European countries. The results of this study can be used to further facilitate research in areas where emission rates serve as an input to environmentally oriented decision problems, such as location planning or routing problems. They might also be used for companies to benchmark their environmental performance. In addition, the derived model of the European rail and road network can be used for follow-up research in the field of intermodal transportation.

The paper is organized as follows. Section 2.2 formally describes the intermodal rail/road network and the used data. Section 2.3 briefly reviews literature on emission estimation models and provides details about the mesoscopic estimation model. Section 2.4 describes the simulation settings and Section 2.5 presents the obtained results. Section 2.6 concludes this paper. The paper is supplemented by an extensive appendix that provides look-up tables for emission rates of road, rail and intermodal rail/road

erational transshipment processes and consists of nodes \mathcal{N}^{trans} (nodes 17 and 18 in the example) and an empty set $\mathcal{E}^{trans} = \emptyset$ as there are no edges between transshipment nodes. The road network $\mathcal{G}^{road}(\mathcal{N}^{road}, \mathcal{E}^{road})$ is an incomplete network described by nodes \mathcal{N}^{road} (nodes 7 to 16 in the example) and edge set $\mathcal{E}^{road} \subset \mathcal{N}^{road} \times \mathcal{N}^{road}$. The bottom layer states the customer network $\mathcal{G}^{cust}(\mathcal{N}^{cust}, \mathcal{E}^{road})$ and consists of all customer nodes \mathcal{N}^{cust} (nodes 1 to 6 in the example) and an empty set \mathcal{E}^{road} as customers are only connected with each other via the road network. The additional cross-layer edge sets $\mathcal{E}^{trans-rail} \subset \mathcal{N}^{rail} \times \mathcal{N}^{trans}$, $\mathcal{E}^{trans-road} \subset \mathcal{N}^{trans} \times \mathcal{N}^{road}$ and $\mathcal{E}^{cust-road} \subset \mathcal{N}^{cust} \times \mathcal{N}^{road}$ connect subgraphs \mathcal{G}^{rail} , \mathcal{G}^{trans} , \mathcal{G}^{road} and \mathcal{G}^{cust} . Railway nodes that qualify for transshipment to the road mode (nodes 19 and 23 in the example) are linked via dedicated transshipment nodes (nodes 17 and 18 in the example) to dedicated road nodes (nodes 9 and 16 in the example). Note that each node in \mathcal{N}^{rail} and \mathcal{N}^{road} is linked to at most one node in \mathcal{N}^{trans} and that each node in \mathcal{N}^{cust} is linked to exactly one node in \mathcal{N}^{road} .

We denote by $(i, j) \in \mathcal{E}$ the edge that connects node $i \in \mathcal{N}$ and node $j \in \mathcal{N}$. We consider asymmetric edge weights because edge characteristics (like gradient i^α and distance d introduced later in Section 2.3) might differ between edges $(i, j) \in \mathcal{E}$ and $(j, i) \in \mathcal{E}$ in a real-world infrastructure network. Eventually, shipments from an origin $i \in \mathcal{N}^{cust}$ to a destination $j \in \mathcal{N}^{cust}$ may use a road-only routing (Figure 2.1a) or an intermodal routing (Figure 2.1b). The road-only routing uses merely the two bottom layers whereas the intermodal routing uses all four layers. In other words, we assume that customers do not have direct access to the rail network, although this could be included in the model without difficulty.

2.2.2 Network Data for the European Rail and Road Network

We instantiate the theoretical network model from Section 2.2.1 to represent the rail/road network of the current EU member states, excluding the island states Cyprus, Ireland and Malta but including the non-EU member states Norway and Switzerland.

The railway network \mathcal{G}^{rail} orients along the core corridors of the TEN-T policy. The use of TEN-T core corridors comes for several reasons: (i) the corridors define all relevant infrastructural elements, (ii) they also define rail line specific restrictions (e.g. a lack of electrification) and (iii) it can be assumed that all core corridors are relevant for intermodal freight transportation. The set of railway nodes \mathcal{N}^{rail} is derived from respective terminals in the TENtec Interactive Map (2018). All these nodes qualify for rail/road transshipment. TEN-T contains at most one terminal for most of the cities.

For cities with more than one terminal, we included only the most central one in our network. This results for example in 14 transshipment nodes for Spain and 4 transshipment nodes for Austria, see Table 2.1. Concerning railway edges \mathcal{E}^{rail} , we only consider existing tracks as derived from Raildar (2018). We supplement the rail network by auxiliary nodes that split some of the edges into two or more parts. This is to represent different edge characteristics, such as traction type or country borders. To increase the network connectivity, we include the projected ‘Tallinn-Helsinki Tunnel’ between Helsinki (Finland) and Tallinn (Estonia), the planned ‘Fehmarn Belt Tunnel’ between Puttgarden (Germany) and Rødby (Denmark), the train ferry that connects Sicily with mainland Italy and the train ferry that connects Rostock (Germany) with Trelleborg (Sweden),

Table 2.1: Descriptive network data for 27 European countries.

country	country code [-]	transshipment nodes [-]	rail line		emission coefficient [gCO ₂ e/kWh]	customer nodes [-]
			electrified [km]	not electrified [km]		
Austria	AUT	4	1,103	66	322	226
Belgium	BEL	7	838	0	261	83
Bulgaria	BGR	4	1,114	0	618	297
Croatia	HRV	2	378	0	487	153
Czech Republic	CZE	6	1,216	75	657	212
Denmark	DNK	2	343	121	364	116
Estonia	EST	1	56	216	878	116
Finland	FIN	5	520	0	207	384
France	FRA	16	4,513	0	100	1,500
Germany	DEU	26	5,176	524	599	956
Greece	GRC	2	435	408	732	353
Hungary	HUN	2	1,276	0	383	248
Italy	ITA	22	3,919	0	413	806
Latvia	LVA	2	45	374	1,110	170
Lithuania	LTU	3	95	493	370	172
Luxembourg	LUX	1	40	0	508	7
Netherlands	NLD	9	585	0	555	92
Norway	NOR	1	169	0	9	528
Poland	POL	9	3,686	100	937	839
Portugal	PRT	5	1,064	0	372	251
Romania	ROU	9	1,494	112	449	630
Slovakia	SVK	2	663	0	412	132
Slovenia	SVN	2	397	109	309	55
Spain	ESP	14	3,911	1,349	321	1,370
Sweden	SWE	5	1,374	0	45	661
Switzerland	CHE	1	509	0	29	108
United Kingdom	GBR	9	1,227	494	593	663
	Σ	171	36,147	4,439		11,128

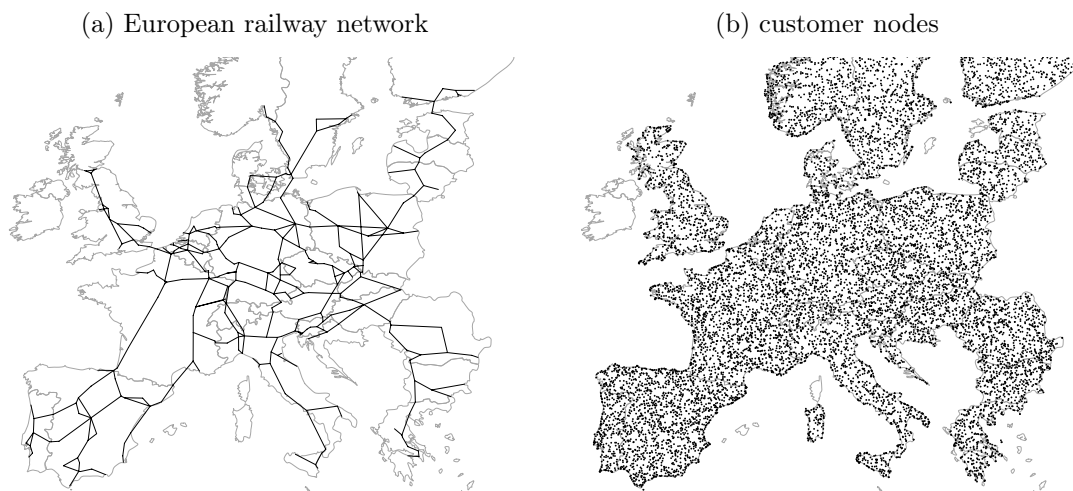


Figure 2.2: Railway network and customer nodes.

see European Parliament (2017), European Commission (2015), BluFerries (2018) and StenaLine (2018). The traction type of the locomotive on each railway track (either diesel or electric) is derived from information of the TEN-T Compliance Maps (2014). In total, \mathcal{G}^{rail} includes 40,586 kilometers of rail tracks, of which 36,147 kilometers are electrified (89%) and 4,439 kilometers are not electrified (11%) and operated with diesel locomotives, see Table 2.1. Figure 2.2a illustrates this railway network.

The road network \mathcal{G}^{road} is derived from the Open Street Map (2018), as provided by Geofabrik (2018). The road network consists of all roads of the type ‘motorway’, ‘trunk’, ‘primary’, ‘secondary’, ‘tertiary’, and ‘service’. To improve the connectivity, we include heavy-good vehicle ferries, for example between Calais (France) and Dover (United Kingdom) as well as between Helsinki (Finland) and Stockholm (Sweden).

2.3 Emission Estimation for Road and Rail Transportation

2.3.1 Literature Review

Numerous papers have investigated the environmental impact of transport activities and reported emission rates for various transport scenarios. Table 2.2 shows a selection of emission rates mentioned in the literature. Clearly, these values are valid only for the particular context considered in the respective study. In addition, some of the studies focus on carbon dioxide only and ignore other greenhouse gases and some of the studies look at well-to-wheel emissions whereas others consider tank-to-wheel emissions only.

Table 2.2: Some emission rates per ton-km for road, rail and intermodal transportation.

source	emissions		context
	value	unit	
road			
de Miranda Pinto et al. (2017)	115	gCO ₂	case study for paper transportation in Brazil
Craig et al. (2013)	78	gCO ₂	North America, varies between 55 and 106 gCO ₂ /ton-km
DEFRA (2017)	77	gCO ₂ e	HGV (> 33 t) in the UK, 50% load
NTM (2017b)	72	gCO ₂ e	EU average for a 34-40 t truck with trailer, 50% load
Winebrake et al. (2008)	48	gCO ₂	case study for the USA (13 t/TEU)
MMEEC (2018)	40	gCO ₂	generic truck with two TEU containers (13 t/TEU)
rail			
DEFRA (2017)	34	gCO ₂ e	freight train in the UK
NTM (2017a)	23	gCO ₂ e	EU average for diesel and electric locomotives
MMEEC (2018)	15	gCO ₂	generic line haul locomotive with 100 well cars (13 t/TEU)
Winebrake et al. (2008)	10	gCO ₂	case study for the USA (13 t/TEU)
intermodal (rail/road)			
Craig et al. (2013)	42	gCO ₂	North America, varies between 18 and 138 gCO ₂ /ton-km
de Miranda Pinto et al. (2017)	18	gCO ₂	case study for paper transportation in Brazil

Therefore, the obtained emission rates might be taken up by other studies that demand emission rates as an input (for example to do eco-oriented transportation planning) but the comparability and explanatory power of the results is then limited. Therefore, it seems reasonable to provide a holistic overview of emission rates that covers a large scale transport system like the European rail/road network.

Generally, emissions caused by a particular transport activity can be computed using emission estimation models. In the literature, numerous models have been proposed that differ in the used data sources and the level of detail of the estimation. Psaraftis and Kontovas (2016) differentiate between top-down (or fuel-based) and bottom-up (or activity-based) methods. Top-down methods use the actual fuel consumption or estimate the fuel consumption of an already conducted transport. Emission factors for the respective fuel type are then used to quantify the GHG emissions. In contrast, bottom-up methods exploit relevant parameters of the transport activity (used vehicle type, distance, etc.) and estimate emissions with the help of look-up values. Another way to classify emission models is to differentiate between microscopic and macroscopic models (Scora and Barth; n.d.). Microscopic models estimate emissions as precisely as possible

by considering detailed physics of the moving vehicle, such as air resistance and rolling resistance. Macroscopic models are less precise and use, similar to bottom-up methods, empirical data to estimate emissions. Macroscopic models usually combine trip specific information, such as road profile and average speed, with vehicle specific information, such as tare weight and fuel type.

A large number of emission estimation models is designed either for road or for rail freight transportation. An overview of models for road transportation is provided by Demir et al. (2011). A popular model in this field is the Comprehensive Modal Emissions Model (CMEM) from Scora and Barth (n.d.). A popular model for rail transportation is the ARTEMIS (Assessment and Reliability of Transport Emission Models and Inventory Systems) model from Lindgreen and Sorenson (2005b). Both models follow the microscopic idea and derive emissions from a very detailed estimation of fuel or energy demands. Emission estimation models that cover both road and rail transportation often follow a macroscopic approach. The EcoTransIT World Initiative (2016) developed the EcoTransIT model that covers all major transportation modes (road, rail, water, air). Another macroscopic model for road and rail is the MEET (Methodologies for Estimating Air Pollutant Emissions from Transport) model from Hickman et al. (1999). The authors derive emission functions and parameters from real-world experiments for various vehicle types. Kirschstein and Meisel (2015) propose a mesoscopic model for road and rail transportation that combines the most relevant factors from microscopic models with empirical data from macroscopic models. The authors follow the physical base model from Ross (1997), which derives the required energy from factors like speed, weight, grade or acceleration. The relevance of these factors has been discussed in several other studies, such as Hickman et al. (1999) or Stead (1999). From the energy demand, the mesoscopic model deducts the amount of emitted greenhouse gases through emission factors. This procedure is similar to other emission estimation models, such as the model from DeLuchi (1991) or the GREET model from Wang (1999). Like Hickman et al. (1999) and others, the mesoscopic model supports trip specific acceleration profiles and thus allows for a consideration of various traffic conditions, like urban traffic and highway traffic. Kirschstein and Meisel (2015) show that this differentiation can have a significant impact on emission rates. Like all other models that cover road and rail, also the mesoscopic model can be used for an environmental assessment of intermodal rail/road transports. For the purpose of our study, the mesoscopic model describes a good trade-off between the required input data and the accuracy of estimated emissions. The next two subsections describe the methodology of the mesoscopic model for road transportation and for rail transportation.

2.3.2 Estimating Emissions from Road Transportation

The mesoscopic model derives emissions for road transportation by estimating the fuel demand of a transport operation. Equation (2.1) represents the main formula for computing GHG emissions and Table 2.3 shows the adopted notation. The formula first estimates the energy demand W_{truck} for moving the truck, taking into account the distance d of a considered trip, the gradient i of the route, the total weight m (including payload $m^{payload}$ and tare weight m^{tare}), the average number of acceleration processes per kilometer n^{acc} and the average speed v of the expected traffic conditions. For details of the corresponding computation, we refer to Kirschstein and Meisel (2015).

$$GHG_{truck} = \left(W_{truck}(d, i, m, n^{acc}, v) \cdot \frac{r^{full} - r^{idle}}{\epsilon^t(v) \cdot p^{vehicle}} + r^{idle} \cdot \frac{d}{v} \right) \cdot k \quad (2.1)$$

Formula (2.1) weights W_{truck} to convert the energy demand into a fuel demand by taking into account the transmission efficiency of the truck $\epsilon^t(v)$, which depends on the average speed v , the maximal power of the engine $p^{vehicle}$ and the fuel consumption rate

Table 2.3: Notation of the mesoscopic model for road transportation.

notation	value	unit	description
trip specific			
W_{truck}	*	kWh	required energy to move the truck
d	*	km	distance
i	*	%	gradient
m	*	t	total weight
$m^{payload}$	*	t	payload
n^{acc}	*	-	average number of accelerations per km
v	*	km/h	average speed
truck and fuel type specific			
m^{tare}	14	t	tare weight of the truck
$\epsilon^t(v)$	~0.88	-	transmission efficiency
$p^{vehicle}$	300	kW	maximal power of the engine
r^{idle}	3	l/h	fuel consumption rate if truck is idle
r^{full}	68.7	l/h	fuel consumption rate if truck is at full power
A	9	m ²	front surface area of the truck
c^{air}	0.6	-	air resistance coefficient
c^{roll}	0.006	-	rolling resistance coefficient
p	0.0811	l/kWh	well-to-wheel energy coefficient (diesel)
k	3.15	kgCO ₂ e/l	well-to-wheel emission coefficient (diesel)

* computed from other parameters or varied in the simulation

if the truck is idle r^{idle} or at full power r^{full} . The calculation requires further truck and fuel type specific parameters, namely the front surface A of the truck, the air resistance coefficient c^{air} , the rolling resistance coefficient c^{roll} and the energy coefficient p for diesel fuel. Corresponding values are also listed in Table 2.3. All values belong to a 40 t diesel truck, which is the vehicle type considered for road transportation throughout our study. Eventually, Formula (2.1) multiplies the fuel demand with a well-to-wheel emission coefficient k to convert the amount of diesel into an amount of CO₂e.

One of the parameters that needs to be provided to the mesoscopic model is the gradient i of the route. This gradient is then used to calculate the power to overcome the difference in altitude, which becomes part of the total energy to move the truck W_{truck} . For a path that connects some origin location with some destination location, an intuitive way to calculate this gradient i is to compare the altitude of the origin with the altitude of the destination. However, this approach can result in the same gradient value for two paths with very different slope profiles, see Figure 2.3. The path from A to B in Figure 2.3a goes through a hilly terrain with partially steep gradients whereas the path from C to D in Figure 2.3b goes through a terrain with a modest but constant gradient. Since the altitude of origins A and C , the altitude of destinations B and D and the distance $d = 50$ km are identical, the simple origin-destination altitude difference leads to the same gradient for both routes and, thus, presumes an identical energy demand for both routes. To resolve this issue, we introduce the concept of the adjusted gradient i^α , where we differentiate between positive and negative slopes. For this, we split the path, which is of total distance d , into n equally sized segments. We refer to the i^{th} segment as z_i and denote by $alt(z_i^1)$ the altitude of the starting point of segment z_i and by $alt(z_i^2)$ the altitude of the ending point of segment z_i . Furthermore, we compute by $u_{z_i} = \max\{alt(z_i^2) - alt(z_i^1), 0\}$ the positive altitude difference in segment z_i and

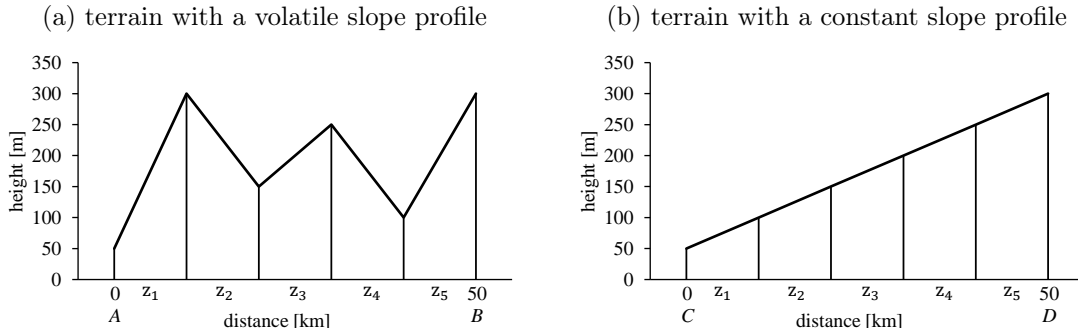


Figure 2.3: Two routes with different slope profiles.

by $v_{z_i} = \max\{alt(z_i^1) - alt(z_i^2), 0\}$ the negative altitude difference in segment z_i . The calculation of the adjusted gradient i^α is shown in Formula (2.2) where $0 \leq \alpha \leq 1$ is a preset weight.

$$i^\alpha = \frac{1}{d} \cdot \sum_{z_i} (u_{z_i} - \alpha \cdot v_{z_i}) \quad (2.2)$$

The idea behind i^α is to fully account for positive slopes (u_{z_i}) and to (partially) subtract negative slopes (v_{z_i}). Note that negative slopes reduce the energy required to overcome other physical forces, such as rolling resistance or air resistance, and thus reduces the total energy demand (Ross; 1997). In addition, new technologies enable energy recoveries from negative slopes, such as the deceleration energy of trains. However, the original gradient i assumes that energy from negative slopes can be recovered totally. This might even lead to situations where energy recovered from negative slopes exceeds all other energy demands and results in a negative overall energy demand, which is definitely unrealistic. With the introduction of α we can control to what extent this energy is recovered. In case $\alpha = 0$ only positive slopes are considered for the calculation of the adjusted gradient and downhill segments are treated like segments with flat terrain. In other words, $\alpha = 0$ means that no energy is recovered from negative slopes at all. With a value of $\alpha > 0$ energy from negative slopes is partially recovered. The extreme case of $\alpha = 1$ represents a full recovery of energy from negative slopes, identical to the original gradient i . In Table 2.4 we show i^α for the examples from Figure 2.3 and for $\alpha \in [0, 0.2, \dots, 1]$. The adjusted gradient in Figure 2.3a increases with lower values of α , because the negative slopes are gradually ignored. For the reversed path that goes from B to A this leads to a change in the sign of i^α . In Figure 2.3b, no segment of the path going from C to D has a negative altitude difference ($v_{z_i} = 0, \forall i = 1, \dots, n$), which makes i^α independent of the value of α . Respectively, for the reversed path that goes from D to C , all segments have a negative altitude difference ($v_{z_i} > 0, \forall i = 1, \dots, n$) and i^α decreases with higher values of α .

Table 2.4: Adjusted gradients i^α (in %) for the paths from Figure 2.3.

α	Figure 2.3a		Figure 2.3b	
	$A \rightarrow B$	$B \rightarrow A$	$C \rightarrow D$	$D \rightarrow C$
0.0	1.10	0.60	0.50	0.00
0.2	0.98	0.38	0.50	-0.10
0.4	0.86	0.16	0.50	-0.20
0.6	0.74	-0.06	0.50	-0.30
0.8	0.62	-0.28	0.50	-0.40
1.0	0.50	-0.50	0.50	-0.50

2.3.3 Estimating Emissions from Rail Transportation

For rail freight transportation, the mesoscopic model differentiates between diesel and electric trains. Still, the main idea for both types of power supply is to estimate the energy demand W_{train} for moving the train and, then, either directly derive the emissions from this amount of energy (electric train) or use an energy coefficient p to first convert the energy demand into a fuel demand (diesel train). Formula (2.3) shows the calculation that is common for both types of power supply. Table 2.5 lists the corresponding notation.

$$GHG_{train} = \frac{W_{train}(d, i, m, n^{car}, n^{acc}, v)}{\epsilon} \cdot p \cdot k \quad (2.3)$$

The energy demand W_{train} is computed from distance d , gradient i , total weight m , number of rail cars n^{car} , number of accelerations per kilometer n^{acc} and average speed v . Here d , i , n^{acc} and v are defined identical to the road model. In contrast, m depends

Table 2.5: Notation of the mesoscopic model for rail transportation.

notation	value	unit	description
trip specific			
W_{train}	*	kWh	required energy to move the train
d	*	km	distance
i	*	%	gradient
m	*	t	total weight
$m^{payload}$	*	t	payload
n^{car}	*	-	number of cars per train
n^{acc}	*	-	average number of accelerations per km
v	*	km/h	average speed
train type specific			
m^{car}	17.7	t	tare weight of a car
m^{loc}	123	t	tare weight of the locomotive
ϵ	*	-	efficiency of the locomotive
p	*	l/kWh	energy coefficient
k	*	*	well-to-wheel emission coefficient
A	10	m ²	front surface area of the train
c_{car}^{air}	0.218	-	air resistance car (3 transport units per car)
c_{loc}^{air}	1.1	-	air resistance locomotive
c_{aux1}^{roll}	0.0005	-	rolling resistance (auxiliary 1)
c_{aux2}^{roll}	0.0006	-	rolling resistance (auxiliary 2)
c_{car}^{roll}	0.0006	-	rolling resistance car
c_{loc}^{roll}	0.004	-	rolling resistance locomotive
* computed from other parameters or varied in the simulation			

on the payload $m^{payload}$, the number of rail cars n^{car} required for carrying this load, the tare weight per car m^{car} and the tare weight of the locomotive m^{loc} . The transmission efficiency of the locomotive ϵ , the energy coefficient p and the emission coefficient k depend on the type of power supply. For diesel trains, ϵ is set to 0.38, p is set to 0.0811 l/kWh and k is set to 3.15 kgCO₂e/l. For electric trains, ϵ is set to 0.65 and p is set to 1 (as it actually plays no role for electric trains). The emission coefficient k used by the electric train is measured in kgCO₂e/kWh and depends on the energy mix of the country within which the train operates. The calculation of W_{train} requires further train type specific parameters, which are listed in Table 2.5 but not described here in further detail. All mentioned values are for a train with a 6-axle locomotive, carrying a varying number of 19.64 m long four-axle ‘Sgis’ cars (Kirschstein and Meisel; 2015, Lindgreen and Sorenson; 2005a,b). These cars can carry at most three 20-foot containers or a total of 62 tons.

2.4 Simulation Settings

Our simulation study aims at estimating emission rates for shipments within and between the considered European countries. Section 2.4.1 describes the creation of shipments and their routing in the network. Section 2.4.2 describes the specification of trip specific parameters for the mesoscopic model and derives an appropriate number of shipments to simulate per country pair. Finally, Section 2.4.3 describes different configurations that are later explored by experiments in Section 2.5.

2.4.1 Generation of Shipments and Routing

We generate shipments within and between 27 European countries. We denote by \mathcal{C} the set of these countries. Given a country pair (c_1, c_2) , with $c_1 \in \mathcal{C}$ and $c_2 \in \mathcal{C}$, we generate a set of shipments \mathcal{S}_{c_1, c_2} for this transport relation. In case of $c_1 = c_2$ these shipments have their origin and destination in the same country whereas in case of $c_1 \neq c_2$ shipments have their origin and destination in different countries.

Each shipment $s \in \mathcal{S}_{c_1, c_2}$ is defined by its payload l_s (in tons), its origin location o_s and its destination location d_s . For the payload l_s , we first draw a random shipment size $t_s \in [6, 7, \dots, 24]$ of transport units (TU). Each such unit corresponds to a 20-ft equivalent container unit or a similar load device. Accordingly, the lowest shipment size of 6 transport units refers to 3 full truck loads or 2 full rail cars whereas the largest shipment size of 24 transport units refers to 12 full trucks or 8 full rail cars. We then

assume a gross weight of 11 t per transport unit for heavy goods and 6 t per transport unit for voluminous goods, which leads to the payload l_s of shipment s . For the origin o_s and the destination d_s , we first preprocess a set of candidate customer node \mathcal{N}_i^{cust} per country $i \in \mathcal{C}$, with $\mathcal{N}^{cust} = \bigcup_{i \in \mathcal{C}} \mathcal{N}_i^{cust}$. Node locations are drawn uniformly from latitude/longitude values that belong to the country, where we exclude locations that are not connected to the road network \mathcal{G}^{road} (for example small islands). The number of candidate locations per country is proportional to the land area of this country. For France, which is the largest country in \mathcal{C} , we draw 1,500 random locations. For each other country, the number of candidate locations derives from its land area in comparison to France. For example, the land area of Latvia is 11.3% of the area of France and we thus generate 170 customer nodes in Latvia. We exclude locations with a latitude north of 63° North, as these are sparsely populated areas in Norway, Sweden or Finland. Figure 2.2b illustrates the nodes \mathcal{N}^{cust} and Table 2.1 shows the number of customer nodes $|\mathcal{N}_i^{cust}|$ per country. For a particular shipment $s \in \mathcal{S}_{c_1, c_2}$, we draw the origin o_s from set $\mathcal{N}_{c_1}^{cust}$ and the destination d_s from set $\mathcal{N}_{c_2}^{cust}$.

For each shipment $s \in \mathcal{S}_{c_1, c_2}$, we compare two possible routings: road-only (RO) and intermodal (IM). For RO, shipment s goes from o_s to d_s solely through the road network \mathcal{G}^{road} . For IM, shipment s goes from o_s to a transshipment node $h_s^o \in \mathcal{N}^{trans}$ in the origin area via \mathcal{G}^{road} , uses the rail network \mathcal{G}^{rail} for rail transportation to a transshipment node $h_s^d \in \mathcal{N}^{trans}$ in the destination area and finally goes from h_s^d to d_s via \mathcal{G}^{road} . We select h_s^o as the closest transshipment node to o_s and h_s^d as the closest transshipment node to d_s , where h_s^o is not necessarily within the same country as o_s and h_s^d is not necessarily within the same country as d_s . The IM routing of shipment s is therefore $o_s \rightarrow h_s^o$ via road, $h_s^o \rightarrow h_s^d$ via rail and $h_s^d \rightarrow d_s$ via road. For short distance shipments, this

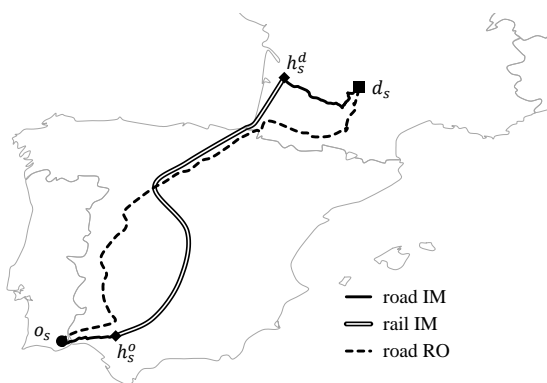


Figure 2.4: Example of an intermodal and a road-only routing from Portugal to France.

might lead to a selection of the same transshipment node $h_s^o = h_s^d$. In this case, the routing does actually not involve a rail transportation and we merely consider road-only transportation for such shipments. Figure 2.4 shows the RO and the IM routing for an exemplary shipment from Portugal to France. In the figure, the solid lines present the pre- and post-haulage $o_s \rightarrow h_s^o$ and $h_s^d \rightarrow d_s$ in the road mode, the two parallel solid lines represent the rail transportation $h_s^o \rightarrow h_s^d$ and the dashed line corresponds to the direct road transportation $o_s \rightarrow d_s$.

2.4.2 Specification of Emission Model Parameters

We now specify the trip specific parameters distance d , gradient i , payload $m^{payload}$, number of rail cars n^{car} , average number of acceleration processes per kilometer n^{acc} and average speed v for a shipment s . We suppress here the shipment subscript s for reasons of readability. Furthermore, we specify the emission coefficient k for electric trains and derive an appropriate number of shipments to simulate for each pair of countries.

Distances d in the road-only mode and in the pre- and post-haulage of intermodal routings refer to the fastest routes in the road network \mathcal{G}^{road} and are calculated with the Open Source Routing Machine (Luxen and Vetter; 2011). Distances d in the rail part of an intermodal routing refer to the shortest routes in the rail network \mathcal{G}^{rail} and are calculated with Raildar (2018).

We approximate the gradients i^α in \mathcal{G}^{road} and \mathcal{G}^{rail} as follows. We consider the straight-line distance d_{o_s, d_s} from o_s to d_s and split this into segments of 10 kilometers each. We use Open Elevation (2018) to obtain the altitude for each segment's start and end point. The gradient is then calculated from the slopes of all segments as described in Section 2.3.2.

For rail transportation, we assume a maximal total length of 740 meter per train (European Parliament and Council; 2013), which limits the number of cars per train to 36. For the calculation of the actual number of cars n^{car} and the payload $m^{payload}$, we assume a basic load of 24 cars, each holding 3 transport units à 9 ton. This load expresses a default train utilization rate of 67% w.r.t. the number of allowed cars per train. This rate is later varied in the experimental study. On top of that comes the shipment load l_s , which makes up the total payload of the train. The total emissions of the train on a specific edge are equally distributed over all cargo units in $m^{payload}$.

Kirschstein and Meisel (2015) showed that also the average number of acceleration processes per kilometer n^{acc} and the average speed v have a high influence on transport related emissions. We therefore use two settings for these values: one for congested traffic

Table 2.6: Traffic conditions for road and rail transportation.

	road		rail	
	congested	free-flowing	congested	free-flowing
average speed v [km/h]	40	80	70	80
average accelerations n^{acc} [per km]	2.5	0.12	0.1	0.01

conditions and one for free-flowing traffic conditions, see Table 2.6. The parameter values for road transportation are based on real-world European driving cycles of high powered cars (André et al.; 2006). For rail transportation, the average speed is based on real-world driving cycles of freight trains in Denmark (Lindgreen and Sorenson; 2005b). The average number of acceleration processes is set to 1 per 100 km for free-flowing traffic conditions and to 1 per 10 km for congested traffic conditions. Note that the average travel speed for rail transportation is rather high for congested traffic conditions. This reflects the freight trains' stop-and-go behavior, which is characterized by an acceleration to full speed between the stops.

For the well-to-wheel emission coefficient k for electric trains on edges \mathcal{E}^{rail} that belong to country $c_i \in \mathcal{C}$, we use the energy mix of this particular country as reported in Moro and Lonza (2018), see Table 2.1. Finally, if ferry transportation is part of the routing, we use an emission rate of 51.35 gCO₂e/ton-km for this leg, see DEFRA (2017).

Having discussed the generation and routing of shipments, as well as the emission model parameters, we can now identify the number of shipments that needs to be simulated for a country pair (c_1, c_2) to obtain a valid estimate of the average emission rate. We derive this number from an analysis of the convergence index (Jung et al.; 2004). The convergence index compares the deviation between the average rate observed after $n \in [1, 2, \dots, N]$ simulated shipments with the average rate observed after simulating a total of N shipments. For this purpose, we simulate $N = 2000$ heavy goods shipments for country pairs (POL, PRT) and (FRA, FRA) . For the first country pair, we expect similar routings for major parts of the journey and thus low variations in the rates. For the second country pair, we expect a high share of pre- and post carriages of variable length and thus higher variations in the rates. Figure 2.5 illustrates the observed convergence of emission rates. The rates are higher for road only transportation than for intermodal transportation but converge in both cases quickly to the final rate observed after $N = 2000$ simulated shipments. For example, the intermodal emission rates for shipments within France are 20.06 gCO₂e/ton-km after simulating 500 shipments and 20.13 gCO₂e/ton-km after simulating 2000 shipments. For shipments between Poland

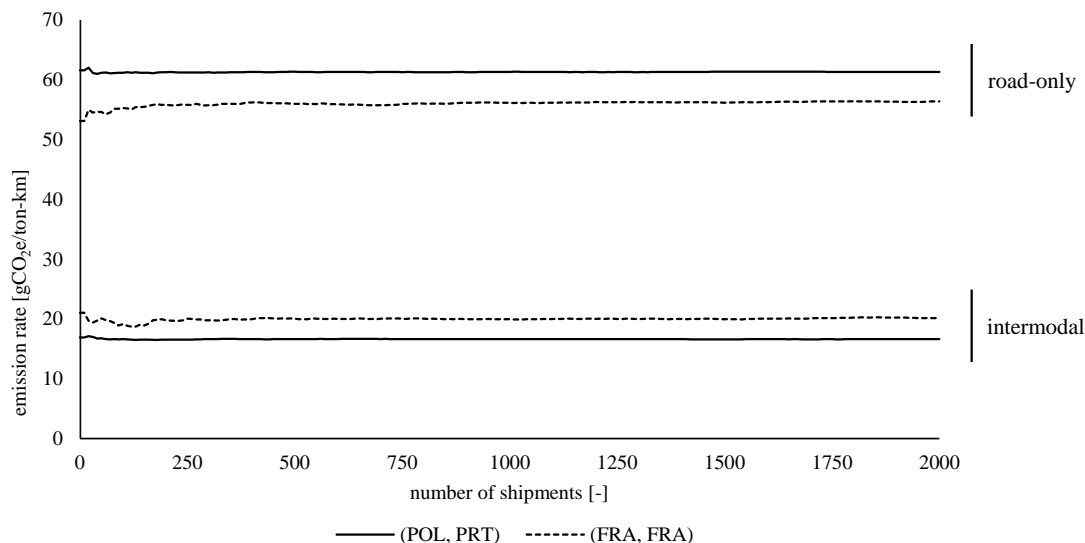


Figure 2.5: Convergence of emission rates for country pairs (POL, PRT) and (FRA, FRA).

and Portugal the rate is 16.64 gCO₂e/ton-km after 500 shipments and 16.62 gCO₂e/ton-km after 2000 shipments. From this analysis, we deduct that 500 shipments produce valid average emission rates and, therefore, we simulate $|\mathcal{S}_{c_1, c_2}| = 500$ shipments for each country pair (c_1, c_2) .

2.4.3 Definition of Simulation Configurations

We conduct our simulation study to calculate average emission rates for various relevant transport situations. We consider varied parameters for shipments (cargo type, size), varied parameters for the emission model (traffic conditions, gradient calculation) and miscellaneous settings of additional parameters (train utilization rates, empty return trips, a green power scenario and emissions from transshipment operations). Table 2.7 provides an overview of all simulation settings. The default setting, configuration I, estimates emission rates with random shipment sizes between 6 and 24 transport units (TU), free-flowing traffic conditions, a value of $\alpha = 0.5$ for computing the adjusted gradient, a train utilization rate of 67%, no empty return trips, the country specific electric power mixes, the current degree of rail line electrification and no emissions from transshipment operations. Since we expect that the cargo weight has a major impact on the emission rates, we differentiate the cargo type in this configuration and all following configurations between heavy and voluminous goods.

In configuration II, we estimate emission rates with the assumption that all ship-

Table 2.7: Configurations of simulation parameters.

	configuration							
	I	II	III	IV	V	VI	VII	VIII
shipment								
cargo type* [-]	h/v	h/v	h/v	h/v	h/v	h/v	h/v	h/v
shipment size t_s [TU]	[6-24]	[7,15,24]	[6-24]	[6-24]	[6-24]	[6-24]	[6-24]	[6-24]
emission model								
congested traffic [%]	0	0	50	0	0	0	0	0
negative slopes α [-]	0.5	0.5	0.5	[0-1]	0.5	0.5	0.5	0.5
miscellaneous								
train utilization [%]	67	67	67	67	[50,78]	67	67	67
empty return trips [-]	no	no	no	no	no	yes	no	no
power mix & electrification [-]	as is	as is	as is	as is	as is	as is	green	as is
transshipment [kgCO ₂ e/TU]	0	0	0	0	0	0	0	[1-25]

* h: heavy, v: voluminous

ments have an identical size c_s of either 7 or 15 or 24 transport units. Configuration III analyses a setting where 50% of the distance in \mathcal{G}^{road} and in \mathcal{G}^{rail} is traveled under congested traffic conditions. Configuration IV looks at the impact of varying values for the parameter α , which determines the consideration of negative slopes in the calculation of the adjusted gradient i^α . Configuration V elaborates the impact of a train utilization rate of 50% and 78%, instead of the default 67%. Configuration VI includes empty vehicle trips in \mathcal{G}^{road} and \mathcal{G}^{rail} for the estimation of emissions from shipment s . With configuration VII we simulate the hypothetical case of a fully electrified rail network in Europe that is powered completely with ‘clean’ electricity. For this purpose, we apply the emission coefficient k from Sweden, which is the lowest k among all the EU member states, to the whole rail network. Finally, with configuration VIII, we consider emissions from transshipment processes in \mathcal{G}^{trans} as it is a relevant issue in green intermodal transportation (Dekker et al.; 2012; Marchant and Baker; 2012). Here, the amount of emitted greenhouse gases reflects the total energy demand of the terminal operations, such as crane liftings, warehousing or administrative actions, that is then allocated to single terminal tasks, see Clausen et al. (2013), Geerlings and Van Duin (2011) and Miodrag et al. (2016). In the study from Geerlings and Van Duin (2011), the authors estimate values of 14 and 23 kgCO₂ per container for two sea-rail transshipment terminals in the Port of Rotterdam and elaborate that terminal layout is important for an accurate estimation. An estimation of transshipment emissions for a 40-foot container in Clausen et al. (2013) yields 6 kgCO₂e for a transshipment from sea to land and 12 kgCO₂e for a transshipment between rail and road. Since rail-road freight terminals can differ substantially in their layout, see Ballis and Golias (2002), we simulate in configuration VIII values between 1 and 25 kgCO₂e per transport unit and per rail/road transshipment operation. With 27

countries considered in our study, 500 shipments per country pair, and a differentiation between heavy and voluminous goods, we simulate a total of 729,000 shipments for each of the eight configurations.

2.5 Results

Our results comprise estimated well-to-wheel emission rates in $\text{gCO}_2\text{e}/\text{ton-km}$ for 729 country pairs. Emission rates reported for a country pair (c_1, c_2) are averages over the shipments $s \in \mathcal{S}_{c_1, c_2}$. For the notation of the country pairs we use the country codes as reported in Table 2.1. We discuss in the following the results of selected country pairs only and refer to the Appendix A for a complete overview of all obtained results. A comprehensive summary of the results is shown in Table 2.8. Details of the results for configuration I and II are described in Section 2.5.1. Section 2.5.2 provides insights into the mesoscopic emission estimation model, including results from configurations III and IV. Finally, Section 2.5.3 presents results from configurations V, VI, VII and VIII.

2.5.1 General Findings

In this section, we look at the spread of emission rates for the 729 country pairs under configuration I. We analyze emission rates from heavy and voluminous goods and we compare rates from road-only routing with rates from intermodal routing. Furthermore, we analyze the impact of the shipment size using configuration II.

A comparison of the emission rates across all country pairs shows that there is a wide spread of emission rates. Figure 2.6 shows the relative frequency of emission rates from heavy shipments (Figure 2.6a) and voluminous shipments (Figure 2.6b) over all 729 country pairs. In general, intermodal routing (black bars) leads to lower average rates than road-only routing (grey bars), which confirms the advantage of rail transportation with respect to eco-friendliness. This finding is in line with other studies like those in

Table 2.8: Aggregated results for simulation configurations I to VIII.

conf.	emission rates for heavy goods [$\text{gCO}_2\text{e}/\text{ton-km}$]				emission rates for voluminous goods [$\text{gCO}_2\text{e}/\text{ton-km}$]			
	road (RO)	intermodal (IM)	rail section	<i>IM-share</i> *	road (RO)	intermodal (IM)	rail section	<i>IM-share</i> *
I	56.8	23.8	18.1	92.7	86.7	29.2	19.4	94.9
II	[55.5-60.7]	[23.1-24.9]	[17.6-18.7]	[92.7-93.1]	[84.3-93.6]	[28.9-30.2]	[19.3-19.4]	[94.8-95.3]
III	64.8	25.7	19.0	93.5	95.6	31.2	20.2	95.2
IV	[48.8-64.9]	[17.7-30.0]	[12.5-23.8]	[89.6-94.6]	[75.9-97.4]	[22.5-36.0]	[13.5-25.3]	[93.8-95.7]
V	56.8	[23.6-24.3]	[17.9-18.7]	[92.3-92.8]	86.7	[28.8-30.1]	[19.0-20.4]	[94.7-95.0]
VI	92.6	32.3	21.9	94.7	152.2	44.7	26.4	95.7
VII	56.8	10.1	2.2	96.9	86.7	14.5	2.3	97.0
VIII	56.8	[23.8-26.6]	18.1	[89.1-92.7]	86.7	[29.2-34.4]	19.4	[91.7-94.9]

* intermodal share (*IM-share*) in %, see Section 2.5.1

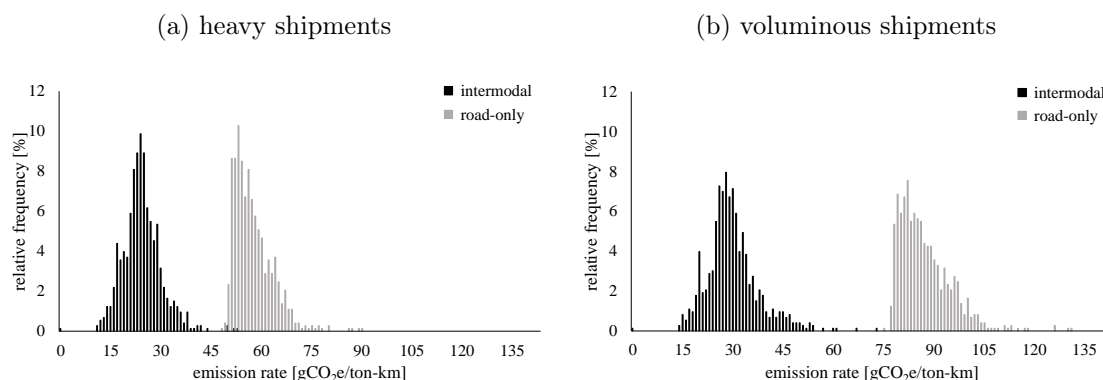


Figure 2.6: Relative frequency of emission rates.

Table 2.2. From our extensive simulation, we observe that emission rates from IM routings are on average 58% below rates from RO routings for heavy goods. For voluminous goods this measure is 66%. Emission rates for IM routings of both heavy and voluminous goods are mostly within a range of 15 to 45 gCO₂e/ton-km. For RO routings, emissions for heavy goods are mostly between 50 to 70 gCO₂e/ton-km and for voluminous goods between 80 to 100 gCO₂e/ton-km. The distribution of RO emissions is positively skewed at rates of about 50 for heavy shipments and about 80 gCO₂e/ton-km for voluminous shipments, see Figure 2.6. This is because the gradient of a route is a major driver of RO emissions, where all country pairs with negligible altitude differences get close to these lower bounds. In contrast, for IM shipments, many more relevant drivers exist (traction type, power mix, etc.) which affects a more symmetric distribution of emission rates.

Figure 2.7 shows the average and extreme emission rates from RO and IM routings of heavy goods under configuration I. The analysis shows that the extreme values for RO routing result from geographical characteristics, such as mountains. Routes with high emission rates pass the Alps, the highest mountain range in Europe, and routes with low emission rates typically involve flat terrain, as is found in Denmark, the Netherlands, Belgium, etc.. In contrast, extreme values from IM routing result from the characteristics of a country's rail system, such as the share of electrification or the used power mix. High emissions are found for Greece, where just about half of the rail lines are electrified in combination with an unfavorable emission coefficient (see Table 2.1) that results from using lignite (brown coal) as a major source of energy (Public Power Corporation S.A.; 2016). Low emissions are found for routes where substantial parts of the rail transportation goes through France, such as (*PRT, LUX*) or (*ESP, BEL*), as most of the rail network is electrified in combination with a low CO₂e-emission coefficient (see Table 2.1) that results from using nuclear power as a major source of energy (Réseau de

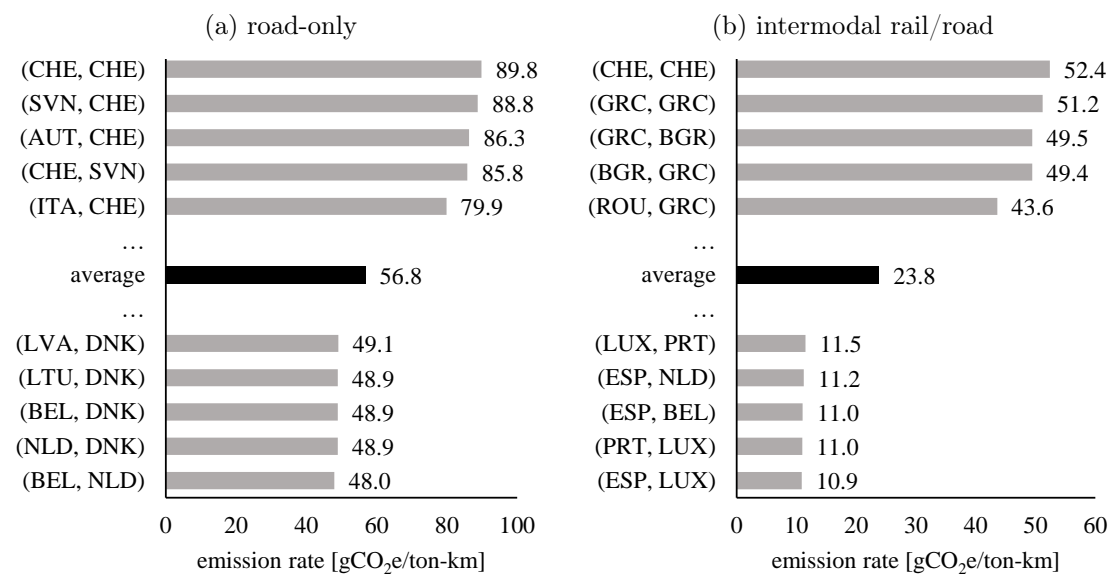


Figure 2.7: Top 5 and bottom 5 emission rates for RO and IM heavy shipments.

Transport d'Électricité; 2017). The spread of emission rates for heavy RO transportation is between 48.0 and 89.8 gCO₂e/ton-km with an average of 56.8 gCO₂e/ton-km. For heavy IM transportation, the spread is between 10.9 and 52.4 gCO₂e/ton-km with an average of 23.8 gCO₂e/ton-km. These observations indicate that the use of a single average emission rate for a large area like Europe can lead to large errors in the estimation of emissions for a particular transport relation or a particular shipment.

The emission rates from shipments with voluminous goods are higher than the emission rates from shipments with heavy goods, see Table 2.8. For example, the average rate over all country pairs from RO routing is 56.8 gCO₂e/ton-km for heavy goods and 86.7 gCO₂e/ton-km for voluminous goods. For IM routing, the rate is 23.8 gCO₂e/ton-km for heavy goods and 29.2 gCO₂e/ton-km for voluminous goods. This finding shows that emission rates from road-only and intermodal routing are both sensitive to additional weight. This motivates presenting separate emission rates for heavy goods and for voluminous goods in all considered simulation configurations. We furthermore observe that the direction of a route can have an impact, i.e. that the results for country pair (c_1, c_2) and country pair (c_2, c_1) are not necessarily identical. However, such differences primarily exist for countries with significantly different average altitudes. For example, emission rates of shipments originating in Switzerland are usually lower than emission rates for shipments that go to Switzerland. This is hardly surprising as Switzerland is the country in Europe with the highest average elevation above sea level.

The comparison of emission rates per ton-km might lead to the conclusion that the intermodal routing of a shipment causes a lower amount of greenhouse gases than a road-only routing. However, this is too short sighted as the actual amount of emissions caused by a shipment also depends on the transport distances in the road and the rail mode, which can differ substantially in the RO and the IM routing. For the further analysis, we define the intermodal-share *IM-share* as the rate of those shipments where the intermodal route emits a lower amount of greenhouse gases than the road-only route. The average *IM-share* over all country pairs is 93% for heavy goods and 95% for voluminous goods. Around 80% of all country pairs have an *IM-share* of 90% or higher. These high values are because many shipments can use the rail mode for a substantial part of their routing. Likewise, short RO distances and high shares of pre- and post-carriages by truck characterize country pairs with low *IM-shares*. Examples are country pairs that include Finland, Norway or Sweden because the sparse rail network in these countries requires substantial pre- or post-carriages by truck. The *IM-share* is also low for country pairs with low electrification of the rail network or with high emission coefficients. For example, the *IM-share* for (*GRC, BGR*) is 48% for shipments with heavy goods and 79% for shipments with voluminous goods. This is because only half of the rail lines in Greece are electrified and both countries Greece and Bulgaria have a power mix with high emission coefficients, see Table 2.1.

The size t_s of a shipment s influences the number of trucks required, respectively the number of rail cars in the IM routing. Figure 2.8 shows the average rates across all country pairs for shipments with random sizes (configuration I) and fixed sizes of 7 or 15 or 24 transport units (configuration II). The results show that the shipment size has only a small impact on the observed emission rates in RO routings. Since we consider quite large shipments of multiple transport units in all experiments, road-only emissions do not differ between even numbers of transport units and the only variance results from shipments with an uneven number of transport units. In this case, the relative impact of the emissions of the single half-filled truck depreciates with larger shipment size and the average emission rates tend towards the emission rates with even numbers of transport units. The impact of the shipment size is even lower in IM routings. The marginal emissions of an additional transport unit are very low, which is because of the high tare weight of trains and their substantial base utilization of 67%.

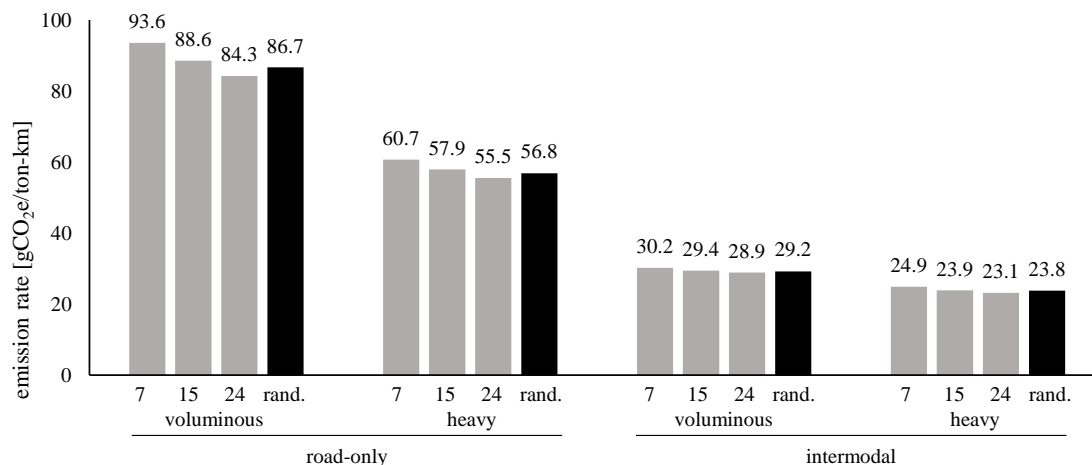


Figure 2.8: Emission rates from fixed shipment sizes (grey bars) and random sizes (black bars).

2.5.2 Emission Model Analysis

In this section, we look at the gradient of a route and the traffic conditions, which are two of the drivers of energy demand in the mesoscopic emission model. To further facilitate the understanding of transport related emissions, we analyze the composition of the total energy demand W . According to Kirschstein and Meisel (2015), W composes of energy to overcome air resistance, energy to overcome rolling resistance, energy to overcome grade and energy to perform accelerations, following the same physical laws for trucks and trains.

Figure 2.9 shows the relative contribution of each of these parts to the total energy demand over all heavy goods shipments in configurations I and III. We see that the energy to overcome air resistance and rolling resistance accounts for more than 50% of the total energy demand, be it for trucks or for trains.

We observe that congested traffic has a stronger impact in RO routing than in IM routing, which is because the power to perform accelerations is more relevant in the road mode. The emission rates across all countries increase for RO routing by 14% (heavy) and by 10% (voluminous) and for IM routing by 8% (heavy) and by 7% (voluminous) when comparing free-flowing traffic and congested traffic, see Table 2.8. The impact of congested traffic conditions on the *IM-share* is 0.9% (heavy) and 0.3% (voluminous). We thus conclude that traffic conditions are important in estimating the height of emissions for a specific transport relation but they hardly determine which routing (RO or IM) is more eco-friendly.

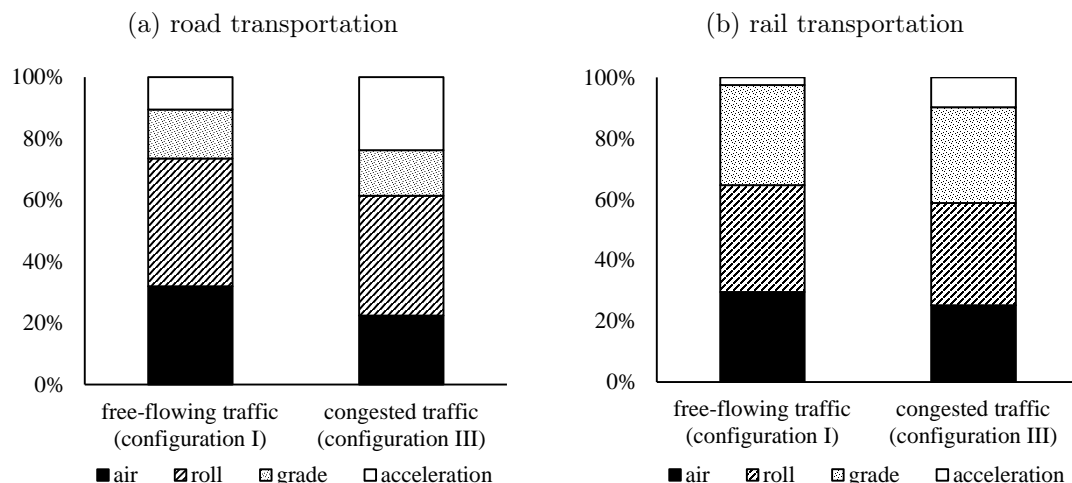


Figure 2.9: Composition of the energy demand of heavy shipments.

With configuration IV, we look at the influence of considering energy from negative slopes through the average adjusted gradient i^α . For $\alpha = 0$, the adjusted gradient considers no energy from negative slopes at all. For $\alpha = 1$, where all energy from negative slopes is recovered, i^α reflects the simple origin-destination altitude difference and is identical to gradient i . For these extreme values, the average emission rate for heavy shipments over all country pairs is 17.7 ($\alpha = 1$) and 30.0 ($\alpha = 0$) for IM routings whereas it is 48.8 ($\alpha = 1$) and 64.9 ($\alpha = 0$) for RO routings. This supports the observation from Figure 2.9 where the relative energy demand to overcome grade is higher for rail transportation than for road transportation. Clearly, these results vary among country pairs. Figure 2.10 shows individual rates for six exemplary country pairs where shipments originate in the Netherlands with values of α being set to 0, 0.2, \dots 1. All country pairs have a similar emission rate for the case $\alpha = 1$, although their geographical characteristics are quite different. Shipments to Denmark, Estonia and Poland do not pass significant elevations, while shipments to Portugal, Bulgaria and Italy have to go through mountain ranges. Emission rates that are calculated with $\alpha = 1$ do not reflect these differences, whereas for lower values of α we see a clear spread in the emission rates that reflects these geographical characteristics. We thus conclude that the adjusted gradient i^α can better capture the characteristics of the diverse transport relations.

2.5.3 Further Configurations

This section looks at the impact of varying train utilization (configuration V), empty returns trips (configuration VI), a fully electrified railway network (configuration VII) and

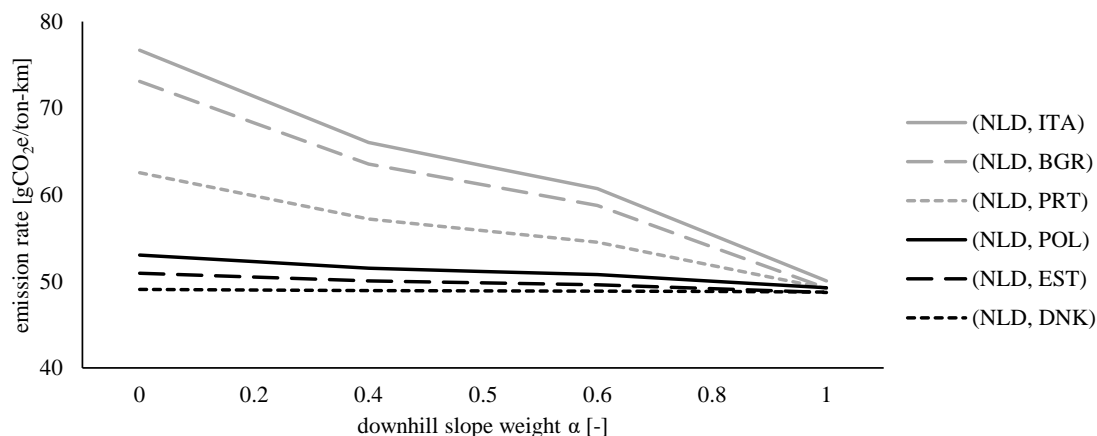


Figure 2.10: Exemplary emission rates of heavy goods from configuration IV.

emissions from transshipment operations (configuration VIII). For these configurations, we focus on discussing the aggregated results from Table 2.8. While configuration I assumes a train utilization rate of 67%, configuration V addresses utilization rates of 50% and 78%. We observe that a higher train utilization rate, expressed through a larger number of transport units and rail cars for the basic load, causes less marginal greenhouse gases from shipment load l_s and thus reduces the emission rate of shipment s . Likewise, a lower train utilization rate allocates more greenhouse gases to s . However, the absolute change is very low such that the average rate for heavy goods in IM routings varies between 23.6 for a train utilization of 78% and 24.3 gCO₂e/ton-km for a utilization of 50%. For voluminous goods the rate varies between 28.8 and 30.1 gCO₂e/ton-km. Since there is hardly any impact on the IM emission rate, there is also hardly any change on the *IM-share*.

The European Norm DIN EN 16258 (2012) states that emissions from transportation should also include vehicle operations from empty trips. Our results so far completely ignored empty trips. With configuration VI, we now consider this and assume empty vehicle return trips for all shipments. For this, we consider for a shipment s a corresponding shipment s' with $o_{s'} = d_s$ and $d_{s'} = o_s$ and load $l_{s'} = 0$. The IM routing for the return trip s' of shipment s is then d_s to h_s^d via road, h_s^d to h_s^o via rail and h_s^o to o_s via road. As expected, the consideration of empty return trips leads to a strong increase in the average emission rates of the freight shipments. The rate across all country pairs increases for RO routing by 63% (heavy) and by 75% (voluminous) and for IM routing by 36% (heavy) and by 53% (voluminous), respectively. Despite of this, we only observe a small increase in the *IM-share* by 2.0% (heavy) and 0.8% (voluminous), see Table 2.8.

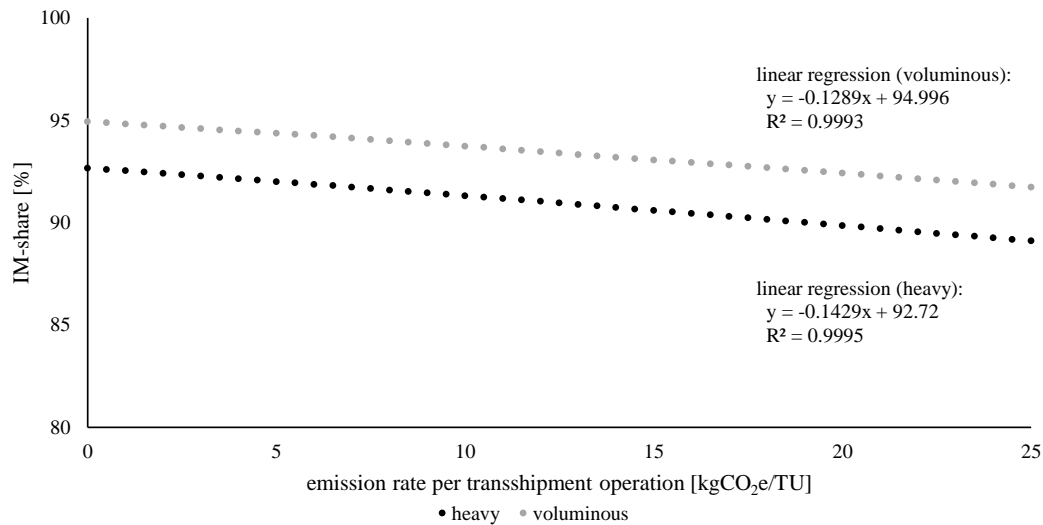


Figure 2.11: *IM-share* depending on the emission rate per transshipment operation.

With configuration VII, we analyze the scenario of a fully electrified railway network. Furthermore, we apply a low emission coefficient of $k = 45$ gCO₂e/kWh to the whole network. This coefficient stems from Sweden, which is the EU member state with the lowest k . As expected, the emission rates from freight transportation on rail sections decrease for nearly all country pairs with an average reduction of around 88%, see Table 2.8. This also leads to increasing *IM-shares*. Since the majority of country pairs already have high *IM-shares* in the base setting (configuration I) we see an increase of this measure of merely 4.2% for heavy goods and 2.1% for voluminous goods in configuration VII. Still, for some country pairs, we observe a much stronger impact of the green and fully electrified rail system. This is the case for countries that currently have high electric emission coefficients, like Latvia, Poland or Estonia. With a total of 438 billion ton-km of rail freight transport in the EU in 2016 (Eurostat; 2018c) and an average reduction of rail emission by 88% in a completely green rail network, the total amount of anthropogenic CO₂e emissions could be reduced by approximately 7.25 million tons.

Finally, in configuration VIII, we consider emissions released during transshipment processes in the intermodal routing. Each of these routings includes two transshipment operations (one from road to rail and one from rail to road) where we assume an identical emission rate per transshipment operation. We varied this rate in the range 1 to 25 kgCO₂e per transshipped transport unit. Figure 2.11 shows the average *IM-share* across all countries depending on the emission rate per transshipment operation. Surprisingly,

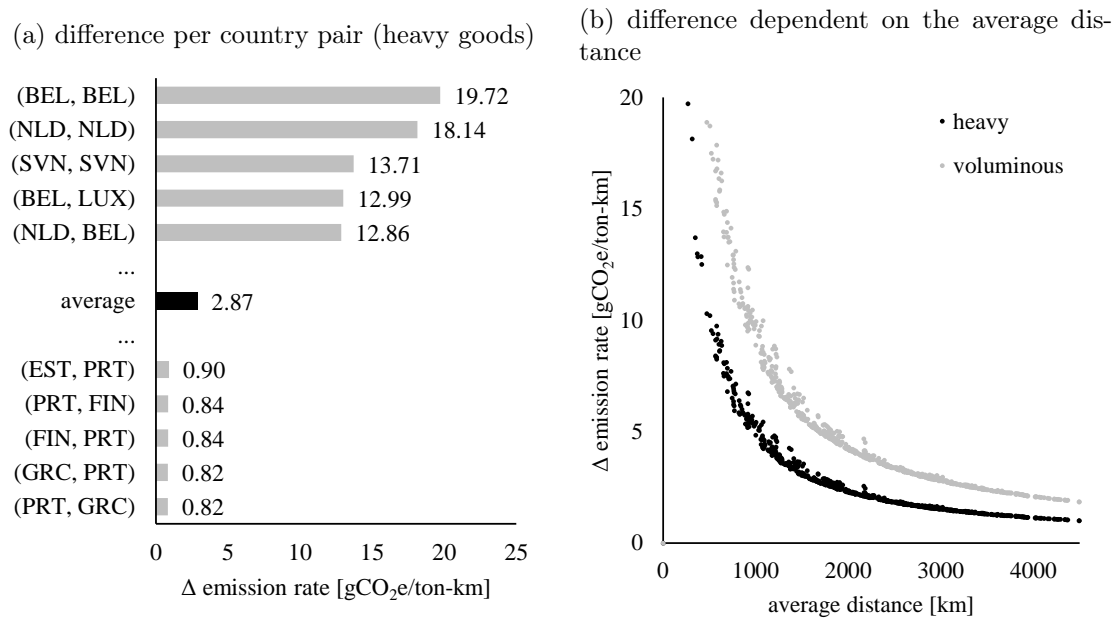


Figure 2.12: Change of IM emissions rates for transshipment emissions of 25 kgCO₂e/TU.

we only observe a very small and constant decrease of about 0.1% per kgCO₂e added to the transshipment emission rate. However, we observe that the impact on the intermodal emission rates can be high for some country pairs. Here, the distance between shipments is the most important driver. This is because the emissions from transshipments are a fixed amount per shipment, which leads to a depreciation of these emissions with increasing distance. Figure 2.12 illustrates this relationship for a very high emission rate per transshipped TU of 25 kgCO₂e. It reports the increase in the intermodal emission rate per ton-km (Δ emission rate), when we compare configuration VIII with configuration I, i.e. if emissions from transshipments are added to the consideration. The five countries with the highest/lowest change in the emission rate per ton-km are shown in Figure 2.12a and the relationship between the change of the emission rate per ton-km and the distance between country pairs is shown in Figure 2.12b. Country pairs with low average distances, like (*BEL, BEL*) or (*NLD, NLD*), show the highest increase and country pairs with high average distances, like (*FIN, PRT*) or (*PRT, GRC*), show the lowest increase. The change in the emission rate is below 4 gCO₂e/ton-km for around 80% of all country pairs for heavy goods. For voluminous goods it is below 7 gCO₂e/ton-km for around 80% of all country pairs. Overall, we conclude that emissions from transshipment processes are relevant in estimating the height of emissions for a specific transport relation and in estimating the *IM-share*, especially for transport relations with low average distances,

whereas we see hardly any impact for transport relations with high average distances.

2.6 Conclusion

In this paper, we have calculated emission rates of intermodal rail/road and road-only transportation of large cargo shipments in Europe. We have described the intermodal rail/road network, the various data sources and the results from a comprehensive simulation study. We found that the average emission rate across all country pairs from road-only routing is 57 gCO₂e/ton-km for heavy goods and 87 gCO₂e/ton-km for voluminous goods. For intermodal routing, we determined rates of 24 gCO₂e/ton-km for heavy goods and 29 gCO₂e/ton-km for voluminous goods. However, there are high variations. Rates for road transportation range from 48 to 131 gCO₂e/ton-km over the considered 729 country pairs. Rates for intermodal transportation range from 11 to 72 gCO₂e/ton-km. The highest emission rates are observed for transports that go through the Alps. Furthermore, we found that intermodal routings emit less greenhouse gases than road-only routings for over 90% of the simulated shipments. Again, this value varies among country pairs and is significantly lower for countries with many non-electrified rail tracks and high emission coefficients for their electricity. In our study, we have identified emission factors that quantify the value of road-only and intermodal emission rates and thus determine which routing is more eco-friendly. Some of these factors are of geographical or physical nature, such as gradient of the route or vehicle size, and thus rather hard or even impossible to change by decision makers from industry. Other factors, like average speed or the share of electrified rail lines, are set by transport operators or public authorities and thus could be addressed by policies that target a reduction of greenhouse gases from freight transportation.

Overall, our results indicate that the use of a single average emission rate for a large area like Europe can lead to substantial errors in the estimation of emissions for individual shipments or particular transport relations. The appendix of this study therefore provides look-up tables for all country pairs and shows the respective emission rates from road, rail and intermodal rail/road transportation as well as the *IM-share* for all considered scenarios. Future research should put a scope on smaller shipments and the impact of freight consolidation. It is also of interest to identify realistic values for the gradient parameter α and to validate our emission estimates through real-work experiment. Finally, we see the in-depth consideration of emissions from transshipment processes as another field of research for gaining deeper insights into the drivers of eco-friendly freight transportation.

Acknowledgments

This research was supported by the German Research Foundation (DFG) under reference 268276815. We thank two anonymous reviewers for their valuable comments which helped to improve the manuscript considerably.

2.7 Appendix A. Supplementary data

Supplementary data associated with this article can be found in the online version of this article and on the website of our department (<https://www.scm.bwl.uni-kiel.de/de/forschung/research-data>).

Bibliography

- André, M., Joumard, R., Vidon, R., Tassel, P. and Perret, P. (2006). Real-world european driving cycles, for measuring pollutant emissions from high-and low-powered cars, *Atmospheric Environment* **40**(31): 5944–5953.
- Ballis, A. and Golias, J. (2002). Comparative evaluation of existing and innovative rail-road freight transport terminals, *Transportation Research Part A: Policy and Practice* **36**(7): 593–611.
- Bauer, J., Bektaş, T. and Crainic, T. G. (2010). Minimizing greenhouse gas emissions in intermodal freight transport: an application to rail service design, *Journal of the Operational Research Society* **61**(3): 530–542.
- Behnke, M. and Kirschstein, T. (2017). The impact of path selection on GHG emissions in city logistics, *Transportation Research Part E: Logistics and Transportation Review* **106**: 320–336.
- Bektaş, T. and Laporte, G. (2011). The pollution-routing problem, *Transportation Research Part B: Methodological* **45**(8): 1232–1250.
- BluFerries (2018). BluFerries: Gruppo Ferrovie Dello Stato Italiane. <http://www.bluferries.it/laflootta.html> (visited on 25.07.2018).
- Clausen, U., Kaffka, J., Döring, L. and Ebel, G. (2013). Container based calculation of greenhouse gas emissions - A method to determine emissions of container handlings in container terminals, *General Proceedings of the 13th World Conference on Transport Research (WCTR)*.
- Comer, B., Corbett, J. J., Hawker, J. S., Korfmacher, K., Lee, E. E., Prokop, C. and Winebrake, J. J. (2010). Marine vessels as substitutes for heavy-duty trucks in great lakes freight transportation, *Journal of the Air & Waste Management Association* **60**(7): 884–890.
- Craig, A. J., Blanco, E. E. and Sheffi, Y. (2013). Estimating the CO₂ intensity of intermodal freight transportation, *Transportation Research Part D: Transport and Environment* **22**: 49–53.
- de Miranda Pinto, J. T., Mistage, O., Bilotta, P. and Helmers, E. (2017). Road-rail intermodal freight transport as a strategy for climate change mitigation, *Environmental Development* **25**: 100–110.

- DEFRA (2017). Department for Environment, Food and Rural Affairs. Greenhouse Gas Reporting: Conversion Factors 2017. <https://www.gov.uk/government/publications/greenhouse-gas-reporting-conversion-factors-2017> (visited on 25.07.2018).
- Dekker, R., Bloemhof, J. and Mallidis, I. (2012). Operations Research for green logistics - An overview of aspects, issues, contributions and challenges, *European Journal of Operational Research* **219**(3): 671–679.
- DeLuchi, M. A. (1991). Emissions of greenhouse gases from the use of transportation fuels and electricity, *Technical report*, Argonne National Lab.
- Demir, E., Bektaş, T. and Laporte, G. (2011). A comparative analysis of several vehicle emission models for road freight transportation, *Transportation Research Part D: Transport and Environment* **16**(5): 347–357.
- DIN EN 16258 (2012). *Methodology for calculation and declaration of energy consumption and GHG emissions of transport services (freight and passengers)*, European Committee for Standardization.
- EcoTransIT World Initiative (2016). EcoTransIT: Ecological Transport Information Tool for Worldwide Transports, Methodology and Data (30.06.2016). . http://www.ecotransit.org/download/ETW_Methodology_Background_Report_2016.pdf (visited on 25.07.2018).
- Ehmke, J. F., Campbell, A. M. and Thomas, B. W. (2016). Data-driven approaches for emissions-minimized paths in urban areas, *Computers & Operations Research* **67**: 34–47.
- European Commission (2015). State aid: Commission approves public financing of Fehmarn Belt fixed rail-road link. http://europa.eu/rapid/press-release_IP-15-5433_en.htm (visited on 25.07.2018).
- European Commission (2018). About TEN-T. <http://ec.europa.eu/transport/infrastructure/tentec/tentec-portal/site/en/abouttent.htm> (visited on 25.07.2018).
- European Parliament (2017). Parliamentary Questions: Tallinn-Helsinki tunnel. <http://www.europarl.europa.eu/sides/getDoc.do?type=WQ&reference=E-2017-004271&language=EN> (visited on 25.07.2018).
- European Parliament and Council (2013). Regulation (EU) No 1315/2013 of the European Parliament and the Council of 11 December 2013 on Union guidelines for

- the development of the trans-European transport network and repealing Decision No 661/2010/EU. <http://data.europa.eu/eli/reg/2013/1315/oj> (visited on 25.07.2018).
- Eurostat (2018a). Freight transport statistics - modal split. http://ec.europa.eu/eurostat/statistics-explained/index.php/Freight_transport_statistics_-_modal_split (visited on 25.07.2018).
- Eurostat (2018b). Greenhouse gas emissions by source sector. http://ec.europa.eu/eurostat/statistics-explained/index.php?title=Greenhouse_gas_emission_statistics (visited on 25.07.2018).
- Eurostat (2018c). Railway freight transport statistics. http://ec.europa.eu/eurostat/statistics-explained/index.php?title=Railway_freight_transport_statistics (visited on 25.07.2018).
- Geerlings, H. and Van Duin, R. (2011). A new method for assessing CO₂-emissions from container terminals: a promising approach applied in Rotterdam, *Journal of Cleaner Production* **19**(6-7): 657–666.
- Geofabrik (2018). OpenStreetMap Data Extracts. <http://download.geofabrik.de/> (visited on 25.07.2018).
- Hawker, J. S., Comer, B., Corbett, J. J., Ghosh, A., Korfmacher, K., Lee, E. E., Li, B., Prokop, C. and Winebrake, J. J. (2010). An integrated model to study environmental, economic, and energy trade-offs in intermodal freight transportation. . 5th International Congress on Environmental Modelling and Software. Ottawa. Canada.
- Hickman, J., Hassel, D., Joumard, R., Samaras, Z. and Sorenson, S. (1999). Methodology for calculating transport emissions and energy consumption. . <https://trimis.ec.europa.eu/sites/default/files/project/documents/meet.pdf> (visited on 25.07.2018).
- Hoffrichter, A., Miller, A. R., Hillmansen, S. and Roberts, C. (2012). Well-to-wheel analysis for electric, diesel and hydrogen traction for railways, *Transportation Research Part D: Transport and Environment* **17**(1): 28–34.
- Jung, J. Y., Blau, G., Pekny, J. F., Reklaitis, G. V. and Eversdyk, D. (2004). A simulation based optimization approach to supply chain management under demand uncertainty, *Computers & chemical engineering* **28**(10): 2087–2106.

- Kirschstein, T. and Meisel, F. (2015). GHG-emission models for assessing the eco-friendliness of road and rail freight transports, *Transportation Research Part B: Methodological* **73**: 13–33.
- Lindgreen, E. B. G. and Sorenson, S. C. (2005a). Driving resistance from railroad trains, *Technical report*, Technical University of Denmark. Department of Mechanical Engineering.
- Lindgreen, E. B. G. and Sorenson, S. C. (2005b). Simulation of energy consumption and emissions from rail traffic, *Technical report*, Technical University of Denmark. Department of Mechanical Engineering.
- Luxen, D. and Vetter, C. (2011). Real-time routing with OpenStreetMap data, *Proceedings of the 19th ACM SIGSPATIAL International Conference on Advances in Geographic Information Systems*, GIS '11, ACM, New York, NY, USA, pp. 513–516.
- Marchant, C. and Baker, P. (2012). Reducing the environmental impact of warehousing, in A. McKinnon, M. Browne and A. Whiteing (eds), *Green logistics: Improving the environmental sustainability of logistics*, 2 edn, Kogan Page Limited London, chapter 8, pp. 175–202.
- McKinnon, A., Browne, M. and Whiteing, A. (2012). *Green logistics: Improving the environmental sustainability of logistics*, 2 edn, Kogan Page Publishers.
- Miodrag, Z., Kaffka, J., Clausen, U., Munsel, L. and Drost, S. (2016). Assessment of emissions caused by logistics handling operations in multimodal-terminals, *Transportation Research Procedia* **14**: 2754–2761.
- MMEEC (2018). Multi-Modal Energy and Emissions Calculator (MMEEC). Rochester Institute of Technology and University of Delaware. <http://clarke.main.ad.rit.edu/LECDM/EmissionsCalc/> (visited on 25.07.2018).
- Moro, A. and Lonza, L. (2018). Electricity carbon intensity in european member states: Impacts on ghg emissions of electric vehicles, *Transportation Research Part D: Transport and Environment* **64**: 5–14.
- NTM (2017a). Network For Transport Measures: Rail cargo transport baselines 2017. <https://www.transportmeasures.org/en/wiki/evaluation-transport-suppliers/rail-cargo-transport-baselines-2017/> (visited on 25.07.2018).

- NTM (2017b). Network For Transport Measures: Road cargo transport baselines 2017. <https://www.transportmeasures.org/en/wiki/evaluation-transport-suppliers/road-transport-baselines-2017/> (visited on 25.07.2018).
- Open Elevation (2018). Open Elevation: A free and open-source elevation API. <https://www.open-elevation.com> (visited on 25.07.2018).
- Open Street Map (2018). OpenStreetMap is the free wiki world map. <https://www.openstreetmap.org> (visited on 25.07.2018).
- Psaraftis, H. N. and Kontovas, C. A. (2016). Transportation Emissions: Some Basics, *Green Transportation Logistics*, Springer, pp. 41–79.
- Public Power Corporation S.A. (2016). Annual Report: January 1st, 2016 - December 31st, 2016. https://www.dei.gr/Documents2/ANNUAL%20REPORT/AR-2016/Annual_Report_2016_EN_WEB.pdf (visited on 25.07.2018).
- Raildar (2018). raildar.fr. <http://raildar.fr/osrm/osrm.html> (visited on 25.07.2018).
- Ross, M. (1997). Fuel efficiency and the physics of automobiles, *Contemporary Physics* **38**(6): 381–394.
- Rudi, A., Fröhling, M., Zimmer, K. and Schultmann, F. (2016). Freight transportation planning considering carbon emissions and in-transit holding costs: a capacitated multi-commodity network flow model, *EURO Journal on Transportation and Logistics* **5**(2): 123–160.
- Réseau de Transport d'Électricité (2017). RTE Open Data platform: Annual French electricity production (TWh) by branch (2017). https://opendata.rte-france.com/explore/dataset/prod_par_filiere/table/?sort=-annee&refine.annee=2017 (visited on 25.07.2018).
- Scora, G. and Barth, M. (n.d.). Comprehensive modal emissions model (CMEM), version 3.01 (Users guide). https://www.cert.ucr.edu/sites/g/files/rcwecm1251/files/2019-07/CMEM_User_Guide_v3.01d.pdf (visited on 19.11.2021).
- Southworth, F. and Peterson, B. E. (2000). Intermodal and international freight network modeling, *Transportation Research Part C: Emerging Technologies* **8**(1): 147–166.
- Stead, D. (1999). Relationships between transport emissions and travel patterns in Britain, *Transport Policy* **6**(4): 247 – 258.

- StenaLine (2018). StenaLineFreight / Routes and Ports / Trelleborg-Rostock. <http://www.stenalinefreight.com/Routes-and-ports/trelleborg-rostock> (visited on 25.07.2018).
- TEN-T Compliance Maps (2014). TEN-T Compliance Maps. TENtec Reporting. European Commission. https://ec.europa.eu/transport/themes/infrastructure/downloads_en (visited on 25.07.2018).
- TENtec Interactive Map (2018). TENtec Interactive Map Viewer. <http://ec.europa.eu/transport/infrastructure/tentec/tentec-portal/map/maps.html> (visited on 25.07.2018).
- Wang, M. Q. (1999). Greet 1.5-transportation fuel-cycle model-vol. 1: methodology, development, use, and results., *Technical report*, Argonne National Lab., IL (US).
- WebGIFT (2018). Online Application of the Geospatial Intermodal Freight Transportation (GIFT) model. Rochester Institute of Technology and University of Delaware. <http://clarke.main.ad.rit.edu/LECDM/Webgift/> (visited on 25.07.2018).
- Winebrake, J. J., Corbett, J. J., Falzarano, A., Hawker, J. S., Korfmacher, K., Ketha, S. and Zilora, S. (2008). Assessing energy, environmental, and economic tradeoffs in intermodal freight transportation, *Journal of the Air & Waste Management Association* **58**(8): 1004–1013.

Chapter 3

Emission-oriented vs. Time-oriented Routing in the European Intermodal Rail/Road Freight Transportation Network

Publication status Published in 2019: Bierwirth C., Kirschstein T., Sackmann D. (eds) Logistics Management (LM19). *Lecture Notes in Logistics*. Springer, Cham, pp. 188–202.

Arne Heinold and Frank Meisel

School of Economics and Business, Kiel University, Kiel, Germany

Abstract This study compares emissions and transit times from an environmentally oriented and a time oriented routing of large freight shipments in the European rail/road transportation network. We use the terminal-and-service selection problem (TSSP) to find the optimal routings under the different objectives. We show that substantial differences exist between the emission oriented routing and the time oriented routing. A large-scale simulation study reveals that shipments in the emission minimizing routing emit on average almost half as much emissions as if they were routed with the objective to minimize transit time. At the same time, the average transit time of shipments in the emission oriented routing almost triples compared to the transit time in the time optimal routing. This shows by experiment that substantial emission reductions can be achieved in the European freight transport sector by a corresponding routing of shipments but

that this comes at the cost of a much lower service quality.

Keywords Emission Rates, Transit Time, European Rail/Road Network, Intermodal Transportation, Mesoscopic Model

3.1 Introduction

Recent studies show that intermodal rail/road freight transportation is usually less harmful to the environment than unimodal road-only transportation, see for example de Miranda Pinto et al. (2018) or Heinold and Meisel (2018). However, using intermodal rail/road transportation also impacts performance measures like transit time or cost. Quantifying the trade-off between these measures is required in order to make informed transportation decisions, but literature provides little in this regard so far. In particular, there is a need for more analysis of large-scale transport systems. In this study, we compare results from an environmentally oriented routing and a time oriented routing within the rail corridors from the Trans-European Transport Network (TEN-T). Our results are based on fixed-sized shipments with random origins and destinations across continental Europe. For these orders, we design a terminal-and-service selection problem (TSSP) to find a desirable path through the considered rail/road network. In total, our network covers more than 11,400 rail services per week and connects more than 19 European countries. The results of our simulation show that there are substantial differences between the emission oriented and the time oriented routings. These differences can be observed for absolute measures of emissions and transit time as well as for distance adjusted rates per kilometer.

The paper is organized as follows. Section 3.2 briefly discusses relevant literature and Section 3.3 describes the considered problem. In Section 3.4, we present the mathematical notations, the optimization model and the used network data. Section 3.5 describes the results from our simulation experiments. Section 3.6 concludes this paper.

3.2 Literature review

In this section, we provide a short overview of selected studies that focus on long-distance road, rail and/or intermodal rail/road transportation with objectives that are either related to the environment and/or related to time. Due to this scope of our study, we do not discuss here related paper that address different transport settings, such as emission

Table 3.1: Selected relevant literature for this study.

references	type	size ^a	modes		objectives	
			road	rail	envir.	time
Figliozzi (2010)	EVRP	med.	✓	-	✓	✓
Bektaş and Laporte (2011)	PRP	small	✓	-	✓	✓
Bauer et al. (2010)	SND	small	✓	✓	✓	✓
Demir et al. (2016)	GISND-TTU	med.	✓	✓	✓	✓
Lam and Gu (2016)	INO	med.	✓	✓	-	✓
Winebrake et al. (2008)	SPP	small	✓	✓	✓	✓
Heinold and Meisel (2018)	SPP	large	✓	✓	✓	-
de Miranda Pinto et al. (2018)	SPP	small	✓	✓	✓	-
Kim and Van Wee (2014)	SPP	small	✓	✓	✓	-
this study	TSSP	large	✓	✓	✓	✓

^a instance size, such as number of nodes or number of rail services

minimization in urban transportation, see Ehmke et al. (2016). Table 3.1 shows an overview of those studies that we discuss in more detail.

Figliozzi (2010) formulates the emissions vehicle routing problem (EVRP) with time windows, capacity constraints and time-dependent travel times. The EVRP considers emissions either as part of a multi-objective function or as a secondary objective in a hierarchical approach. Bektaş and Laporte (2011) present the pollution routing problem (PRP), which is based on a vehicle routing problem with time windows for homogeneous trucks. The authors consider several objectives, such as minimizing distance, travel time or greenhouse gas emissions. The mentioned studies consider merely the road mode. For a detailed review of green vehicle routing problems we refer to Lin et al. (2014). Bauer et al. (2010) present a service network design (SND) formulation that considers greenhouse gas emissions as a primary objective with both modes, road and rail. The authors test their model on a small real-world network between Austria and Poland. Demir et al. (2016) also investigate a service network design problem and introduce the green intermodal service network design problem with travel time uncertainty (GISND-TTU). The authors apply their model on a small intermodal network, covering trains, trucks and inland vessels, and compare results for the objectives time and emissions. Lam and Gu (2016) present a bi-objective intermodal network optimization (INO) for hinterland transportation, including the road and the rail mode. The authors use cost and time as objectives and model governmental carbon emission restrictions per transport unit as additional constraints in their mathematical model. Winebrake et al. (2008) describe the

geospatial intermodal freight transport (GIFT) model, which allows a path evaluation for the dimensions time and emissions. The model is demonstrated as a shortest path problem (SPP) in three case studies in northern USA. A recent study of Heinold and Meisel (2018) uses a simulation approach to estimate emissions of the shortest path for road-only and intermodal rail/road transportation for 27 countries in Europe. The authors show that intermodal transportation is less harmful to the environment for more than 90% of the simulated orders. However, the selection of the used transshipment terminals at the origin area and at the destination area is solely based on distance, which might not be optimal if scheduled rail services have to be considered and transit time is to be minimized. Similarly, de Miranda Pinto et al. (2018) use the nearest train station in a shortest path based case study for the Brazilian paper and cellulose pulp sector. The authors show that intermodal transportation could reduce emissions by up to 77.4% compared to road-only transportation. Kim and Van Wee (2014) assess shortest paths with emissions in road-only, intermodal rail/road and intermodal vessel/road transports between Rotterdam and Gdansk. The authors use fix road-distances of at most 50 km for road transportation at each end of the intermodal transport chain. In contrast, the TSSP in our study considers multiple transshipment terminals for the orders and, thus, includes a terminal selection problem when searching for the time- and emission-minimizing routings of freight shipments all across Europe.

3.3 Problem description

The problem addressed in this study is to find optimal paths for orders with origins and destinations across Europe. For an individual order, the problem corresponds to a shortest path problem in a directed network with arc weights corresponding to transit times and/or emissions. Thereby multiple time-sensitive arcs can exist between two nodes as there might be multiple rail services offered between two terminals, see Figure 3.1. In the figure, the three arcs represent three scheduled rail services between the two Portuguese rail stations Entroncamento and Lisbon. The trains operate on different weekdays, depart and arrive at different times and emit different amounts of greenhouse gases. The latter is because transit time is closely related to speed, which is an important factor in estimating emissions from rail transportation.

Common shortest path algorithms, such as the algorithms of Dijkstra et al. (1959) or Floyd (1962), cannot be used to solve this kind of problem because they cannot deal with multiple time-dependent arcs between a pair of nodes. Instead, we model the problem addressed in this paper as a special case of a service network design problem, see Crainic

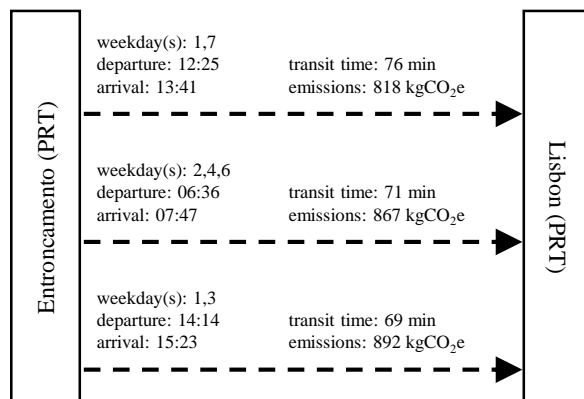


Figure 3.1: Representation of rail services as multiple time-sensitive arcs.

(2000). Here, we consider only one order at a time and assume enough capacity for this order for all services in the rail network. We name this modified service network design problem a terminal-and-service selection problem (TSSP). Clearly, the routing of an individual order could also be considered as a time-dependent shortest path problem. Anyhow, we model it here as a variant of the service network design problem because the TSSP can be extended towards multiple orders in future research easily. For the considered order, we measure emissions for the path that minimizes total transit time and measure the transit time for the path that minimizes total emissions. In other words, we solve the TSSP once under the objective to minimize transit time and once under the objective to minimize emissions but analyze in both cases also the secondary performance measure.

3.4 Methodology and data

3.4.1 Terminal-and-service selection problem (TSSP)

We search here for the path of a single freight shipment with origin o , destination d and departure time \bar{t} through a network with multiple time-sensitive arcs. We model this as a TSSP. For this, we define with \mathcal{N} the set of nodes in the network, which consist of transshipment terminals \mathcal{T} , the order's origin o and the order's destination d . Each node $i \in \mathcal{N}$ is associated with emissions e_i^{tship} that are caused by transshipping the order at this facility and time t_i^{tship} that is required for the transshipment of the considered order at node i . With \mathcal{S} we denote the set of services, which include road services and rail services. Here, for a service $s \in \mathcal{S}$, $o_s \in \mathcal{N}$ is the origin node, $d_s \in \mathcal{N}$ is the destination

Table 3.2: Sets, parameters and decision variables in the TSSP.

name	description
\mathcal{N}	set of nodes
\mathcal{T}	set of transshipment terminals
\mathcal{S}	set of services
o	origin of the order
d	destination of the order
\bar{t}	departure time of the order
o_s	origin of service $s \in \mathcal{S}$
d_s	destination of service $s \in \mathcal{S}$
e_s^{trans}	emissions caused by using service $s \in \mathcal{S}$ for shipping the order
t_s^{dep}	scheduled departure time of service $s \in \mathcal{S}$ at node o_s
t_s^{dur}	transit time of service $s \in \mathcal{S}$
suc_s	succeeding service ($suc_s \in \mathcal{S}$) of rail service $s \in \mathcal{S}$
e_i^{tship}	emissions caused by a transshipment process at node $i \in \mathcal{N}$
t_i^{tship}	required time for a transshipment process at node $i \in \mathcal{N}$
x_s	= 1 if service $s \in \mathcal{S}$ is used
y_s	= 1 if transshipment at the end of service $s \in \mathcal{S}$ (at node d_s) is required
t_i	ready-for-departure time at node $i \in \mathcal{N}$

node, e_s^{trans} are the emissions emitted from transporting the order from o_s to d_s using service s , t_s^{dep} is the scheduled departure time at node o_s , t_s^{dur} is the transit time and $suc_s \in \mathcal{S}$ the succeeding service of service s that is conducted by the particular vehicle that performs service s . We use suc_s to model trains with multiple stops, as each link between two stops is modeled as a service on its own. Transshipment processes between a service s and a subsequent service s' are only required if s' is not the succeeding service $suc_s \in \mathcal{S}$ of the same train, i.e. if $s' \neq suc_s$. Note that we set $t_s^{dep} = \bar{t}$ for all services $s \in \mathcal{S}$ where $o_s = o$, which means that the departure times of truck services that depart at origin o is set to the orders departure time. Binary decision variable x_s is equal to 1 if service $s \in \mathcal{S}$ is used in the routing and variable y_s is equal to 1 if a transshipment is required at node $d_s \in \mathcal{N}$. Decision variable t_i states the "ready-for-departure" time at node $i \in \mathcal{N}$, which is the arrival time of a service s at node $d_s = i$ plus the transshipment time t_i^{tship} if transshipment is required at node i . Table 3.2 provides an overview of sets, parameters and decision variables. The mathematical formulation of the mixed integer linear program is as follows.

$$\min t_d - \bar{t} \quad (3.1)$$

$$\min \sum_{s \in \mathcal{S}} (e_s^{trans} \cdot x_s) + \sum_{s \in \mathcal{S}: d_s \neq d} (e_{d_s}^{tship} \cdot y_s) \quad (3.2)$$

subject to

$$\sum_{s \in \mathcal{S}: o_s = o} x_s = \sum_{s \in \mathcal{S}: d_s = d} x_s = 1 \quad (3.3)$$

$$\sum_{s \in \mathcal{S}: o_s = d} x_s = \sum_{s \in \mathcal{S}: d_s = o} x_s = 0 \quad (3.4)$$

$$\sum_{s \in \mathcal{S}: o_s = i} x_s = \sum_{s \in \mathcal{S}: d_s = i} x_s \leq 1, \forall i \in \mathcal{T} \quad (3.5)$$

$$(x_s = 0) \implies (y_s = 0), \forall s \in \mathcal{S} \quad (3.6)$$

$$(x_s = 1) \implies (y_s = 1 - x_{suc_s}), \forall s \in \mathcal{S} \quad (3.7)$$

$$t_i = \sum_{s \in \mathcal{S}: d_s = i} x_s \cdot (t_s^{dep} + t_s^{dur}) + y_s \cdot t_{d_s}^{tship}, \forall i \in \mathcal{T} \quad (3.8)$$

$$(x_s = 1) \implies (t_{o_s} \leq t_s^{dep}), \forall s \in \mathcal{S}, d_s \neq d \quad (3.9)$$

$$(x_s = 1) \implies (t_{o_s} + t_s^{dur} = t_d), \forall s \in \mathcal{S}, d_s = d \quad (3.10)$$

$$x_s, y_s \in \{0, 1\}, \forall s \in \mathcal{S} \quad (3.11)$$

$$t_i \geq \bar{t}, \forall i \in \mathcal{N} \quad (3.12)$$

Objective (3.1) finds the path with the shortest transit time and Objective (3.2) finds the path that emits the lowest amount of greenhouse gases. Constraints (3.3) state that the order has to leave the origin and that the order has to arrive at the destination.

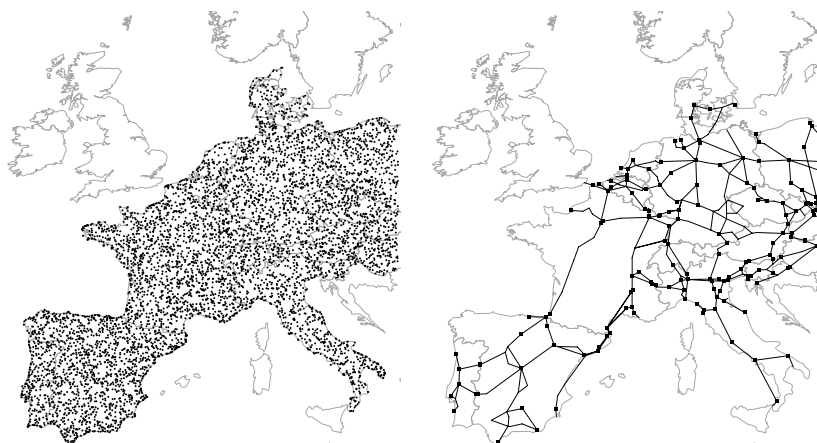


Figure 3.2: Randomly created locations (left) and TEN-T railway corridors (right) for continental Europe.

Constraints (3.4) ensure that the routing of the order does not use services that end at the origin o or that start at the destination d , which guarantees a cycle-free routing. The balance of flow for the rail stations is described by Constraints (3.5). The binary transshipment variable is set by Constraints (3.6) and (3.7). Constraints (3.8) to (3.10) state time-related restrictions. Finally, the domains of the decision variables are defined in Constraints (3.11) and (3.12). We implement this TSSP formulation with Version 12.7.1.0 of the IBM ILOG CPLEX Optimization Studio software and solve the problem with a time limit of 300 seconds per order.

3.4.2 European road and rail network data

We solve the TSSP repeatably for a large amount of randomly drawn orders across continental Europe where each order has a load of 18 tons (i.e. about one truckload). Regions that can only be reached via ferries, tunnels or large road-detours (e.g. Sicily, Norway, Ireland) and regions that are located east of longitude 19° East are excluded (e.g. Greece, Bulgaria, Romania). Overall, we consider 6,213 randomly created locations as potential origins and destinations of the orders, see Figure 3.2 (left).

The infrastructural rail network data is based on maps from the Trans-European Transport Network which are provided by the European Commission, see TEN-T Compliance Maps (2019) and TEN-T Interactive Maps (2019). If these maps indicate the traction type of a rail section as electric, we consider the country specific electric power mix as described in Moro and Lonza (2018) for computing the emissions of trains. Otherwise, we assume diesel traction for a train. For the time oriented routing, we use

Table 3.3: Parameter values for the emission estimation.

parameter	truck	train ^a
acc. ^b	0.12	0.05
distance	Open Source Routing Machine	Raildar (2019)
gradient ^c	Open Elevation (2019)	Open Elevation (2019)
payload	18 tons	646 tons
rail cars	n/a	24 rail cars
speed	Open Source Routing Machine	PaP Catalogue (2019) ^d

^a these values are identical for both electric and diesel trains

^b number of acceleration processes per kilometer

^c adjusted gradient with $\alpha = 0.5$, see Heinold and Meisel (2018)

^d combined with distance from Raildar (2019)

timetables provided at the TEN-T Customer Information Platform, which are available for eight core corridors, see PaP Catalogue (2019). The rail services considered in this study are thus limited to these corridors, see Figure 3.2 (right). We assume that every stop mentioned in the timetables qualifies for rail/road transshipment. We combine the information from the timetables with distances from Raildar (2019) to calculate the average speed of trains. For some rail services, this can lead to very high or very low values, for example if the timetables do not mention waiting times at intermediate stops. Therefore, we require the speed to be at least 40 km/h and at most 120 km/h for such services. We model rail services for one full week, which is sufficient to reach every potential destination from every potential origin. For the road network, we use raw data from Open Street Map (2019), as is provided by Geofabrik (2019), and calculate travel time and distance with the Open Source Routing Machine, see Luxen and Vetter (2011). The calculated time is the pure driving time and, thus, does not conform to regulations about drivers' working hours, which may vary between countries. As a general rule the "daily driving time shall not exceed nine hours", see Article 6 in EC Regulation 561/2006 (2006). Therefore, for reasons of simplicity, we do not include break times, if a truck service takes at most 9 hours. However, for truck services where the driving time exceeds 9 hours, we add another 15 hours break time for each full 9 hours of driving time. Additional information on the processing of the road and rail network data can be found in Heinold and Meisel (2018).

For estimating emissions from road and rail transportation, several models were developed, see Hickman et al. (1999), Lindgreen and Sorenson (2005), Scora and Barth

(2006) or Wang (1999). In these studies, emissions usually refer to carbon dioxide equivalents (CO₂e) to convert all kinds of greenhouse gases that occur in vehicle operations into CO₂-equivalents. We use the mesoscopic emission estimation model from Kirschstein and Meisel (2015) to estimate emissions from road and rail transportation in the TSSP. The mesoscopic model allows an individual setting of model parameters while keeping the computational effort at a moderate level. Table 3.3 provides an overview of relevant parameters and their data sources. Note that the payload set for the trains corresponds to a utilization rate of around 70%. Although this rate could be varied, it was shown in Heinold and Meisel (2018) that its impact on the emission rate of an order is relatively low. For each transshipment operation we assume a processing time of 30 minutes and emissions of 20 kgCO₂e for all terminals \mathcal{T} , see Geerlings and Van Duin (2011) and Clausen et al. (2013). For additional information on the mesoscopic model, we refer to Kirschstein and Meisel (2015), Behnke and Kirschstein (2017) and Heinold and Meisel (2018).

3.5 Simulation

3.5.1 Generation of orders

We model intermodal transportation as a three-leg transport chain, consisting of rail transportation between two selected rail/road transshipment terminals (which might consist of multiple consecutive rail services) as well as a road service from the orders origin o to a starting rail terminal and a road service from the last rail terminal to destination d . Thus, we disregard truck transportation between rail services (e.g. road-rail-road-rail-road), although the model presented in Section 3.4.1 could cover such transport chains too. We consider the twenty closest terminals to the origin and destination as candidates for rail/road transshipment and leave it to the optimization to find the most appropriate transshipment terminals for each order.

Each order is associated with a randomly drawn origin and destination. To simulate orders that are relevant for intermodal transportation, we require the air-line distance between origin and destination to be at least 300 kilometers. The departure time \bar{t} of each order is a randomly generated timestamp in minutes between $[1, 2, \dots, 10\ 079]$, where 1 stands for Monday at 0:01 and 10 079 for Sunday at 23:59. If an order uses a rail service $s \in \mathcal{S}$, we apply a payload based allocation scheme and allocate $18\text{t}/646\text{t} = 2.8\%$ of the total emissions $e^{trans}(s)$ that are caused by the whole train to the considered order.

We use the convergence index from Jung et al. (2004) to find a sufficient number of

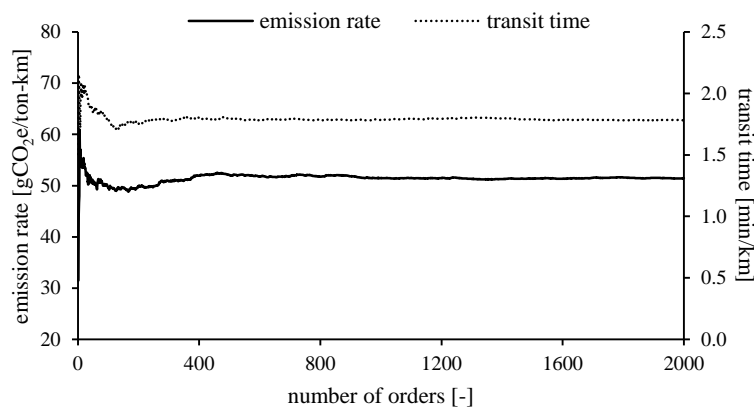


Figure 3.3: Convergence of the average emission rate and transit time.

simulated orders for a reliable estimation of emission rates and transit times, see Figure 3.3. We see that 2000 orders lead to negligibly low variations in the average estimated emissions per ton-km and in the average estimated transit time per km. Therefore, all results reported in the following stem from a simulation of 2000 transport orders.

3.5.2 Results

For all simulated orders, we compare the emission oriented routing and the time oriented routing. Table 3.4 presents relevant measures from both routings. As expected, the average emissions (in kgCO₂e) are lower and the average transit times (in h) are higher for orders that are routed with an emission oriented objective. More precisely, in the time oriented routing, orders have an average transit time of 35 hours and arrive at the destination on average 65 hours earlier compared to the emission oriented routing. This decrease in transit time corresponds to an average increase of emitted greenhouse gases of 563 kgCO₂e per order. In other words, orders that are routed with an emission oriented objective require on average 890 kgCO₂e which is 40% less than in the time oriented route, while the average transit time almost triples to 101 hours on average.

Remember that the distance between origin o and destination d is at least 300 km for all simulated orders. However, despite of this requirement, not all orders use rail transportation in the optimal solution. Around 2% of the orders in the emission oriented routing and around 26% of the orders in the time oriented routing use road services exclusively. These road-road routings can only happen for orders where potential transshipment terminals at the origin area overlap with potential transshipment terminals at the destination area. If this is the case, the use of rail services could involve detours that result in higher emissions and/or higher transit times compared to not using rail services

Table 3.4: Results obtained from the simulation experiments.

	emission oriented	time oriented	Δ
avg. emissions [kgCO ₂ e]	890.1	1,453.0	+562.9
avg. emission rate [gCO ₂ e/ton-km]	51.5	81.7	+30.2
avg. transit time [h]	100.8	35.5	-65.3
avg. transit time [min per km]	5.9	1.8	-4.1
avg. truck dist [km]	354	859	+505
intermodal route [%]	97.8	73.8	-24.0
same routing [%]	2.0	2.0	0.0

at all. However, the majority of the considered orders uses at least one rail service in the optimal solution. For these orders, time oriented routings often select transshipment terminals where the orders' waiting time for the next rail service is low and where well-connected rail services can be used for the rail routing. This practice can lead to longer distances for truck transportation in the time oriented routing. The average truck distance from pre- and post-carriage is 859 km in the time oriented routing whereas it is only 354 km in the emission oriented routing. Eventually, for 2.0% of all orders, the time oriented routing uses the same services as the emission oriented routing. In other words, the chosen objective impacts the selected route for the vast majority of 98% of all orders.

Figure 3.4 shows the emission oriented and the time oriented routing for an exemplary order from France to Germany. The weekdays and times in the graph refer to the departure at the nodes. In the emission oriented routing, transshipment terminals are selected that are close to the origin and destination and the rail transportation involves a detour via Belgium and the Netherlands. In contrast, the time oriented routing selects more distant terminals, which leads to rail transportation with much lower detouring. In addition, the used rail services in the time oriented routing are well synchronized and incur only little waiting time at rail stations while the used rail services in the emission oriented routing can imply long waiting times between two rail services.

The total emissions and the total transit time increase with the distance between origin o and destination d . To partly control for this, the environmental impact can be measured as gCO₂e/ton-km and the transit time as min/km. In Figure 3.5 we put the (o, d) -airline distance of the orders in relation to the emission rate in the emission oriented

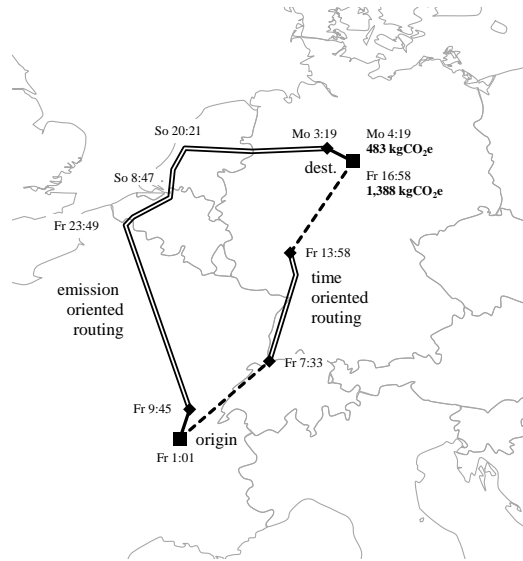


Figure 3.4: Example of an emission oriented and a time oriented routing from France to Germany.

routing (left graph) and in relation to the transit time per km in the time oriented routing (right graph).

For the emission rate ($\text{gCO}_2\text{e}/\text{ton-km}$) we observe a non-linear decrease with increasing distances. This is because truck transportation between transshipment terminals and origin/destination causes relatively high emissions per ton-km. This amount depreciates

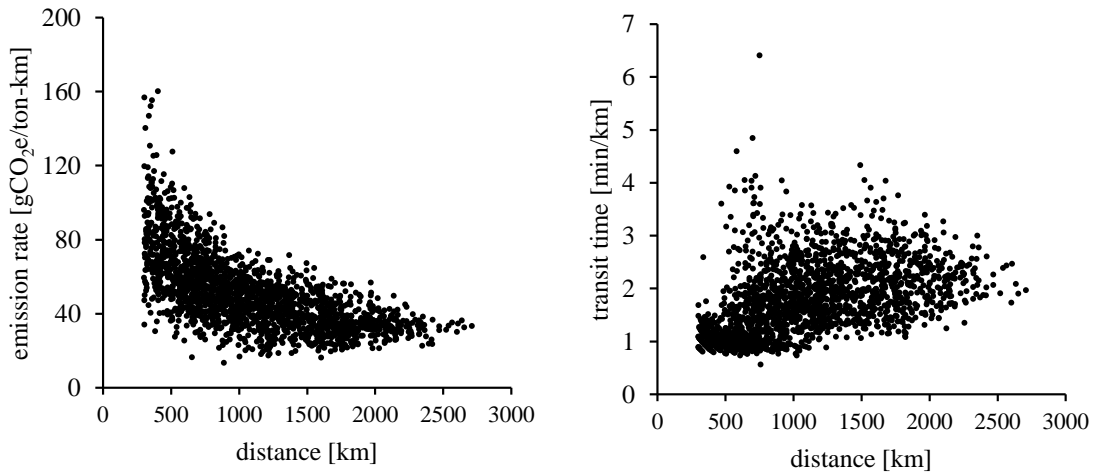


Figure 3.5: Relation between emission rates (left), transit times (right) and (o, d) -airline distance.

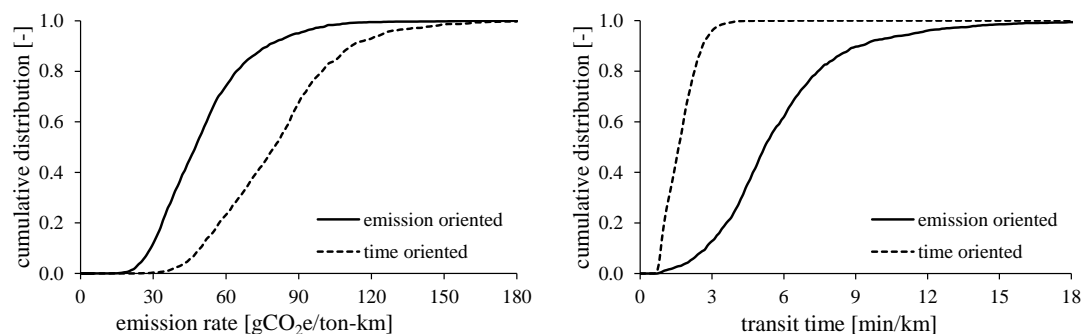


Figure 3.6: Cumulative distribution function of emission rates (left) and transit times (right) for both routing options.

with increasing intermodal transport distances of orders, as the use of the eco-friendly rail mode becomes more and more relevant. The transit time (min/km) appears to increase slightly with the orders distance. This can be explained with additional transshipment operations and waiting times at rail stations as increasing distances usually result in using more rail services.

We further specify the range of emission rates and transit times per km in Figure 3.6. Here, we depict the cumulative distribution function of emission rates and transit times for both routing options. In general, orders in the emission oriented routing have a lower emission rate (left graph) and a higher transit time (right graph) compared to if they were routed with the objective to minimize time. For example, 50% of the orders (median) have an emission rate of at most 48.4 gCO₂e/ton-km and a transit time of at most 5.3 min/km in the emission oriented routing whereas the emission rate is at most 80.8 gCO₂e/ton-km and the transit time is at most 1.7 min/km in the time oriented routing. The cumulative distribution functions also indicate that the range of optimal values for emission rates and transit times is narrower if the objective includes emissions or time, respectively. In particular, the interquartile range, which indicates the difference between the 75% and the 25% quantile, for emission rates is $61.5 - 36.6 = 24.9$ in the emission oriented routing and $96.0 - 62.6 = 33.4$ in the time oriented routing. The interquartile range for transit times is $7.0 - 4.1 = 2.9$ in the emission oriented routing but only $2.2 - 1.2 = 1.0$ in the time oriented routing.

3.6 Conclusion

In this paper, we compare the emission oriented routing with the time oriented routing of large freight shipments that have origins and destinations all across Europe. We use

the terminal-and-service selection problem (TSSP) to solve the routing problem for each considered order. Our results are based on a simulation of 2000 fixed-sized orders in the European rail/road network. The network consists of realistic timetables for trains and realistic driving times for trucks. We show that substantial differences exist between an emission oriented and a time oriented routing. The average amount of emitted greenhouse gases is 890 kgCO₂e in the emission oriented routing and 1,453 kgCO₂e in the time oriented routing. The average transit time is 101 hours in the emission oriented routing and around 36 hours in the time oriented routing. The average emission rate is 51 gCO₂e/ton-km in the emission oriented routing and 81 gCO₂e/ton-km in the time oriented routing. The average transit time is 5.9 min/km in the emission oriented routing and 1.8 min/km in the time oriented routing. All results show that the chosen objective has a tremendous impact on the chosen route and its performance measures. We also show that truck services are more relevant in time-oriented routings but that the tightly scheduled rail services of the European TEN-T corridors are often competitive even if transit time is to be minimized. If emissions are to be minimized, intermodal transportation clearly dominates road transportation with substantially lower total emissions for almost all considered orders. Future research can consider the interdependencies of orders that are jointly routed through the network and the impact of stochastic departures and transit times on the reliability of intermodal transport options. Furthermore, it could be interesting to investigate the limitations of the current train network and possibilities to extend it.

Acknowledgments

This research was funded by the German Research Foundation (DFG) under reference 268276815. We thank three anonymous reviewers for their valuable comments which helped to improve the manuscript considerably.

Bibliography

- Bauer, J., Bektaş, T. and Crainic, T. G. (2010). Minimizing greenhouse gas emissions in intermodal freight transport: an application to rail service design, *Journal of the Operational Research Society* **61**(3): 530–542.
- Behnke, M. and Kirschstein, T. (2017). The impact of path selection on ghg emissions in city logistics, *Transportation Research Part E: Logistics and Transportation Review* **106**: 320–336.
- Bektaş, T. and Laporte, G. (2011). The pollution-routing problem, *Transportation Research Part B: Methodological* **45**(8): 1232–1250.
- Clausen, U., Kaffka, J., Döring, L. and Ebel, G. (2013). Container based calculation of greenhouse gas emissions—a method to determine emissions of container handlings in container terminals, *General Proceedings of the 13th World Conference on Transport Research (WCTR)*.
- Crainic, T. G. (2000). Service network design in freight transportation, *European journal of operational research* **122**(2): 272–288.
- de Miranda Pinto, J. T., Mistage, O., Bilotta, P. and Helmers, E. (2018). Road-rail intermodal freight transport as a strategy for climate change mitigation, *Environmental development* **25**: 100–110.
- Demir, E., Burgholzer, W., Hrušovský, M., Arıkan, E., Jammernegg, W. and Van Woensel, T. (2016). A green intermodal service network design problem with travel time uncertainty, *Transportation Research Part B: Methodological* **93**: 789–807.
- Dijkstra, E. W. et al. (1959). A note on two problems in connexion with graphs, *Numerische mathematik* **1**(1): 269–271.
- EC Regulation 561/2006 (2006). Regulation (EC) No 561/2006 of the European Parliament and of the Council of the European Union. <https://eur-lex.europa.eu/LexUriServ/LexUriServ.do?uri=CELEX:32006R0561:EN:HTML> (visited on 22.01.2019).
- Ehmke, J. F., Campbell, A. M. and Thomas, B. W. (2016). Data-driven approaches for emissions-minimized paths in urban areas, *Computers & Operations Research* **67**: 34–47.

- Figliozzi, M. (2010). Vehicle routing problem for emissions minimization, *Transportation Research Record* **2197**(1): 1–7.
- Floyd, R. W. (1962). Algorithm 97: shortest path, *Communications of the ACM* **5**(6): 345.
- Geerlings, H. and Van Duin, R. (2011). A new method for assessing co2-emissions from container terminals: a promising approach applied in rotterdam, *Journal of cleaner Production* **19**(6-7): 657–666.
- Geofabrik (2019). OpenStretMap Data Extracts. <https://download.geofabrik.de/> (visited on 22.01.2019).
- Heinold, A. and Meisel, F. (2018). Emission rates of intermodal rail/road and road-only transportation in europe: A comprehensive simulation study, *Transportation Research Part D: Transport and Environment* **65**: 421–437.
- Hickman, J., Hassel, D., Joumard, R., Samaras, Z. and Sorenson, S. (1999). Methodology for calculating transport emissions and energy consumption. <https://trimis.ec.europa.eu/sites/default/files/project/documents/meet.pdf> (visited on 22.01.2019).
- Jung, J. Y., Blau, G., Pekny, J. F., Reklaitis, G. V. and Eversdyk, D. (2004). A simulation based optimization approach to supply chain management under demand uncertainty, *Computers & chemical engineering* **28**(10): 2087–2106.
- Kim, N. S. and Van Wee, B. (2014). Toward a better methodology for assessing co2 emissions for intermodal and truck-only freight systems: A european case study, *International Journal of Sustainable Transportation* **8**(3): 177–201.
- Kirschstein, T. and Meisel, F. (2015). Ghg-emission models for assessing the eco-friendliness of road and rail freight transports, *Transportation Research Part B: Methodological* **73**: 13–33.
- Lam, J. S. L. and Gu, Y. (2016). A market-oriented approach for intermodal network optimisation meeting cost, time and environmental requirements, *International Journal of Production Economics* **171**: 266–274.
- Lin, C., Choy, K. L., Ho, G. T., Chung, S. H. and Lam, H. (2014). Survey of green vehicle routing problem: past and future trends, *Expert systems with applications* **41**(4): 1118–1138.

- Lindgreen, E. and Sorenson, S. C. (2005). Simulation of energy consumption and emissions from rail traffic, *Technical University of Denmark. Department of Mechanical Engineering*. http://orbit.dtu.dk/files/3413826/lindgreen_sorenson.pdf (visited on 22.01.2019).
- Luxen, D. and Vetter, C. (2011). Real-time routing with openstreetmap data, *Proceedings of the 19th ACM SIGSPATIAL international conference on advances in geographic information systems*, pp. 513–516.
- Moro, A. and Lonza, L. (2018). Electricity carbon intensity in european member states: Impacts on ghg emissions of electric vehicles, *Transportation Research Part D: Transport and Environment* **64**: 5–14.
- Open Elevation (2019). Open Elevation: a free and open-source elevation API. <https://open-elevation.com> (visited on 17.01.2019).
- Open Street Map (2019). OpenStreetMap is the free wiki world map. <https://www.openstreetmap.org> (visited on 17.01.2019).
- PaP Catalogue (2019). Annual catalogue of the pre-arranged paths (PaP) 2019. https://cip.rne.eu/apex/f?p=212:170:2793393320158::::P170_BOOKS_LIST:504556 (visited on 22.01.2019).
- Raildar (2019). raildar.fr. <http://raildar.fr/osrm/osrm.html> (visited on 22.01.2019).
- Scora, G. and Barth, M. (2006). Comprehensive modal emissions model (cmem), version 3.01, *User guide. Centre for environmental research and technology. University of California, Riverside* **1070**: 79. https://www.cert.ucr.edu/cmем/docs/CMEM_User_Guide_v3.01d.pdf (visited on 22.01.2019).
- TEN-T Compliance Maps (2019). TEN-T Compliance Maps. TENtec Reporting. European Commission. https://ec.europa.eu/transport/themes/infrastructure/downloads_en (visited on 21.01.2019).
- TEN-T Interactive Maps (2019). TEN-T Interactive Maps. TENtec Reporting. European Commission. <http://ec.europa.eu/transport/infrastructure/tentec/tentec-portal/map/maps.html> (visited on 21.01.2019).
- Wang, M. Q. (1999). Greet 1.5: Transportation fuel-cycle model. vol. 1: Methodology, development, use, and results, *Technical report*, Argonne National Laboratory. <https://greet.es.anl.gov/files/20z8ihl0> (visited on 21.01.2019).

Bibliography

Winebrake, J. J., Corbett, J. J., Falzarano, A., Hawker, J. S., Korfmacher, K., Ketha, S. and Zilora, S. (2008). Assessing energy, environmental, and economic tradeoffs in intermodal freight transportation, *Journal of the Air & Waste Management Association* **58**(8): 1004–1013.

Chapter 4

Comparing Emission Estimation Models for Rail Freight Transportation

Publication status Published in 2020: *Transportation Research Part D: Transport and Environment* 86: 102468.

Arne Heinold

School of Economics and Business, Kiel University, Kiel, Germany

Abstract This study reviews emission estimation models that aim at providing realistic estimates of the emitted greenhouse gases from rail freight transportation. Five models are considered: two models from the MEET project, the ARTEMIS model, the EcoTransIT World model, and the Mesoscopic model. For each of the five models, this paper describes the estimation principles, methodology, and procedure, as well as relevant input parameters. An experimental study demonstrates the impact of train and trip specific parameters on each model's emission estimate. Results are presented for varying values of a train's number of wagons, the payload per wagon, the average speed, the trip distance, the number of stops, and the altitude profile along the route. In doing so, given a specific transportation scenario, the paper supports decision makers from industry and researchers to find and apply an appropriate emission estimation model for evaluating the eco-friendliness of rail freight transportation.

Keywords Rail Freight Transportation, Emission Estimation Models, Comparative Study,

4.1 Introduction

There is a recent revival of using rail transportation to match the constantly increasing global freight volume (International Energy Agency; 2019). The International Transport Forum (2019) expects global rail freight volumes to grow 2.7% per year between 2015 and 2030, with some countries having significantly higher growth rates (e.g., in 2017, growth rates are 13.3%, 6.4%, 5.5%, and 5.2% for China, Russia, India, and the USA, respectively). Recent infrastructural developments demonstrate this growth, such as the ‘silk railway’ initiated by the Chinese government to reduce transportation time between China and Europe (The Times; 2020). Further, transportation makes up for about 25% of global energy-related CO₂ emissions (IPPC; 2018; Eurostat; 2020) and the rail mode is often considered as a mean to reduce total emissions from transportation. For example, recent studies show that using intermodal rail/road transportation instead of road-only transportation can reduce the overall transport emissions, e.g., Craig et al. (2013), Kiyota et al. (2015), de Miranda Pinto et al. (2018), or Heinold and Meisel (2018, 2019). These studies analyze different transport scenarios and apply diverse emission estimation models to measure the environmental impact of the considered modes of transportation. Demir et al. (2011) provide a comparative analysis of several vehicle emission models for road freight transportation. As far as is known, there is no such analysis of emission estimation models for rail freight transportation.

This study fills this gap by reviewing and comparing five emission estimation models for rail freight transportation. The selected models provide an overview of the most common approaches. For this, two models from the MEET project (Hickman et al.; 1999), the ARTEMIS model (Lindgreen and Sorenson; 2005a,b), the EcoTransIT World (ETW) model (EcoTransIT World Initiative; 2019), and the Mesoscopic model (Kirschstein and Meisel; 2015) are considered in this study. In a first step, each model’s estimation principles, methodology, input parameters, and procedures are explained. Then, in a second step, the impact of varying values of a train’s number of wagons, the payload per wagon, the average speed, the trip distance, the number of stops, and the altitude profile along the route is demonstrated in an experimental study. Here, a typical freight train serves as a base scenario and results are presented for each of the considered experimental settings, which results in emission rates for a large amount of potential transport scenarios. Finally, in a third step, this paper discusses scenarios in which it might be appropriate

to select one or another of the considered models.

With this, the main contribution of this paper is twofold. Firstly, the models' detailed description with a consistent notation allows a direct and precise application of the models. All models are implemented in Python and the code is made publicly available, see Appendix A. Secondly, the results of the experimental study demonstrate the impact of relevant train and trip specific parameters on each model's emission estimate. In doing so, given a specific transportation scenario, the paper supports decision makers from industry and researchers to find and apply an appropriate emission estimation model for evaluating the eco-friendliness of rail freight transportation.

The rest of this paper is organized as follows. Section 4.2 describes general principles of estimating emissions from rail freight transportation. Section 4.3 describes each of the considered emission estimation models in detail. The experimental study in Section 4.4 demonstrates the impact of train and trip parameters on each model's emission estimate. Section 4.5 discusses the selection of an appropriate model for a given transport scenario. Section 4.6 concludes this paper.

4.2 Principles of estimating emissions from rail freight transportation

This section describes the fundamental principles of estimating emissions from rail freight transportation. Here, emissions refer to all greenhouse gases that result from the combustion of fuel and electricity to power freight transport equipment, most notably, carbon dioxide (CO_2), nitrogen oxides (NO_x), sulfur dioxide (SO_2), and non-methane hydrocarbons (NMHCs). These gases are subsumed under the single measure of carbon dioxide equivalents (CO_2e) that is then used to measure transport related emissions, see Piecyk et al. (2012). Generally, transport related emissions can be distinguished by their life-cycle phase, which refers to either well-to-tank (WTT), tank-to-wheel (TTW), or well-to-wheel (WTW) emissions (e.g., Moro and Lonza; 2018). Well-to-tank emissions include all emissions that are emitted in the production and distribution of the used energy source, such as emissions at power plants or emissions from tank trucks that refuel gas stations. In contrast, tank-to-wheel emissions describe the instant emissions from the energy that is required to move the considered vehicle. Typically, for diesel trains, these are emissions from burning the used type of fuel. Finally, well-to-tank and tank-to-wheel emissions add up to well-to-wheel emissions. Note that, in carbon accounting, emissions are further differentiated according to their scope (GHG Protocol; 2020, p. 25), which,

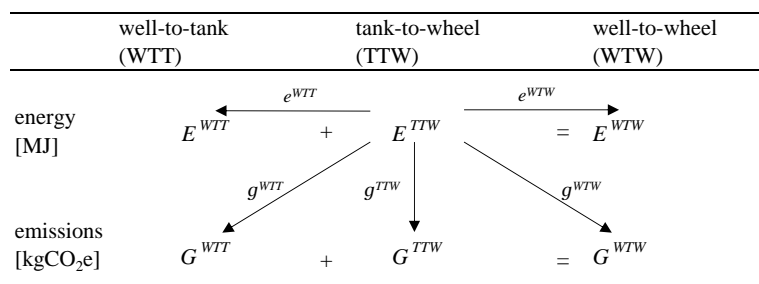


Figure 4.1: Structure of estimating energy and emissions from rail transportation.

however, is not considered in this study.

For each phase (WTT, TTW, and WTW), it is possible to estimate the energy and emissions of a train on a specific trip. Furthermore, by using so-called energy and emission factors, a distinct relation between each phase's energy and emission estimate can be drawn. Figure 4.1 demonstrates this by using the definition of these factors that is also used in European norm DIN EN 16258 (2012). In particular, TTW emissions G^{TTW} (kgCO₂e) are calculated from the actual TTW energy E^{TTW} (MJ) consumed by the train and emission factor g^{TTW} (kgCO₂e/MJ) and, likewise, energy and emission factors e^{WTW} (MJ/MJ) and g^{WTW} (kgCO₂e/MJ) can be directly applied to the TTW energy E^{TTW} for calculating WTW energy and emissions, respectively. Finally, it is also possible to derive the WTT energy and emissions from the TTW energy consumption, by applying energy and emission factors e^{WTT} (MJ/MJ) and g^{WTT} (kgCO₂e/MJ), respectively. Here, artificial energy factor e^{WTT} shows the energy in the production and distribution processes per unit of energy that is required to move the train. For several train and engine types, these emission and energy factors are provided by the literature. If this is the case, a train's emissions and energy can be derived solely from its TTW energy consumption. Thus, most emission estimation models, including the ones considered in this study, present a methodology to estimate the TTW energy consumption.

4.3 Emission estimation models

Emission estimation models usually follow a microscopic or a macroscopic approach. The former is based on a detailed consideration of the underlying physical principles of the moving vehicle and the latter is primarily based on aggregated statistical data of the transportation process. So-called mesoscopic models rely on a mixture of micro- and macroscopic principles. This paper considers models from each of the three approaches

Table 4.1: Consistent notation of common trip and train parameters.

parameter	description	unit
d	trip's distance	m or km
h	trip's altitude difference	m
m_{loc}	train's locomotive weight	kg or ton
m_t	train's total weight	kg or ton
m_{tl}	train's payload	kg or ton
m_{te}	train's empty weight	kg or ton
m_w	wagon's total weight	kg or ton
m_{we}	wagon's empty weight	kg or ton
m_{wl}	wagon's payload	kg or ton
m_{wm}	wagon's max. payload	kg or ton
n_{ax}	wagon's number of axles	-
n_w	train's number of wagons	-
n_s	trip's number of stops (excl. last stop)	-
v	train's average speed	m/s or km/h

(micro-, macro-, and mesoscopic) and, with this, it provides a comprehensive overview of commonly used approaches for estimating emissions. Thereby, early seminal models (MEET from 1999, ARTEMIS from 2005) and recent, more practically oriented models (global ETW from 2010, Mesoscopic from 2015) are explained in this section. The models analyzed in this study are presented in the order of their year of publication (oldest to newest). Table 4.1 provides the notation for the trip's distance, the trip's altitude difference, the train's weights, the train's number of wagons and axles, the trip's number of stops, and the train's average speed. This notation is consistently used across all the considered models and further notation that is specific the models is introduced in the respective subsections.

4.3.1 MEET

Hickman et al. (1999) present Methodologies for Estimating Emissions from Transport (MEET). The work provides estimation models for road, rail, sea, and air transportation of passengers and freight. For rail transportation, the general idea is to estimate a TTW-energy consumption rate in kJ per ton and kilometer with an estimation function that is parameterized with empirical or train specific data. This rate is then used to calculate the train's total energy consumption through considering the train's payload and the traveled distance. The MEET project proposes two models for estimating energy consumption rates.

The first model, also referred to as the empirical MEET model, describes the energy consumption rate as a function of the train's average speed v and the distance d_s between

two stops.

Formula (4.1) shows the estimation of the energy per ton and kilometer for a large freight train if the distance between two stops d_s is between 80 and 200 kilometers. Here, A_0 and A_1 are train type specific parameters that were derived from an empirical study.

$$E_1 \stackrel{[kJ/ton \cdot km]}{=} \stackrel{[-]}{A_0} + \stackrel{[-]}{A_1} \cdot \frac{\stackrel{[km/h]^2}{v^2}}{\stackrel{[km]}{\ln(d_s)}}, \quad d_s \in [80, 200] \quad (4.1)$$

The second model, also referred to as the steady state MEET model, derives the train's energy consumption rate from its steady state loading, see Formula (4.2). Here, the rate is calculated from average speed v , number of stops n_s , distance d , maximum speed v_{max} , and gradient h . Note that v is the train's average speed and v_{max} its maximal speed to which it accelerates along the considered trip. Parameters B_0 , B_1 , and B_2 consider train type specific characteristics and parameter $g = 9.81 \text{ m/s}^2$ is the gravitational acceleration.

$$E_2 \stackrel{[kJ/ton \cdot km]}{=} \stackrel{[-]}{B_0} + \stackrel{[-]}{B_1} \cdot \frac{[m/s]}{v} + \stackrel{[-]}{B_2} \cdot \frac{[m/s]^2}{v^2} + \frac{[-]}{d} \cdot \frac{[m/s]^2}{2} + \frac{[m/s]^2}{g} \cdot \frac{[m]}{d} \quad (4.2)$$

Both, the first model (empirical) and the second model (steady state), estimate the train's energy consumption rate in kJ per ton and kilometer independent of the locomotive or engine type (diesel or electric). For trains hauled by a locomotive with an electric engine, the energy consumption rate can be directly used to estimate the total consumed TTW energy in MJ, see Formula (4.3). Index $i \in \{1, 2\}$ is used to differentiate between the two models. For trains hauled by a locomotive with a diesel engine, the consumed energy needs to be adjusted for the diesel-electric efficiency. This can be done by either considering the efficiency through the emission factors (Hickman et al.; 1999, p. 346, Table F9) or by using a diesel-electric efficiency rate ϵ^{de} . The energy estimate in MJ from the second approach is described by Formula (4.4).

$$E_i^{TTW \text{ elec.}} \stackrel{[MJ]}{=} \frac{[kJ]}{E_i} \cdot \stackrel{[ton]}{m_{tl}} \cdot \stackrel{[km]}{d} \cdot 10^{-3}, \quad \forall i \in \{1, 2\} \quad (4.3)$$

$$E_i^{TTW\ diesel} = E_i^{TTW\ elec.} \cdot \frac{1}{\epsilon_{de}}, \quad \forall i \in \{1, 2\} \quad (4.4)$$

4.3.2 ARTEMIS

Lindgreen and Sorenson (2005b,a) present an emission estimation model for rail transportation as part of a more comprehensive project on the Assessment and Reliability of Transport Emission Models and Inventory Systems (ARTEMIS). The model is based on a detailed analysis of the physical principles that describe the required energy to move a train. In particular, it estimates the train's energy consumption (in J) by integrating its driving resistance over the traveled distance d , see Formula (4.5). Thereby, the driving resistance constitutes of rolling resistance F_R , aerodynamic resistance F_L , gradient resistance F_S , and acceleration resistance F_A . Each of these resistances can be calculated from trip and train specific parameters, see Formulas (4.6) to (4.9).

$$E_3 = \int \left(F_R + F_L + F_S + F_A \right) \Delta d \quad (4.5)$$

$$F_R = C_R \cdot m_t \cdot g \quad (4.6)$$

$$F_L = \frac{1}{2} \cdot \rho \cdot C_L \cdot A \cdot v^2 \quad (4.7)$$

$$F_S = m_t \cdot g \cdot \frac{h}{d} \cdot 1000 \quad (4.8)$$

$$F_A = m_t \cdot a \quad (4.9)$$

Parameter $g = 9.81 \text{ m/s}^2$ is the gravitational acceleration, parameter $\rho = 1.2 \text{ kg/m}^3$ is the air density, parameter A is the train's front surface, parameter a is the train's acceleration, and parameters C_R and C_L are train specific rolling and aerodynamic coefficients,

respectively. The last two parameters require additional calculations (Kirschstein and Meisel; 2015; Lindgreen and Sorenson; 2005a,b) that are described in Formulas (4.10) and (4.11). Here, parameters c_R^{loc} , c_R^{car} , c_1 , c_2 , c_L^{loc} , and c_L^{car} , are rolling and aerodynamic constants of the considered locomotive and wagons/cars, respectively.

$$C_R^{[-]} = c_R^{loc[-]} \cdot \frac{m_{loc}^{[t]}}{m_t^{[t]}} + c_R^{car[-]} \cdot \frac{m_w^{[t]} \cdot n_w^{[-]}}{m_t^{[t]}} + \frac{n_{ax}^{[-]} \cdot n_w^{[-]}}{10 \cdot m_t^{[t]} \cdot g^{[m/s^2]}} + c_1^{[-]} \cdot \frac{[\frac{km}{h}]}{100} + c_2^{[-]} \cdot \left(\frac{[\frac{km}{h}]}{100} \right)^2 \quad (4.10)$$

$$C_L^{[-]} = c_L^{loc[-]} + c_L^{car[-]} \cdot n_w^{[-]} \quad (4.11)$$

If speed v and acceleration a are constant, the integral from Formula (4.5) can be solved by using Formula (4.12). The variables x_1 and x_2 describe the distance of this (constant) speed-acceleration section, i.e., speed v and acceleration a do not change here. For example, considering a trip with a total distance of 750 meters: if a train travels with $v = 50$ km/h and $a = 0.2$ m/s² for first 500 meters, then, $x_1 = 0$ and $x_2 = 500$ for this first section, and, if the train travels with $v = 100$ km/h and $a = 0.1$ m/s² on the following 250 meters, then, $x_1 = 500$ and $x_2 = 750$ for the second section.

$$E_3^{[J]} = (F_R^{[N]} + F_L^{[N]} + F_S^{[N]} + F_A^{[N]}) \cdot (x_2^{[m]} - x_1^{[m]}) \quad (4.12)$$

Theoretically, one could split the actual trip into a sufficiently large number of sections with constant speed and acceleration, then calculate the energy per section by Formula (4.12), and sum up the values of all sections to come up with an estimate of the whole trip's energy. Clearly, this is not a practical approach and, instead, the authors propose a so-called matrix approach. This approach follows a three step process.

Firstly, a train-specific energy matrix is calculated for various speed-acceleration combinations. The authors suggest acceleration intervals of 0.1 m/s² (i.e., $C = \{0, 0.1, \dots, 1\}$) and speed intervals of 10 km/h (i.e., $V = \{0, 10, \dots, 140\}$). The energy matrix considers the energy from rolling resistance F_R , aerodynamic resistance F_L , and acceleration resistance F_A . The energy from gradient resistance F_S is not considered in the matrix as it depends on the trip's geographical characteristics (slope profile) and not on the train's acceleration or speed. Instead, the authors suggest to calculate it for the whole trip in

		speed interval														
		140 - 130	130 - 120	120 - 110	110 - 100	100 - 90	90 - 80	80 - 70	70 - 60	60 - 50	50 - 40	40 - 30	30 - 20	20 - 10	10 - 0	
acceleration interval	0.9 - 1.0	0.00	0.00	0.00	0.00	0.00	0.00	0.00	0.00	0.00	0.00	0.00	0.00	0.00	0.00	0.00
	0.8 - 0.9	0.00	0.00	0.02	0.00	0.00	0.00	0.00	0.00	0.04	0.01	0.02	0.01	0.00	0.00	
	0.7 - 0.8	0.00	0.00	0.00	0.00	0.00	0.00	0.00	0.00	0.00	0.00	0.00	0.00	0.00	0.00	
	0.6 - 0.7	0.00	0.00	0.00	0.00	0.00	0.00	0.00	0.00	0.00	0.00	0.00	0.00	0.00	0.00	
	0.5 - 0.6	0.00	0.00	0.17	0.09	0.07	0.02	0.00	0.05	0.03	0.00	0.01	0.00	0.00	0.00	
	0.4 - 0.5	0.00	0.00	0.08	0.02	0.02	0.12	0.12	0.07	0.06	0.05	0.01	0.01	0.00	0.00	
	0.3 - 0.4	0.05	0.05	0.00	0.00	0.00	0.00	0.00	0.05	0.00	0.00	0.00	0.00	0.00	0.00	
	0.2 - 0.3	0.09	0.19	0.47	0.31	0.35	0.35	0.35	0.09	0.09	0.11	0.11	0.05	0.04	0.00	
	0.1 - 0.2	0.71	1.23	0.76	0.92	0.71	0.64	0.59	0.47	0.29	0.37	0.22	0.11	0.03	0.01	
	0.0 - 0.1	11.49	12.30	9.80	4.25	2.55	1.44	0.00	0.50	0.79	0.17	0.57	0.38	0.20	0.01	

Figure 4.2: Spatial distribution of speed-acceleration combinations of train GP7523 between Glostrup (DK) and Fredericia (DK) (Lindgreen and Sorenson; 2005b).

the third step of the matrix approach.

Secondly, a trip-specific distribution matrix is determined for all considered speed-acceleration combinations. The authors propose to either use a spatial distribution matrix, indicating the train's traveled distance in each speed-acceleration interval, or a temporal distribution matrix, indicating the train's traveled time in each speed-acceleration interval. Figure 4.2 shows the spatial distribution matrix of the exemplary train GP7523 between the cities of Glostrup (DK) and Fredericia (DK), which the authors derive from analyzing empirical data. For example, the value 11.49% (bottom left corner) states the share of the distance where the considered train traveled with an acceleration between 0 and 0.1 m/s² and a speed between 130 and 140 km/h. The authors suggest to use only those sections of the trip where the train accelerates ($a \geq 0$). For the exemplary train GP7523, this is the case for 55.36 % and 57.61 % of its distance and time, respectively. Note that, by doing so, potential energy gains from regenerative braking are not considered here.

Finally, in a third step, the train-specific energy matrix and the trip-specific distribution matrix are combined in order to estimate the energy of a specific train on a specific trip. This is done in Formula (4.13). The first part of the formula combines the two matrices: for a matrix element (i, j) ($i \in C, j \in V$), e_{ij} describes the value of the energy matrix (F_R , F_L , and F_A) and p_{ij} describes the value of the distribution matrix. The second part of the formula calculates the energy from the gradient resistance (F_S).

$$E_3 = d \cdot \sum_{i \in C, j \in V} e_{ij} \cdot p_{ij} + d \cdot F_S \quad (4.13)$$

Energy E_3 is the kinetic energy that is required to move the train. The train's efficiency is then used to convert this energy to the actual energy demand of the train.

Formulas (4.14) and (4.15) state the estimated TTW energy in MJ for trains' hauled by electric and diesel locomotives, respectively. Here, ϵ^e and ϵ^d are the corresponding efficiency rates of the locomotive's engine.

$$E_3^{TTW\ elec.} \overset{[MJ]}{=} E_3 \overset{[J]}{\cdot} \frac{\overset{[-]}{1}}{\epsilon^e} \cdot 10^{-6} \quad (4.14)$$

$$E_3^{TTW\ diesel} \overset{[MJ]}{=} E_3 \overset{[J]}{\cdot} \frac{\overset{[-]}{1}}{\epsilon^d} \cdot 10^{-6} \quad (4.15)$$

4.3.3 EcoTransIT World

The EcoTransIT World (ETW) calculator presents a methodology to estimate emissions for the transport of goods between two locations (EcoTransIT World Initiative; 2019). Thereby, the model considers modes truck, train, airplane, sea ship, and barge as well as transshipment operations between the modes. The results from the ETW model are in accordance with European norm DIN EN 16258 (2012) and the GLEC Framework (Smart Freight Centre; 2020). An implementation of the model is available online at www.ecotransit.org. This website also provides a detailed description of the methodology as well as regular updates of the used parameters and functions.

For rail transportation with electric locomotives, the ETW model uses an empirical function to estimate the specific energy consumption per gross ton and kilometer, see Formula (4.16). The authors recommend to use the function for trains with a gross load of at most $m_t = 2,200$ t and to use a constant value of 10 Wh/ton·km for larger trains ($m_t > 2,200$ t). The parameter s captures the slope profile of the trip: $s = 0.9$ in flat terrain, $s = 1.0$ in hilly terrain, and $s = 1.1$ in mountainous terrain.

$$\overset{[Wh/ton \cdot km]}{E_4} = 1200 \cdot \overset{[ton]}{m_t}^{-0.62} \cdot \overset{[-]}{s} \quad (4.16)$$

To convert the energy consumption per gross ton and kilometer to an energy consumption per net ton and kilometer, the model uses a so-called net-gross relation r . This parameter r considers the train's capacity utilization c , the wagon's empty weight m_{we} , and the wagon's max. load m_{wm} , see Formula (4.17).

$$r = \frac{c}{c + m_{we} / m_{wm}} \quad (4.17)$$

The capacity utilization c is calculated by considering the train's load factor l as well as the train's empty trip factor e , see Formula (4.18). The load factor l is the ratio of the wagon's payload to the wagon's capacity (m_{wl}/m_{wm}) and the empty trip factor e is the ratio of the empty traveled distance to the loaded traveled distance (d_{empty}/d_{loaded}). If empty trips are not considered, the train's load factor l is equal to the train's capacity utilization c , i.e., ($d_{empty} = 0$) \implies ($c = l$).

$$c = \frac{l}{1 + e} \quad (4.18)$$

Remember that the energy estimate E_4 is based on empirical observations of an electric train. However, the authors argue that this functional relationship can also be used to estimate the energy from trains hauled by a diesel locomotive, simply by using the diesel-electric efficiency ϵ^{de} . The TTW energy in MJ is then estimated by Formula (4.19) for electric trains and by Formula (4.20) for diesel trains.

$$E_4^{TTW\ elec.} = \frac{1}{r} \cdot \frac{Wh}{ton \cdot km} \cdot m_{tl} \cdot d \cdot 3.6 \cdot 10^{-3} \quad (4.19)$$

$$E_4^{TTW\ diesel} = E_4^{TTW\ elec.} \cdot \frac{1}{\epsilon^{de}} \quad (4.20)$$

4.3.4 Mesoscopic model

Kirschstein and Meisel (2015) propose the Mesoscopic model to estimate emissions from road and rail freight transportation. The Mesoscopic model combines physical principles from microscopic models, such as the ARTEMIS model, with empirical data from macroscopic models, such as the ETW model. With this, the authors claim to provide a model that combines 'the preciseness of micro-models while requiring only little more information than macro-models' (Kirschstein and Meisel; 2015, p. 13).

The Mesoscopic model is based on the same physical principles that are also used in the ARTEMIS model, see Section 4.3.2. Thereby, the authors use W-equivalent formulations of the resistances. In particular, the power to overcome air resistance p^{air} , rolling resistance p^{roll} , and gradient resistance p^{grade} are calculated by Formulas (4.21) to (4.23). Here, parameters c^{air} and c^{roll} are train specific coefficients for the estimation of aerodynamic and rolling resistances, respectively. For these parameters, the Mesoscopic model uses the calculation methods from the ARTEMIS model ($c^{air} \Leftrightarrow C_L$, $c^{roll} \Leftrightarrow C_R$), see Formulas (4.10) and (4.11).

$$p^{air} \stackrel{[kW]}{=} \frac{1}{2000} \cdot c^{air} \stackrel{[-]}{\cdot} \rho \stackrel{[kg/m^3]}{\cdot} A \stackrel{[m^2]}{\cdot} v \stackrel{[m/s]^3}{^3} \quad (4.21)$$

$$p^{roll} \stackrel{[kW]}{=} c^{roll} \stackrel{[-]}{\cdot} m_t \stackrel{[t]}{\cdot} g \stackrel{[m/s^2]}{\cdot} v \stackrel{[m/s]}{v} \quad (4.22)$$

$$p^{grade} \stackrel{[kW]}{=} m_t \stackrel{[t]}{\cdot} g \stackrel{[m/s^2]}{\cdot} v \stackrel{[m/s]}{v} \cdot \frac{h}{d} \stackrel{[m]}{[m]} \quad (4.23)$$

Remember that the ARTEMIS model uses the matrix-approach to consider the energy consumption at different speed-acceleration combinations. In contrast to this, the Mesoscopic model uses an approximation function to estimate the energy from acceleration processes. Specifically, the authors propose Function (4.24) to estimate the energy from acceleration processes W_{train}^{inert} , which considers the train's total weight m_t and the train's average speed v . The authors show that W_{train}^{inert} describes a good fit for a freight train's acceleration energy that is required for a single acceleration process up to speed v .

$$W_{train}^{inert} \stackrel{[kWh]}{=} \frac{0.52}{2 \cdot 3600} m_t \stackrel{[t]}{\cdot} \left(\frac{[m/s]}{v} \right)^2 \quad (4.24)$$

The Mesoscopic model uses this approximation to estimate the trip's acceleration energy, which is less data demanding compared to the matrix approach used in the ARTEMIS model. In particular, Formula (4.25) then estimates the train's total energy

by considering the required energy to overcome air, rolling, gradient, and acceleration resistance. For the acceleration resistance, the required energy for a single acceleration processes (W_{train}^{inert}) is multiplied with the total number of accelerations ($n^{acc} \cdot d$) along the route. In this context, n^{acc} is the average number of acceleration processes per kilometer ($n^{acc} = (n_s + 1) / d$) and serves to reflect different traffic conditions.

$$E_5^{[kWh]} = \frac{d^{[km]}}{v^{[km/h]}} \cdot \left(p^{air^{[kW]}} + p^{roll^{[kW]}} + p^{grade^{[kW]}} \right) + n^{acc^{[-]}} \cdot d^{[km]} \cdot W_{train}^{inert^{[kWh]}} \quad (4.25)$$

Like in the ARTEMIS model, this energy estimate is the kinetic energy to move the train and the actual energy demand depends on the engine type. This is considered through efficiency rates ϵ^e (electric locomotive) and ϵ^d (diesel locomotive), see Formulas (4.26) and (4.27).

$$E_5^{TTW^{[MJ]}_{elec}} = E_5^{[kWh]} \cdot \frac{1^{[-]}}{\epsilon^e} \cdot 3.6 \quad (4.26)$$

$$E_5^{TTW^{[MJ]}_{diesel}} = E_5^{[kWh]} \cdot \frac{1^{[-]}}{\epsilon^d} \cdot 3.6 \quad (4.27)$$

Table 4.2: Train and trip parameters that are varied in the experiments.

nr	parameter	unit	range	default	considered in the model? ^{a)}				
					1	2	3	4	5
train									
1	number of wagons n_w	-	2-42	20	-	-	✓	✓	✓
2	payload per wagon m_{wt}	t	10-62	38	-	-	✓	✓	✓
3	average speed v	km/h	40-140	90	✓	✓	(-)	-	✓
trip									
4	distance d	km	40-440	240	✓	✓	✓	-	✓
5	number of stops n_s	-	1-5	2	✓	✓	(-)	-	✓
6	altitude difference h	m	0-400	200	-	✓	✓	✓	✓

^{a)} 1: MEET (empirical), 2: MEET (steady state), 3: ARTEMIS, 4: ETW, 5: Mesoscopic

4.4 Experiments

The purpose of the experiments is to demonstrate the impact of common train and trip parameters on the estimated emissions of the considered models. In particular, the experiments analyze the impact of varying values of a train's number of wagons, the payload per wagon, the average speed, the trip distance, the number of stops, and the altitude profile along the route. Table 4.2 shows the range within which these parameters are varied, their default values (which represent a typical freight train in Germany, see FIS (2020)), and whether these parameters are explicitly considered by the models as inputs, or not. The analysis of each parameter's impact helps in understanding each model's methodology. Further, by using such a wide range of values for the varied parameters, the results of the experiments provide estimates of emission rates for various transport scenarios. The model and simulation parameters that are used in the experiments are described in Section 4.4.1 and the results are described in Sections 4.4.2 to 4.4.7.

4.4.1 Model and simulation parameters

The experiments cover trains that are either hauled by a locomotive with an electric engine or by a locomotive with a diesel engine. For both cases, a six-axle locomotive (frontal area $A = 10 \text{ m}^2$, locomotive weight $m_{loc} = 123 \text{ t}$) is assumed to carry a varying number of wagons of the type 'sgis 716' ($n_{ax} = 4$ axles, empty weight $m_{we} = 23 \text{ t}$, maximal load $m_{wm} = 61 \text{ t}$). It is assumed that each wagon is loaded with three 20-ft containers, that each wagon's payload m_{wl} includes the empty weight of the containers, and that each wagon's payload m_{wl} is equally distributed among all containers. The efficiency of diesel and electric trains is set to $\epsilon^d = 0.35$ and $\epsilon^e = 0.65$ (Lindgreen and Sorenson; 2005b, p. 27), respectively, and the diesel-electric efficiency is set to $\epsilon^{de} = 0.37$ (EcoTransIT World Initiative; 2019, p. 63).

For the energy estimate with the empirical MEET model (E_1), the parameters A_0 and A_1 correspond to a large freight train with an empty mass of 600 t and are set to 63 and 0.019 (Hickman et al.; 1999, p. 223), respectively. Furthermore, it is assumed that stops n_s are uniformly distributed across the trip such that the distance between any two consecutive stops is the same, i.e., $d_s = d/(n_s + 1)$. For the MEET's energy estimate that is based on the train's steady state loading (E_2), it is assumed that the maximal speed v_{max} is a multiple of the average speed v ($v_{max} = 1.5 \cdot v$) and that $B_0 = 24.7$, $B_1 = 0$, and $B_2 = 0.0845$ (Hickman et al.; 1999, p. 223).

The matrix approach of the ARTEMIS model is used with the spatial distribution of the freight train between Glostrup and Fredericia, see Figure 4.2. Clearly, this causes

misleading emission rates in the experiments as the distribution matrix is based on a specific freight train in Denmark, e.g., whose total payload is only 126 tons whereas it is 760 tons for this study's default train. However, using appropriate speed-accelerations for each experimental setting requires a vast amount of detailed real-world rail freight data. The issue of data availability is discussed in more detail in Section 4.5. The following values are used to calculate the train specific rolling and aerodynamic coefficients C_R and C_L that are used in the ARTEMIS and Mesoscopic model: $c_R^{car} = 0.0006$, $c_R^{loc} = 0.004$, $c_1 = 0.0005$, $c_2 = 0.0006$, $c_L^{loc} = 1.1$, and $c_L^{car} = 0.218$ (Lindgreen and Sorenson; 2005a, p. 7-8, 29).

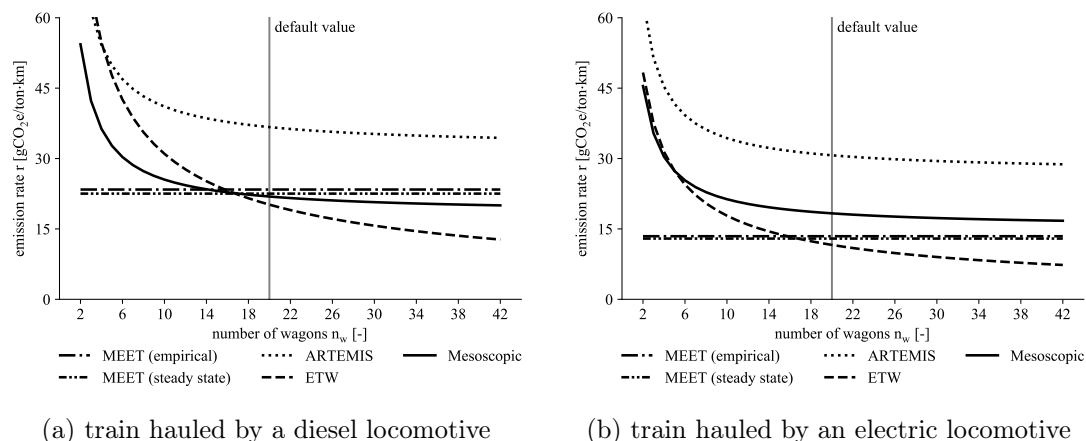
The ETW model uses parameter s to consider the slope profile of the trip. In the experiments, the altitude difference h between the origin location and the destination location is used as a proxy for s . In particular, it is assumed that $s = 0.9$ for altitude differences below 100 meters ($h < 100$), $s = 1.0$ for altitude difference between 100 and 300 meters ($100 \leq h \leq 300$), and $s = 1.1$ for altitude differences of more than 300 meters ($h > 300$). Empty trips are not considered in the experiments, e.g., $d_{empty} = 0$ and $d_{loaded} = d$.

As explained in Section 4.2, energy and emission factors can be used to convert a TTW energy estimate (E^{TTW}) to a WTW emission estimate (G^{WTW}), see Figure 4.1. For trains hauled by electric locomotives, the emission factor resulting from the EU-28 average energy supply is used, i.e., $g^{WTW} = 137$ gCO₂e/MJ (EcoTransIT World Initiative; 2019, Tab. 52), and for trains hauled by locomotives that generate their power from diesel fuel, the emission factor resulting from a 7% bio-diesel is used, i.e., $g^{WTW} = 88.21$ gCO₂e/MJ (DIN EN 16258; 2012, Tab. A.4). For both train types, total WTW emissions are calculated with Formula (4.28).

$$G^{WTW} = E^{TTW} \cdot g^{WTW} \quad (4.28)$$

In the following sections, experimental results are mainly presented in terms of WTW emission rates r in gCO₂e/ton·km. These rates are computed by dividing total emissions G^{WTW} by the train's payload m_{tl} and the trip's distance d , see Formula (4.29).

$$r = \frac{G^{WTW}}{m_{tl} \cdot d} \quad (4.29)$$


 Figure 4.3: WTW emission rate r for a varying number of wagons n_w .

4.4.2 Number of wagons

Figure 4.3 shows the WTW emission rate r for a train with a varying number of wagons n_w . Results are presented for a train that is hauled by a diesel locomotive (Figure 4.3a) and for a train that is hauled by an electric locomotive (Figure 4.3b). It can be seen that an increasing number of wagons leads in all models other than MEET and under both engine types to degressive emission rates. In other words, the emission rate decreases with a larger number of wagons at a decreasing marginal rate. This is because some of the train’s total emissions are fix and independent of the number of wagons, such as the emissions caused from moving the locomotive. Thus, since total emissions are equally distributed over the train’s total payload in emission rate r , each additional wagon decreases the share of ‘wagon-independent’ emissions per payload and ton. In contrast, the MEET models already estimate a rate per (loaded) ton and kilometer, which makes their estimated emission rates independent of a varying number of wagons.

Remember that all of the considered models estimate an energy demand that is somehow independent of the engine type. Thus, differences between diesel and electric locomotives arise from energy factors, emission factors, and efficiency rates, which are assumed to be equal in all models and for all experiments. For each model, this leads to a similar pattern of emission rates for both engine types. This is why the following sections concentrate on results solely for one engine type, namely diesel.

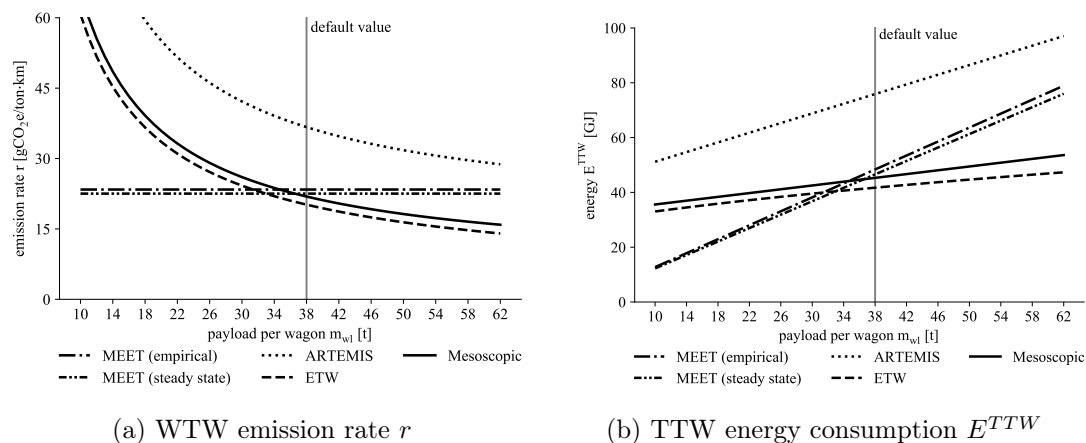


Figure 4.4: Emission rate and energy consumption for a varying payload per wagon m_{wl} (diesel train).

4.4.3 Payload per wagon

Figure 4.4 shows the train’s WTW emission rate r (Figure 4.4a) and the train’s TTW energy E^{TTW} (Figure 4.4b) for varying values of the payload per wagon m_{wl} . It can be seen that an increasing payload per wagon results in a degressive emission rate in the ARTEMIS, ETW, and Mesoscopic model. The explanation is similar to the one given for a varying number of wagons, see Section 4.4.2. In particular, an increasing payload per wagon decreases the share of ‘payload-independent’ emissions, such as the emissions caused from moving the locomotive or the wagon’s empty weight, per payload and ton, which leads to degressive emission rates in models other than MEET. In contrast, energy in the MEET models is already estimated per (loaded) ton and kilometer, which leads to constant emission rates under varying values for the payload per wagon. Total TTW energy E^{TTW} increases with a higher payload per wagon in all models. This increase is linear in the MEET models, the ARTEMIS model, and the Mesoscopic model and almost linear in the ETW model. Note that the ‘payload-independent’ energy can be easily identified in Figure 4.4b as it is at $m_{wl} = 0$. As mentioned before, energy estimates are directly linearly related to emission estimates through energy and emission factors, see Figure 4.1. This is why the following sections present results only for the emission rate r . However, all findings also apply to energy measures and the emission values can easily be converted to energy values simply by using the respective energy and emission factors.

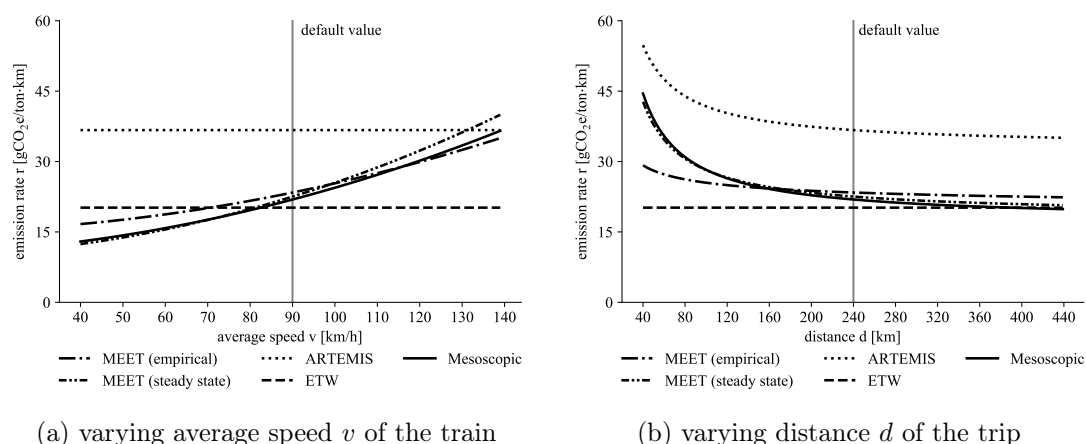


Figure 4.5: WTW emission rate r for a varying average speed v and a varying distance d (diesel train).

4.4.4 Speed

Figure 4.5a shows the WTW emission rate r for varying values of the train's average speed v . It can be seen that the average speed has no impact in the ARTEMIS model and the ETW model. For the ARTEMIS model, this is because the same speed-acceleration distribution from Figure 4.2 is used in all experiments. Clearly, this is unrealistic as different average speeds also result in different speed-acceleration distributions. Yet, it was not possible to find empirical data for all the speed-acceleration intervals that were considered in the experiments. For ETW, average speed has no impact on the emission rate because the ETW energy estimate only depends on the train's total weight and the trip's slope profile, see Formula (4.16). In contrast, the emission rate estimated with the MEET models or the Mesoscopic model increases quadratically with the average speed. The quadratical increase derives directly from the respective formulas, see Formulas (4.1) for MEET (empirical), (4.2) for MEET (steady state), and (4.24) for the Mesoscopic model.

4.4.5 Distance

Figure 4.5b shows the WTW emission rate r for varying values of the trip's distance d . As already described in the previous section on the impact of speed, the ETW energy estimate only depends on the train's total weight and the trip's slope profile. Thus, the traveled distance has no impact on the emission rate if it is estimated with the ETW model. For all other models, increasing distance leads to degressive emissions rates. This is because the models incorporate that increasing distance usually leads to fewer

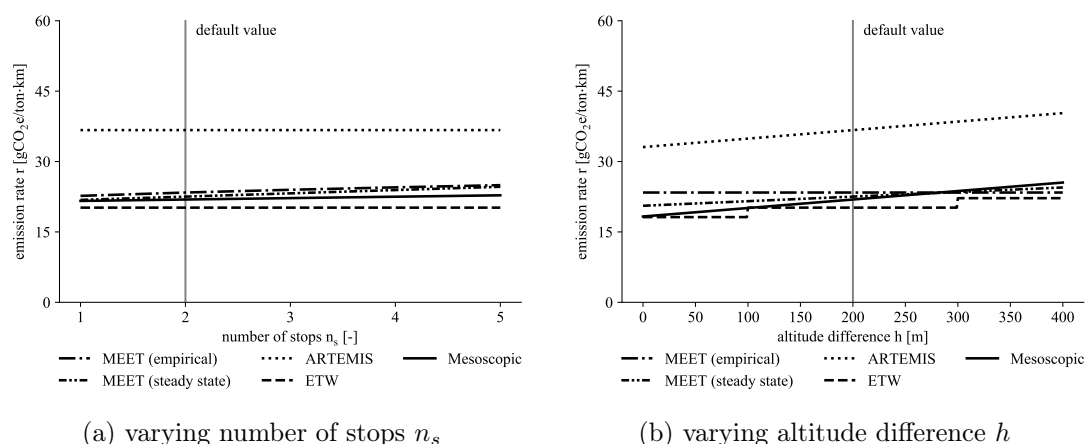


Figure 4.6: WTW emission rate r for a varying number of stops n_s and a varying altitude difference h (diesel train).

acceleration processes per kilometer. Thus, the emissions from acceleration processes become less relevant with increasing distance. Note that emission rates are very high for small distances (e.g., for $d < 80$). The reason for this is that most models are designed for typical train transportation scenarios which involve larger distances. For too short distances, estimates are therefore unrealistic. The empirical MEET model explicitly states that it should only be applied to trips of which the distance between the stops is between 80 and 200 kilometers.

4.4.6 Number of stops

The number of stops are used to capture the train's energy that results from acceleration processes. Such accelerations are required at the beginning of the trip as well as after each stop. Figure 4.6a shows that the WTW emission rate r increases with the number of stops in the MEET models and in the Mesoscopic model whereas it is constant in the ARTEMIS model and in the ETW model. For the ARTEMIS model, this is because the number of stops are not explicitly considered by the matrix approach. However, the approach implicitly considers the number of acceleration processes through the distribution of speed-acceleration combinations. More precisely, a higher number of stops usually implies a higher probability for intervals of low speed and high accelerations. But, as the same speed-acceleration distribution is used in all experiments, the number of stops has no impact here. The ETW model uses empirical data to estimate the energy and emissions. Similar to speed and distance, the number of stops is not considered as an independent variable which results in a constant emission rate for a varying number of the stops.

4.4.7 Altitude difference

Finally, Figure 4.6b shows the impact of the trip's gradient on the WTW emission rate r . There are two ways how the models consider this. Firstly, by using the altitude difference h between the origin and the destination (MEET steady state, ARTEMIS, and Mesoscopic) and secondly, by using slope profile s (ETW). The empirical MEET model does not consider altitudes, which results in constant emission rates. In contrast, increasing altitude differences result in continuously increasing emission rates in the MEET model (steady state), in the ARTEMIS model, and in the Mesoscopic model, whereas they result in discontinuously increasing emission rates in the ETW model. The last is because slope profile s is assumed to change at pre-defined altitude differences of $h = 200$ and $h = 400$ meters. Note that only positive changes (uphill) are considered in this experiment. However, the reverse results arise for downhill slopes. This is because the considered models do not differentiate between the direction (sign) of the slope which implicitly assumes a total recovery of the uphill consumed energy when going downhill again. Heinold and Meisel (2018) suggest using an adjusted variant for the slope that only considers parts of the recovered energy from negative slopes.

4.5 Selecting an appropriate model

As there exist numerous models for estimating emissions, it is a challenging task to select an appropriate model for a specific transport scenario, especially, as the availability of data often limits the choice of applicable models. For example, whereas a train's traveled distance might be known (or can be calculated from public sources), its actual speed and acceleration profile is often unknown. Some models, such as ETW, therefore concentrate on input factors that are easy to collect, e.g., a train's total weight. The experiments in the previous section have shown which input factors are most relevant to each of the models. Figure 4.7 sums up the results. The figure shows the impact of the train's number of wagons (row 1), the train's payload per wagon (row 2), the train's speed (row 3), the trip's distance (row 4), the trip's number of stops (row 5), and the trip's altitude difference (row 6) on each model's emission estimate (column 1 to 5). In contrast to Table 4.2, which indicates whether those parameters are considered in a model, or not, Figure 4.7 makes it easy to spot how they are captured in a model's emission rate. For example, looking at the ETW model (column 4), the emission rate decreases with an increasing number of wagons or payload per wagon, it remains constant for variations in speed, distance, or number of stops, and it discontinuously increases with increasing altitude differences.

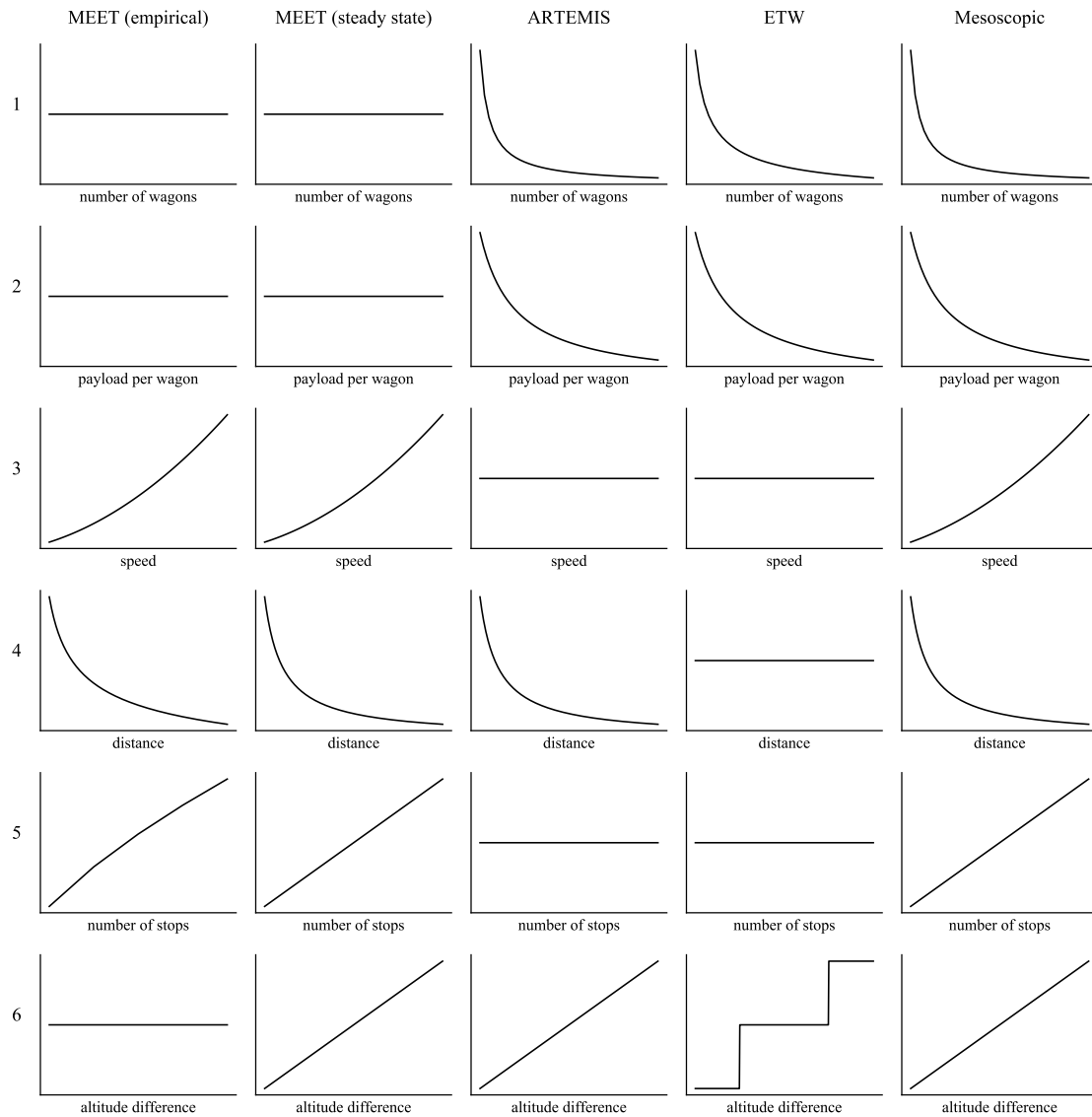


Figure 4.7: Impact of varying train and truck parameters (rows) on each model’s WTW emission rate (columns).

Similarly, for a specific parameter, it is easy to identify the parameter’s impact on each model’s emission rate. For example, looking at the row of parameter speed (row 3), it can be seen that the emission rate quadratically increases if it is estimated with the MEET models or the Mesoscopic model, whereas the emission rate is constant if it is estimated with the ARTEMIS model or the ETW model. However, the same speed-acceleration matrix is used in the ARTEMIS model, even for the experiments that vary speed and number of stops.

In addition to these common trip and train parameters, all of the models considered in this paper use some kind of statistical parameters or functions, such as a train's physical resistances, to estimate emissions. The availability of up-to-date values for these parameters might be another key consideration, especially, as regular updates might be required due to technological advancements. Overall, some models need only a few data inputs but generate quite coarse results. These models might still be useful in a rail project proposal or feasibility analysis. On the contrary, other models might be more preferred in detail design phases when the alignment of the transport scenario is almost determined, which might be the case for shippers or logistics service provider.

Anyhow, even with all input data available to apply the models, it is not possible to tell which of the models results in the 'best' estimate, as the 'true' emissions require an actual measurement of emissions. For example, the diesel default train used in the experiments results in emission rates of 20.17, 21.90, 22.52, and 23.39 gCO₂e/ton·km using the ETW, Mesoscopic, MEET (steady state), and MEET (empirical) model, respectively. While these estimates are similar to each other as well as similar to other estimates found in the literature, e.g., the Network for Transport Measures (2018) reports average emission rates of 23 gCO₂e/ton·km for diesel freight trains in the EU, it is not possible to say which of the models is absolutely better than another. Furthermore, the experiments in Section 4.4 have demonstrated that differences between the models might be significantly higher for other transport scenarios. Thus, it might not be reasonable to exclusively use one or another model, but, instead, use several models covering different aspects of the considered train and trip.

4.6 Conclusion

This paper has reviewed five emission estimation models for rail freight transportation. In particular, two models from the MEET project, the ARTEMIS model, the ETW model and the Mesoscopic model have been considered. These models quantify emissions by estimating a train's tank-to-wheel energy consumption. For this, the models use train and trip specific parameters that have been described in detail in this paper. Engine type specific energy and emission factors are then used to convert energy estimates into emission estimates.

An computational study has analyzed the impact of relevant parameters on the estimated emissions. In particular, results have been presented for varying values of a train's number of wagons, the payload per wagon, the average speed, the trip distance, the number of stops, and the altitude profile along the route. The analysis has shown that

the parameters impact on the well-to-wheel emission rate (gCO₂e/ton·km) is considered differently in the five models: increasing number of wagons or payloads per wagon lead to a degressive emission rate in three models and have no impact on the emission rate in two models, increasing speed increases the emission rate in three models and has no impact on the emission rate in two models, increasing distance decreases the emission rate in four models and has no impact on the emission rate in one model, an increasing number of stops increases the emission rate in three models and has no impact on the emission rate in two models, and an increasing altitude difference increases the emission rate in four models and has no impact on the emission rate in one model. This study has also discussed transport scenarios in which each of the models can be applied to. Here, the availability of data plays a vital role as some models require a substantial amount of specific input data, such as technical parameters about the locomotive. Despite of this, it has been shown that the models lead to similar estimates for a realistic default train. Overall, it has been shown that it is the considered transport scenario that decides which model is most appropriate to estimate emissions from rail freight transportation.

This study has concentrated on the most prominent parameters but did not vary all possible parameters. For example, the rolling and aerodynamic coefficients (used in the ARTEMIS and Mesoscopic model) have not been varied in the experiments, although they can have a significant impact on the estimated energy/emissions. However, a proper setting of these parameters is challenging as they depend on, for example, train-type specific characteristics, and it would be interesting to provide an overview of these parameters for several common train-types. The matrix approach of the ARTEMIS model uses trip-specific distribution matrices to capture realistic speed-acceleration combinations. The same distribution from a freight train in Denmark has been used throughout the experiments. It is left for future research to collect real data for trains' driving cycles in order to build distribution matrices for additional transportation scenarios. Finally, Hickman et al. (1999) and Lindgreen and Sorenson (2005a,b) already provide some findings on the actual emissions that are emitted by a freight train. It would be interesting to update and extend these results and, for example, to investigate the impact of technological improvements on the emitted emission.

Acknowledgments

This research was supported by the German Research Foundation (DFG) under reference 268276815. Special thanks go to three anonymous reviewers for their valuable comments which helped to improve the manuscript considerably.

4.7 Appendix A. Python scripts

The Python code with the implementations of the emission estimation models are available as additional files in the electronic appendix of this paper. These scripts can be used to reproduce all results from the experimental study. They can also be used for performing own calculations. All data and material is also available from the corresponding author on request.

Bibliography

- Craig, A. J., Blanco, E. E. and Sheffi, Y. (2013). Estimating the CO₂ intensity of intermodal freight transportation, *Transportation Research Part D: Transport and Environment* **22**: 49–53.
- de Miranda Pinto, J. T., Mistage, O., Bilotta, P. and Helmers, E. (2018). Road-rail intermodal freight transport as a strategy for climate change mitigation, *Environmental Development* **25**: 100–110.
- Demir, E., Bektaş, T. and Laporte, G. (2011). A comparative analysis of several vehicle emission models for road freight transportation, *Transportation Research Part D: Transport and Environment* **16**(5): 347–357.
- DIN EN 16258 (2012). Methodology for calculation and declaration of energy consumption and GHG emissions of transport services (freight and passengers).
- EcoTransIT World Initiative (2019). Ecological Transport Information Tool for Worldwide Transports. Methodology and Data. Update 2019. . https://www.ecotransit.org/download/EcoTransIT_World_Methodology_Data_Update_2019.pdf (visited on 20.06.2020).
- Eurostat (2020). Greenhouse gas emission statistics - emission inventories. https://ec.europa.eu/eurostat/statistics-explained/index.php?title=Greenhouse_gas_emission_statistics_-_emission_inventories (visited on 20.06.2020).
- FIS (2020). Forschungs-Informationssystem: Betriebstechnische Grenzparameter für Güterzüge. . <https://www.forschungsinformationssystem.de/servlet/is/324625/> (visited on 20.06.2020).
- GHG Protocol (2020). The greenhouse gas protocol: A corporate accounting and reporting standard. <https://ghgprotocol.org/sites/default/files/standards/ghg-protocol-revised.pdf> (visited on 20.06.2020).
- Heinold, A. and Meisel, F. (2018). Emission rates of intermodal rail/road and road-only transportation in Europe: A comprehensive simulation study, *Transportation Research Part D: Transport and Environment* **65**: 421–437.
- Heinold, A. and Meisel, F. (2019). Emission oriented vs. time oriented routing in the european intermodal rail/road freight transportation network, *in* C. Bierwirth, K. Thomas

- and D. Sackmann (eds), *Logistics Management. Lecture Notes in Logistics.*, Springer, pp. 188–202.
- Hickman, J., Hassel, D., Joumard, R., Samaras, Z. and Sorenson, S. (1999). Methodology for calculating transport emissions and energy consumption. <https://trimis.ec.europa.eu/sites/default/files/project/documents/meet.pdf> (visited on 20.06.2020).
- International Energy Agency (2019). The future of rail: Opportunities for energy and the environment. <https://www.iea.org/reports/the-future-of-rail> (visited on 20.06.2020).
- International Transport Forum (2019). ITF Transport Outlook 2019. . https://doi.org/10.1787/transp_outlook-en-2019-en (visited on 20.06.2020).
- IPPC (2018). Global warming of 1.5°C. . https://www.ipcc.ch/site/assets/uploads/sites/2/2019/06/SR15_Full_Report_High_Res.pdf (visited on 20.06.2020).
- Kirschstein, T. and Meisel, F. (2015). GHG-emission models for assessing the eco-friendliness of road and rail freight transports, *Transportation Research Part B: Methodological* **73**: 13–33.
- Kiyota, A. S., Yoshizaki, H. T. Y. and Massara, V. M. (2015). Analysis of greenhouse gases in the emissions of Brazilian freight transport, *International Journal of Low-Carbon Technologies* **10**(4): 438–440.
- Lindgreen, E. B. G. and Sorenson, S. C. (2005a). Driving resistance from railroad trains, *Technical report*, Technical University of Denmark. Department of Mechanical Engineering.
- Lindgreen, E. B. G. and Sorenson, S. C. (2005b). Simulation of energy consumption and emissions from rail traffic, *Technical report*, Technical University of Denmark. Department of Mechanical Engineering.
- Moro, A. and Lonza, L. (2018). Electricity carbon intensity in European Member States: Impacts on GHG emissions of electric vehicles, *Transportation Research Part D: Transport and Environment* **64**: 5–14.
- Network for Transport Measures (2018). Rail cargo transport baselines 2018. <https://www.transportmeasures.org/en/wiki/evaluation-transport-suppliers/rail-cargo-transport-baselines-2017/> (visited on 20.06.2020).

Piecyk, M., Cullinane, S. and Edwards, J. (2012). Assessing the external impacts of freight transport, *in* A. McKinnon, M. Browne and A. Whiteing (eds), *Green logistics: Improving the environmental sustainability of logistics*, 2 edn, Kogan Page Limited London, New York, chapter 2, pp. 31–50.

Smart Freight Centre (2020). Global logistics emissions council (GLEC): The global method for calculation and reporting of logistics emissions. <https://www.smartfreightcentre.org/en/how-to-implement-items/what-is-glec-framework/58/> (visited on 20.06.2020).

The Times (2020). Xi's 'Silk Railway' halves delivery time to Europe. <https://www.thetimes.co.uk/article/xis-silk-railway-halves-delivery-time-to-europe-wft98n7z6> (visited on 20.06.2020).

Chapter 5

Emission Limits and Emission Allocation Schemes in Intermodal Freight Transportation

Publication status Published in 2020: *Transportation Research Part E: Logistics and Transportation Review* 141: 101963.

Arne Heinold and Frank Meisel

School of Economics and Business, Kiel University, Kiel, Germany

Abstract The problem addressed in this paper seeks for an optimal routing of freight orders through an intermodal transportation network. We consider the case of environmentally aware customers that request to ship orders with no more than a specified amount of greenhouse gases, which establishes so-called emission limits. In order to ensure that a routing plan complies with each order's emission limit, it is necessary to estimate emissions caused by the used transport services and to allocate these emissions to the orders. We model this problem under cost-, emission- and service-objectives and apply it to an intermodal rail/road network in Europe.

Keywords Intermodal Transportation, Service Selection Problem, Emission Limits, Emission Estimation, Emission Allocation

5.1 Introduction

Within the last years, an increasing environmental awareness in different areas of modern societies can be observed. One form of this development are eco-labels that indicate the energy consumption or the carbon footprint of products or services (Thøgersen and Nielsen; 2016). It is not surprising that such overall environmental cautiousness is carried over to the decision-making processes in transportation and logistics companies (e.g., DHL; 2019; UPS; 2019).

In this study, we model a service selection problem (SSP) where a set of orders, which is placed by customers, is to be routed through an intermodal network of road and rail transportation services. Thereby, we consider the case of environmentally aware customers that request to ship orders with no more than a specified amount of greenhouse gases, so called *emission limits*. The planning task is (i) to come up with a routing plan, (ii) to estimate the corresponding emissions, and (iii) to implement emission allocation schemes such that the solution complies with each order's emission limit. The routing plan indicates the services used as well as the transshipment processes required between the services. Overall, the problem addressed in this paper covers two types of decisions. Firstly, the decision about the routing and transshipment of the orders and, secondly, the decision about each service's emission allocation scheme. Since the orders are typically placed by customers and the services are typically operated by one or several companies, these decisions might be made by different actors. However, there are also settings where one decision maker is in charge of making both decisions. For example, a freight agent could act between the customers and the service operators, selecting both the services to be used and the emission allocation schemes that fit to the customers' environmental preferences. The freight agent then prescribes the required schemes for the service operators (e.g., if the agent possesses the market power) or uses this information for negotiations with the service operators. For this reason, we consider a model where both decisions are made holistically by one decision maker. Throughout this study, we consider an *egalitarian allocation* scheme and a *payload-based allocation* scheme as alternatives for emission allocation. With these schemes, we allocate emissions from a transportation service, such as a truck or a train, to orders that use this service. In particular, the egalitarian scheme allocates the same amount of emissions to each order of a service and the payload-based scheme allocates emissions to orders based on the orders' contribution to a service's overall payload. For reasons of comparison, we also present results for the case where all services consistently use the egalitarian allocation scheme and for the case where all services consistently use the payload-based allocation scheme. Note that by

letting the model select the services' allocation schemes, an order's route might involve services that use different schemes. This helps in respecting an order's emission limit. For example, if an order exceeds its emission limit in a routing-solution under a consistent application of a single allocation scheme, then, by changing the allocation scheme on some of the used services, the emissions assigned to this particular order could fall below the emission limit. The freedom to apply different allocation schemes on different services is in accordance with the European norm on the calculation and declaration of emissions of transport services (DIN EN 16258; 2012). Overall, the **Service Selection Problem** in our study considers **T**ransshipment processes, **A**llocation schemes per service and **L**imits on the emissions per order in an **E**mission-oriented setting. We refer to this problem as **SSP-TALE** and formulate it for cost-, emission- and service-objectives.

With this study, we are, to the best of our knowledge, the first to present the problem of routing orders with order-specific emission limits through an intermodal network of transportation services where the emission allocation schemes are selected for each service. We show how to model and solve the corresponding problem. We analyze the impact of orders' emission limits, which serve as an indicator for customers' environmental cautiousness, on the routing of individual orders as well as their impact on the overall network costs and emissions. In addition, we show how the choice of emission allocation schemes can change the routing plan and, thus, the optimal solution under each of the considered objectives. Finally, we also present insights on the settings in which the model is likely to select either the egalitarian or the payload-based emission allocation scheme for the services in the considered network.

The rest of this paper is organized as follows. Section 5.2 presents an overview of relevant literature. Section 5.3 describes the SSP-TALE and its mathematical formulation. Section 5.4 presents extensive experimental results that are based on real-world data. In particular, we consider the routing of orders between Portugal and the Netherlands and between Italy and Denmark in the European intermodal rail/road network. Section 5.5 concludes this paper.

5.2 Literature review

In this section, we provide an overview of studies on environmentally oriented routing in transportation networks. We mainly focus on studies that address intermodal freight networks consisting of road and rail services. We also include some relevant unimodal studies that address the allocation of emissions to orders. Table 5.1 shows an overview of all considered studies, together with the central problem features that are relevant in

Table 5.1: Overview of selected relevant literature.

reference			objective			emissions			emission limits	
	multimodal	unimodal	costs	emissions	service level / time	transportation	transshipment	allocation selection ^a	network wide	per order
Bauer et al. (2010)	✓	-	-	✓	✓	✓	-	-	-	-
Rudi et al. (2016)	✓	-	✓	✓	✓	✓	✓	-	-	-
Sun and Lang (2015)	✓	-	✓	✓	-	✓	-	-	-	-
Qu et al. (2016)	✓	-	✓	✓	-	✓	-	-	-	-
Baykasoğlu and Subulan (2016)	✓	-	✓	✓	✓	✓	-	-	-	-
Demir et al. (2016)	✓	-	✓	✓	✓	✓	✓	-	-	-
Sharma and Mathew (2011)	✓	-	-	✓	✓	✓	-	-	-	-
Heinold and Meisel (2018)	✓	-	-	✓	-	✓	✓	-	-	-
Heinold and Meisel (2019)	✓	-	-	✓	✓	✓	✓	-	-	-
Lam and Gu (2016)	✓	-	✓	-	✓	✓	-	-	✓	-
Kirschstein and Bierwirth (2018)	-	✓	-	✓	-	✓	-	✓	-	-
Kellner and Schneiderbauer (2019)	-	✓	-	✓	-	✓	-	✓	-	-
this study	✓	-	✓	✓	✓	✓	✓	✓	(✓)	✓

^a studies that use multiple schemes for allocating emissions to orders

relation to our study. A more general overview of studies concerning multimodal freight transportation is provided by SteadieSeifi et al. (2014).

Bauer et al. (2010) extend a service network design problem by considering a minimization of total emissions emitted by the services in the network as well as the more traditional objective of minimizing total transportation time of orders. The authors perform a computational study for a rail/road network that covers Austria, the Czech Republic and Poland and compare solutions for both objectives. In contrast to the time minimizing solution, the emission minimizing solution results in fewer used services and higher waiting times for transshipping orders between services. Rudi et al. (2016) formulate a capacitated multi-commodity network flow model with the objectives to minimize costs, transit times and emissions of the transport and transshipment processes. The model considers in-transit inventory and finds an optimal solution for the routing and transshipment of products. Sun and Lang (2015) consider the problem of routing commodities through a rail/road transportation network. The authors consider schedule-based rail services and time-flexible road services and apply their model to a large-scale problem of bringing containers from inland cities to seaports in China. The

objective is to minimize total costs for transportation, transshipment, inventory, pick-up and delivery as well as CO₂ emissions from transportation. Qu et al. (2016) present a similar problem and consider services' fixed and variable costs, transshipment costs as well as emissions. Here, the authors also consider transshipment costs that occur if an order has to change between one mode of transportation to another (e.g., from road to rail). Baykasoğlu and Subulan (2016) consider a multimodal transportation problem with the objectives to minimize transport costs, transit time or transport-related emissions. The authors consider a multi-period scenario and test their model on data from an international logistics company in Turkey. Demir et al. (2016) describe a green intermodal service network design problem with travel time uncertainty. The objective of the model is to minimize a weighted cost function that considers direct transportation, transit time, and emissions. Thereby, the authors consider emissions from transportation and transshipment processes. A sample average approximation algorithm is used to find robust solutions under uncertain travel times. Sharma and Mathew (2011) consider as objectives the minimization of transit time and transport emissions in a multi-objective network design problem with various road modes. The authors formulate the problem as a bi-level model with an upper level decision on the road network design and a lower level decision on the routing in this network. Heinold and Meisel (2018) provide a comprehensive overview of emission rates for European rail/road intermodal and road-only transportation. For this, the authors conduct a systematic simulation study for the rail/road Trans-European Transport Network where they consider emissions from transportation and transshipment processes. In a follow-up study, Heinold and Meisel (2019) propose a model to route an individual order through an intermodal transportation network with the objective to minimize total emissions or transit time. The authors measure emissions and transit time from transportation and transshipment processes under both objectives and present comprehensive results for a large number of artificial orders that are shipped across Europe. Lam and Gu (2016) present a model to find an optimal routing for shipping containers in a port hinterland by using trucks, trains, and barges. A bi-objective optimization approach is used to demonstrate the trade-offs between costs and transit time. The model considers the environmental impact of a solution by restricting the total amount of emitted greenhouse gases through a hard constraint. The authors argue that such limit could be imposed by governmental or regulatory authorities. Chen et al. (2014) consider emission reduction targets in an intermodal waterway-road network. The authors provide a model that determines a routing for the orders under the objective of minimizing state subsidies. Thereby, restrictions enforce certain carbon emission reduction targets, such as reducing network emissions by at least 15%. Similarly, Chen and

Wang (2016) analyze the selection of transport modes under different emission reduction policies. In particular, the authors consider the cap policy and the cap-and-trade policy that both set an overall limit for the network emissions. Anyhow, the latter two studies are only little related to our research as they consider the problem from the point of view of transport policy makers whereas our paper considers the problem from the point of view of a logistics service provider.

The previously mentioned studies apply to networks with multiple modes of transportation. Thereby, total emissions are either considered as an objective to minimize or as a limit on the overall network emissions. Studies that incorporate the selection of emission allocation schemes into routing decisions so far consider only one transportation mode. For example, Kirschstein and Bierwirth (2018) propose a road-only selective traveling salesman problem with emission allocation schemes. The problem is to find a vehicle route that minimizes the amount of greenhouse gases that is allocated to one specific order. For this purpose, the model also decides on the emission allocation scheme to use. Here, either a distance based allocation or an egalitarian allocation can be selected to distribute the total route-emissions among the orders. Kellner and Schneiderbauer (2019) further analyze the effect of allocation schemes in road transportation. The authors consider three problem types: a vehicle routing problem (VRP), a road-only network flow model (NFM), and a mixed VRP-NFM model. The authors apply various allocation schemes, including schemes that are based on principles of game theory, to each considered problem type. The authors show by experiment that emission allocation schemes that are based on the orders' individual travel distances lead to emission allocations that are similar to an allocation based on Shapley values, which serves as a benchmark allocation method. Note that Kirschstein and Bierwirth (2018) and Kellner and Schneiderbauer (2019) both analyze schemes that allocate total network emissions to individual orders. In contrast, we consider this in more detail for a situation where emission allocation schemes are selected for each service, rather than applying one scheme to the overall network. With this, it is possible to use different emission allocation schemes for the services within the considered transportation network. Accordingly, we do not consider allocation schemes that use the Shapley value or the travel distance of the orders, as these imply using the same allocation scheme for all services. Instead, we concentrate on the service-specific egalitarian scheme and payload-based scheme.

In contrast to the existing literature, the problem addressed in this paper is to route orders with *individual emission limits* through an intermodal network where we consider emissions from transportation and transshipment processes and also *select allocation schemes* to allocate these emissions to orders. The emission limits reflect individual

customer preferences on the environmental impact of their shipment. As shown above, hard emission limits on a network level have been considered in some studies but no study considered emission limits per order so far. We fill this gap by presenting a model that considers emission limits per order, which, through the sum over all orders' emission limits, also imposes an overall network limit. We implement such limits as soft constraints and use the number of orders that can be routed within their emission limit as a service-oriented performance measure. We do not consider time as an additional service-oriented measure although some of the above studies include this in their analysis. This is because the focus of our study is on describing interdependencies of orders' emission limits, orders' routings, and services' emission allocation schemes. We refer to Heinold and Meisel (2019) for a study that compares the emission-oriented and the time-oriented routing of orders in an intermodal network. Furthermore, although we formulate the model as an intermodal transportation problem, it can also be applied to settings with only one mode of transportation, simply by restricting the set of considered services. In our experiments, we consider orders each of a size of one or more container units (TEU) as these are candidates for intermodal transportation. However, the presented formulation of the SSP-TALE also fits to scenarios with smaller order sizes.

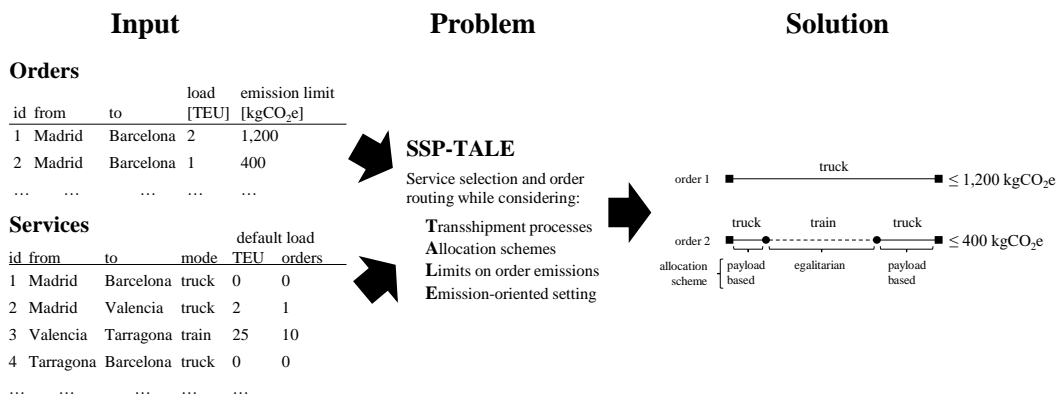


Figure 5.1: Structure of the service selection problem with transshipment processes, allocation schemes per service and limits on order emissions in an emission-oriented setting (SSP-TALE).

5.3 The SSP-TALE model

5.3.1 Problem description and notation

In the following, we provide a formal description of the considered problem. An overview of the used notation is provided in Table 5.2. We model the transportation network as a graph $\mathcal{G}(\mathcal{N}, \mathcal{S})$. The set of nodes \mathcal{N} represents the origins and destinations of orders and services. The set of arcs \mathcal{S} describes all services that operate between the nodes of the network. Each service $s \in \mathcal{S}$ connects an origin node a_s and a destination node b_s . We allow parallel services between two nodes in order to model services of different types (e.g., truck or train) that connect the same pair of nodes. The problem of the SSP-TALE is to find an optimal routing plan for a given set of orders \mathcal{O} in network \mathcal{G} , as is conceptually sketched in Figure 5.1.

For each order $o \in \mathcal{O}$, a number q_o of 20-ft container units (TEU) is to be shipped from a given origin node $a_o \in \mathcal{N}$ to a given destination node $b_o \in \mathcal{N}$ ($a_o \neq b_o$). In our study, each TEU corresponds to 12 tons of cargo, such that two TEU are equivalent to one full truck load of a 40-ft container à 24 tons.

The binary decision variable x_{os} is used to denote if order o uses service s ($x_{os} = 1$) or not ($x_{os} = 0$). Similarly, binary decision variable y_{os} is used to denote if order o requires transshipment at the destination b_s of service s ($y_{os} = 1$) or not ($y_{os} = 0$). To identify transshipment processes, the parameter $suc_s \in \mathcal{S}$ indicates the succeeding service of a service $s \in \mathcal{S}$. For example, if two adjacent train services s_1 and s_2 with $b_{s_1} = a_{s_2}$ are conducted by the same train, we have $suc_{s_1} = s_2$. Then, an order that uses both services s_1 and s_2 requires no transshipment at location b_{s_1} as it stays on the train. However, transshipment is required at node $b_{s_1} = a_{s_2}$ if s_2 is not conducted by the same train, which is indicated by parameter $suc_{s_1} \neq s_2$. Note that using binary decision variables to indicate if an order o is transported with or transshipped after a service s implies that payload q_o is not split when being transported from a_o to b_o . Transporting one TEU with service $s \in \mathcal{S}$ causes costs r_s^{tport} and emissions e_s^{tport} . Transshipping one TEU at node $i \in \mathcal{N}$ causes costs r_i^{tship} and emissions e_i^{tship} . For a specific service $s \in \mathcal{S}$, we denote by \bar{c}_s the capacity and by \underline{c}_s the default load of that service, both expressed in TEU. Here, default load \underline{c}_s refers to the amount of transport units that use service s independently of the routing of orders \mathcal{O} . Thus, the total load of a service s composes of its default load \underline{c}_s and order load $\sum_{o \in \mathcal{O}} x_{os} \cdot q_o$. The number of orders that make up for default load \underline{c}_s is denoted by \underline{m}_s .

We use equivalents of carbon dioxide (CO₂e) to subsume the environmental impact of several relevant greenhouse gases and refer to these jointly as "emissions" (e.g., Piecyk

et al.; 2012). The SSP-TALE considers emission limits set by customers. Such a limit \bar{e}_o states the maximal amount of emissions (including emissions from transportation as well as emissions from transshipment) that is allowed for order $o \in \mathcal{O}$. We use five decision variables to capture emissions: (i) E_s^c states the amount of emissions of a service s that are allocated to its default orders \underline{m}_s , (ii) E_{os}^{tport} states the transport emissions of a service s that are allocated to order o , (iii) E_{oi}^{tship} states the transshipment emissions of order o

Table 5.2: Sets, parameters and decision variables in the SSP-TALE.

name	description
nodes	
\mathcal{N}	set of nodes ($\mathcal{N} = \bigcup_{o \in \mathcal{O}} \{a_o, b_o\} \cup \bigcup_{s \in \mathcal{S}} \{a_s, b_s\}$)
r_i^{tship}	costs in \$/TEU caused by transshipping one TEU at node $i \in \mathcal{N}$
e_i^{tship}	emissions in kgCO ₂ e/TEU caused by transshipping one TEU at node $i \in \mathcal{N}$
orders	
\mathcal{O}	set of orders
q_o	payload of order $o \in \mathcal{O}$ (in TEU)
a_o, b_o	origin/destination location (node) of order $o \in \mathcal{O}$, $a_o, b_o \in \mathcal{N}$
\bar{e}_o	emission limit of order $o \in \mathcal{O}$ (in kgCO ₂ e)
services	
\mathcal{S}	set of services
a_s, b_s	origin/destination location (node) of service $s \in \mathcal{S}$, $a_s, b_s \in \mathcal{N}$
suc_s	succeeding service of service $s \in \mathcal{S}$, $suc_s \in \mathcal{S}$
\underline{c}_s	default load of service $s \in \mathcal{S}$ (in TEU)
\bar{c}_s	maximal load (capacity) of service $s \in \mathcal{S}$ (in TEU)
\underline{m}_s	number of orders that make up for default load \underline{c}_s of service $s \in \mathcal{S}$
r_s^{tport}	cost rate (\$/TEU) for transporting one TEU with service $s \in \mathcal{S}$
e_s^{tport}	emission rate (kgCO ₂ e/TEU) for transporting one TEU with service $s \in \mathcal{S}$
decision variables	
x_{os}	= 1 if order $o \in \mathcal{O}$ uses service $s \in \mathcal{S}$, 0 otherwise
y_{os}	= 1 if order $o \in \mathcal{O}$ is transshipped at the end of service $s \in \mathcal{S}$ (i.e., at node $b_s \in \mathcal{N}$), 0 otherwise
z_s	= 1 if the egalitarian and = 0 if the payload-based allocation scheme is used for service $s \in \mathcal{S}$
E_s^c	emissions allocated to default orders \underline{m}_s of service $s \in \mathcal{S}$
E_{os}^{tport}	emissions allocated to order $o \in \mathcal{O}$ for using service $s \in \mathcal{S}$
E_{oi}^{tship}	emissions from transshipping order $o \in \mathcal{O}$ at node $i \in \mathcal{N}$
E_o^{ex}	excess emissions, i.e., the amount of emissions allocated to order $o \in \mathcal{O}$ that exceeds emission limit \bar{e}_o
E_o^{lim}	= 1 if emissions allocated to order o exceed the order's emission limit \bar{e}_o ($E_o^{ex} > 0$), 0 otherwise

at a node $i \in \mathcal{N}$, (iv) E_o^{ex} states the amount of emissions that exceeds the emission limit \bar{e}_o of order o and (v) E_o^{lim} is a binary variable to indicate if emissions of order o are higher than its limit ($E_o^{ex} > 0 \implies E_o^{lim} = 1$), or not ($E_o^{ex} = 0 \implies E_o^{lim} = 0$). Furthermore, the binary decision variable z_s is equal to 1 if the egalitarian scheme (EA) is used for allocating emissions to orders of service s . If $z_s = 0$, the payload-based allocation scheme (PA) is used for this service.

For a service $s \in \mathcal{S}$, the egalitarian scheme ($z_s = 1$) allocates the same amount of emissions to all orders that use the service, independent of each order's actual payload. Thereby, the set of orders comprises both, the \underline{m}_s default load orders and those orders $o \in \mathcal{O}$ that are assigned to the service by the model (i.e., $x_{os} = 1$). For an order $o \in \mathcal{O}$ that uses service $s \in \mathcal{S}$, the allocated transport emissions E_{os}^{tport} are then determined by Formula (5.1). Here, the nominator describes the total transport emissions $e_s^{tport} \cdot (\underline{c}_s + \sum_{o' \in \mathcal{O}} q_{o'} \cdot x_{o's})$ of service s and the denominator corresponds to the total number of orders $\underline{m}_s + \sum_{o' \in \mathcal{O}} x_{o's}$ that use service s . Note that Formula (5.1) is non-linear. We provide in Section 5.3.2 a linearized formulation of the respective model constraints.

$$(z_s = 1 \wedge x_{os} = 1) \implies E_{os}^{tport} = \frac{e_s^{tport} \cdot (\underline{c}_s + \sum_{o' \in \mathcal{O}} q_{o'} \cdot x_{o's})}{\underline{m}_s + \sum_{o' \in \mathcal{O}} x_{o's}}, \forall o \in \mathcal{O}, s \in \mathcal{S} \quad (5.1)$$

In contrast, a service $s \in \mathcal{S}$ that uses the payload-based scheme ($z_s = 0$) allocates the same amount of emissions to each transported TEU and, thus, considers an order's contribution q_o to the total load ($\underline{c}_s + \sum_{o' \in \mathcal{O}} q_{o'} \cdot x_{o's}$) of this service, see Formula (5.2). Here, the total emissions of service s are allocated equally among all TEUs of this service and are then multiplied with the number of TEUs that correspond to order o .

$$\begin{aligned} (z_s = 0 \wedge x_{os} = 1) \implies E_{os}^{tport} &= q_o \cdot \frac{e_s^{tport} \cdot (\underline{c}_s + \sum_{o' \in \mathcal{O}} q_{o'} \cdot x_{o's})}{\underline{c}_s + \sum_{o' \in \mathcal{O}} q_{o'} \cdot x_{o's}} \\ &= q_o \cdot e_s^{tport}, \forall o \in \mathcal{O}, s \in \mathcal{S} \end{aligned} \quad (5.2)$$

Note that, irrespective of the applied allocation scheme, transport emissions of service $s \in \mathcal{S}$ are only allocated to order $o \in \mathcal{O}$ if the order uses this service, i.e., ($x_{os} = 0$) $\implies E_{os}^{tport} = 0$. Emissions from transshipping an order $o \in \mathcal{O}$ at the end-node b_s of service $s \in \mathcal{S}$ are fully assigned to the order, i.e., $E_{ob_s}^{tship} = q_o \cdot e_s^{tship} \cdot y_{ob_s}$. An illustrative example of the SSP-TALE model is provided in Appendix A.

5.3.2 Optimization model

In this section, we present a MIP formulation for the SSP-TALE, considering four performance measures F1 to F4 that can serve as objectives, see Functions (5.3a) to (5.3d). The orders' total costs and emissions from transportation and transshipment are calculated by performance measures "order costs" (F1) and "order emissions" (F2), respectively. The total excess emissions that result from exceeding orders' emission limits are calculated by performance measure "excess emissions" (F3). The number of orders that exceed their emission limit are calculated by performance measure "red orders" (F4). We solve this multi-objective problem hierarchically, i.e., we consider one of these performance measures as primary objective and the others as subordinate objectives. For example, using F1 (order costs) as primary objective and F2 (order emissions) as secondary objective results in minimal emissions for order set \mathcal{O} within the cost-minimizing solution. Of course, such a multi-objective problem can also be solved with other techniques. Linear weighting might be used but it is then the task to find proper weights for performance measures of different units. We refer to Marler and Arora (2004), Jozefowiez et al. (2008), and Deb (2014) for an overview of multi-objective optimization. In our study, we use the hierarchical approach as it clearly distincts the roles of the performances measures. In our experiments in Section 5.4, we use each combination of two out of the four measures F1 to F4 as primary and subordinate objectives, which leads to a total of 12 hierarchical objective-pairs being considered.

$$\min F1 = \sum_{o \in \mathcal{O}} \sum_{s \in \mathcal{S}} q_o \cdot (r_s^{tport} \cdot x_{os} + r_{b_s}^{tship} \cdot y_{os}) \quad \text{"order costs"} \quad (5.3a)$$

$$\min F2 = \sum_{o \in \mathcal{O}} \left(\sum_{s \in \mathcal{S}} E_{os}^{tport} + \sum_{i \in \mathcal{N}} E_{oi}^{tship} \right) \quad \text{"order emissions"} \quad (5.3b)$$

$$\min F3 = \sum_{o \in \mathcal{O}} E_o^{ex} \quad \text{"excess emissions"} \quad (5.3c)$$

$$\min F4 = \sum_{o \in \mathcal{O}} E_o^{lim} \quad \text{"red orders"} \quad (5.3d)$$

subject to

$$\sum_{s \in \mathcal{S} | a_s = a_o} x_{os} = 1, \quad \forall o \in \mathcal{O} \quad (5.4)$$

$$\sum_{s \in \mathcal{S} | b_s = b_o} x_{os} = 1, \quad \forall o \in \mathcal{O} \quad (5.5)$$

$$\sum_{s \in \mathcal{S} | b_s = i} x_{os} = \sum_{s \in \mathcal{S} | a_s = i} x_{os}, \forall o \in \mathcal{O}, i \in \mathcal{N} \setminus \{a_o, b_o\} \quad (5.6)$$

$$\sum_{s \in \mathcal{S} | b_s = a_o} x_{os} + \sum_{s \in \mathcal{S} | a_s = b_o} x_{os} = 0, \forall o \in \mathcal{O} \quad (5.7)$$

Constraint (5.4) states that each order $o \in \mathcal{O}$ has to depart at its origin a_o and Constraint (5.5) states that the order has to arrive at its destination b_o . Constraint (5.6) describes each order's balance of flow at all other nodes of the network, i.e., an order which enters a node also has to leave that node. Constraint (5.7) prevents subtours by prohibiting orders to use services that arrive at their origin a_o or depart at their destination b_o . Thus, the constraint ensures for all orders a cycle-free routing from the origin- to the destination-nodes.

$$y_{os} \geq x_{os} - x_{o, suc_s}, \forall o \in \mathcal{O}, s \in \mathcal{S} \quad (5.8)$$

$$c_s + \sum_{o \in \mathcal{O}} q_o \cdot x_{os} \leq \bar{c}_s, \forall s \in \mathcal{S} \quad (5.9)$$

Constraint (5.8) is used to set the transshipment decision variable y_{os} . Here, a transshipment operation y_{os} for an order o after using a service s is only required if service's s succeeding service suc_s is not used by this order. Decision variable y_{os} is never set unintentionally to value 1 as transshipment operations result in costs and emissions, one of which is always minimized in objectives F1 to F4. Constraint (5.9) describes the capacity restrictions of the services. Note that this constraint also implies that the complete order quantity q_o is shipped with service s if this service is used by order o ($x_{os} = 1$).

$$E_{oi}^{tship} = e_i^{tship} \cdot q_o \cdot \sum_{s \in \mathcal{S} | b_s = i} y_{os}, \forall o \in \mathcal{O}, i \in \mathcal{N} \quad (5.10)$$

$$E_s^c + \sum_{o \in \mathcal{O}} E_{os}^{tport} = e_s^{tport} \cdot \left(c_s + \sum_{o \in \mathcal{O}} q_o \cdot x_{os} \right), \forall s \in \mathcal{S} \quad (5.11)$$

$$E_{os}^{tport} \leq M_{os}^1 \cdot x_{os}, \forall o \in \mathcal{O}, s \in \mathcal{S} \quad (5.12)$$

$$E_s^c = 0, \forall s \in \mathcal{S} | \underline{m}_s = 0 \quad (5.13)$$

Emissions that result from transshipment operations are calculated by Constraint (5.10) and emissions that result from transportation are calculated by Constraint (5.11). Note

that Constraint (5.11) also ensures that all transport emissions are distributed among the default load and the orders $o \in \mathcal{O}$, which implies that all emissions of a service are allocated. Constraint (5.12) ensures that emissions from a service s can only be allocated to an order o if this order uses service s ($x_{os} = 1$). Here, M_{os}^1 is a sufficiently large positive number ("big M ") whose value is defined in Appendix B together with all other M -values appearing in the following constraints. Constraint (5.13) states that no emissions E_s^c can be allocated to a service if a service has no default load ($\underline{m}_s = 0$).

$$E_{o_1s}^{tport} - E_{o_2s}^{tport} \leq M_{o_1s}^2 \cdot (3 - x_{o_1s} - x_{o_2s} - z_s), \quad \forall o_1, o_2 \in \mathcal{O}, s \in \mathcal{S} | \underline{m}_s = 0 \quad (5.14)$$

$$E_{o_2s}^{tport} - E_{o_1s}^{tport} \leq M_{o_2s}^2 \cdot (3 - x_{o_1s} - x_{o_2s} - z_s), \quad \forall o_1, o_2 \in \mathcal{O}, s \in \mathcal{S} | \underline{m}_s = 0 \quad (5.15)$$

$$\frac{E_s^c}{\underline{m}_s} - E_{os}^{tport} \leq M_s^3 \cdot (2 - x_{os} - z_s), \quad \forall o \in \mathcal{O}, s \in \mathcal{S} | \underline{m}_s > 0 \quad (5.16)$$

$$E_{os}^{tport} - \frac{E_s^c}{\underline{m}_s} \leq M_{os}^4 \cdot (2 - x_{os} - z_s), \quad \forall o \in \mathcal{O}, s \in \mathcal{S} | \underline{m}_s > 0 \quad (5.17)$$

The egalitarian allocation of emissions to orders in \mathcal{O} is described by Constraints (5.14) to (5.17). Services with no default load ($\underline{m}_s = 0$) are treated in (5.14) and (5.15). They allocate the same emissions pairwise to orders o_1 and o_2 that both use service s . Constraints (5.16) and (5.17) handle services that have a default load ($\underline{m}_s > 0$). Here, the emissions E_{os}^{tport} allocated to order o are set equal to the emissions allocated to each order of the default load which is computed by $\frac{E_s^c}{\underline{m}_s}$. Constraints (5.14) and (5.15) are based on the implementation of the egalitarian scheme in the selective traveling salesman problem of Kirschstein and Bierwirth (2018). This implementation is a linearization of the generic but non-linear Equation (5.1) that was presented in Section 5.3.1.

$$E_s^c - e_s^{tport} \cdot c_s \leq M_s^5 \cdot z_s, \quad \forall s \in \mathcal{S} \quad (5.18)$$

$$e_s^{tport} \cdot c_s - E_s^c \leq M_s^6 \cdot z_s, \quad \forall s \in \mathcal{S} \quad (5.19)$$

$$E_{os}^{tport} - e_s^{tport} \cdot q_o \cdot x_{os} \leq M_{os}^7 \cdot (1 - x_{os} + z_s), \quad \forall o \in \mathcal{O}, s \in \mathcal{S} \quad (5.20)$$

$$e_s^{tport} \cdot q_o \cdot x_{os} - E_{os}^{tport} \leq M_{os}^8 \cdot (1 - x_{os} + z_s), \quad \forall o \in \mathcal{O}, s \in \mathcal{S} \quad (5.21)$$

The payload-based allocation of emissions is modeled by Constraints (5.18) and (5.19) for the default load of service s and by Constraints (5.20) and (5.21) for the transport

emissions E_{os}^{tport} of order o using service s . Remember that $z_s = 0$ indicates that the PA-scheme is applied to service s .

$$E_o^{ex} \geq \sum_{s \in \mathcal{S}} E_{os}^{tport} + \sum_{i \in \mathcal{N}} E_{oi}^{tship} - \bar{e}_o, \forall o \in \mathcal{O} \quad (5.22)$$

$$E_o^{ex} \leq M_o^9 \cdot E_o^{lim}, \forall o \in \mathcal{O} \quad (5.23)$$

$$E_s^c, E_{os}^{tport}, E_{oi}^{tship}, E_o^{ex} \geq 0, \forall o \in \mathcal{O}, s \in \mathcal{S}, i \in \mathcal{N} \quad (5.24)$$

$$x_{os}, y_{os}, z_s, E_o^{lim} \in \{0, 1\}, \forall o \in \mathcal{O}, s \in \mathcal{S} \quad (5.25)$$

Constraint (5.22) calculates the emissions that exceed order o 's emission limit \bar{e}_o . If this value is strictly positive, the binary indicator E_o^{lim} is set to 1 by Constraint (5.23). Note that E_o^{ex} and E_o^{lim} are never unintentionally larger than 0 if these measures are considered as primary or subordinate objectives. Finally, the domains of the decision variables are described by Constraints (5.24) and (5.25). The implementation is enhanced by bounds that limit the range of possible values for decision variables E_s^c , E_{oi}^{tship} , and E_{os}^{tport} . A description of these bounds is provided together with the large numbers M in Appendix B. We use version 12.7.1.0 of IBM ILOG CPLEX for solving this formulation of the SSP-TALE.

5.4 Experiments with real-world data

5.4.1 Data

For the following experiments, we use the SSP-TALE model to route a fixed number of orders through the European intermodal rail/road network. Thereby, we compare results from country pairs Portugal and the Netherlands (PT-NL) as well as Italy and Denmark (IT-DK). Orders between these countries can be candidates for intermodal rail/road transportation due to the long distances. The results from these country pairs are used to demonstrate the impact of SSP-TALE's features whereas for other country pairs results might differ. For example, Arnold et al. (2004) show that modal shares are also sensitive to costs of track gauge changes which could be incorporated when considering countries with differing track gauge.

The considered rail network is based on the core corridors described in the Trans-European Transport Network (TEN-T), see PaP Catalogue (2019) and TENtec Reporting

(2014, 2019). Figure 5.2a illustrates this network. Full data of the network is provided in Appendix C. Road network data is extracted from Open Street Map (2019) using Geofabrik (2019). We apply the Open Source Routing Machine to obtain truck routes within this road network, see Luxen and Vetter (2011). Figure 5.2b shows an exemplary routing through the road network from a customer node in Portugal to five rail/road transshipment terminals on the Iberian Peninsula.

For the rail services, we model an artificial mix of light and regular trains, see Figure 5.2a. Here, regular trains operate on main axes across Europe, such as the "west-to-east" axis or "north-to-south" axis, and light trains are used as feeders to the regular trains. Overall, we model 88 light trains and 18 regular trains that are also described in Appendix C. We assume for both train types a maximum capacity of $\bar{c}_s = 108$ TEUs, which corresponds to 36 wagons à 3 TEU. For the default load of a service s , we use values of $\underline{c}_s = 25$ TEU for light trains and $\underline{c}_s = 40$ TEU for regular trains. These default loads are chosen because they pose constellations where the selection of the services' allocation schemes is not trivial. This is further explained in Section 5.4.6, where we present results for varying values of \underline{c}_s . A train's remaining capacity $\bar{c}_s - \underline{c}_s$ can be used for loads q_o of orders \mathcal{O} . The number of external orders \underline{m}_s is randomly drawn between 1 and 10 for both train types. For the road services, we model heavy trucks. We

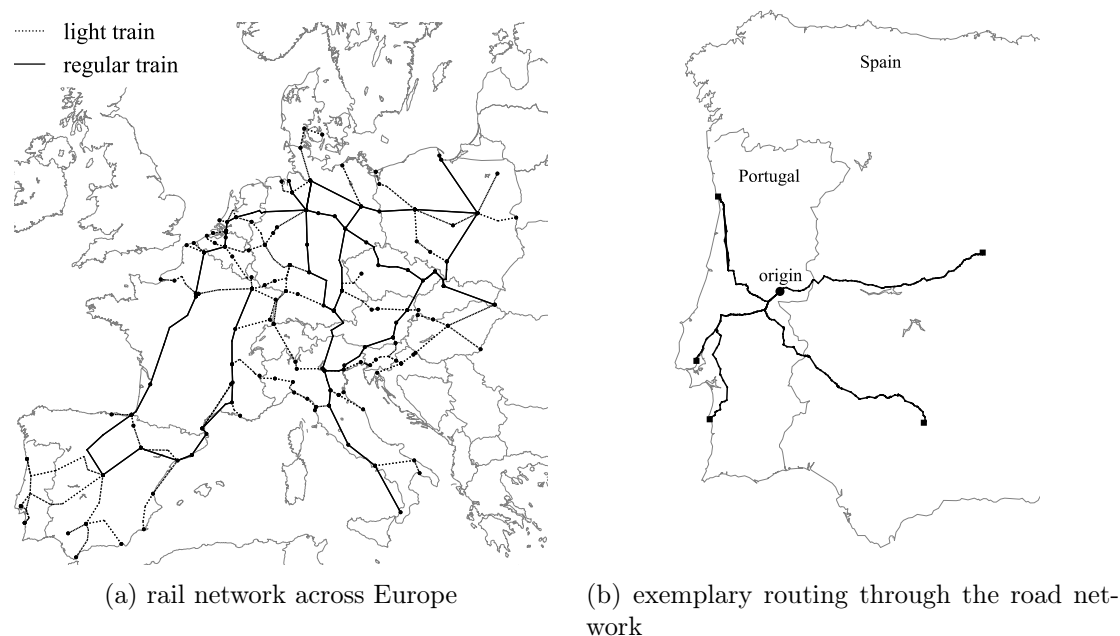


Figure 5.2: Considered rail network and exemplary routing through the road network.

consider road services that connect each order’s origin location directly to the five closest transshipment terminals. Likewise, road services that connect a destination location to five nearby terminals are established. For an order o , and each such road service s , we assume that the maximum capacity of the road service equals the quantity of the related order ($\bar{c}_s = q_o$). Thus, as each truck can carry at most two TEU, a road service can correspond to multiple trucks. Road services s are assumed to have no default load ($\underline{c}_s = \underline{m}_s = 0$).

Throughout this study, we assume transshipment costs of $r_i^{tship} = 40$ \$/TEU and transshipment emissions of $e_i^{tship} = 15$ kgCO₂e/TEU for all nodes $i \in \mathcal{N}$, see Clausen et al. (2013), Geerlings and van Duin (2011), and Janic (2007). The services’ cost rates r_s^{tport} (\$/TEU) are 1.67 \$ cents/ton·km for train transportation and 5.23 \$ cents/ton·km for truck transportation (Forkenbrock; 2001). The services’ emission rates e_s^{tport} , measured in kgCO₂e per TEU, of truck and train freight transportation are calculated with average country-pair specific values provided by Heinold and Meisel (2018), see Table 5.3. Emission rates differ between country pairs because countries have their own geographical and/or infrastructural characteristic (e.g., crossing the Alps, density of the rail network, degree of electrification in the rail network, source of electricity, etc.) and they differ between light and regular trains because each train type has a different default weight resulting from default load \underline{c}_s .

For each order $o \in \mathcal{O}$, a random origin a_o and a random destination b_o are drawn within the borders of the respective country. We draw order quantities q_o between 1 and 8 TEUs. For the emission limit \bar{e}_o of an order o , we multiply the order’s road-only emissions with a weight p . Here, road-only emissions of an order o refer to the emissions that result from shipping the load q_o directly by truck from the order’s origin to its destination. Note that such truck services are not contained in set \mathcal{S} as we look for analyzing intermodal operations. For eco-aware customers, it is reasonable to assume that $p < 1$ as transporting goods solely by truck usually causes higher emissions than using intermodal rail/road transportation (e.g., Heinold and Meisel; 2018). In other words, parameter p describes the share of road-only emissions that a customer is willing to accept for an intermodal

Table 5.3: Emission rates from truck and train freight transportation.

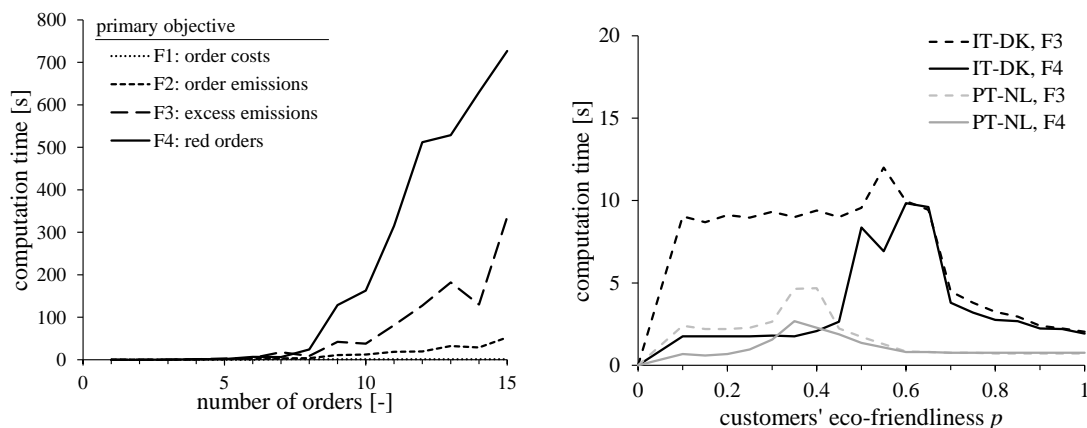
country pair	emission rate [gCO ₂ e/ton·km]		
	light train	regular train	truck
PT-NL	10.0	9.3	53.3
IT-DK	24.9	23.4	59.4

transportation. However, it is difficult to preset a particular value of p as it is an indicator for the environmental cautiousness of an individual customer. Therefore, we vary this parameter in our experiment in Section 5.4.3.

All results presented in this paper are based on solving 25 instances for each of the considered country pairs, using either five or eight orders per instance ($|\mathcal{O}| = \{5, 8\}$). Note that by considering at most 8 orders of 8 TEUs each, the capacities of trains are not a limiting factor here. This relatively small number of orders already represents a realistic setting for the considered problem. For example, if all of the 8 orders are transported with the same train service, these orders could make up for nearly 60% of this train's capacity. Furthermore, the services' default loads can be seen as several independent orders that have already been assigned to these services, for example, in previous planning periods. These orders are assumed here to have no preferences regarding their environmental impact. Thus, the default load of a service s could also be modeled as many artificial orders between the service's origin a_s and destination b_s . However, by modeling them collectively as "default load", it is possible to reduce the computational challenge of solving the problem. A more enhanced analysis on the computation time is provided in the following section.

5.4.2 Computation time

This first experiment analyzes the computation time that is required for solving the SSP-TALE instances. The experiment is conducted on a computer with 32 GB RAM and an



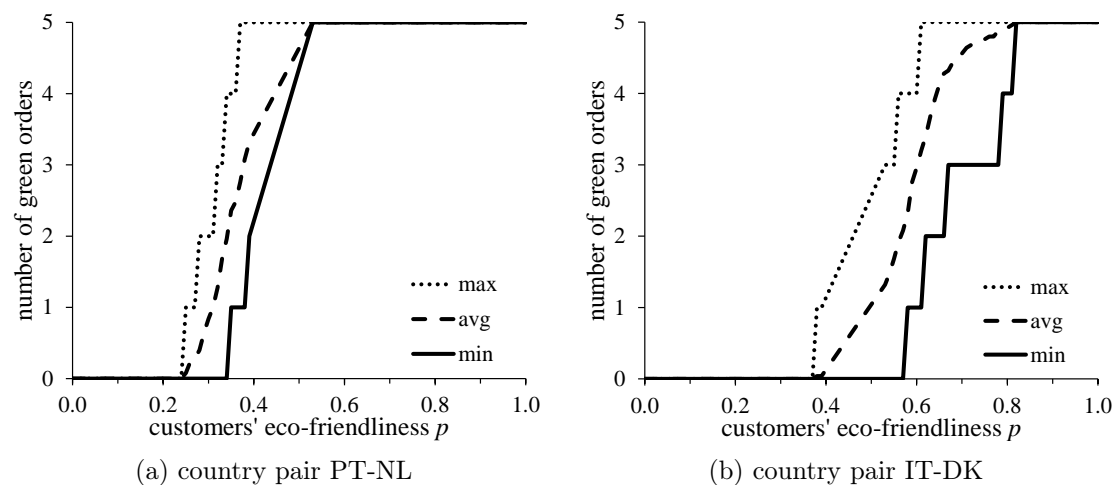
(a) different number of orders (PT-NL, $p = 0.35$).

(b) varying values of parameter p (5 orders).

Figure 5.3: Average computation time for a varying number of orders and varying values of p .

i7-8700 CPU processor with 3.2 GHz. The computation time depends on several factors which are interdependent with each other. We start reporting computation times under objectives F1 to F4 for instances with a varying number of orders. Figure 5.3a shows the average computation time (in seconds) for shipping 1 to 15 orders from Portugal to the Netherlands. As expected, more orders lead to a higher computation time. More interestingly, the computational challenge rises for objectives "excess emissions" (F3) and "red orders" (F4), which are the two novel objectives introduced in this study. This is because F3 and F4 consider whether an order is routed within its emission limit \bar{e}_o , which requires the model to take into account decision variables E_o^{ex} and E_o^{lim} , respectively, and to make order-specific allocation decisions. In contrast, these variables can be ignored in the solution process under objectives F1 and F2. Furthermore, it is not even possible to find an optimal solution for every large instance under objectives F3 and F4 within a given runtime of 60 minutes. For example, this holds for 6 out of 25 instances with 15 orders under objective F4. These instances were therefore excluded from the results in Figure 5.3. Note that the results are obtained from strengthened models that use the cuts and big-M values in Appendix B. For example, if instances 1-10 (5 orders, PT-NL, objective F4, flexible EA/PA allocation) are solved without these cuts, no optimal solution is found within 300 seconds for four instances (average gap 40%) and the average computation time of the remaining six instances is 79 seconds. In contrast, using the cuts, an optimal solution for all ten instances is found within an average runtime of 2 seconds.

Figure 5.3b shows the average computation time under the more time-consuming objectives F3 and F4 for shipping five orders between PT-NL and IT-DK under varying values of the customers' eco-friendliness p . It can be seen that the computation time behaves differently for the two country pairs. This is because the country-specific emission rates and the different network structures offer diverse country-specific options for routing orders and for respecting emission limits. In particular, there exist more possible routings for orders from Italy to Denmark compared to orders from Portugal to the Netherlands. The figure also shows that it is relatively easy to solve instances where p is either very low or very high. For extreme values of p , it is relatively easy for the model to find an optimal solution as either all or none of the orders can be shipped within their emission limit. Consequently, it is most challenging to come up with an optimal solution if customers ask for a medium level of eco-friendliness. A similar observation can be made for varying values of the services' default loads. Here, it is not challenging for the model to find an optimal solution if the selection of the services' allocation schemes is straightforward. For example, if the services' default load is relatively large compared to the size of the

Figure 5.4: Number of green orders for varying values of p .

orders that are to be routed, the egalitarian scheme always allocates more emissions to the orders than the payload scheme and, thus, the payload scheme is used under the service-oriented objectives F3 and F4.

Overall, these results show that the computation time depends on several factors. The most important ones are as follows: (i) considered number of orders $|\mathcal{O}|$, (ii) chosen objective, (iii) considered country pair, (iv) level of customers' eco-friendliness p , and (v) difficulty to select the services' allocation schemes (depends on order size and default load).

5.4.3 Customers eco-friendliness (p-value)

We start by investigating the impact of parameter p , which indicates the level of eco-friendliness sought by the shippers of orders \mathcal{O} . We analyze for varying values of p , the number of orders that do not exceed their emission limit (referred to as *green orders*), which is the difference between the total number of orders $|\mathcal{O}|$ and the number of orders that exceed their emission limit (referred to as *red orders*). These results are obtained by using primary objective "red orders" (F4) which minimizes the number of red orders and, thus, maximizes the number of green orders.

Figure 5.4 shows the minimal, average and maximal number of green orders over the 25 test instances for both country pairs with five orders per instance, using varied values of $p \in [0, 1]$. If parameter $p = 1$, the minimal number of green orders is 5 for both country pairs. This means, that there is a solution for all instances in which all orders are routed within their emission limits if these limits are sufficiently high. In

contrast, if $p = 0.35$ for country pair PT-NL, the minimal number of green orders is 1, the average is 2.36 and the maximum is 4 over the 25 test instances. Thus, if customers request that the intermodal transport's emissions are at most 35% of the direct road-only transport's emissions ($p = 0.35$), the model finds solutions where on average around half of the considered orders are routed within their limit.

For country pair IT-DK, if $p = 0.55$, the average number of green orders is 1.68. In addition, this p -value can result in solutions where no orders are routed within their emission limits (minimal number of green orders is 0) or where at most 3 orders are routed within their emission limit (maximal number of green orders). Thus, despite of a higher p -value, the average number of green orders is lower for country pair IT-DK compared to PT-NL. This is because country-specific emission rates for truck and train transportation are used and their ratio is closely related to the impact of the p -value on the number of green orders. For example, the ratios of emissions from truck and regular trains are 0.39 for IT-DK but only 0.17 for PT-NL. In other words, train transportation between Portugal and the Netherlands causes relatively low emissions compared to Italy and Denmark, which allows, for the same p -value, more green orders for country pair PT-NL compared to IT-DK. Due to this country-pair specific spread, the further results presented in this paper use $p = 0.35$ for country pair PT-NL and $p = 0.55$ for country pair IT-DK as these represent interesting constellations for the considered problem.

5.4.4 Emission limits and order emissions

We analyze in this section the impact of primary objectives F1 to F4 on the emissions allocated to the orders. For this, we show exemplary results from a selected test instance with five orders between Portugal and the Netherlands, see Figure 5.5. We use objective "order emissions" (F2) as secondary objective and the values atop of the bars measure the difference between the emissions allocated to the orders and their respective emission limit (shown as black bar in Figure 5.5). This value is measured in tCO_{2e} and positive (+) for the case of red orders and negative (-) for the case of green orders. There are three red orders (2, 4 and 5) under objective "order costs" (Figure 5.5a), two red orders (4 and 5) under objectives "order emissions" and "excess emissions" (Figures 5.5b and 5.5c), and only one red order (4) under objective "red orders" (Figure 5.5d). Thus, the number of red orders differs among the solutions and reaches its minimum only under the corresponding objective "red orders" (F4). In contrast, objective F2 minimizes the total emissions that are allocated to the orders which, at the same time, implies two red orders (4 and 5). Consider now that the emission limit of order 5 increases by 0.07 tCO_{2e}

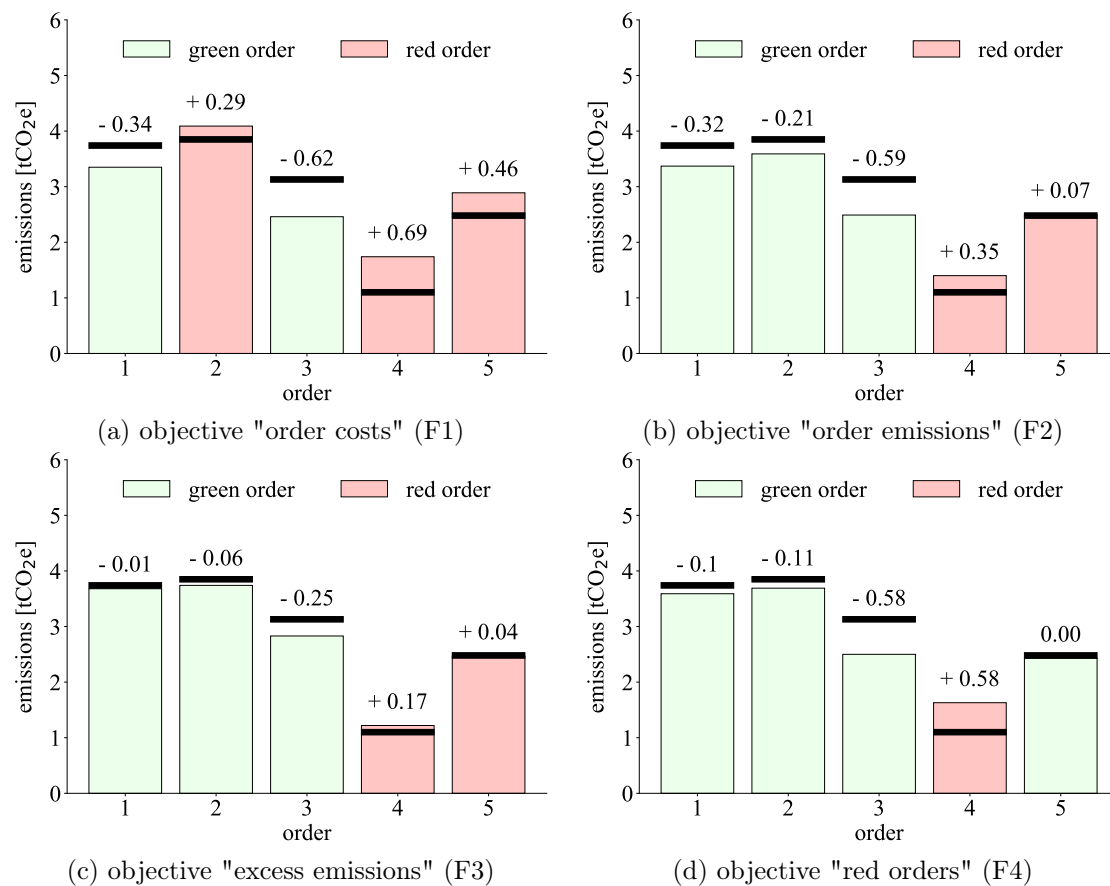


Figure 5.5: Emissions per order under primary objectives F1 to F4 (instance 17, PT-NL).

(which is the order's excess emission under F2). Then, the solution that minimizes the total order emissions (F2) and the solution that minimizes the total number of red orders (F4) would be the same. However, using the emission limits as they are, order 5 becomes "green" under objective F4 only by allocating more emissions to the other orders 1 to 4. This can be done by changing the services' allocation schemes or by changing the other orders' routings. Either way, this shows that the allocation of emissions to a particular order also depends on the emission limits of other orders. We refer to the second example in Appendix A for a further illustration of this finding.

Note that each solution in Figure 5.5 comes up with a different allocation of emissions. In other words, total order emissions increase by considering the orders' emission limits. Figure 5.6 further illustrates this by showing the emissions that are allocated to the orders (performance measure F2) in each of the 25 PT-NL instances with five orders, using F1 to F4 as primary objectives. In the figure, the orders are sorted by decreasing values of the order emissions under secondary objective F2. It can be seen that the emissions allocated

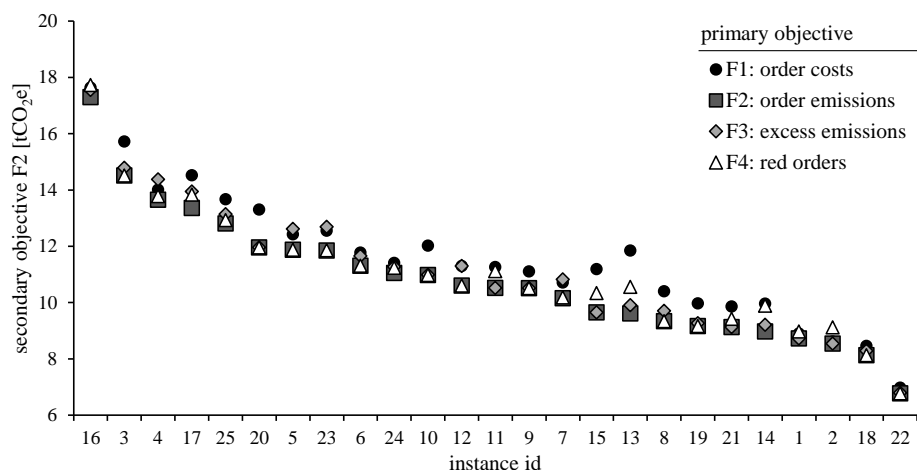


Figure 5.6: Emissions per instance under primary objectives F1 to F4 (five orders, PT-NL).

to the orders under the different objectives constitute a lower bound and an upper bound. The lower bound is obtained for all instances if "order emissions" (F2) is considered as primary objective. The upper bound follows from primary objective "order costs" (F1) for 18 instances, from objective "excess emissions" (F3) for four instances and from objective "red orders" (F4) for three instances. Thus, as expected, using performance measures related to emission limits (F3 and F4), usually lead to solutions where less emissions are allocated to the considered orders than in minimum-cost solutions. At the same time, there is no substantial difference in the emissions allocated to the orders between objectives "excess emissions" (F3) and "red orders" (F4).

5.4.5 Allocation schemes and order size

So far, the results are based on the assumption that the model selects the emission allocation scheme for each service individually. To analyze the impact of this degree of freedom, we now look at the case where all services exclusively use either the payload-based or the egalitarian allocation scheme. Figure 5.7 shows the total emissions (F2) that are allocated to the orders for the 25 instances of country pair PT-NL (five orders each), considering the three allocation policies (exclusively EA; exclusively PA; flexible EA/PA). Here, the instances are sorted by their total order size ($\sum_{o \in \mathcal{O}} q_o$), where 13 TEU and 35 TEU is the lowest and highest total order size, respectively. We make the following observations. If instances have a small total order size, e.g., below about 20 TEU, the exclusive PA scheme allocates less emissions to the considered orders than the

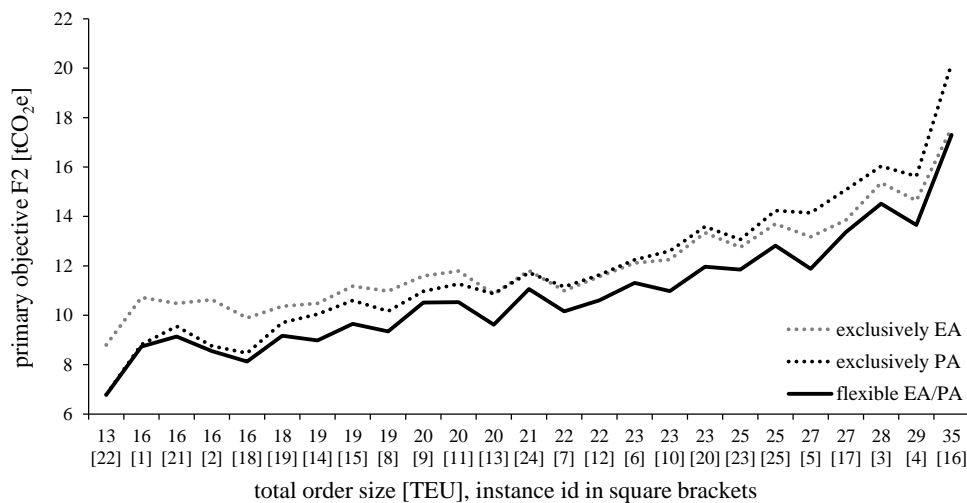


Figure 5.7: Emissions per instance for three emission allocation cases (five orders, PT-NL).

exclusive EA scheme. In contrast, if instances have a higher order size, the exclusive EA scheme allocates less emissions to the considered orders than the exclusive PA scheme. Thus, the size of the instance appears to be a good indicator for comparing the emissions that are allocated under the two exclusive policies. Moreover, this observation for five orders per instance seems to be very similar to the allocation scheme that is selected if a single order uses a service. Here, if the order is relatively small, then lowest emissions are allocated to the order under the payload-based scheme. Likewise, if the order is relatively large, then lowest emissions are allocated to the order under the egalitarian scheme. This is because the egalitarian scheme implicitly balances the emissions caused by the default load with the emissions caused by the order, which is more beneficial if the considered order is relatively large. Section 5.4.6 provides additional insights on this topic by presenting results for varying values of the services' default loads. We refer to Appendix A for an illustrative example with a single order. Anyhow, for the instances considered in this study, it can be seen that having the freedom of choosing the allocation scheme (flexible EA/PA) allocates lowest emissions to orders for all instances, which in most cases outperforms both of the pure allocation schemes. In general, the exclusive use of the PA (EA) scheme can only be optimal for instances with a relatively low (high) total order size. A mix of these two schemes is optimal for instances with a total order size that is in-between these two extremes.

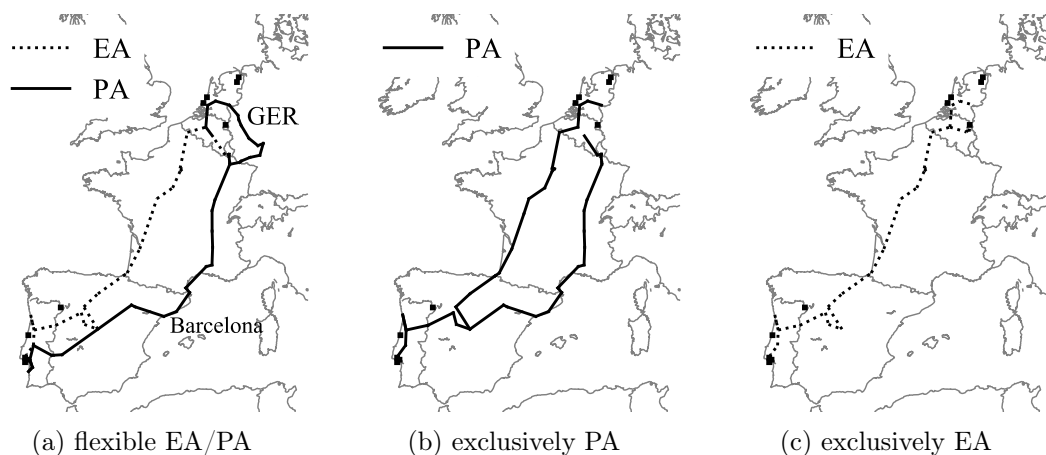


Figure 5.8: Used rail services for three emission allocation policies (instance 10, five orders, PT-NL).

5.4.6 Allocation schemes and default load

We now analyze the impact of the allocation schemes on the routing as well as the impact of the default load on the chosen allocation scheme. Figure 5.8 demonstrates the impact on the orders' routing if services are forced to use a specific emission allocation scheme. The figure shows for a selected test instance the used services and their allocation schemes for each of the three allocation policies. It can be seen that the used services strongly differ for the three policies. For example, the services through Germany are only used if the model is free to select between the EA and PA allocation scheme (Figure 5.8a) whereas the train services along Barcelona are only used if the PA scheme is allowed for these services (Figures 5.8a and 5.8b). In this example, if the EA scheme is prescribed for all services, most orders use the same set of rail services (Figure 5.8c). The selection of the allocation scheme and, thus, the routing of the orders is strongly affected by the composition of the default load (size and number of orders). So far, the results are based on the assumption of having rail services with a fixed default load size \underline{c}_s and a randomly drawn number of external orders $\underline{m}_s \in [1, 10]$. In the following experiment, we set the number of default orders to $\underline{m}_s = 5$ and solve the instances with default loads of $\underline{c}_s = 1, 2, \dots, 50$ TEU. Figure 5.9 shows the results under primary objective "order emissions" (F2) for the three emission allocation policies. We make the following observations. If the EA scheme is used exclusively, an increasing default load increases the emissions that are allocated to the orders. In contrast, these emissions are not affected if the PA scheme is used exclusively. The latter is because the emission rate is independent of the default load in this experiment. Furthermore, if the size of the services' default load

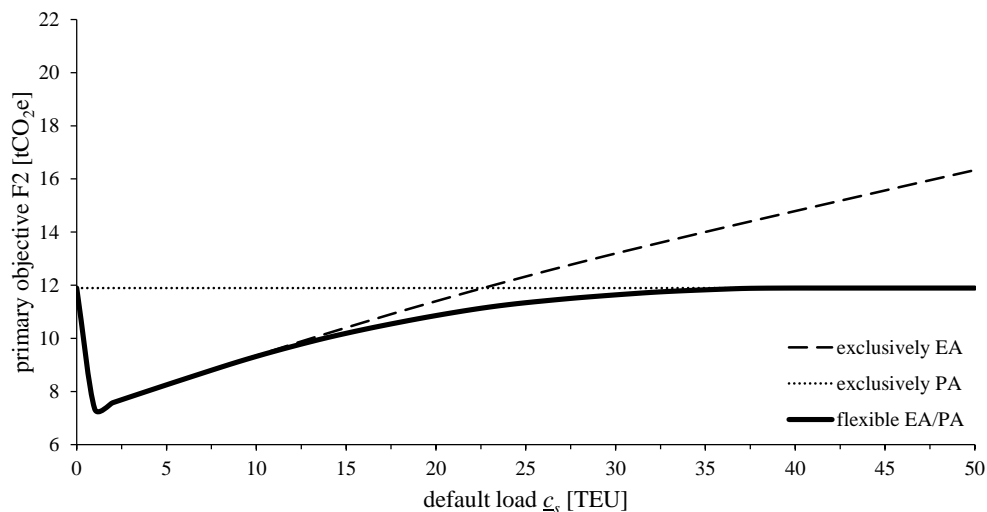


Figure 5.9: Average emissions over all instances for varying values of default load (five orders, PT-NL).

c_s is low, then the EA scheme allocates less emissions to the considered orders compared to the PA scheme. Likewise, if the size of the services' default load c_s is high, then the PA scheme allocates less emissions to the considered orders compared to the EA scheme. However, if c_s is somewhere in-between, then the policy that flexibly combines both allocation schemes outperforms all pure allocation policies. Note that this observation is in line with the findings about the order size from Section 5.4.5. In fact, it is the relation between the order size and the default load size that jointly decides upon the allocation schemes that are used for the services.

5.4.7 Overall results for five and eight orders and both country pairs

The previous sections primarily presented results for five orders and country pair PT-NL. We now extend this analysis by considering five or eight orders that have to be shipped from Portugal to the Netherlands or from Italy to Denmark. Table 5.4 shows the results from a hierarchical optimization, using objectives F1 to F4 either as a primary objective and/or as a secondary objective. Results are presented as averages over the 25 instances for each country pair with either five or eight orders per instance. The values in the table correspond to the performance measures of the secondary objective, which is stated at the top of a column. For example, using F1 as primary objective gives minimal average values of F1 = 20.13 thous. \$, F2 = 11.59 tCO₂e, F3 = 1.38 tCO₂e and F4 = 3.36 red orders, see first line in Table 5.4. Conversely, from looking at the first column in

Table 5.4: Average results from a hierarchical optimization over 25 instances.

		secondary objective							
		five orders				eight orders			
		F1 [thous. \$]	F2 tCO ₂ e	F3 tCO ₂ e	F4 [red orders]	F1 [thous. \$]	F2 tCO ₂ e	F3 tCO ₂ e	F4 [red orders]
primary objective	PT-NL ($p = 0.35$)								
	F1: order costs	20.13 ¹	11.59 ⁴	1.38 ⁴	3.36 ³	33.61 ¹	20.30 ⁴	3.25 ⁴	6.44 ²
	F2: order emissions	20.68 ³	10.82 ¹	0.86 ²	3.32 ²	34.83 ⁴	19.08 ¹	2.25 ²	6.52 ³
	F3: excess emissions	20.72 ⁴	11.10 ³	0.79 ¹	3.40 ⁴	34.76 ³	19.29 ²	2.19 ¹	6.52 ³
	F4: red orders	20.26 ²	11.05 ²	0.97 ³	2.64 ¹	34.45 ²	20.17 ³	3.24 ³	5.56 ¹
	IT-DK ($p = 0.55$)								
	F1: order costs	15.66 ¹	15.04 ³	1.24 ³	3.76 ²	24.35 ¹	23.24 ³	2.05 ³	5.68 ²
	F2: order emissions	16.01 ⁴	14.71 ¹	1.03 ²	3.88 ³	24.88 ³	22.39 ¹	1.67 ²	5.80 ³
F3: excess emissions	15.99 ³	14.79 ²	0.99 ¹	4.04 ⁴	24.90 ⁴	22.89 ²	1.45 ¹	6.08 ⁴	
F4: red orders	15.80 ²	15.08 ⁴	1.37 ⁴	3.32 ¹	24.66 ²	23.46 ⁴	2.54 ⁴	4.52 ¹	

superscripts 1-4 refer to the rank of the column's measure (1 = lowest value; 4 = highest value)

Table 5.4, the average minimal costs that are allocated to the orders (F1) for shipping five orders from Portugal to the Netherlands are 20.13 under primary objective F1, 20.68 under F2, 20.72 under F3, and 20.26 under F4. The superscripts shown in the table refer to the rank of the secondary objective's value, where 1 refers to the lowest and 4 to the highest value. In addition, the bold values highlight the value of rank 1, as this is the minimum of the corresponding primary objective.

Using the ranks, it is easy to compare results for the secondary objective's performance measure. For example, the highest average number of red orders (F4) is always achieved under primary objective "excess emissions" (F3). In particular, the average number of red orders is 3.40 out of five orders and 6.52 out of eight orders for country pair PT-NL as well as 4.04 out of five orders and 6.08 out of eight orders for country pair IT-DK. However, the average difference in the number of red orders under primary objectives F1 to F3 is quite small for instances from both country pairs. For performance measure "excess emissions" (F3), we see a relatively high difference between the lowest and the highest value, which indicates that excess emissions are strongly influenced by the chosen primary objective. For example, this difference is 0.38 tCO₂e (+39%) and 1.09 tCO₂e (+76%) for five and eight orders shipped from Italy to Denmark. From this, it can be concluded that F3 chooses more orders where emissions exceed the limit by only a small amount and F4 chooses then a lower number of orders where the emissions exceed the limit by a somewhat higher amount per order. In contrast, the primary objective's relative impact on performance measures F1 and F2 is less strong and lies between 2.2% and 3.6% for costs (F1) and between 2.5% and 7.1% for emissions (F2). In other words,

using F2, F3, or F4 as primary objective increases costs by at most 3.6% and using F1, F3, or F4 as primary objective increases emissions by at most 7.1%. Overall, the results from Table 5.4 show the trade-offs that are implied by considering orders' emission limits. The basic findings from the previous sections apply to five and eight orders as well as to both country pairs. Neither minimizing total costs nor minimizing total emissions leads to a routing where as many orders as possible are routed within their emission limit, i.e., where the number of green orders is maximized.

5.4.8 Network results

Remember that the performance measures F1 to F4 solely capture the effects for order set \mathcal{O} . Therefore, in this section, we provide results for measures that consider network-wide costs and emissions from both, the orders and the default load of services. In particular, we use performance measures "network costs" (F5) and "network emissions" (F6), see Formulas (5.26a) and (5.26b). Note that objectives "order costs" (F1) and "network costs" (F5) always lead to the same routing. This is because we consider no cost allocation schemes and it is therefore reasonable to use services with low cost rates under both objectives. In Formula (5.26a), this can be easily seen as the constant term $\sum_{s \in \mathcal{S}} c_s \cdot r_s^{tport}$ is added to performance measure F1. In contrast, objective "order emissions" (F2) minimizes the emissions that are allocated to the orders by either changing the services' allocation scheme or the orders' routing. If the latter is the case, the optimal solutions and network-wide emissions are usually different under objectives F2 and F6. Anyhow, since the total size of the orders is usually small compared to the total size of the services' default load, we only see little differences in this network-wide measure.

$$\min F5 = F1 + \sum_{s \in \mathcal{S}} c_s \cdot r_s^{tport} \quad \text{"network costs"} \quad (5.26a)$$

$$\min F6 = F2 + \sum_{s \in \mathcal{S}} E_s^c \quad \text{"network emissions"} \quad (5.26b)$$

Figure 5.10 shows the network-wide emissions (F6) under primary objectives F1 to F6 for shipping five or eight orders from Portugal to the Netherlands. Thus, the figure shows the minimal network-wide emissions using the optimal value for performance measures F1 to F6. The values are averages of the 25 instances per setting. As mentioned before, the network-wide impact of the chosen objective is limited. For example, the difference between the highest and the lowest value is only 0.26 tCO₂e and 0.56 tCO₂e for the shipping of five and eight orders, respectively. However, the analysis confirms that network-wide emissions are not minimized by minimizing order costs, order emissions,

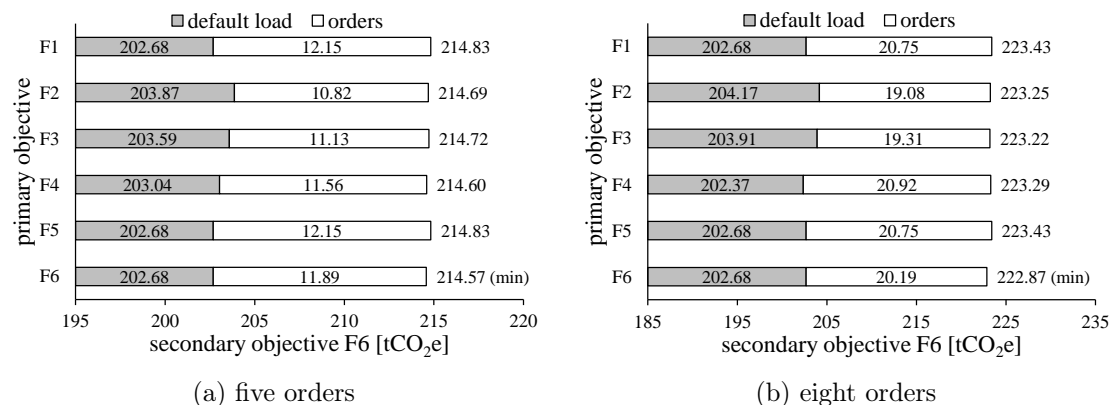


Figure 5.10: Average results for performance measure "network emissions" (PT-NL).

excess emissions, or the number of red orders.

5.5 Conclusion

In this study, we have considered the case of environmentally cautious customers that request to ship orders through an intermodal network where each order is associated with an emission limit. To reveal if an order is routed such that it stays below its limit, it is necessary to allocate emissions from the used transport services to the orders that use this service. We have considered two emission allocation schemes (egalitarian and payload-based) and let an optimization model select the appropriate scheme for each service. Overall, the problem has been modeled as a **S**ervice **S**election **P**roblem with **T**ransshipment operations, **A**llocation schemes and emission **L**imits in an **E**missions-oriented setting (SSP-TALE). We have solved the problem for cost-, emission- and service-objectives. We have also minimized the number of orders that are routed above their emission limits, which might be a more practical objective for logistics service providers compared to the pure emission-minimizing objective which is often proposed in the vehicle routing literature.

We have tested our approach for a real-world intermodal rail/road network in Europe. In particular, instances of five or eight orders that have to be shipped from Portugal to the Netherlands or from Italy to Denmark have been considered. Experiments have shown the impact of both, the number of orders as well as the country pair, on the results of the considered performance measures. We have shown the interrelations of routing decisions, emission allocation schemes, and emission limits. In particular, solutions where most orders comply with their emission limits are different from solutions where total emissions or total costs are minimized solely. We have also demonstrated

that the emissions allocated to an order can increase if a tight emission limit exists for other orders. This is because emission limits impact the selection of allocation schemes and the interdependent routing of orders. Furthermore, our analysis has shown that a payload-based allocation of emissions is often beneficial for orders of small sizes and an egalitarian allocation of emissions is often beneficial for orders of large sizes. Likewise, an egalitarian allocation of emissions is often beneficial if the size of the services' default load is small and a payload-based allocation of emissions is often beneficial if the default load size is large. If both, the orders and the default load, are of medium size, it is often optimal to mix these allocation policies.

Future research may consider the schedules of rail services to analyze the trade-off between transit time and emission limits, and, with this, consider a traditional service-objective. However, powerful heuristics are then required to solve large-scale instances with a large number of orders. In addition, a multi-period planning may yield more possibilities to route orders and, thus, to comply with the orders' emission limits. Another interesting extension could be to explicitly consider customers' willingness to pay for green transportation.

Acknowledgments

This research was supported by the German Research Foundation (DFG) under reference 268276815. We thank three anonymous reviewers for their valuable comments which helped to improve the manuscript considerably.

5.6 Appendix A. Illustrative example of the SSP-TALE

We present two illustrative examples that demonstrate the interdependencies of emission allocation schemes and emission limits. The same network with the same services is used in both examples. However, the first example considers the case of *one* order with a varied order size and the second example the case of *two* orders with fixed but different order sizes. The considered network consists of only two nodes a and b . Each order o is routed from its origin node $a_o = a$ to its destination node $b_o = b$. Thereby, an order o can either use service s_1 or service s_2 which are two direct, parallel, train services that connect node $a = a_{s_1} = a_{s_2}$ with node $b = b_{s_1} = b_{s_2}$. The distance between the nodes is assumed to be 150 kilometer. Service s_1 is a light train and service s_2 is a regular train, both with $\underline{m}_{s_1} = \underline{m}_{s_2} = 10$. All other data is used as described in Section 5.4.1.

		allocated emissions [kgCO ₂ e]			
		egalitarian		payload-based	
service	s_1	E_s^c	E_{os}^{tport}	E_s^c	E_{os}^{tport}
		s_1	857	86	873
	s_2	1,244	124	1,303	65

(a) $q_o = 2$ TEU

		allocated emissions [kgCO ₂ e]			
		egalitarian		payload-based	
service	s_1	E_s^c	E_{os}^{tport}	E_s^c	E_{os}^{tport}
		s_1	952	95	873
	s_2	1,333	133	1,303	163

(b) $q_o = 5$ TEU

Figure 5.11: Results for an example with one order of different sizes.

We now illustrate with the first example the functioning of the emission allocation schemes and the impact of the order size on the selection of the scheme used per service. For this, we consider the case where a single order o is to be shipped (i.e., $\mathcal{O} = \{o\}$) from origin a_o to destination b_o with a load of either $q_o = 2$ TEU (= 24 t) or $q_o = 5$ TEU (= 60 t). Figures 5.11a and 5.11b report for both order sizes the emissions that are allocated to the default load (E_s^c) and to the considered order o (E_{os}^{tport}) using either service s_1 or s_2 under the egalitarian (EA) or payload-based (PA) allocation scheme. For the order size $q_o = 2$, the lowest emissions allocated to order o are 65 kgCO₂e, which results from using service s_2 with a payload-based allocation scheme, see Figure 5.11a. For the order size $q_o = 5$, using service s_1 and an egalitarian allocation effects lowest emissions of 95 kgCO₂e, see Figure 5.11b. Thus, a payload based allocation is more attractive for small order sizes and an egalitarian allocation of emissions is more attractive for larger order sizes.

For the routing of multiple orders, the amount of emissions allocated to a particular order also depends on the routing of the other orders, which will be shown in the second example. In addition, the second example demonstrates the impact of emission limits on the decisions made as well as such limits' impact on the total network emissions. For this, we route two orders $\mathcal{O} = \{o_1, o_2\}$ from node a to node b and, thus, consider the interaction of two jointly routed orders. The quantity of the first order is $q_{o_1} = 2$ TEU and the quantity of the second order is $q_{o_2} = 5$ TEU. Each service s_1 or s_2 can either be used by o_1 or o_2 or both, respectively, and emissions on each service can either be allocated with the EA or the PA scheme. Thus, in this example, there exist four routing possibilities and four allocation possibilities. Figure 5.12a reports for each such routing-allocation combination the split of total emissions. The numbers in the square bracket atop of the bars serve as index of these combinations. The figure shows that each routing combination leads to different amounts of total greenhouse gases although the differences are small due to the small example size. This amount has its minimum of 2,404 kgCO₂e if both orders use train s_2 (solutions [13] to [16]) and its maximum of 2,421 kgCO₂e if

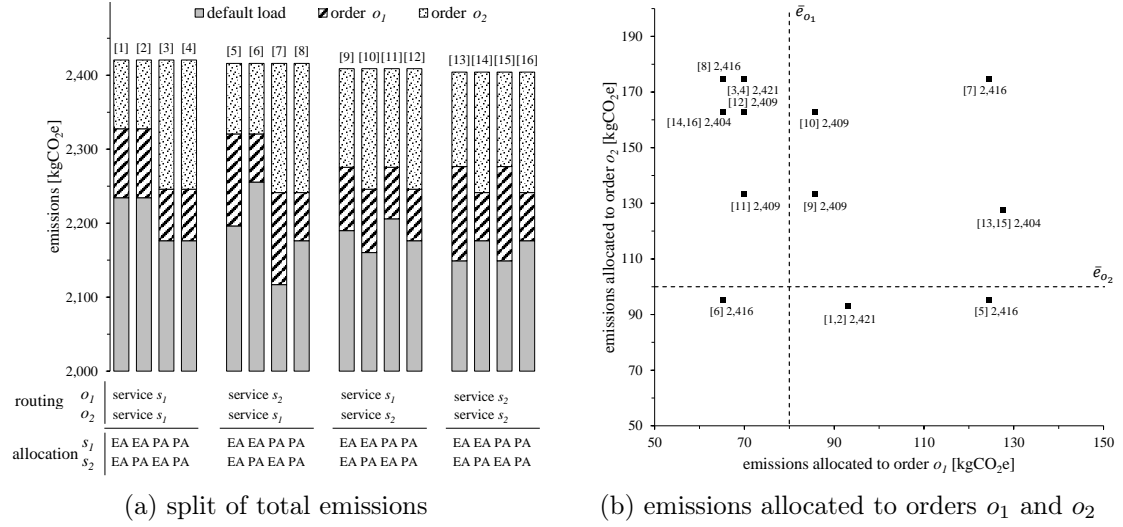


Figure 5.12: Solutions for all routing-allocation possibilities in the example with two orders.

both orders use train s_1 (solutions [1] to [4]). However, under each routing possibility, the selected emission allocation scheme of the used services decides upon the emissions that are actually allocated to the orders. For example, if both orders use service s_1 , it is possible to either allocate 93 kgCO₂e to each of the orders (solutions [1] and [2]) or 70 kgCO₂e to order o_1 and 175 kgCO₂e to order o_2 (solutions [3] and [4]). Figure 5.12b shows all possible combinations to distribute emissions among orders o_1 and o_2 . The number(s) in the square brackets refer to the routing-allocation combination from Figure 5.12a and the value next to the brackets refers to the total emissions of a solution. Here, it can be seen that the emission minimizing solutions [13] to [16] result from either allocating 128 kgCO₂e to both orders (EA, [13] and [15]) or from allocating 65 kgCO₂e to order o_1 and 163 kgCO₂e to order o_2 (PA, [14] and [16]).

We now consider the impact of an emission limit $\bar{e}_{o_1} = 80$ for order o_1 , which is represented by the vertical dotted line in Figure 5.12b. If this emission limit is considered as a hard constraint, we are only left with eight routing-allocation solutions, as all other solutions would allocate more emissions to order o_1 than allowed by the respective limit. Out of the remaining solutions, the lowest emissions allocated to order o_2 are 95 kgCO₂e, see solution [6]. However, if emission limit \bar{e}_{o_1} is not considered as a hard constraint, solutions [1] and [2] would allocate less than 95 kgCO₂e to order o_2 . In other words, the emission limit of order o_1 restricts attractive routing-allocation solutions that minimize the emissions allocated to order o_2 . If we additionally consider a hard emission limit of $\bar{e}_{o_2} = 100$ for order o_2 (represented by the horizontal dotted line in Figure 5.12b),

solution [6] remains as the only feasible solution. Here, the allocated emissions comply to both orders' emission limits and the total emissions, consisting of default and order emissions, are 2,416 kgCO₂e. At the same time, solution [6] results in 12 kgCO₂e more emissions than solutions [13] to [16] that effect minimum total emissions of 2,404 kgCO₂e.

5.7 Appendix B. Implementation of the SSP-TALE

We present in this section the methodology to calculate suitable large numbers (big M) and bounds on the emissions allocated to default loads and orders to tighten the SSP-TALE model. For each service s , we consider the minimal and maximal emissions than can be allocated to default load E_s^c and orders E_{os}^{tport} by using either the PA or the EA scheme. Table 5.5 shows the corresponding values.

If service s uses the PA scheme, the emissions allocated to the default orders are simply calculated by multiplying the services' emission rate e_s^{tport} with default load \underline{c}_s and the emissions allocated to an order o are calculated by multiplying the services' emission rate e_s^{tport} with order load q_o . In contrast, if service s uses the EA scheme, the allocated emissions are calculated by considering the number of orders that can use service s . Clearly, as the number of orders using a service s depends on the routing in the considered solution, it is not possible to predict the exact emissions that are allocated to each order under the EA scheme. However, it is possible to calculate a lower bound and an upper bound for the emissions per order under the EA scheme. For this, we consider order sizes q_o , default load \underline{c}_s and the number of default orders \underline{m}_s . Remember that the general procedure of an egalitarian allocation is to divide a service's total emissions by the number of orders that use the service. For example, if only a single order o uses a service s ($x_{os} = 1$ and $x_{o's} = 0$, $\forall o' \in \mathcal{O} | o' \neq o$), the emissions per order

Table 5.5: Emissions for the default load and the orders under both allocation schemes.

	default emissions E_s^c	order emissions E_{os}^{tport} (if $x_{os} = 1$)
payload-based allocation (PA)	$e_s^{tport} \cdot \underline{c}_s$	$e_s^{tport} \cdot q_o$
egalitarian allocation (EA)		
lower bound	$\underline{m}_s \cdot \min\left(\frac{e_s^{tport} \cdot \underline{c}_s}{\underline{m}_s}, \min_{o \in \mathcal{O}} LB_{os}\right)$	LB_{os} as computed by (5.27)
upper bound	$\underline{m}_s \cdot \max\left(\frac{e_s^{tport} \cdot \underline{c}_s}{\underline{m}_s}, \max_{o \in \mathcal{O}} UB_{os}\right)$	UB_{os} as computed by (5.28)

are calculated by $\frac{e_s^{tport} \cdot (\underline{c}_s + q_o)}{\underline{m}_s + 1}$. The lower bound LB_{os} and the upper bound UB_{os} for the emissions allocated to order o by using service s under emission allocation scheme EA can be calculated by using Formulas (5.27) and (5.28). Here, we consider the $2^{|\mathcal{O}|}$ order-combinations of orders \mathcal{O} , the so-called powerset $P(\mathcal{O})$. For example, the size of the powerset is 32 for the case of 5 orders ($P(\mathcal{O}) = \{\emptyset, \{o_1\}, \{o_2\}, \dots, \{o_1, o_2, o_3, o_4, o_5\}\}$), where each order o is included in $\frac{|P(\mathcal{O})|}{2} = 16$ sets.

$$LB_{os} = \min_{P' \in P(\mathcal{O}) | o \in P'} \left(\frac{e_s^{tport} \cdot (\underline{c}_s + \sum_{o' \in P'} q_{o'})}{\underline{m}_s + |P'|} \right), \forall o \in \mathcal{O}, s \in \mathcal{S} \quad (5.27)$$

$$UB_{os} = \max_{P' \in P(\mathcal{O}) | o \in P'} \left(\frac{e_s^{tport} \cdot (\underline{c}_s + \sum_{o' \in P'} q_{o'})}{\underline{m}_s + |P'|} \right), \forall o \in \mathcal{O}, s \in \mathcal{S} \quad (5.28)$$

We illustrate the allocation under the EA scheme by considering five orders with order quantities $q_1 = 1, q_2 = 3, q_3 = 5, q_4 = 6$ and $q_5 = 8$ and a service s with emission rate $e_s^{tport} = 1 \text{ kgCO}_2\text{e}$, default load $\underline{c}_s = 20$ and $\underline{m}_s = 7$ default orders. Figure 5.13a shows the emissions per order for all those sets $P' \in P(\mathcal{O})$ that use service s , e.g., $x_{os} = 1 \forall o \in P'$ and $x_{os} = 0 \forall o \in P \setminus P'$. In the figure, the horizontal lines (solid black) are the lower and upper bounds for the emissions per order for using service s . If only the most light weight order o_1 uses service s , the service's total emissions (21 kgCO₂e) are equally distributed over $\underline{m}_s + 1 = 8$ orders, resulting in 2.6 kgCO₂e for each of the eight orders (lower bound). In contrast, if orders 3, 4 and 5 use service s , the service's

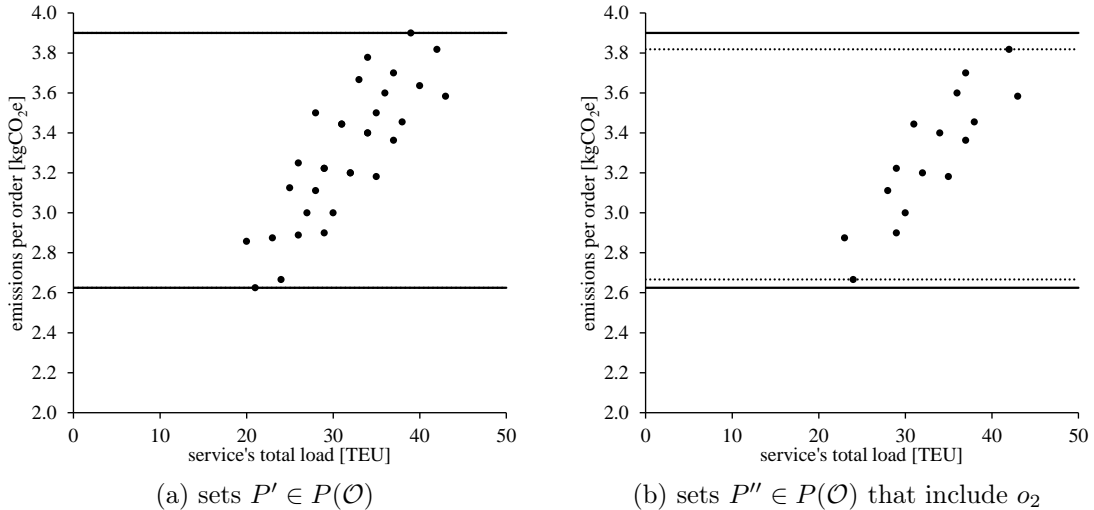


Figure 5.13: Emissions per order from sets of powerset $P(\mathcal{O})$.

total emissions (39 kgCO₂e) are equally distributed over $\underline{m}_s + 3 = 10$ orders, resulting in 3.9 kgCO₂e for each of the ten orders (upper bound). Thus, the emissions per order usually increase with the services' load but the extreme values depend on the service's load and number of orders. Figure 5.13b shows the emissions per order for all sets P'' of powerset $P(\mathcal{O})$ that use service s and include order o_2 . Here, the bounds (grey dotted lines) that result from sets $P'' \in P(\mathcal{O})$ are more restrictive than the general bounds that result from considering all sets $P' \in P(\mathcal{O})$. In other words, it is reasonable to calculate bounds for each order-service-combination.

Using this information, Formulas (5.29) to (5.35) derive the large numbers M for the SSP-TALE model. For M_o^9 it is not possible to calculate an appropriate value. However, our experiments indicate that usually all orders can be routed within their emission limit if $p = 1$, e.g., if the emission limit is equivalent to the road-only emissions. We simply use a multiple of the emission limit, although, theoretically, the excess emissions might be higher but we consider such a solution as unacceptable for logistics service providers.

$$M_{os}^1 = M_{os}^2 = \max(e_s^{tport} \cdot q_o, UB_{os}), \forall o \in \mathcal{O}, s \in \mathcal{S} \quad (5.29)$$

$$M_s^3 = \max\left(\frac{e_s^{tport} \cdot \underline{c}_s}{\underline{m}_s}, \max_{o \in \mathcal{O}} UB_{os}\right), \forall s \in \mathcal{S} \quad (5.30)$$

$$M_{os}^4 = e_s^{tport} \cdot q_o, \forall o \in \mathcal{O}, s \in \mathcal{S} \quad (5.31)$$

$$M_s^5 = \underline{m}_s \cdot \max_{o \in \mathcal{O}} UB_{os}, \forall s \in \mathcal{S} \quad (5.32)$$

$$M_s^6 = e_s^{tport} \cdot \underline{c}_s, \forall s \in \mathcal{S} \quad (5.33)$$

$$M_{os}^7 = UB_{os}, \forall o \in \mathcal{O}, s \in \mathcal{S} \quad (5.34)$$

$$M_{os}^8 = e_s^{tport} \cdot q_o, \forall o \in \mathcal{O}, s \in \mathcal{S} \quad (5.35)$$

$$M_o^9 = 100 \cdot \bar{e}_o, \forall o \in \mathcal{O} \quad (5.36)$$

Finally, Constraints (5.37) and (5.38) limit the range of possible values for the emissions allocated to the services' default loads \underline{c}_s , Constraints (5.39) define the maximal emis-

sions for the transshipment of an order $o \in \mathcal{O}$ at node $i \in \mathcal{N}$ and Constraints (5.40) define minimal transport emissions allocated to an order $o \in \mathcal{O}$ if service $s \in \mathcal{S}$ is used ($x_{os} = 1$). Overall, Constraints (5.37) to (5.40) impose cuts and improve the computational performance significantly, see Section 5.4.2.

$$E_s^c \geq \underline{m}_s \cdot \min \left(\frac{e_s^{tport} \cdot \underline{c}_s}{\underline{m}_s}, \min_{o \in \mathcal{O}} LB_{os} \right), \quad \forall s \in \mathcal{S} \quad (5.37)$$

$$E_s^c \leq \underline{m}_s \cdot \max \left(\frac{e_s^{tport} \cdot \underline{c}_s}{\underline{m}_s}, \max_{o \in \mathcal{O}} UB_{os} \right), \quad \forall s \in \mathcal{S} \quad (5.38)$$

$$E_{oi}^{tship} \leq e_i^{tship} \cdot q_o, \quad \forall o \in \mathcal{O}, i \in \mathcal{N} \quad (5.39)$$

$$E_{os}^{tport} \geq x_{os} \cdot \min (e_s^{tport} \cdot q_o, LB_{os}), \quad \forall o \in \mathcal{O}, s \in \mathcal{S} \quad (5.40)$$

5.8 Appendix C. Rail network data

The experiments in our study are based on a real-world rail network, see Section 5.4. For the description of this network we refer to the online appendix of this paper (<https://doi.org/10.1016/j.tre.2020.101963>).

Bibliography

- Arnold, P., Peeters, D. and Thomas, I. (2004). Modelling a rail/road intermodal transportation system, *Transportation Research Part E: Logistics and Transportation Review* **40**(3): 255–270.
- Bauer, J., Bektaş, T. and Crainic, T. G. (2010). Minimizing greenhouse gas emissions in intermodal freight transport: an application to rail service design, *Journal of the Operational Research Society* **61**(3): 530–542.
- Baykasoğlu, A. and Subulan, K. (2016). A multi-objective sustainable load planning model for intermodal transportation networks with a real-life application, *Transportation Research Part E: Logistics and Transportation Review* **95**: 207–247.
- Chen, K., Yang, Z. and Notteboom, T. (2014). The design of coastal shipping services subject to carbon emission reduction targets and state subsidy levels, *Transportation Research Part E: Logistics and Transportation Review* **61**: 192–211.
- Chen, X. and Wang, X. (2016). Effects of carbon emission reduction policies on transportation mode selections with stochastic demand, *Transportation Research Part E: Logistics and Transportation Review* **90**: 196–205.
- Clausen, U., Kaffka, J., Déring, L. and Ebel, G. (2013). Container based calculation of greenhouse gas emissions – a method to determine emissions of container handlings in container terminals, *General Proceedings of the 13th World Conference on Transport Research (WCTR)*.
- Deb, K. (2014). Multi-objective optimization, *Search Methodologies*, Springer, pp. 403–449.
- Demir, E., Burgholzer, W., Hrušovský, M., Arıkan, E., Jammerneegg, W. and Van Woensel, T. (2016). A green intermodal service network design problem with travel time uncertainty, *Transportation Research Part B: Methodological* **93**: 789–807.
- DHL (2019). Green logistics solutions. . https://www.dhl.com/en/logistics/green_logistics_solutions.html (visited on 12.12.2019).
- DIN EN 16258 (2012). *Methodology for calculation and declaration of energy consumption and GHG emissions of transport services (freight and passengers)*, European Committee for Standardization.

- Forkenbrock, D. J. (2001). Comparison of external costs of rail and truck freight transportation, *Transportation Research Part A: Policy and Practice* **35**(4): 321–337.
- Geerlings, H. and van Duin, R. (2011). A new method for assessing CO₂-emissions from container terminals: a promising approach applied in Rotterdam, *Journal of Cleaner Production* **19**(6-7): 657–666.
- Geofabrik (2019). OpenStreetMap Data Extracts. <http://download.geofabrik.de/> (visited on 12.12.2019).
- Heinold, A. and Meisel, F. (2018). Emission rates of intermodal rail/road and road-only transportation in Europe: A comprehensive simulation study, *Transportation Research Part D: Transport and Environment* **65**: 421–437.
- Heinold, A. and Meisel, F. (2019). Emission Oriented vs. Time Oriented Routing in the European Intermodal Rail/Road Freight Transportation Network, in C. Bierwirth, K. Thomas and D. Sackmann (eds), *Logistics Management. Lecture Notes in Logistics.*, Springer, pp. 188–202.
- Janic, M. (2007). Modelling the full costs of an intermodal and road freight transport network, *Transportation Research Part D: Transport and Environment* **12**(1): 33–44.
- Jozefowicz, N., Semet, F. and Talbi, E.-G. (2008). Multi-objective vehicle routing problems, *European Journal of Operational Research* **189**(2): 293–309.
- Kellner, F. and Schneiderbauer, M. (2019). Further insights into the allocation of greenhouse gas emissions to shipments in road freight transportation: the pollution routing game, *European Journal of Operational Research* **278**(1): 296–313.
- Kirschstein, T. and Bierwirth, C. (2018). The selective Traveling Salesman Problem with emission allocation rules, *OR Spectrum* **40**(1): 97–124.
- Lam, J. S. L. and Gu, Y. (2016). A market-oriented approach for intermodal network optimisation meeting cost, time and environmental requirements, *International Journal of Production Economics* **171**: 266–274.
- Luxen, D. and Vetter, C. (2011). Real-time routing with OpenStreetMap data, *Proceedings of the 19th ACM SIGSPATIAL International Conference on Advances in Geographic Information Systems*, GIS '11, ACM, New York, NY, USA, pp. 513–516.
- Marler, R. T. and Arora, J. S. (2004). Survey of multi-objective optimization methods for engineering, *Structural and Multidisciplinary Optimization* **26**(6): 369–395.

- Open Street Map (2019). OpenStreetMap is the free wiki world map. <https://www.openstreetmap.org> (visited on 12.12.2019).
- PaP Catalogue (2019). Annual catalogue of the pre-arranged paths (PaP) 2019. https://cip.rne.eu/apex/f?p=212:170:16987342585315::::P170_BOOKS_LIST:504556 (visited on 12.12.2019).
- Piecyk, M., Cullinane, S. and Edwards, J. (2012). Assessing the external impacts of freight transport, in A. McKinnon, M. Browne and A. Whiteing (eds), *Green logistics: Improving the environmental sustainability of logistics*, 2 edn, Kogan Page Limited London, chapter 2, pp. 31–50.
- Qu, Y., Bektaş, T. and Bennell, J. (2016). Sustainability SI: multimode multicommodity network design model for intermodal freight transportation with transfer and emission costs, *Networks and Spatial Economics* **16**(1): 303–329.
- Rudi, A., Fröhling, M., Zimmer, K. and Schultmann, F. (2016). Freight transportation planning considering carbon emissions and in-transit holding costs: a capacitated multi-commodity network flow model, *EURO Journal on Transportation and Logistics* **5**(2): 123–160.
- Sharma, S. and Mathew, T. V. (2011). Multiobjective network design for emission and travel-time trade-off for a sustainable large urban transportation network, *Environment and Planning B: Planning and Design* **38**(3): 520–538.
- StadieSeifi, M., Dellaert, N. P., Nuijten, W., Van Woensel, T. and Raoufi, R. (2014). Multimodal freight transportation planning: A literature review, *European Journal of Operational Research* **233**(1): 1–15.
- Sun, Y. and Lang, M. (2015). Modeling the multicommodity multimodal routing problem with schedule-based services and carbon dioxide emission costs, *Mathematical Problems in Engineering* **2015**.
- TENtec Reporting (2014). TEN-T Compliance Maps. European Commission. https://ec.europa.eu/transport/themes/infrastructure/downloads_en (visited on 12.12.2019).
- TENtec Reporting (2019). TEN-T Interactive Maps. European Commission. <http://ec.europa.eu/transport/infrastructure/tentec/tentec-portal/map/maps.html> (visited on 12.12.2019).

Bibliography

Thøgersen, J. and Nielsen, K. S. (2016). A better carbon footprint label, *Journal of Cleaner Production* **125**: 86–94.

UPS (2019). Ups: Commitment to sustainability. . <https://www.ups.com/us/en/services/resource-center/Commitment-to-Sustainability.page> (visited on 12.12.2019).

Chapter 6

Eco-Labeling of Freight Transport Services: Design, Evaluation and Research Directions

Publication status Resubmitted after major revision to *Journal of Industrial Ecology* (19.11.2021). Currently under review (second round).

Thomas Kirschstein¹, Arne Heinold², Martin Behnke¹, Frank Meisel², and Christian Bierwirth¹

¹: School of Economics and Business, Martin-Luther-University, Halle, Germany

²: School of Economics and Business, Kiel University, Kiel, Germany

Abstract The idea of eco-labeling is to provide customers with an easy-to-understand signal regarding the ecological impact of using a product or service. With this paper, we propose an eco-labeling system for freight transportation. We discuss design options based on a common emission reporting standard and a related communication protocol. We further explain a procedure for deriving labels for shipments of goods and provide examples illustrating and evaluating the labeling process at selected land-based freight transport services. Results indicate that eco-labels can grade the environmental impact of a transport service reliably, even if heterogeneous goods are moved together. Finally, we outline challenges for future research associated with eco-labeling in freight transportation markets.

Keywords Eco-labeling, EN 16258, Emission allocation, GHG Reporting Standard, Sustainable transportation

6.1 Introduction

Passenger and freight mobility is responsible for about 14% of the global anthropogenic greenhouse gas (GHG) emissions, with a share of up to 25% in highly industrialized economies (IPCC; 2014). Prominent GHGs are Carbon Dioxide (CO₂), Methane, Nitrous Oxide, Ozone, Chlorofluorocarbons and other halogenated gases (EPA; 2021). To measure the negative effects of any GHG, its *global warming potential* (GWP) can be set in relation to the GWP of CO₂, which is then referred to in units of CO₂-equivalents (CO₂e). While the major part of mobility-related CO₂e emissions worldwide stem from passenger transportation, the role of freight transportation is still substantial. For example, road freight transportation emitted 2.4 Gt of CO₂e worldwide in 2018, see Figure 6.5 (appendix).

Diverse political initiatives aim at limiting global warming by cutting transport-related GHG emissions. Noteworthy activities are stricter standards for exhaust systems of combustion engines, governmental promotions of electric vehicles, and CO₂ taxation. All this is discussed under the designation of green transportation in the literature with a focus often put on harmonizing environmental targets and traditional business objectives, see Dekker et al. (2012), Savelsbergh and Woensel (2016).

This paper provides a novel view on green freight transportation, by asking how a transport service, i.e. the movement of a good from a point of origin to a point of destination, should be organized to match a customer's ecological expectation. We develop a categorical labeling system, similar to eco-labels known in consumer product markets. The label generates a signal that shippers can use to express and adjust their ecological preferences. Along with an eco-label, a communication protocol illustrates the information flows of the labeling process. Checking whether or not a transport service's environmental performance is compatible with the shippers' ecological preferences is not an easy task, especially when different transport modes, and vehicles with a changing degree of consolidation are involved.

To the best of our knowledge, the paper provides the first design for an eco-labeling system that targets logistic services and operations. It is organized as follows. Section 6.2 outlines reporting standard EN 16258, which forms the basis of the proposed eco-labeling system. In Section 6.3, we describe the communication flow between shippers and carriers

necessary to measure a service's ecological footprint. Section 6.4 introduces the labeling system design. We define indicator values for measuring environmental performances of transport processes. The approach is evaluated in Section 6.5 by a study on different services. The paper ends with an outlook on future research topics related with eco-labeling in logistics in Section 6.6 and a conclusion in Section 6.7.

6.2 Emission reporting standard EN 16258

A major component of every eco-labeling system is a standardized procedure to ascertain the ecological impact of products or services, e.g. in terms of GHG emissions caused by making the product or by consuming the service. For transport services, such a procedure has been proposed by the European Committee for Standardization (2013).

The European Norm EN 16258 defines a widely applicable GHG emission reporting standard for the transport industry. It prescribes that carriers (1) quantify the emissions that are caused by the conducted transport processes, (2) that they allocate these emissions to the transport orders moved in the processes, and (3) that they report the environmental performance to their customers (shippers).

A so-called *vehicle operation system* (VOS) forms the basis for calculating emissions according to EN 16258. It is constituted by physical movements of vehicles from some point of origin to some point of destination, also referred to as *vehicle trips*. Vehicle trips include loaded trips and empty trips necessary to reach customers or depots. The norm prescribes that the total energy consumption and GHG emissions associated with a VOS must be allocated completely to the involved transport orders. EN 16258 generally recommends to use *ton-kilometers* as allocation measure but it allows other measures, if suitable, like *transport distance*, *loading weight*, *pallet-kilometer*, and even combinations thereof. If transport distance is considered in the emission allocation process it should relate to crow-fly or shortest travel distances between the order's pickup and delivery locations, which provokes less bias than realized travel distances do (Davydenko et al.; 2014; Kellner; 2016).

For each VOS an allocation rule has to be applied consistently, meaning that transport orders carried together on a leg are treated the same way. Emission allocation starts with the amount of fuel or electricity a vehicle consumes when conducting a trip. For reporting purposes the true energy consumption can be taken ex post, while for planning purposes it has to be estimated. Various models are available to estimate the energy consumption of a vehicle trip at different scales of accuracy, see Demir et al. (2014) for an overview.

Given the true or estimated energy consumption f_i (in liters of fuel or kilowatt) for

a vehicle serving leg i , the corresponding GHG emission e_i , measured in kg CO₂e, is calculated by

$$e_i = f_i \cdot c_s^{GHG}. \quad (6.1)$$

Here, c_s^{GHG} denotes a *conversion factor* for the energy source s used in the process. For oil-based fuels c_s^{GHG} indicates the GHG volume emitted by burning one liter of fuel, measured in kg CO₂e/l. Corresponding emission coefficients for various fuels are provided by the European Committee for Standardization (2013).

Once the GHG emission e_i is determined for leg i , it is allocated in portions of e_{ij} to the transport orders $j \in J_i$ moved in the process. Let ω_j denote the value of the selected allocation measure regarding transport order $j \in J_i$. The allocation weight of order j is computed as the relative share of ω_j against the total value of all orders $k \in J_i$. Hence, the portion of emission e_{ij} assigned to order j is given by

$$e_{ij} = \frac{\omega_j}{\sum_{k \in J_i} \omega_k} \cdot e_i. \quad (6.2)$$

An example is shown in Table 6.5 in the appendix. Here, two orders are moved together by a van. The total emission produced on leg 1 is $e_1 = 60$ kg CO₂e. The table indicates that fairly different emission allocations are realizable for the process. An *egalitarian allocation* of emissions happens by the pallet-kilometer measure. According to EN 16258 an egalitarian allocation is also generally admissible.

In case of a multi-leg transport process, the emission quantity e_j assigned to order j finally results from the sum of quantities assigned to j for each leg traveled. This yields

$$e_j = \sum_{i \in I_j} e_{ij}, \quad (6.3)$$

where I_j denotes the set of legs used by transport order j .

The reporting standard EN 16258 allows carriers to slightly affect the emission declaration process by selecting the allocation rule. This can evoke unequal treatment of shippers which is criticized in the literature (Zhu et al.; 2014; Davydenko et al.; 2014; Kellner; 2016). On the other hand, it enables carriers to balance heterogeneous customer preferences, e.g. if shippers accept a surcharge for low-emission services while others expect low transport rates (Kirschstein and Bierwirth; 2018).

6.3 Communication structure

An eco-label for freight transportation aims at easing and improving the communication between shippers and carriers:

1. Looking for environmental friendly transports, a shipper has to choose a shipping option for a specific good from a set of alternatives.
2. When shippers contract carriers, shippers would like to express their ecological preferences.
3. After a carrier has fulfilled an order, the shipper wants to assess the carbon footprint of the shipment.

To come up with an eco-labeling procedure for shipping options using different transport modes and services, we capture the communication between shippers and carriers by the protocol displayed in Figure 6.1. It illustrates a series of steps for data transformation and decision making on both sides. Some steps can be done by either party or by an intermediary forwarder. The protocol neglects price negotiation. We retrace it step by step below.

S1: Transmit freight documents. Shippers prepare cargo, i.e. specific sets of physical goods, to be transported according to spatial and temporal coordinates. Freight

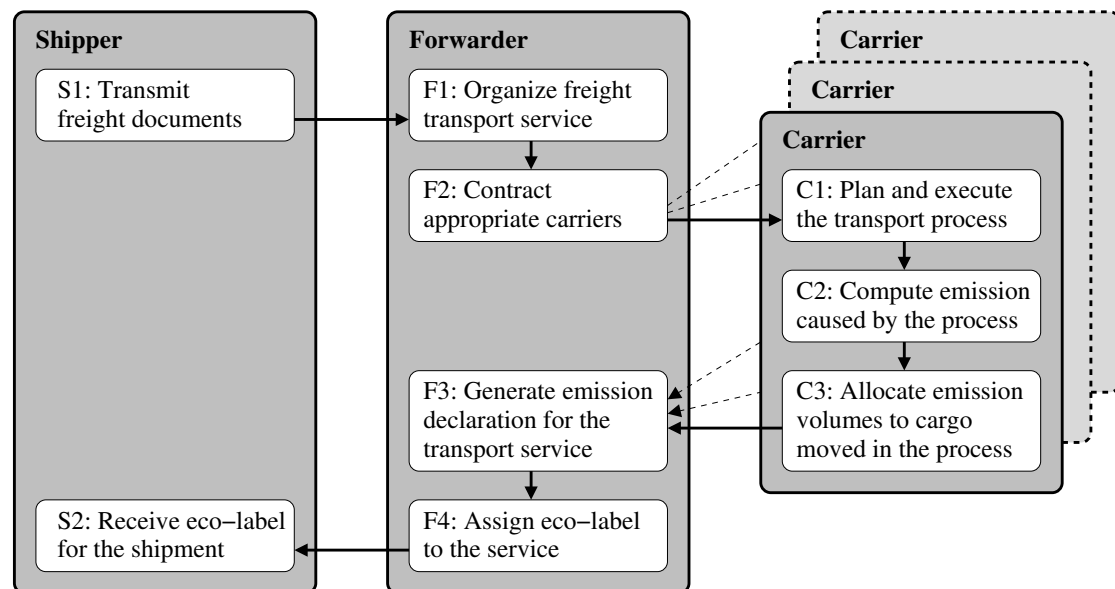


Figure 6.1: Communication protocol of an eco-labeling process.

documents provide the data relevant for freight transportation like the loading weight of cargo (payload), space requirements, handling instructions, pickup-&-delivery locations, time windows, etc.

F1: Organize freight transport service. The forwarder configures the *transport service* according to the requirements specified by the shipper. Often a transport route is split up into a chain of transport *legs*. The physical movement of freight along a *transport chain* is done by vehicles like trucks or trains which is called a *transport process*. Transport processes can be organized as *full truck- or trainload* (FTL) services or as part load services, called *less-than-full truck- or trainload* (LTL). In FTL mode the shipper utilizes the entire vehicle capacity, whereas in LTL mode, goods of multiple shippers are moved together in the process. The forwarder has to select suitable transport processes for each leg of the transport chain. Moreover, logistic operations taking place at transshipment terminals are scheduled. In a planning procedure, the forwarder might choose a preferred transport service after receiving the estimated GHG emissions from the carriers (step F3) and calculating the associated eco-label (step F4). Thereby, the shippers' preferences for eco-sensitivity, cost, time, etc. can be taken into account.

F2: Contract appropriate carriers. To implement the projected transport service, the forwarder has to identify and contract appropriate logistic service providers. Apart from carriers, terminal and warehouse operators can be involved. For simplicity the protocol neglects service operators others than carriers. The negotiations between forwarder and carriers may address pricing, service quality, and environmental compatibility of operations. As a result, the forwarder places a *transport order* for each leg of the transport chain with a particular carrier.

C1: Plan and execute the transport process. Carriers typically receive many transport orders from shippers and forwarders in a period. To satisfy the agreed service quality at reasonable cost, they consolidate LTL services, combining general cargo at nearby destinations into larger entities. These entities are assigned to vehicles offering sufficient transport capacity before their routes and schedules are determined. To solve these complex problems, powerful planning tools are available, also with a scope on minimizing transport-related emissions, see e.g. Jabali et al. (2012), Fukasawa et al. (2016), or Dabia et al. (2017).

C2: Compute emission caused by the process. From the viewpoint of carriers, a transport process generally starts and ends at a vehicle depot. Start depot and end depot, however, must not necessarily match. When the process is completed, the consumed energy is read off directly from the vehicles' fuel gauge or electricity meter. For planning purposes, the energy demand can be estimated by using a suitably calibrated, transport-mode specific energy consumption model, see e.g. Kirschstein and Meisel (2015). We refer to Demir et al. (2014) and Heinold (2020) for reviews on emission estimation models for transporting freight using trucks and trains, respectively. Finally, Equation (6.1) calculates the emission volume e_i caused by the process on leg i from the spent energy and an associated GHG conversion factor.

C3: Allocate emission volumes to cargo moved in the process. If a single transport order j is moved in a process, its emission volume is directly declarable by $e_{ij} = e_i$. Otherwise, the carrier selects an allocation rule and divides e_i among the jointly moved orders according to Equation (6.2).

F3: Generate emission declaration for the transport service. The forwarder collects the GHG emission reports from the carriers engaged in the service and calculates the carbon footprint of the shipment using Equation (6.3). A certified emission declaration provides ecological information for the shipper on the entire service as well as on each of its legs.

F4: Assign eco-label to the service. To provide a simple but qualified assessment of the emission declaration, the forwarder assigns an eco-label to the transport service, which is described in detail in Section 6.4.

S2: Receive eco-label for the shipment. The shipper receives an emission declaration and an eco-label for the shipment carried out on its behalf.

6.4 Eco-labeling system design

We present a design for an eco-labeling of freight transport services which is flexibly applicable to large-sized shipments, e.g. several containers, as well as smaller units like pallets or even individual parcels. We discuss general requirements of such a labeling system in Section 6.4.1. Afterwards, we derive reference emission rates and grading schemes in Sections 6.4.2 and 6.4.3.

6.4.1 General requirements

Eco-labeling is a widely discussed market-based approach for grading the energy efficiency and sustainability of products and services (Prieto-Sandoval et al.; 2016). The general interest in eco-labeling bases on the assumption that consumers can process ecological product information in the purchase decision easier when it is systematically aggregated through a label (Salzman; 1997; Heinzle and Wüstenhagen; 2012). Likewise, scientific literature dealing with the effects of eco-labeling and GHG emission reporting in supply chains grows rapidly in recent years. Gopalakrishnan et al. (2020) assume that supply chain leaders who are motivated to reduce GHG emissions can leverage their knowledge on interrelated sources of GHG emission in their supply chains through reallocating emission volumes among suppliers in a footprint-balanced manner. A good deal of research concentrates on design questions for product-specific eco-labels and technical implementations. For an overview, we refer to Liu et al. (2016) who survey common standards for GHG reporting and the implementation of eco-labeling systems in selected industrial countries.

Previous work has demonstrated that emission reporting and eco-labeling can be effective in gaining eco-efficiency in face of heterogeneous technologies and information asymmetries between independent actors. But with regard to freight transportation markets there are only a few recent studies addressing the applicability of eco-labeling to achieve a transparent grading of energy efficiency. Baumeister et al. (2020) analyze the impact of an eco-label in the booking decision of air passenger transportation. Results from a discrete choice analysis suggest that such labels indeed provide an incentive for passengers to choose flights that are considered to be more environmentally friendly. In this context, Baumeister and Onkila (2017) present results from twelve expert interviews highlighting criteria in the development of eco-labels in the airline industry. Similarly, Poulsen et al. (2017) assess best practices regarding eco-labels from several industries and state that the shipping industry falls short on meeting them.

Based on consumer and manufacturer responses, Banerjee and Solomon (2003) have

evaluated several eco-labeling programs in the U.S. It was found that public programs are more successful in promoting energy efficiency than private programs because governmental support is capable of intensifying a program's credibility, financial stability, and long-term viability. More generally, Harbaugh et al. (2011) stress that eco-labels need to be designed and configured reliably and transparently. Otherwise, obliquity and mistrust may spoil the steering effect of the label information. In addition, Murali et al. (2019) argue that consistent eco-labeling standards foster eco-sensitive decision making when actors face a lack of eco-credibility. Summarizing this analysis, we conclude that an eco-label for the transport industry should be certified by a public organization and possess the following properties:

- *Applicability*: The label must be applicable to all kinds of transport technologies.
- *Effectiveness*: The label must clearly address an ecological target figure.
- *Consistency*: The label must reflect the ecological impact of transport services consistently.
- *Simplicity*: The label must be sufficiently simple to apply and easy to interpret.

Applicability means that the labeling system works for all kinds of transport modes, vehicles, and types of traction. This is mandatory because different technologies may interact in a transport chain. Effectiveness means that the label catches a proper assessment of the environmental impact of a transport service (Salzman; 1997). Consistency ensures that the label allows decision makers to compare the ecological impact of transport services (Clift et al.; 2005). Finally, simplicity means that the label is designed such that a third party can interpret it correctly without much effort.

According to Wiel and McMahon (2005) two types of eco-labels are distinguished, *endorsement labels* and *comparison labels*. Endorsement labels are single-grade labels signaling that a product or a service fulfills a set of criteria. Comparison labels are multi-grade labels based on an ecological performance measure. They allow a relative comparison between two or more entities. Wiel and McMahon (2005) further distinguish comparison labels as *categorical labels* and *continuous labels*. A *categorical label* uses discrete categories such that an entity falls exactly into one category. A *continuous label* positions the entity on a cardinal scale to indicate its ecological performance.

We propose a categorical label for an ecological assessment of freight transport services. A major advantage of categorical labels is that consumers can easily spot the relative performance gap between two compared entities. They indicate, in particular, the distance to the best-in-class entity with respect to a particular eco-measure.

6.4.2 Reference base for transport emissions

An appropriate ecological assessment of freight transportation requires comprising the so called *tank-to-wheel* emission (TTW), which is produced while a vehicle is moved, and the *well-to-tank* (WTT) emission, which arises along the supply chains providing fuel and electricity. Both add up to the well-to-wheel (WTW) emission (Brinkman et al.; 2005). For an ecological assessment of a transport service, the WTW-emission caused by the involved transport processes is put into relation to the logistic performance achieved by the service. According to this ratio, a categorial labeling system can assign a service into one of a set of categories.

In order to determine reasonable category boundaries for a labeling system, we analyze CO₂e emission data reported for freight transportation processes within and between 27 European countries. The data has been recorded in a simulation study of Heinold and Meisel (2018). It involves a total of 4,374 continental transport relations for shipping containerized transport units (TU) each with a payload of 6, 11, or 22 tons. For each relation, 500 shipments with individual pickup and delivery locations are routed in road-only mode and in rail-road mode. Based on the model of Kirschstein and Meisel (2015) the CO₂e emission is determined for each route. The underlying road- and rail-networks base on Open Street Map (2021) and the Trans-European Transport Network (European Commission; 2021). Figure 6.2a shows the resulting distribution of GHG emission rates produced per TU and kilometer (TU-km).

The observed emission rates for land-based containerized transportation range between 70 g CO₂e/TU-km and 1,200 g CO₂e/TU-km. The overall distribution shows three peak regions at 200, 550 and 800 g CO₂e/TU-km, respectively. We recognize five categories of emission rates for TU-shipments. The first category A is reserved for a few

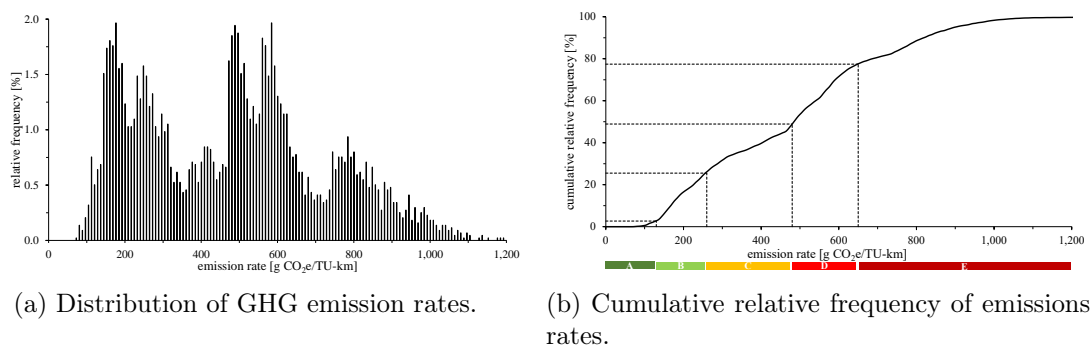


Figure 6.2: Frequency and cumulative frequency of emissions rates in European land-based container transportation (Heinold and Meisel; 2018).

shipments with emission rates lower than rates belonging to the first peak region of the distribution. The second category B addresses those shipments that fall into this region. The third category C covers the range of shipments falling between the first and the second peak region, while the fourth category D addresses shipments belonging to the second peak region. Category E takes up the rest of the shipments including those of the third peak region.

The chosen number of categories is in line with other transport-related eco-labeling systems, e.g., Baumeister and Onkila (2017) review cases of five to seven categories in the aviation sector. The boundaries between the categories become evident by the cumulative distribution of the emission rates shown in Figure 6.2b. About 3% of the shipments fall into category A, with emission rates of at most 130 g CO₂e/TU-km. The further boundaries are set to 260, 480, and 650 g CO₂e/TU-km for labels B to E, comprising about 22%, 23%, 28%, and 23% of the shipments, respectively. Note that the proposed setting reflects a reached state of technology. Boundaries need to be adjusted when technological, infrastructural, or organizational innovation succeeds.

6.4.3 Grading eco-performance of transport services

An often used ecological performance indicator for a transport service divides the volume of CO₂e allocated to the service by the payload of cargo given in tons, and the direct travel distance given in kilometer. Measuring the ecological transport performance in g CO₂e per ton-kilometer (tkm) seems appropriate for heavy goods whereas for volume goods emissions are better accounted by a volume-based (m³km) or pallet-based (pkm) measure.

To address this issue we transfer the category boundaries shown in Figure 6.2b into corresponding eco-labels for heavy goods and volume goods. In line with Heinold and Meisel (2018), we assume that an average TU represents 12.5 tons of payload and 17 pallets which utilizes a heavy truck with a capacity of 25 t and 34 pallets by 50%. For payload capacity the boundary of category A (130 g CO₂e/TU-km) results in $\frac{130 \text{ g CO}_2\text{e}}{12.5 \text{ t}} \approx 10 \text{ g CO}_2\text{e}/\text{tkm}$, and for pallet space in $\frac{130 \text{ g CO}_2\text{e}}{17 \text{ pal.}} \approx 8 \text{ g CO}_2\text{e}/\text{pkm}$. The boundaries of the remaining categories are computed accordingly. This leads to the payload-based and the pallet-based labeling systems shown in Figure 6.3.

As an illustrative example, we consider two shipments which are moved together for a distance of 100 km. Shipment 1 (2) weighs 1 ton (0.5 tons) placed on a single pallet (two pallets). In the process 3 kg CO₂e is allocated to each shipment. For payload-based labeling, Shipment 1 achieves an emission rate of $\frac{3000 \text{ g CO}_2\text{e}}{1\text{t}\cdot 100\text{km}} = 30 \text{ g CO}_2\text{e}/\text{tkm}$ and is

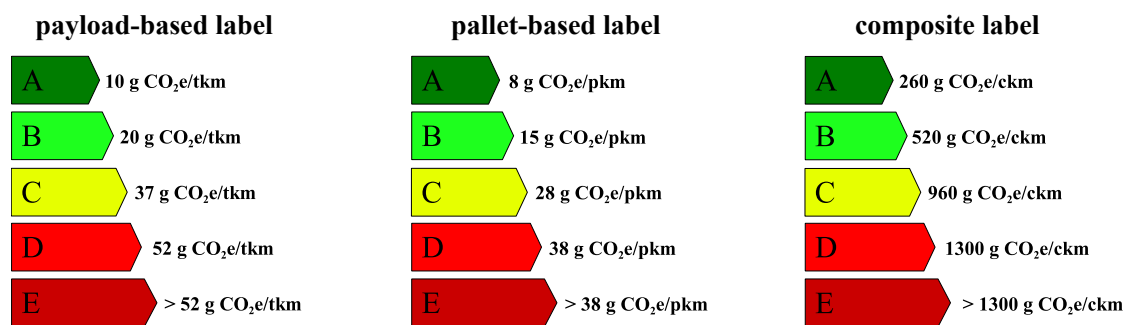


Figure 6.3: Three eco-labeling systems for freight transport services.

labeled as C. Accordingly, Shipment 2 achieves a rate of $= 60 \text{ g CO}_2\text{e/tkm}$ labeled by E. Under pallet-based labeling, the rates are $\frac{3000 \text{ g CO}_2\text{e}}{1\text{p}\cdot 100\text{km}} = 30 \text{ g CO}_2\text{e/pkm}$ and $15 \text{ g CO}_2\text{e/pkm}$ which corresponds to labels D and B, respectively. Note that the payload-pallet ratio of Shipment 1 exceeds the TU's critical ratio of $\frac{12.5}{17}$ ton per pallet, why it is better off under payload-based eco-labeling. On the contrary, shipments that underscore the critical ratio benefit from pallet-based eco-labeling.

A way to unify different performance indicators has been proposed by Davydenko et al. (2014). Let c_i denote the vehicle capacity of type $i \in \{\text{payload, pallets, space, volume, } \dots\}$. Furthermore, let m_{ij} denote the percentage of capacity i which is occupied in the vehicle by transport order j . Then,

$$u_j = \max_i \left(\frac{m_{ij}}{c_i} \right) \quad (6.4)$$

represents the demand of capacity critical for shipment j in a transport process involving arbitrary goods. For an ecological assessment of the shipment its emission declaration can be normalized by the value of u_j . The resulting emission rate is measured in g CO₂e per ckm (*percentage of the composite capacity utilization and kilometer*).

The right-most picture of Figure 6.3 shows the transition of the composite performance measure into a labeling system. Due to the assumption that an average TU exploits the container capacities by 50%, the boundary of label A calculates to $\frac{130 \text{ g CO}_2\text{e}}{50\%} \approx 260 \text{ g CO}_2\text{e/ckm}$. Supposed $c_{\text{payload}} = 25$ ton and $c_{\text{pallet}} = 34$ pallets hold in our example, we obtain $u_1 = \max(1/25, 1/34) = 1/25$ for Shipment 1, and $u_2 = \max(0.5/25, 2/34) = 1/17$ for Shipment 2. The corresponding composite emission rates reveal $\frac{3000 \text{ g CO}_2\text{e}}{1/25 \cdot c \cdot 100\text{km}} = 750 \text{ g CO}_2\text{e/ckm}$ and $510 \text{ g CO}_2\text{e/ckm}$ for the shipments, labeled as C and B respectively. This is in accordance with the stronger labels achieved by the shipments under a payload- or pallet-based labeling system. As the composite-

capacity-based labeling system generally selects the strongest label obtainable for a shipment, it is applied in the rest of the paper, if not stated otherwise.

6.5 Evaluation of eco-labeling systems

In this section, we evaluate the proposed eco-labeling systems at numerical examples. For this, we present the corresponding data in Section 6.5.1 and four transport scenarios in Sections 6.5.2 to 6.5.5.

6.5.1 Transport order data and transport services

For an evaluation of the eco-labeling system displayed in Figure 6.3, we consider two transport orders carried out by four different transport services. Order HG consists of a heavy good with a loading weight of 20 tons placed on 7 pallets. Order VG represents a volume good of 5 tons placed on 27 pallets. The values have been chosen such that both orders can be considered for an individual carriage by a standard truck as well as for a joint carriage, which will perfectly exploit the truck capacities Table 6.6 in the appendix summarizes the order data together with the required transport performances and capacity utilization levels.

Transport orders HG and VG have pickup locations P_1 and P_2 within the same region (the pickup region) and delivery locations D_1 and D_2 within the same delivery region. The pickup and delivery locations are only reachable by road. The direct road transport distances are 200 km for each order. We further assume that a terminal T_1 is available in the pickup region within a 5 km distance to the pickup locations P_1 and P_2 . This terminal serves for transshipping cargo from the road mode to the rail mode and as start and end point of truck routes that collect the cargo. In the delivery region, terminal T_2 is at a distance of 5 km to the delivery locations D_1 and D_2 . The terminals are connected by a rail line of 220 km length that is regularly served by rail trains. Figure 6.4a shows the transport network connecting the pickup places P_1 and P_2 with each other and with the rail terminals T_1 and T_2 as well as the delivery places D_1 and D_2 .

Freight transport services for the two transport orders must realize a door-to-door transport chain. The chain can utilize a single vehicle or multiple vehicles combining a single or multiple modes of transport, and involve several transshipment processes of goods. If no transshipment is involved, we refer to it as a *direct transport service*. As mentioned in Section 6.3, direct services are further classified as FTL services, where goods of a single shipper ride alone, and as LTL services, where the carrier consolidates

goods of multiple shippers to improve vehicle utilization.

For transport services involving transshipment of goods we refer to definitions provided by the Economic Commission for Europe (2001). A service is referred to as *multimodal* if the movement of goods is realized by two or more modes of transport, and *unimodal* otherwise. Multimodal services generally allow for handling and storing goods when changing modes. In case the movement of goods happens in one and the same loading unit, the transport is called *intermodal*. A multimodal transport service with intermediate storage can be advantageous if transport orders are given on a regular basis. To achieve economies of scale, shippers can bundle multiple orders into larger shipments.

The following services are taken into consideration:

1. FTL road transportation
2. LTL road transportation
3. Multimodal rail-road transportation without intermediate storage of goods (intermodal)
4. Multimodal rail-road transportation with intermediate storage of goods

For road transports, a diesel-powered heavy truck is used. Its fuel consumption per kilometer is defined by $f(p) = 0.22 + 0.14 \cdot \frac{p}{c}$, where 0.22 is the baseline fuel consumption of the empty truck and 0.14 is the marginal fuel consumption of a fully loaded truck, p is the carried payload and $c = 25$ ton is the payload capacity of the truck (see Schmied and Knörr; 2013). Next to transport trips, repositioning trips of empty trucks are included in each scenario. For rail transports, electrified freight trains are used. Two service types are offered by a rail company. Short-trains operate in the general cargo market where a shipment must be at least a pallet. Long-train services are reserved for shipments of complete truckloads. The energy consumption for short-trains is 30 kWh per kilometer and for long-trains 35 kWh per kilometer reflecting the trains' different total weights (Schmied and Knörr; 2013). Emission coefficients of 3.15 kg CO_{2e} per liter of Diesel and 0.5 kg CO_{2e} per kWh electricity are applied (Schmied and Knörr; 2013). Details on the energy demands for the transport services are outlined in Figure 6.4. Technical parameters of the vehicles considered in the following scenarios are summarized in Table 6.7.

6.5.2 FTL road transportation

In the baseline scenario, orders HG and VG are served individually by two heavy trucks. These trucks start their tours empty at T_1 , pick up load at P_1 and P_2 , respectively, deliver

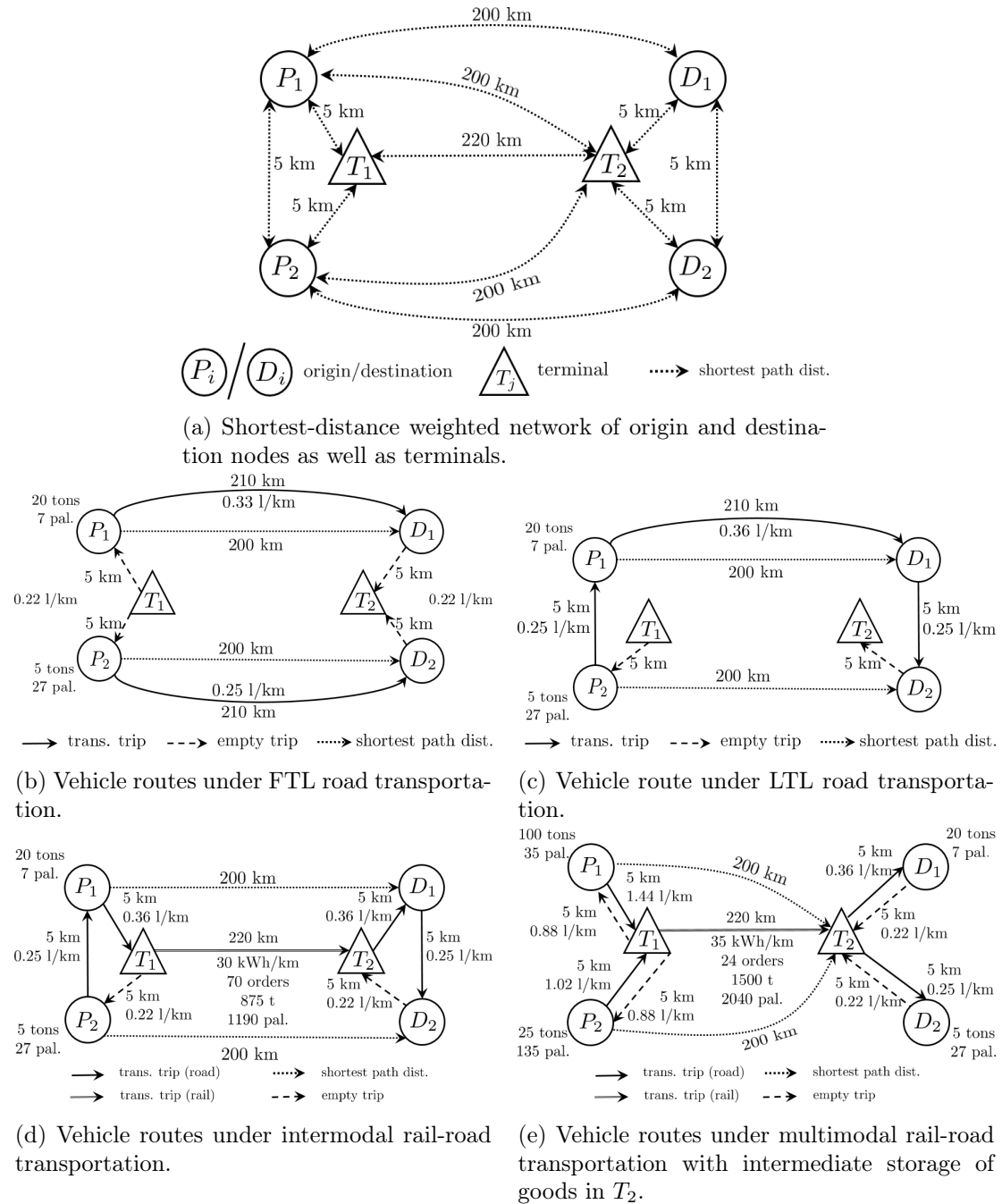








Figure 6.4: Vehicle routes for all transport services along with energy demand rates

Table 6.1: Emission declarations and eco-labels under FTL road transportation.

order	declaration	payload-based label		pallet-based label		composite label	
	(kg CO ₂ e)	(g CO ₂ e/tkm)		(g CO ₂ e/pkm)		(g CO ₂ e/ckm)	
HG	225	56		161		1,406	
VG	172	172		32		1,083	
Σ	397						

it at D_1 and D_2 , respectively. Afterwards, they return empty to terminal T_2 . Usually, shortest routes to a destination cannot be realized exactly due to breaks, refueling stops etc. This is reflected by a detour of 10 km such that a traveling distance of 210 km results for the transport leg of the trip. Figure 6.4b displays the activities along with the relevant data.



A heavy truck spends $f(0) = 0.22$ liter of Diesel per kilometer if going empty, $f(20) = 0.22 + 0.14 \cdot \frac{20}{25} \approx 0.33$ liter while moving HG, and $f(5) = 0.22 + 0.14 \cdot \frac{5}{25} \approx 0.25$ liter while moving VG. Hence, fuel consumption is $5 \cdot 0.22 + 210 \cdot 0.33 + 5 \cdot 0.22 = 71.5$ liter along the route that serves HG and $5 \cdot 0.22 + 210 \cdot 0.35 + 5 \cdot 0.22 = 54.7$ liter for the route that serves VG. The corresponding CO₂e emissions are $71.5 \cdot 3.15 \approx 225$ kg and $54.7 \cdot 3.15 \approx 172$ kg, respectively, leading to a total emission of 397 kg CO₂e for both orders.

Eco-labels are derived for the transport services by calculating the corresponding CO₂e emission rates per ton kilometer (tkm), pallet kilometer (pkm), and composite capacity kilometer (ckm), see Table 6.1. It indicates that label E is awarded in most cases. Road mode is obviously not an eco-friendly solution for long-haul transports. However, the pallet-based system still awards label D to the service of VG. Recall that the composite-based system always selects the capacity maximally utilized by an order. For order VG this is pallet-space with a relative utilization of $\frac{27}{34}$. This yields an emission rate of 1,083 g CO₂e/ckm (= 172 kg/CO₂e divided by $\frac{27}{34}$ and 200 km direct distance) and reveals label D just like the pallet-based labeling system.

6.5.3 LTL road transportation

A better consolidation of freight is reached when orders HG and VG are shipped together. Figure 6.4c shows the route taken by the LTL service. A single empty truck starts at terminal T_1 , picks up load successively at P_2 and P_1 , delivers it at D_1 and D_2 , before

Table 6.2: Emission declaration, allocation and eco-labels under LTL road transportation (values in CO₂e).

allocation order	payload		pallets		egalitarian		
	kg	g/ckm	kg	g/ckm	kg	g/ckm	
HG	202	1,263	52	325	127	793	
VG	51	321	201	1,266	127	800	
Σ	253		253		253		

returning empty to terminal T_2 . For the longest part of the journey, the truck is fully occupied in terms of payload and pallet space. The fuel consumption on this leg accounts for $f(25) = 0.22 + 0.14 \cdot \frac{25}{25} \approx 0.36$ liter per km. In total, the truck consumes 80.3 liters Diesel and emits 253 kg CO₂e.

Following EN 16258, the emission quantity of 253 kg CO₂e is allocated to orders HG and VG either in proportion to payload, pallets, or egalitarian, see Table 6.2. The emission declarations are lower for the LTL service than for the FTL service with the only exception of order VG. It receives a declaration of 201 kg CO₂e from pallet-proportional emission allocation. Obviously, when heavy and volume goods are moved together, the CO₂e share of heavy goods benefits from a pallet-based emission allocation while volume goods benefit from a payload-based allocation. Supposed that the involved parties are likewise eco-sensitive, egalitarian allocation balances shares most fairly.

Note that composite labeling systems generally awards stronger labels to the LTL service than to the FTL service. Either HG or VG can reach label B at the expense of the other order, which achieves label D. In case both shipper are eco-sensitive they can jointly reach label C with the LTL service.

6.5.4 Multimodal rail-road transportation without intermediate storage of goods (intermodal)

An intermodal rail-road transport service divides the transport chain of the orders into three legs, the pre-, main-, and post-carriage. During pre-carriage the movement of goods is executed by a single truck that starts its tours empty at the depot in T_1 and ends there for transshipping the cargo onto a train. Post-carriage of both orders is performed by a truck that starts its route in T_2 where it picks up the goods from the train and delivers them before returning empty to T_2 . The routes of the vehicles are shown in Figure 6.4d. The total fuel consumption of the trucks is $2 \cdot 5 \cdot (0.22 + 0.25 + 0.36) = 8.3$ liters of Diesel,

Table 6.3: Emission declaration, allocation and eco-labels under intermodal rail-road transportation (values in CO₂e).

order	on road		on rail							
	allocation	payload			pallets		egalitarian			
		kg	g/ckm	label	kg	g/ckm	label	kg	g/ckm	label
HG	payload	96	600	C	40	250	A	68	425	B
	pallets	81	506	B	25	156	A	53	331	B
	egalitarian	89	556	C	33	206	A	60	375	B
VG	payload	24	151	A	80	504	B	52	327	B
	pallets	40	252	A	96	605	C	68	428	B
	egalitarian	32	202	A	88	554	C	60	378	B

leading to an emission of 26.2 kg CO₂e.

The main carriage is performed by an electrified short-train. It spends $220 \text{ km} \cdot 30 \text{ kWh/km} = 6,600 \text{ kWh}$ of energy on the rail leg which causes a CO₂e emission of $6,600 \cdot 0.5 = 3,300 \text{ kg}$. We further assume that the train moves 70 transport orders with a total of 875 tons and 1,190 pallets between the two terminals. This means that both, the average demand of payload capacity and the average demand of pallet capacity of both orders exactly meet the average capacity demand of all orders moved in the process. Hence, a share of $2 \cdot \frac{3,300}{70} = 94.3 \text{ kg CO}_2\text{e}$ falls upon orders HG and VG for the rail leg, no matter what allocation rule the rail carrier applies. Thus, a total of $26.2 + 94.3 \approx 120 \text{ kg CO}_2\text{e}$ is assigned to both orders by the intermodal service, which is less than in FTL and LTL services.

Since the intermodal service involves multiple transport processes, the allocation rules selected by the carriers can vary. We assume that the road carriers apply the same rule. Various emission declarations are yet possible for orders HG and VG. Table 6.8 in the appendix shows corresponding emission declarations for road and rail legs. Nine combinations of emission allocation rules are possible and assessed by the composite labeling system in Table 6.3. It indicates that the allocation rule used in the main carriage shows a larger impact than the rule used for pre- and post-carriages. As before, HG benefits from pallet-based allocation and VG from payload-based allocation. Both orders can achieve the strongest label A at their own, provided the allocation rule on the rail leg is chosen to their advantage. With egalitarian allocation applied to the rail leg, both achieve label B, no matter which allocation rule is used on the road legs. This

signals the environmental compatibility of rail freight transportation.

6.5.5 Multimodal rail-road transportation with intermediate storage of goods







To study multimodal transportation, we regard the order quantities of HG and VG as a regular customer period demand. We further assume that a warehouse is available at terminal T_2 which can be used for an intermediate storage of goods. This setting enables shipping goods in larger amounts leading to a better transport consolidation such that larger and more energy-efficient vehicles like long-trains can be used.

For an evaluation of the multimodal rail-road service we consider transport quantities for both goods which are a fivefold of the period demand. These quantities can be moved to T_1 by four complete truckloads each. The trucks are fully utilized regarding either payload ($4 \cdot 25 = 5 \cdot 20$ tons) or pallet space ($4 \cdot 34 = 5 \cdot 27 + 1$ pallets) in seven of the eight trips. Merely a single pallet storage place is not occupied in one of the trips. As road transportation on leg 1 takes place in FTL mode, GHG emissions are directly declarable for pre-carriage. To get rid of emission allocation for post-carriage, we suppose that the road transport from T_2 to the delivery places is done in unconsolidated FTL mode, too. On this leg capacity is utilized by 80%. An allocation of transport emissions is only necessary on the rail leg, which comprises the long-train rail transport between T_1 and T_2 . Figure 6.4e displays the outlined logistic activities for the multimodal service.

The total GHG emission produced by the service is calculated as follows: Leg 1 of the transport chain comprises four fully utilized truck transports for each good. Those four trucks cause $3.15 \cdot 5 \cdot (0.88 + 1.44) \approx 37$ kg CO₂e for HG and $3.15 \cdot 5 \cdot (0.88 + 1.02) \approx 30$ kg CO₂e for VG. The electrified long-train operating on leg 2 consumes $220 \text{ km} \cdot 35 \text{ kWh/km} = 7,700$ kWh of energy. It causes total emissions of $7,700 \cdot 0.5 = 3,850$ kg CO₂e. We assume that 24 orders with a total of 1,500 tons and 2,040 pallets are moved together in the rail process with an average of 62.5 tons and 85 pallets per order. Like for the short-train, this is in line with the joint capacity demand of the heavy and the volume good. Consequently, a share of $2 \cdot \frac{3,850}{24} \approx 321$ kg CO₂e falls upon both orders, whatever allocation rule is selected. To attribute GHG emissions to the periodic orders, the emission volumes calculated for leg 1 and 2 are divided by five periods. Emissions on leg 3 are directly declarable like for leg 1. They account for $3.15 \cdot 5 \cdot (0.22 + 0.36) \approx 9.2$ kg CO₂e for the heavy good and $3.15 \cdot 5 \cdot (0.22 + 0.25) \approx 7.4$ kg CO₂e for the volume good and are respected in every period.

Table 6.4 shows the emission declaration of the orders on each leg and the eco-

Table 6.4: Emissions declaration, allocation and eco-labels under multimodal transportation.

order	allocation	declaration (kg CO ₂ e) on			(kg CO ₂ e)	(g CO ₂ e/ckm)	
		leg 1	leg 2	leg 3	total		
HG	payload	7.3	51.4	9.2	68	340	
	pallets	7.3	13.2	9.2	30	150	
	egalitar.	7.3	32.1	9.2	49	245	
VG	payload	6.0	12.8	7.4	26	131	
	pallets	6.0	51.0	7.4	64	322	
	egalitar.	6.0	32.1	7.4	46	232	

labels achievable by the multimodal transport. Emission allocation only takes place on leg 2, which represents the major part of the transport. The multimodal service improves the eco-performance of the transport operations once more. Allowing for an intermediate storage, it allocates 96 kg CO₂e to HG in the maximum which is a 29% reduction against intermodal transportation. The eco-labels signal this trend very clearly. Whatever emission rule the rail carrier selects, the transport orders receive at least label B. With the egalitarian allocation rule, the service even achieves label A for both orders. It must be noted, however, that GHG emission caused by warehousing operations, is disregarded in the analysis.

6.5.6 Evaluation summary

For an evaluation of the proposed approach we recall the requirements formulated in Section 6.4.1. To overcome the limitation of labeling approaches which are based on single performance measures (like ton-kilometers or pallet-kilometers) a composite-capacity based label has been developed for the transport industry. It supports shippers in finding eco-compatible transport options and makes searches for a best-fitting label redundant. The proposed label design relies on a consistent calculus regarding energy generation, transformation, and consumption. Regarding *applicability* it supports an appropriate consideration of vehicles classes driven by electric or combustion engines, and it covers future technologies like fuel cells as well. It is likewise *effective* by addressing the release of GHG on a unique and quantitative basis.

Consistency means that a labeling system signals the ecological impact of different transport services adequately, which is not that straight to judge for the composite-

capacity based labeling system. Four services have been investigated. Even though their environmental ranking is straightforward, the responded signals are not that definite in every single case. The reason is that freight consolidation complicates emission allocation. For one and the same transport order and service, not a single but a range of different labels is achievable depending on the allocation rule selected. Table 6.9 in the appendix summarizes the ranges of labels assignable to the two transport orders in view of the four services. Selecting an allocation rule gives carriers an important instrument at hand to enhance the performance of eco-sensitive shippers. Supposed all shippers are equally sensitive, the question arises with which rule the best common label is obtained. For the transport orders in our example this is the egalitarian allocation rule. The last line of Table 6.9 shows the best labels that HG and VG can obtain together in a consolidated transport service. A clear grading is recognizable between LTL road transportation, intermodal transportation and multimodal transportation which is consistent with the services' total emission quantities for both orders.

Regarding *simplicity*, our approach is not that clear yet. While its application is technically controllable and reliable, the outcome is not always simple to interpret regarding the unit of composite capacity. This might be subject of future research, next to the research opportunities that we outline in the following.

6.6 Research directions

We present a list of research opportunities that might be investigated in the context of eco-labels for freight transportation. Clearly, we can only touch these issues here and the provided list is certainly not complete.

Operations management and integration into planning systems: Eco-labels can be used as a way to communicate a customer's environmental preference regarding a shipment. Then, this information, i.e., the eco-label, needs to be considered proactively in the operational planning and decision making of logistics service providers. For this purpose, it needs to be investigated how labels can be incorporated into optimization models and solution methods for vehicle routing problems, inter- and multimodal transportation planning, service network design, transport mode selection and further related problems. We refer to Bektaş et al. (2019) for a general overview on the role of operations research in green freight transportation. In this context, it will be interesting to investigate different ways of integrating eco-labels in optimization models. For example, labels might be considered as soft or hard constraints as well as (part of) the objective with which the fulfilment of eco-labels would work as a customer-related service level. On this basis, it

would be interesting to compare a setting in which shipments are either in accordance with their eco-label, or not, with a setting considering also the magnitude of not fulfilling a label. For this, eco-labels can be converted to emission limits that state a shipment's absolute amount of emissions resulting from the corresponding eco-label (Heinold and Meisel; 2020).

Emission allocation: As illustrated in Section 6.5.5, choosing an emission allocation rule is a crucial decision for the implementation of a labeling system, especially if heterogeneous goods share the same service. Our example captured just a few out of many available allocation rules (see e.g. Kellner and Otto; 2012) and highlighted their effects in an illustrative way. Therefore, more detailed analyses of product-specific allocation rules as well as their (game-)theoretic properties and practical effectiveness are due.

Adjustment of the label's reference base: A weak spot of categorial labels is that it suffices to underscore the upper bound of a category just marginally in order to achieve it. Hence, services may receive the same label even if they have quite diverse environmental performances. This effect may be compensated partly by defining a larger number of categories, but it remains unclear whether this is a proper countermeasure in general. It is also known that labels can become a victim of their own success (Heinzele and Wüstenhagen; 2012) if best-in-class categories are achieved more and more easily due to technological progress. This raises a need for regularly re-assessing the category boundaries to push companies towards more eco-friendliness in the long run.

Political implications and steering effects: Politics pursues eco-initiatives to foster green transportation, e.g., by implementing policies to shift freight from road to rail. This raises the question of how a transport-related eco-label as proposed by this paper can support such policies. More generally, it is important to evaluate the overall environmental effect to be expected at a local and global scale. In particular, it might be interesting to analyze how overall emissions are affected by the introduction of eco-labels and to compare this change with other eco-oriented policies like emission reduction targets or carbon taxes. This is, we expect some interesting findings regarding research on how eco-labels work as a steering effect towards more sustainable transport solutions.

Competitive advantage, business models and consumer behavior: If shippers and logistic service providers express eco-friendliness of their products and services by an eco-labeling system, it is worth analyzing the competitive advantage they gain. Corresponding research could comprise, for example, investigating how customers value a better eco-label category and whether this can be turned into a higher willingness-to-pay such that a carrier's profit increases. In this context, an open question is what new business models

could emerge from the introduction of such labels and how companies incorporate eco-labeling when negotiating with business partners or in pricing decisions for their products and services. For instance, Agatz et al. (2021) analyzes the interactions between price and eco-labeling incentives for time slot selection in a home delivery service. They conclude from experiments and simulations that eco-labels are more effective than price incentives in fostering more sustainable customer decisions.

Label propagation in supply chains and inclusion of further processes: Almost any industry-made product consists of a wide range of materials and components that usually stem from a large number of spatially distributed suppliers. Nowadays, many supply chain parties determine and report the carbon footprint of their products. What is still lacking are mechanisms for consolidating such information along horizontal and vertical partnerships. This also calls for new tasks and roles such as the one of an environmentally-oriented supply chain leader, see Gopalakrishnan et al. (2020). The required transactions may call for an adaptation of the logistics-oriented communication protocol from Section 6.3. From this, a better understanding could be obtained on how to propagate and harmonize eco-labels of converging and diverging material flows. The adaptation might also strive for an inclusion of emissions caused by the involved transshipment and warehousing processes. However, communication flows and labeling procedures should be kept as simple as possible ensuring a comprehensible and trustworthy labeling of products and services.

6.7 Conclusion

The paper proposes a categorial, comparison eco-label for the freight transportation industry. The label fosters transparency of the eco-friendliness of transport processes with regard to their emitted greenhouse gases. The gained transparency can be exploited by freight forwarders to differentiate their services from those of (less eco-friendly) competitors, by shippers to express their eco-friendliness, and by other stakeholders for further purposes like reporting or statistics. We have discussed design issues of such a label and procedures of the labeling process for transport services and orders. We derived three labeling systems. The first one assesses emissions per ton-kilometer, which is particularly useful for shipments involving heavy goods. The second system assesses emissions per pallet-kilometer, which is most suitable for volume goods. The third system flexibly adapts the labeling to the most intensively used capacity dimension of a transport process. This system is generally applicable even for processes that involve a mix of heavy goods and volume goods.

We provided examples of how to implement the label in different transport management settings. Our analyses showed that choosing an emission allocation rule and labeling system can yield very different labels for a particular shipment. Still, the labels fulfill general expectations such as that consolidated transports achieve better labels than non-consolidated transports.

Finally, we proposed directions for future research, including topics in operations management but also further topics that address policy issues, incentives and others. We have sketched those challenges that we consider most relevant, which might be considered subjective.

Data Availability Statement

The data supporting the findings of this study are available in the supporting information of this article. They consist of a file containing the raw simulation results underlying the GHG emission rate distribution in Section 4.3.

Acknowledgments

This research was supported by the German Research Foundation (DFG) under reference 268276815.

6.8 Appendix A. Figures and Tables

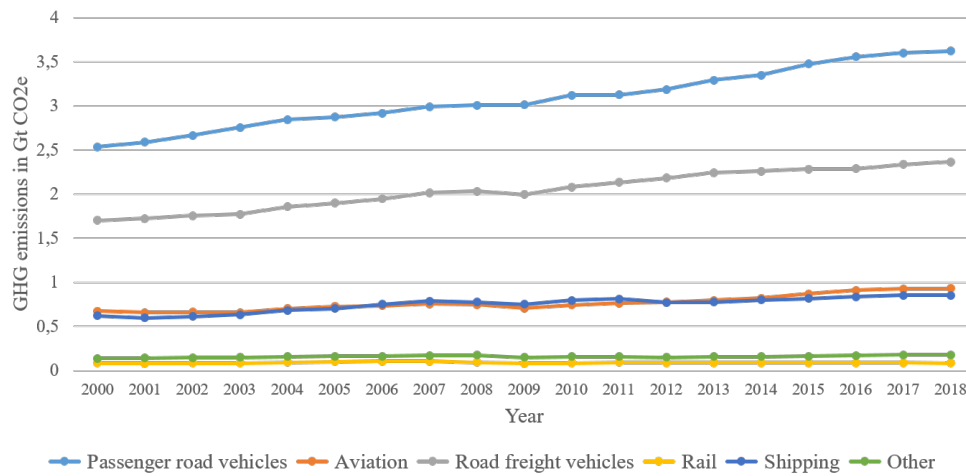


Figure 6.5: Transport-related CO₂e emissions worldwide, 2000-2018. Source: International Energy Agency (2020)

Table 6.5: Comparison of allocation measures compliant with EN 16258: A van moves two orders $j = 1, 2$ on transport leg $i = 1$. Its total emission is $e_1 = 60$ kg CO₂e.

order j	direct distance (km)	payload (ton)	ton kilometer (tkm)	pallets (pc)	pallet-km (pkm)
1	50	0.400	20	2	100
2	100	0.600	60	1	100
Σ	150	1.000	80	3	200
emission allocation (kg CO ₂ e)					
$e_{1,1}$	20	24	15	40	30
$e_{1,2}$	40	36	45	20	30

Table 6.6: Transport order data and utilization rates for individual carriage by a heavy truck.

order	distance (km)	payload (ton)	pallets (pc)	performance		utilization	
				(tkm)	(pkm)	(%weight)	(%space)
HG	200	20.0	7	4,000	1,400	0.800	0.206
VG	200	5.0	27	1,000	5,400	0.200	0.794

Table 6.7: Vehicle data for transport modes used in section 6.5.

vehicle	measure	FTL	LTL	intermodal	multimodal
truck	payload capacity [t]	25	25	25	25
	pallet space capacity [# pal.]	34	34	34	34
	total # orders/vehicle	1	2	2	1
train	total payload [t]	-	-	875	1500
	total pallets [# pal.]	-	-	1190	2040
	total # orders/vehicle	-	-	70	24

Table 6.8: Emission allocation (in kg CO₂e) for pre/post-carriage (road) and main carriage (rail).

allocation: order	payload	pallets	egalitarian	payload	pallets	egalitarian
	pre/post-carriage (road)			main carriage (rail)		
HG	21.0	5.4	13.1	75.4	19.4	47.1
VG	5.2	20.8	13.1	18.9	74.9	47.1
Σ		26.2			94.3	

Table 6.9: Ranges of allocated emissions (in kg CO₂e) and associated labels achieved by four transport services. Eco-labels are recorded as obtained from the order of payload-based, pallet-based and egalitarian allocation.

order	FTL	LTL	intermodal	multimodal
HG	225 	52-202 	25-97 	30-68
VG	172 	51-201 	24-96 	26-64
common best label				

Bibliography

- Agatz, N., Fan, Y. and Stam, D. (2021). The impact of green labels on time slot choice and operational sustainability, *Production and Operations Management* (In Press).
- Banerjee, A. and Solomon, B. D. (2003). Eco-labeling for energy efficiency and sustainability: a meta-evaluation of US programs, *Energy Policy* **31**(2): 109 – 123.
- Baumeister, S. and Onkila, T. (2017). An eco-label for the airline industry?, *Journal of Cleaner Production* **142**: 1368–1376.
- Baumeister, S., Zeng, C. and Hoffendahl, A. (2020). The effect of an eco-label on the booking decisions of air passengers, *Transport Policy* (In Press).
- Bektaş, T., Ehmke, J. F., Psaraftis, H. N. and Puchinger, J. (2019). The role of operational research in green freight transportation, *European Journal of Operational Research* **274**(3): 807–823.
- Brinkman, N., Wang, M., Weber, T. and Darlington, T. (2005). Well-to-wheels analysis of advanced fuel/vehicle systems: A north american study of energy use, greenhouse gas emissions, and criteria pollutant emissions, *Technical report*, EERE Publication and Product Library.
- Clift, R., Malcolm, R., Baumann, H., Connell, L. and Rice, G. (2005). Eco-labels and electric monks, *Journal of Industrial Ecology* **9**(3): 4–7.
- Dabia, S., Demir, E. and Woensel, T. V. (2017). An exact approach for a variant of the pollution-routing problem, *Transportation Science* **51**(2): 607–628.
- Davydenko, I., Ehrler, V., de Ree, D., Lewis, A. and Tavasszy, L. (2014). Towards a global CO2 calculation standard for supply chains: Suggestions for methodological improvements, *Transportation Research Part D: Transport and Environment* **32**: 362–372.
- Dekker, R., Bloemhof, J. and Mallidis, I. (2012). Operations research for green logistics - an overview of aspects, issues, contributions and challenges, *European Journal of Operational Research* **219**(3): 671 – 679.
- Demir, E., Bektaş, T. and Laporte, G. (2014). A review of recent research on green road freight transportation, *European Journal of Operational Research* **237**(3): 775–793.

- Economic Commission for Europe (2001). Terminology on combined transport, *Technical report*, United Nations/ Economic Commission for Europe. <https://unece.org/DAM/transport/wp24/documents/term.pdf>, accessed 2021-05-10.
- EPA (2021). United States Environmental Protection Agency - Global Greenhouse Gas Emissions Data. <https://www.epa.gov/ghgemissions/global-greenhouse-gas-emissions-data>, accessed 2021-05-10.
- European Commission (2021). About TEN-T. <http://ec.europa.eu/transport/infrastructure/tentec/tentec-portal/site/en/abouttent.htm>, accessed 2021-05-10.
- European Committee for Standardization (2013). Methodology for calculation and declaration of energy consumption and GHG emissions of transport services (freight and passengers) EN 16258.
- Fukasawa, R., He, Q. and Song, Y. (2016). A branch-cut-and-price algorithm for the energy minimization vehicle routing problem, *Transportation Science* **50**(1): 23–34.
- Gopalakrishnan, S., Granot, D., Granot, F., Sošić, G. and Cui, H. (2020). Incentives and emission responsibility allocation in supply chains, *Management Science* (In Press).
- Harbaugh, R., Maxwell, J. W. and Roussillon, B. (2011). Label confusion: The groucho effect of uncertain standards, *Management Science* **57**(9): 1512–1527.
- Heinold, A. (2020). Comparing emission estimation models for rail freight transportation, *Transportation Research Part D: Transport and Environment* **86**: 102468.
- Heinold, A. and Meisel, F. (2018). Emission rates of intermodal rail/road and road-only transportation in Europe: A comprehensive simulation study, *Transportation Research Part D: Transport and Environment* **65**: 421 – 437.
- Heinold, A. and Meisel, F. (2020). Emission limits and emission allocation schemes in intermodal freight transportation, *Transportation Research Part E: Logistics and Transportation Review* **141**: 101963.
- Heinzle, S. L. and Wüstenhagen, R. (2012). Dynamic adjustment of eco-labeling schemes and consumer choice - the revision of the EU energy label as a missed opportunity?, *Business Strategy and the Environment* **21**(1): 60–70.
- International Energy Agency (2020). Transport sector CO₂ emissions by mode in the sustainable development scenario 2000-2030, <https://www.iea.org/topics/transport>, accessed 2021-05-10.

- IPCC (2014). Climate change 2014: Mitigation of climate change. contribution of working group iii to the fifth assessment report of the intergovernmental panel on climate change, www.ipcc.ch/site/assets/uploads/2018/02/ipcc_wg3_ar5_full.pdf, accessed 2021-05-10. Edenhofer, O.; R. Pichs-Madruga; Y. Sokona; E. Farahani; S. Kadner; K. Seyboth; A. Adler; I. Baum; S. Brunner; P. Eickemeier; B. Kriemann; J. Savolainen; S. Schlömer; C. von Stechow; T. Zwickel; J.C. Minx (ed.).
- Jabali, O., Van Woensel, T. and de Kok, A. (2012). Analysis of travel times and CO₂ emissions in time-dependent vehicle routing, *Production and Operations Management* **21**(6): 1060–1074.
- Kellner, F. (2016). Allocating greenhouse gas emissions to shipments in road freight transportation: Suggestions for a global carbon accounting standard, *Energy Policy* **98**: 565–575.
- Kellner, F. and Otto, A. (2012). Allocating CO₂ emissions to shipments in road freight transportation, *Journal of Management Control* **22**(4): 451–479.
- Kirschstein, T. and Bierwirth, C. (2018). The selective travelling salesman problem with emission allocation rules, *Operations Research Spectrum* **40**(1): 97–124.
- Kirschstein, T. and Meisel, F. (2015). GHG-emission models for assessing the eco-friendliness of road and rail freight transports, *Transportation Research Part B: Methodological* **73**: 13–33.
- Liu, T., Wang, Q. and Su, B. (2016). A review of carbon labeling: Standards, implementation, and impact, *Renewable and Sustainable Energy Reviews* **53**: 68–79.
- Murali, K., Lim, M. K. and Petruzzi, N. C. (2019). The effects of ecolabels and environmental regulation on green product development, *Manufacturing & Service Operations Management* **21**(3): 519–535.
- Open Street Map (2021). OpenStreetMap is the free wiki world map. <https://www.openstreetmap.org>, accessed 2021-05-10.
- Poulsen, R. T., Hermann, R. R. and Smink, C. K. (2017). Do ecolabels lead to better environmental outcomes in the international shipping industry? Paper presented at 24th NFF Conference, Bodø, Norway.

- Prieto-Sandoval, V., Alfaro, J. A., Mejía-Villa, A. and Ormazabal, M. (2016). Eco-labels as a multidimensional research topic: Trends and opportunities, *Journal of Cleaner Production* **135**: 806–818.
- Salzman, J. (1997). Informing the green consumer: The debate over the use and abuse of environmental labels, *Journal of Industrial Ecology* **1**(2): 11–21.
- Savelsbergh, M. and Woensel, T. V. (2016). 50th anniversary invited article - city logistics: Challenges and opportunities, *Transportation Science* **50**(2): 579–590.
- Schmied, M. and Knörr, W. (2013). Calculating GHG emissions for freight forwarding and logistics services in accordance with EN 16258, *Technical report*. https://www.clecat.org/media/CLECAT_Guide_on_Calculating_GHG_emissions_for_freight_forwarding_and_logistics_services.pdf, accessed 2021-05-10.
- Wiel, S. and McMahon, J. E. (2005). *Energy-efficiency labels and standards: a guidebook for appliances, equipment and lighting*, Collaborative Labeling and Appliance Standards Program (CLASP), Washington D.C.
- Zhu, W., Erikstad, S. O. and Nowark, M. P. (2014). Emission allocation problems in the maritime logistics chain, *EURO Journal on Transportation and Logistics* **3**(1): 35–54.

Chapter 7

Primal-Dual Value Function Approximation for Stochastic Dynamic Intermodal Transportation with Eco-labels

Publication status Submitted to *Transportation Science* (04.10.2021). Currently under review (first round).

Arne Heinold¹, Marlin Wolf Ulmer², and Frank Meisel¹

¹: School of Economics and Business, Kiel University, Kiel, Germany

²: Department of Business Administration, Otto-von-Guericke-Universität, Magdeburg, Germany

Abstract Eco-labels are a way to benchmark transportation shipments with respect to their environmental impact. In contrast to an eco-labeling of consumer products, emissions in transportation depend on several operational factors like the mode of transportation (e.g., train or truck) or a vehicle's current and potential future capacity utilization when new orders are added for consolidation. Thus, satisfying eco-labels and doing this cost-efficiently is a challenging task when dynamically routing orders in an intermodal network. In this paper, we model the problem as a multi-objective sequential decision process and propose a reinforcement learning method, value function approximation (VFA). VFAs frequently simulate trajectories of the problem and store observed

values (violated eco-labels and costs) and states aggregated to a set of features. The observations are used for improved decision making in the next trajectory. For our problem, we face two additional challenges when applying a VFA, the multiple objectives and the ‘delayed’ realization of eco-label satisfaction due to future consolidation. For the first, we propose different feature sets dependent on the objective function’s focus, costs or eco-labels. For the latter, we propose enhancing the suboptimal decision making and observed pessimistic *primal* values within the VFA-trajectories with optimistic *dual* ex-post evaluation when all information of a trajectory is known. This enhancement is a general methodological contribution to the literature of approximate dynamic programming and will likely improve learning for other problems as well. We show the advantages of both components in a comprehensive study for intermodal transport via train and trucks in Europe.

Keywords Intermodel Transportation, Sustainable Transportation, Eco-label, Multi-objective Stochastic Dynamic Decision Making, Approximate Dynamic Programming, Value Function Approximation, Primal-Dual VFA, Objective-specific Feature Selection

7.1 Introduction

Transportation of freight and passengers is a main contributor to the anthropogenic greenhouse gas emissions (European Environment Agency; 2021) and a rising public and political awareness of it forces logistics companies to offer more sustainable transport solutions. A popular method for benchmarking products, services, or facilities according to their environmental impact is to use eco-labels (e.g., Lorenzo-Toja et al.; 2016). Such labels generally indicate the relative environmental impact according to a preset performance scheme using an intuitive traffic-light coloring system. Recently, first approaches were made to transfer the concept of eco-labels to transportation to demonstrated applications in practical settings (e.g., Heinold and Meisel; 2020). Figure 7.1a illustrates such a scheme for the transportation sector using eco-labels A, B, and C. Logistics companies can then let customers specify a desired eco-label for an order or communicate an order’s achieved label to gain a competitive advantage. Either way, the emissions promised through eco-labels then ought to be met in the transport operations for the orders.

In contrast to an eco-labeling of consumer products (e.g., for the annual electricity consumption of a refrigerator), emissions in transportation depend on several operational factors such as freight consolidations and a vehicle’s capacity utilization, see e.g., Demir

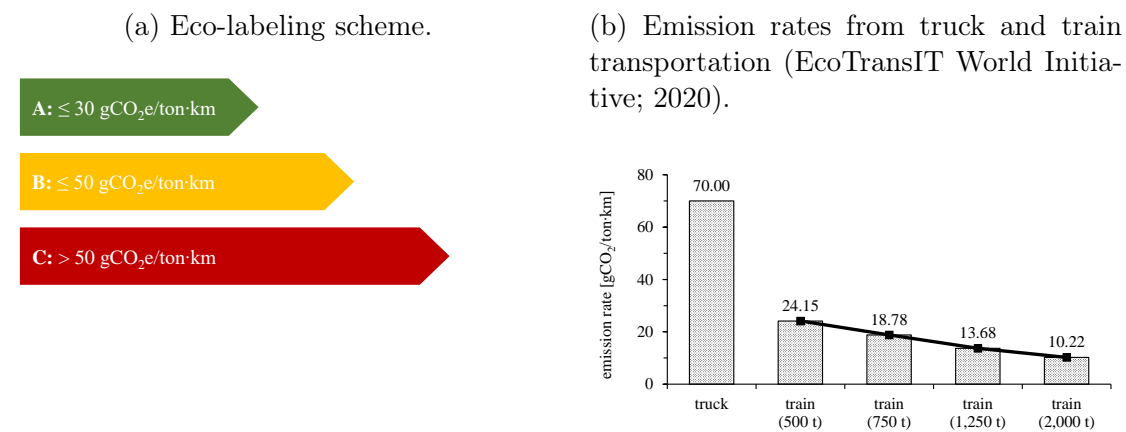


Figure 7.1: Considered eco-labeling scheme (a) and load-dependent emissions rates (b).

et al. (2011), Heinold (2020). For example, Figure 7.1b shows that a freight train's emission rate per ton-km decreases, the more load the train carries, i.e., the emission rate and the payload weight are negatively correlated. Next to the high cost-pressure in the transportation industry, this emphasizes the need for consolidating freight orders which is particularly relevant in networks with multiple transport modes. Moreover, such intermodal problems often deal with transport demand that reveals over time and requires a decision making under uncertainty regarding the consolidation of freight (e.g., Rivera and Mes; 2017a). Therefore, decision makers dispatching orders over time need to find a balance between complying with orders' eco-labels as specified by customers and the resulting overall transportation costs. In this paper, we address the challenge of balancing costs and satisfied eco-labels for a stochastic and dynamic decision making problem in intermodal rail-road transportation. We consider a train with limited capacity operating on a fixed schedule where transport orders consisting of full truckloads appear spontaneously over time and request a certain eco-label. For each order, it needs to be decided whether to route it intermodally using the train for the long-haul carriage or directly using trucks only. The chosen transport routes impact costs and the percentage of achieved eco-labels, which are considered in a weighted objective function.

Finding effective solutions for this problem is difficult in two ways. First, we have to make the routing decisions for already known orders and, second, we have to anticipate a decision's impact on the future for which orders are not known yet. To tackle this, we propose to use a mixed-integer programming approach in combination with value function approximation (VFA) with basis functions, a solution class from approximate dynamic programming (Powell; 2011). The linear basis functions use so-called features

whose weights are learned in VFA iteratively in a forward programming fashion using simulated outcomes. The features also work as a parametric representation of the large problem space inherent to the considered problem. For the decision making in VFA, we formulate a mixed-integer linear program that incorporates the basis functions. This method needs to cope with two aspects specific to our setting: (i) learning the feature weights is difficult as the achieved eco-label of an order depends on its own routing as well as the consolidation decisions for future orders, i.e., it is only known for an order once it arrives at its destination as the calculation of emissions requires full knowledge of the train's payload for each relevant service leg, and (ii) we deal with a multi-objective problem considering eco-labels and costs. To address the learning challenges, we propose a learning strategy that enhances the trajectory obtained from the suboptimal forward decisions in the VFA algorithm (primal) with the trajectory obtained from solving each iterations distinct decision problem to optimality ex-post (dual). That is, we solve for the dual trajectory a decision problem at each stage assuming the realized outcome from the iteration's forward exploration would have been known. We refer to this approach as primal-dual VFA. To the best of our knowledge, we are the first to combine both trajectories in the learning process of a transportation problem. To address the multi-objective nature of the problem, we design objective-specific feature sets that take up the factors influencing eco-labels and costs. Overall, our paper makes contributions to the problem as well as to the general methodology on approximate dynamic programming. These contributions are as follows.

- We are the first to consider eco-labels in stochastic dynamic intermodal transportation and present a comprehensive multi-objective stochastic dynamic model.
- We present an anticipating solution method considering the unique challenges found in freight consolidation. This method enables effective real-time decision making for our problem.
- We enhance the learning in value function approximation with the ex-post solutions. This enhancement is a general methodological contribution to the literature on approximate dynamic programming and will likely improve VFA for other problems as well.
- We show the importance and benefits of designing feature sets with respect to the weight in the multi-objective decision problem.

- We perform comprehensive experiments to analyze the impact of eco-labels on costs and their impact on the embedded decisions in intermodal networks.

The remainder of this paper is organized as follows. Section 7.2 provides an overview of the related literature and identifies the research gaps addressed in this paper. Section 7.3 outlines the problem with its distinctive characteristics and formulates it as a sequential decision process. Section 7.4 motivates and describes our solution approach. Section 7.5 presents experimental results. Section 7.6 concludes the paper.

7.2 Related literature

We contribute to the literature on multimodal transportation as well as to the literature on VFA. We provide reviews for each of these research directions in a distinct section: Section 7.2.1 provides an overview of multimodal studies relevant to our problem and Section 7.2.2 focuses on studies using value function approximation to solve transportation problems.

7.2.1 Multimodal transportation

We use the term multimodal to refer to the potential usage of more than one transport mode and, with this, intermodal studies are considered as well as they describe a particular type of multimodal transportation in which the same transport unit is used for shipping an order. We also consider studies on synchronomodal transportation that usually deal with operational issues regarding the synchronization of orders' time windows and modes' schedules (e.g. Rivera and Mes; 2017b). In this context, this section reviews two problem classes of multimodal transportation: (i) multimodal transportation problems that consider environmental aspects, and (ii) multimodal transportation problems that take place in a stochastic and dynamic environment. There are only few papers considering aspects of both classes. We refer to Crainic and Kim (2007) and Steadie Seifi et al. (2014) for general reviews on multimodal transportation and to Delbart et al. (2021) for a review on uncertainty in intermodal and synchronomodal transportation. The very recent survey of Archetti et al. (2021) also emphasizes that investigating multi-objective problems with environmental aspects (such as carbon emissions) are a valuable topic for future research. Table 7.1 lists multimodal papers that are closely related to our study. The table indicates for each paper if it considers stochastic and/or dynamic elements, if it treats emissions as part of the objective function and/or as a restriction in

Table 7.1: Overview of multimodal studies related to our problem.

reference	stochastic	dynamic	emissions		type
			objective	restriction	
Bauer et al. (2010)	-	-	✓	-	intermodal
Heinold and Meisel (2019)	-	-	✓	-	intermodal
Rudi et al. (2016)	-	-	✓	-	intermodal
Sun and Lang (2015)	-	-	✓	-	multimodal
Baykasoğlu and Subulan (2016)	-	-	✓	-	intermodal
Lam and Gu (2016)	-	-	-	✓	intermodal
Chen et al. (2014)	-	-	-	✓	intermodal
Heinold and Meisel (2020)	-	-	✓	✓	intermodal
Demir et al. (2016)	✓	-	✓	-	intermodal
Zhao et al. (2018)	✓	-	✓	-	intermodal
Jiang, Zhang, Meng and Liu (2020)	✓	-	-	✓	multimodal
Mes and Iacob (2016)	✓	-	✓	-	sychromodal
Resat and Turkay (2019)	✓	-	✓	-	sychromodal
Hrušovský et al. (2020)	✓	-	✓	-	intermodal
Li et al. (2015)	✓	✓	-	-	intermodal
Rivera and Mes (2017a)	✓	✓	-	-	intermodal
Rivera and Mes (2019)	✓	✓	-	-	sychromodal
van Heeswijk et al. (2018)	✓	✓	✓	-	intermodal
this study	✓	✓	✓	✓	intermodal

the mathematical model, and, if it relates to multimodal, intermodal, or sychromodal transportation.

As a first problem class, we consider environmentally oriented studies in multimodal networks. The environmental impact of transportation is usually measured in terms of the resulting emissions and, then, modeled either as objective or as restriction. When considered as objective, most studies compare the emission minimizing solutions with solutions using other, more traditional, objectives, such as transit times (e.g., Bauer et al.; 2010; Heinold and Meisel; 2019) or costs (e.g., Rudi et al.; 2016). However, emissions can also be considered as part of such a traditional objective, for example, by converting emissions into a monetary value (e.g., Sun and Lang; 2015) or by setting preset values to each of the potentially conflicting objectives in a goal programming approach (e.g., Baykasoğlu and Subulan; 2016). Studies that strictly restrict emissions are less common. Lam and Gu (2016) study the trade-off between costs and time, while considering an overall network wide emission limit as a hard constraint. The authors argue that such a limit can result from environmental regulations imposed by a government. Similar approaches consider so-called emission reduction targets that state a reduction of the as-is network emissions. This approach is, for example, used in Chen et al. (2014) for a multimodal coastal liner routing problem. A recent study from Heinold and Meisel (2020) introduces emission limits to reflect customers' environmental preferences regarding the

transportation of orders in an intermodal rail/road network. Thereby, an individual emission limit is stated for each order, expressing the maximal amount of transport-induced emissions that can be allocated to a particular order. The authors treat these limits both as a hard and as a soft constraint and solve the problem hierarchically with different objectives such as costs, emissions, and number of orders that are routed within their emission limit. Note that using emission limits is closely connected to using our study's concept of eco-labels. For example, it is possible to convert an order's total emission limit (measured in gram of carbon-dioxide equivalent emissions (gCO₂e)) to a relative eco-label (measured in gCO₂e/ton·km) by taking into account the order's payload weight (in ton) and its direct distance (in km) between the origin and the destination location.

So far, all of the aforementioned studies cover problems in deterministic and static environments. There are only a few studies that deal with uncertainty in the context of environmentally oriented multimodal transportation. Demir et al. (2016) propose a green service network design problem in which the demand as well as the travel times of vehicles are uncertain. Emissions are considered next to time and costs in a weighted multi-objective mixed-integer linear program, which is then applied to several artificial and real-world test instances. Zhao et al. (2018) consider uncertain demand and supply in an intermodal empty container re-positioning problem. Here, the authors explicitly address emissions as part of a weighted cost function and model the problem as a chance-constrained non-linear integer program. Jiang, Zhang, Meng and Liu (2020) consider demand uncertainty in a multimodal network design problem with emission reduction targets. Research on synchronodal transportation usually considers uncertainty for the vehicles' travel times or as unexpected events that then lead to disruptions. Mes and Iacob (2016) introduce a synchronodal planning algorithm allowing decision makers to select from a restricted list of multimodal routes. The authors consider objectives costs, delays, and emissions and apply the approach to the problem of a logistics service provider in the Netherlands. Resat and Turkay (2019) present a discrete-continuous optimization model to solve complex synchronodal routing problems including decisions on the routing and fleet size. Pareto optimal solutions for objectives costs, travel time, and emissions are obtained by applying the ϵ -constraint method. Hrušovský et al. (2020) propose a decision support methodology that connects ex-ante offline planning (before the transport has started) with online re-planning (in case of disruptions during the transport). With this, the problem also addresses aspects of synchronodal transportation and is then solved for objectives costs, time, and emissions.

The second problem class considers multimodal transportation problems with stochas-

tic *and* dynamic elements. In this regard, dynamic refers to settings in which multiple decision points are considered, e.g., decision problems spanning over time. As far as is known, there is no study in this class that considers environmental aspects by eco-labels. Moreover, there are only a few studies that explicitly address stochastic dynamic problems in multimodal networks. For example, Li et al. (2015) approach a dynamic intermodal freight transport problem in which demand and traffic conditions are both uncertain. The authors use a problem formulation with a terminology similar to the one that is also used in sequential decision processes. A preceding horizon control algorithm is proposed as solution method and its performance is demonstrated in a simulation study. Rivera and Mes (2017a) study an intermodal freight selection problem in which it is central to assign containers either to a long-haul round trip with a barge or to a direct trip with a truck. The problem spans over multiple periods and, in each period, an uncertain container demand appears at an inland terminal that needs to be transported to deep-sea terminals, using one of the aforementioned transport options. The problem is modeled as a Markov Decision Process (MDP) and solutions are obtained with a forward programming algorithm from the field of VFA. Rivera and Mes (2019) also consider an integrated scheduling of drayage and long-haul operations in which the latter is modeled as an MDP and solved via VFA. The aforementioned multimodal stochastic dynamic transportation studies do not consider sustainability aspects in their analyses. In contrast, van Heeswijk et al. (2018) use a multi-objective function considering costs and monetized emissions in an intermodal freight consolidation problem with reloads. The focus is on shipments of small volume (less-than-truckload) that are then consolidated to container loads at the intermodal hubs. Similarly to Mes and Iacob (2016), the authors use an arc expansion approach to generate a restricted list of promising transport routes and then identify and evaluate corresponding consolidation opportunities.

Our paper addresses both of the above discussed problem classes by investigating a stochastic dynamic intermodal transportation problem with order-specific eco-labels. To comply with the specified eco-labels, the corresponding maximal amount of emissions allowed for an order is (softly) restricted in the underlying model. From this, we consider costs and the fulfillment of eco-labels as two objectives in a multi-objective problem setting.

7.2.2 Improved value function approximation

This section discusses means to improve VFA in transportation planning and beyond. VFA is one of the solution classes being available in approximate dynamic programming

(Powell; 2009, 2011) and has been gained increasing attention in recent years, particularly in the emerging research on stochastic dynamic transportation in unimodal networks (e.g., van Heeswijk et al.; 2019; Ulmer et al.; 2019; Ulmer; 2020; Ulmer and Savelsbergh; 2020; Ulmer et al.; 2020). The general idea in VFA is to learn a ‘good’ decision policy from a large number of problem trajectories that are computed with simulation and forward decisions. Thereby, after each (new) trajectory, the policy is updated such that it becomes better and better with each run and, eventually, the policy can be used to generate good solutions within a relatively short computation time in real-world applications. More details on the principles of VFA are provided in Section 7.4.

Learning in VFA is especially difficult in the algorithm’s first iterations as its initialization is often based on a myopic policy. At the same time, the performance of VFA depends on an effective learning at the beginning of the algorithm as early approximations provide the foundation for future updates, i.e., it is important to bring approximations ‘on the right track’. Consequently, the function used in the updating process has received special attention as it is a vital determinant for speed and quality of VFA’s learning process, see e.g. George and Powell (2006); Schaul et al. (2013); Smith (2017). In this context, Ulmer and Thomas (2020) discuss differences in how to aggregate and store the value of a state. The authors compare parametric VFA, which enables a fast but inaccurate learning, with non-parametric VFA, which leads to accurate approximations but is computationally expensive and therefore slow in the solution process. The authors then propose a meso-parametric VFA that aims at exploiting the benefits of both parametric and non-parametric VFA. Their approach is demonstrated on a capacitated customer order acceptance problem with stochastic requests. George et al. (2008) propose using VFA with multiple lookup tables each at a different level of aggregation. The authors demonstrate the concept of using two levels of aggregation, one rough and one detailed level, and discuss the ‘optimal weight’ of considering the information stored in the two tables for the estimation. This means that an estimate is not obtained from using information from one lookup table (as in traditional VFA) but rather from using information from two (or even more) lookup tables. In doing so, good estimates are obtained by putting a higher weight on the rough lookup table in early iterations and a higher weight on the detailed lookup table in later iterations. Ulmer et al. (2018) present a dynamic lookup table approach that focuses on the learning at the early iterations of the VFA algorithm. In particular, the authors propose a method in which the updating increases in its granularity over the learning process. With this, rough approximations are obtained in the beginning that then become more accurate while the algorithm progresses over further iterations. The method is evaluated on a

dynamic vehicle routing problem with stochastic customer requests.

There is also general methodological work on improving VFAs or using primal and dual solutions for dynamic decision making. Jiang and Powell (2015) improve the updating process in VFA by assuming and exploiting monotonicity of the value function. This assumption is reasonable as it is commonly found in many real-world applications. The authors propose an updating function that explicitly considers the monotone structure by prescribing observed values to unexplored areas of the value function. A faster and better learning of their approach is demonstrated on three problem domains and compared to several other approaches from approximate dynamic programming and reinforcement learning.

Very recently, Jiang, Al-Kanj and Powell (2020) and Shar and Jiang (2020) propose the idea of using primal and dual bounds in a Monte Carlo tree search (MCTS) and in Q-Learning (QL), respectively. MCTS is an online lookahead method, where states are evaluated via simulation. In Jiang, Al-Kanj and Powell (2020), the simulated primal outcome is combined with an ex-post solution to evaluate a decision. However, the values are not used for learning. Shar and Jiang (2020) approximates state values as well as upper and lower bounds simultaneously via QL. QL works similar to VFA as it iteratively explores the large-dimensional state space by simulation. However, it evaluates state-action pairs instead of post-decision states which becomes challenging when the decision space increases. Shar and Jiang (2020) use the lower and upper bounds for penalizing decisions within the learning trajectories and show the superiority of their approach for several toy problems with relatively small decision and state spaces. Our approach shows similarities in using the primal and dual values for guiding decision making and learning. However, we directly integrate the bounds into the update of the VFA. Further, we analyze the performance of our method for a real-world size transportation problem with a very large state space and a combinatorial decision space.

7.3 Stochastic dynamic intermodal transportation with eco-labels

This section describes the stochastic dynamic intermodal transportation problem with eco-labels. Section 7.3.1 presents an application-oriented outline of the problem, Section 7.3.2 provides an illustrative example, and Section 7.3.3 formally describes its sequential decision process.

7.3.1 Problem description

We consider a problem where full truck load (FTL) orders dynamically occur over a time horizon and are shipped long-haul via two different modes of transportation. Each order comprises an individual origin, a destination, a payload, and an *eco-label*. The eco-label indicates the permissible emissions per ton-km the order is allowed to cause. It expresses the shipper’s individual environmental preference. Thereby, emissions are measured in terms of equivalents of carbon dioxide (CO₂e) per ton (t) and per kilometer (km) and, with this, the term ‘emissions’ subsumes several relevant greenhouse gases, such as carbon dioxide (CO₂), nitrogen oxides (NO_x), sulfur dioxide (SO₂), and non-methane hydrocarbons (NMHCs) (e.g., Piecyk et al.; 2012). Figure 7.1a shows the eco-labeling scheme used throughout this paper. The scheme results from the distribution of emission rates obtained from a large-scale simulation study of freight shipments in the European rail/road network (Heinold and Meisel; 2018) and comprises three different eco-labels A,B, and C with decreasing strictness. An order with eco-label A has to be transported with an emission rate of at most 30 gCO₂e/ton·km, an order with eco-label B has to be transported with an emission rate of at most 50 gCO₂e/ton·km, and an order with eco-label C has no preference regarding its emission rate.

For transportation, the logistics service provider has access to two modes of transportation: direct transport via truck from a shipment’s origin to its destination or consolidated transport via rail. The transportation cost of trucks depend on several factors, such as distance, empty returns, or if they are owned by the company or booked via an online freight exchange platform (Miller et al.; 2020). Emissions of a truck transportation depend directly on the origin and destination of the order and, as we consider large orders, we assume a constant emission rate per driven vehicle-kilometer corresponding to a regular fully loaded 40-ton truck, depicted in the first bar in Figure 7.1b. Regarding costs, we assume that trucks operate with a constant cost rate per kilometer that can differ dependent on the aforementioned factors. For rail transportation, a single, high-capacity train visits a set of predefined stops over the planning horizon. For example, the train starts in Scandinavia, traverses Germany and Austria, and eventually ends its trip in the south of Italy. At each stop along the route, the train can load/unload ‘nearby’ orders requiring only a short time driving. In order to use the train, an order must be transported via truck to a nearby stop before the train arrives (‘pre-carriage’) where it is then loaded onto the train (‘main-carriage’), and, eventually, transported via truck from a subsequent stop of the train to the final destination (‘post-carriage’). An order’s costs and emissions are an outcome of these carriages. Like for trucks, we consider a

constant cost rate per cargo unit for the train. This is because the scheduled train operates independently of the decisions made in our problem, from which we can assume that cargo units can be booked on the train at a fixed price. The emissions for orders transported via train depend on the pre- and post-carriage distances to those train stops that are selected for loading and unloading an order as well as on the overall load of the train between these two stops. For the train, we assume a degressive emission rate per ton-km that reduces with the train's total payload. Figure 7.1b shows the emission rates assumed for the freight train, which are derived from the emission estimation model of the EcoTransIT World Initiative (2020). It illustrates that the emission rate per ton-km decreases with a higher payload utilization of the train.

For each stop of the train, the service provider decides about the transport of the nearby orders; direct transport via truck, shipment via train from this stop, or postponement of the shipment decision in case the order can also be loaded at a future stop of the train. Once an order is decided to be loaded onto the train, trucks are booked for the pre- and post-carriage and the customer is informed, implying that the routing of this order cannot be changed in future periods. Figure 7.2 illustrates an order's corresponding possible routings. The dashed lines in the figure represent truck transportations, used in the pre- and post-carriage to/from the terminals and for the direct (road-only) routing whereas the solid lines represent the transportation via train. In the figure, three terminals qualify for loading (I, II, III) and two terminals for unloading (X, XI), resulting in six possible intermodal paths for this order.

While the train traverses along its route, new orders are placed by the customers

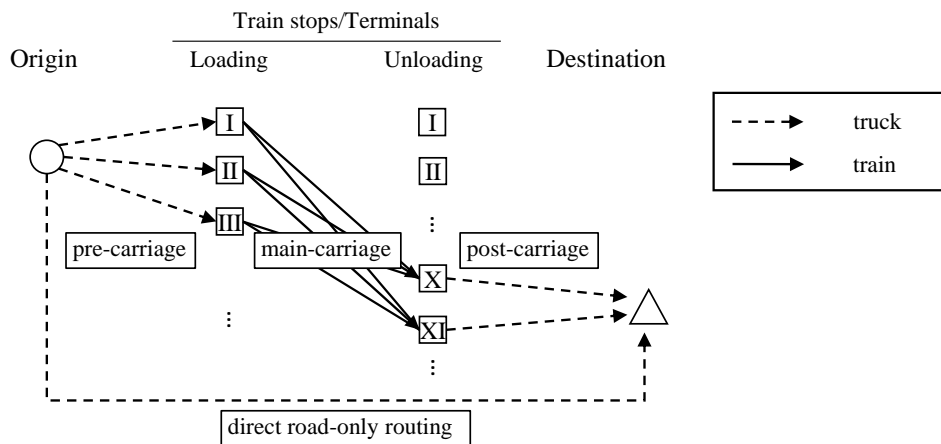


Figure 7.2: Illustration of an order's possible routings.

which leads to a stochastic and dynamic planning environment. When making a decision, the service provider has two objectives: minimizing the overall transportation costs and minimizing the number of orders that violate their requested eco-labels. In contrast to eco-labels in other domains, e.g. for electronics or buildings, the final emissions per order are not yet known when a transport decision is to be made. This is because they depend on the consolidation effects of the train with already loaded orders as well as with future loads at later stops. Thus, the emissions that are to be allocated to an order and the actually achieved eco-label only become known once the order arrives at its destination.

7.3.2 Illustrative example

We provide an illustrative example of the resulting stochastic dynamic intermodal transportation problem with eco-labels. We use here the terms of the sequential decision process that is later formalized in the next subsection. Figure 7.3a shows a state, Figure 7.3b shows for a potential decision the resulting post-decision spate, and Figure 7.3c shows the next state after a transition. Squares represent the three terminals that the train visits in this example where a cross inside a square indicates the current stop of the train. Circles represent the origin locations of the three orders that occur in the course of time and triangles represent their destinations. The eco-label requested for an order is shown at the bottom of its origin location. Potential pre- and post-carriages via truck are shown as arcs. Direct truck transportation is not depicted in the figure for reasons of simplicity. We assume that the train is empty at the beginning and has a sufficiently large capacity to jointly transport all considered orders.

In Figure 7.3a, the train just arrived at the first terminal. Here, orders 1 and 2 have been placed by the customers and can be loaded onto the train at the train's current stop at terminal I or at its next stop at terminal II. Order 1 can be unloaded at terminal III only and order 2 can be unloaded at terminals II or III. Thus, there are three possible paths for order 1 (loading at I and unloading at III; loading at II and unloading at III; direct shipping) and four possible paths for order 2 (loading at I and unloading at II; loading at I and unloading at III; loading at II and unloading at III; direct shipping). This illustrates that already small intermodal networks can contain a substantial number of transport options. In general, if an order has n terminals for being loaded and m terminals for being unloaded, we face up to $(n \times m) + 1$ paths for the case that the two sets of terminals are disjoint. Figure 7.3b describes a feasible decision in which orders 1 and 2 are loaded onto the train at terminals I and II, respectively, and unloaded at terminal III. Such a decision results from considering objectives costs and eco-labels.

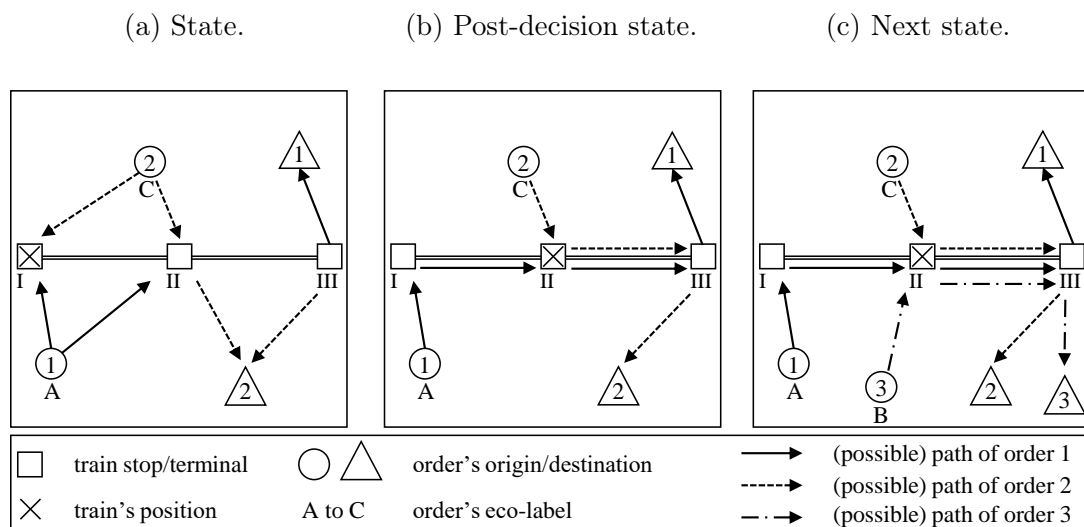


Figure 7.3: Illustration of the stochastic dynamic intermodal transportation problem with eco-labels.

For example, order 1 might be assigned to the first terminal as its requested eco-label A requires as much rail transportation as possible. In contrast, the eco-label of order 2 is only C and the more nearby terminal II might be selected as this results in lower trucking costs (compared to a routing via terminal I). After making these decisions, the train moves to the next station and, with this, Figure 7.3b represents the corresponding post-decision state. Figure 7.3c depicts the next state in which new information has become available. In particular, the new order 3 appears with its corresponding possible intermodal path: loading at terminal II and unloading at terminal III. Furthermore, the set of paths of all other orders is updated in the transition: selected paths including stops that have been visited before are fixed (in this example, the path for order 1 that required a loading at terminal I) and not selected paths including stops that have been visited before are excluded as they can no longer be selected in the new state (in this example, paths for order 2 that required a loading a terminal I).

7.3.3 Sequential decision process

We use the framework of sequential decision processes to formally describe the problem (Powell; 2021). We start by introducing some general notation and then subsequently define states, decisions, rewards, post-decision states, stochastic information, transitions, and the optimal policy. Table 7.2 provides an overview of the notation.

General notation.

We define the sequence of decision points as $\mathcal{T} = [1, 2, \dots, T]$. This sequence corresponds to the set of transshipment terminals visited by the train along its route such that 1 is the

Table 7.2: Overview of the notation used in the sequential decision process.

name	description
General notation	
\bar{e}_o	upper emission limit induced by eco-label λ_o of an order $o \in \mathcal{O}_t$
q_o	payload quantity of an order $o \in \mathcal{O}_t$
t_p^1 / t_p^2	loading/unloading terminal of a path $p \in \mathcal{P}_t$
λ_o	eco-label of an order $o \in \mathcal{O}_t$
\mathcal{T}	set of decision points / train stops / terminals
\mathcal{O}_t	set of orders in decision point $t \in \mathcal{T}$
\mathcal{P}_t	set of paths in decision point $t \in \mathcal{T}$
\mathcal{P}_t^o	set of paths of an order $o \in \mathcal{O}_t$ in decision point $t \in \mathcal{T}$
\mathcal{T}_p	set of terminals visited by a path $p \in \mathcal{P}_t$
State	
\mathbf{f}_t	binary vector describing which orders violate their eco-label in a state S_t
$f_t(o)$	=1, if order $o \in \mathcal{O}$ violates its eco-label in a state S_t , =0 else
\mathbf{r}_t	binary vector describing which paths are used in a state S_t
$r_t(p)$	=1, if path $p \in \mathcal{P}$ is used in a state S_t , =0 else
S_t	state in decision point $t \in \mathcal{T}$
Decision	
$e_t^x(p)$	overall emissions (truck and train) of path $p \in \mathcal{P}$ under the decision in a state S_t , =0 else
$l_t^x(t')$	load of the train at terminal $t' \in \mathcal{T}$ under the decision in a state S_t , =0 else
L^{\max}	capacity of the train
\mathbf{x}_t	binary vector describing which paths are used under the decision in a state S_t
$x_t(p)$	=1, if path $p \in \mathcal{P}_t$ is used under the decision in a state S_t , =0 else
$\mathcal{X}(S_t)$	set of feasible decisions in a state S_t
Reward	
c_p	overall costs (truck and train) of a path $p \in \mathcal{P}_t$
$e_t^{\text{train}}(l_t^x(t'))$	train emissions under a load $l_t^x(t')$
e_t^{truck}	truck emissions of a path $p \in \mathcal{P}_t$
\mathbf{f}_t^x	binary vector describing which orders violate their eco-label under a decision \mathbf{x}_t
$f_t^x(o)$	=1, if order $o \in \mathcal{O}$ is routed in accordance to its eco-label under a decision \mathbf{x}_t , =0 else
$R(\cdot)$	reward function
$R^C(\cdot)$	reward function for objective costs
$R^E(\cdot)$	reward function for objective eco-labels
α	parameter to weight $R^C(\cdot)$ and $R^E(\cdot)$ in the objective function
Post-decision state	
\mathcal{P}_t^x	set of paths in a post-decision state S_t^x
$\mathcal{P}^{o,x}$	set of available paths of an order $o \in \mathcal{O}$ in a post-decision state S_t^x
S_t^x	post-decision state in decision point $t \in \mathcal{T}$
Stochastic information	
$\tilde{\omega}_{t+1}$	stochastic information in decision point $t+1 \in \mathcal{T}$
$\tilde{\mathcal{O}}_{t+1}$	set of new orders in decision point $t+1 \in \mathcal{T}$
$\tilde{\mathcal{P}}_{t+1}$	set of new paths in decision point $t+1 \in \mathcal{T}$
Ω	set of stochastic information
Transition	
$S^M(\cdot)$	system model function to transform to the next state
Optimal policy	
$V_t(S_t^x)$	value of post-decision state S_t^x
π	policy describing a decision for each decision point
Π	set of all policies

first stop and T is the last stop. The set of orders being known at decision point $t \in \mathcal{T}$ is denoted with \mathcal{O}_t . For each order $o \in \mathcal{O}_t$, we deduce a set of paths \mathcal{P}_t^o . This set contains the feasible intermodal paths of an order o (as was illustrated in the example) and a path for the direct transportation via truck between the order's origin and destination. We denote the loading and unloading terminal of an intermodal path $p \in \mathcal{P}_t^o$ by t_p^1 and t_p^2 , respectively, and the set of all terminals that are involved in this path by \mathcal{T}_p . For paths corresponding to a direct (truck only) routing, this set is empty ($\mathcal{T}_p = \emptyset$). The set of all paths being relevant at a decision point t is denoted by $\mathcal{P}_t = \bigcup_{o \in \mathcal{O}_t} \mathcal{P}_t^o$. Each order o is also associated with a load q_o and an eco-label λ_o . To check whether an order o violates its requested eco-label λ_o , we further calculate an emission limit \bar{e}_o . This limit states the highest amount of emissions allowed for this order according to its requested eco-label. We calculate the limit by using order o 's load, the direct origin-destination distance, and the emission rate of the corresponding eco-label as shown in Figure 7.1a.

State.

A state S_t at decision point $t \in \mathcal{T}$ is described by tuple $S_t = (\mathcal{O}_t, \mathcal{P}_t, \mathbf{r}_t, \mathbf{f}_t)$ and contains all information required to make a decision. In particular, \mathcal{O}_t is the set of orders placed until t , \mathcal{P}_t is the set of paths as defined before, $\mathbf{r}_t = [r_t(p)]_{p \in \mathcal{P}_t}$ is a $|\mathcal{P}_t|$ -dimensional binary vector describing for each path p whether it is part of the current solution ($r_t(p) = 1$), or not ($r_t(p) = 0$), and $\mathbf{f}_t = [f_t(o)]_{o \in \mathcal{O}_t}$ is an $|\mathcal{O}_t|$ -dimensional binary vector describing for each order o whether it currently violates its eco-label ($f_t(o) = 1$), or not ($f_t(o) = 0$). Note that vector \mathbf{f}_t can be derived from vector \mathbf{r}_t (as will be shown in the next paragraph) and is only included in the definition of the state for reasons of readability.

Decision.

The set of feasible decisions in a state S_t at decision point $t \in \mathcal{T}$ is described with $\mathcal{X}(S_t)$. A single decision $\mathbf{x}_t \in \mathcal{X}(S_t)$ is defined as a $|\mathcal{P}_t|$ -dimensional binary vector describing for each path p whether it is used under the decision ($x_t(p) = 1$), or not ($x_t(p) = 0$), see Equation (7.1).

$$\mathbf{x}_t = [x_t(p)]_{p \in \mathcal{P}_t} \tag{7.1}$$

There are two restrictions for a decision to be feasible. First, exactly one path must be selected per order, see Equation (7.2), and, second, the capacity of the train L^{\max} cannot be exceeded, see Equation (7.3). Thereby, the load of the train $l_t^x(t')$ at terminal $t' \in \mathcal{T}$

under decision \mathbf{x}_t is calculated by summing up the load q_o of all orders o whose selected path involves terminal t' .

$$\sum_{p \in \mathcal{P}_t^o} x_t(p) = 1, \quad \forall o \in \mathcal{O}_t \quad (7.2)$$

$$l_t(t') = \sum_{o \in \mathcal{O}_t} \left(q_o \cdot \sum_{p \in \mathcal{P}_t^o: t' \in \mathcal{T}_p} x_t(p) \right) \leq L^{\max}, \quad \forall t' \in \mathcal{T} \quad (7.3)$$

Reward.

We consider a multi-objective problem and use parameter α to weight objectives costs and eco-labels. A pure cost minimization is achieved by setting $\alpha = 1$ and a pure minimization of the number of orders violating their eco-label results from $\alpha = 0$. We use the term ‘reward’ to describe the contribution of a decision towards each of these objectives. As we have a minimization problem, our goal is to minimize this ‘reward’. We then consider marginal rewards instead of absolute rewards (Ulmer et al.; 2020) that is motivated by the fact that the actually achieved eco-label of an order can change at later decision points due to the load-dependent emission rate of the train. For example, an order’s eco-label might be violated at the time it is loaded onto the train at stop t_p^1 if the train is quite empty at that point, but the eco-label might be fulfilled at the unloading stop t_p^2 , if later decisions increase the train’s payload utilization and, with this, reduces the emission rate per cargo unit.

To evaluate whether or not an order $o \in \mathcal{O}_t$ violates its eco-label λ_o , we calculate the emissions $e_t^x(p)$ of a path $p \in \mathcal{P}_t$ under a decision \mathbf{x}_t by Equation (7.4). Here, the path’s emissions resulting from truck transportation are denoted with e_p^{truck} , considering emissions from pre- and post-carriage for intermodal paths and emissions from direct road-only transportation for unimodal paths. The emissions from train transportation per unit of load q_o are denoted by $e^{train}(l_t^x(t'))$ and depend on the train’s total payload $l_t^x(t')$ at a terminal $t' \in \mathcal{T}$. The evaluation of the eco-labels under the current decision \mathbf{x}_t is then done for each order using Equation (7.5). Here, we define $\mathbf{f}_t^x = [f_t^x(o)]_{o \in \mathcal{O}_t}$ as a $|\mathcal{O}_t|$ -dimensional binary vector describing for each order o whether it violates its eco-label λ_o ($f_t^x(o) = 1$), or not ($f_t^x(o) = 0$), under the current decision \mathbf{x}_t .

$$e_t^x(p) = e_p^{truck} + q_o \cdot \sum_{t' \in \mathcal{T}_p \setminus \{t_p^2\}} e^{train}(l_t^x(t')), \quad \forall o \in \mathcal{O}_t, p \in \mathcal{P}_t^o \quad (7.4)$$

$$f_t^x(o) = \begin{cases} 1, & \text{if } \sum_{p \in \mathcal{P}_t^o} x_t(p) \cdot e_t^x(p) > \bar{e}_o \\ 0, & \text{else} \end{cases}, \quad \forall o \in \mathcal{O}_t \quad (7.5)$$

With this, the marginal reward $R(\cdot)$ under a decision \mathbf{x}_t is computed by Equation (7.6). This formula takes into account the marginal costs and eco-label violations. The marginal costs R_t^C are calculated in Equation (7.7) where c_p denotes the costs of using a path $p \in \mathcal{P}_t$ and the marginal reward R_t^E regarding the eco-labels in Equation (7.8). These rewards are calculated as the difference in costs/eco-label violations between the newly planned paths and the previous ones.

$$R(S_t, \mathbf{r}_t, \mathbf{x}_t, \mathbf{f}_t, \mathbf{f}_t^x) = \alpha \cdot R_t^C(S_t, \mathbf{r}_t, \mathbf{x}_t) + (1 - \alpha) \cdot R_t^E(S_t, \mathbf{f}_t, \mathbf{f}_t^x) \quad (7.6)$$

with

$$R_t^C(S_t, \mathbf{r}_t, \mathbf{x}_t) = \sum_{p \in \mathcal{P}_t} c_p \cdot (x_t(p) - r_t(p)) \quad (7.7)$$

$$R_t^E(S_t, \mathbf{f}_t, \mathbf{f}_t^x) = \sum_{o \in \mathcal{O}_t} (f_t^x(o) - f_t(o)) \quad (7.8)$$

Post-decision state.

We use the two-step transition in which we first transit to a post-decision state S_t^x considering the decision \mathbf{x}_t and afterward to the new state S_{t+1} considering the new information. Thus, the transition to the post-decision state is fully deterministic and formally defined as the state that is reached by making decision \mathbf{x}_t in state S_t : $S_t^x = (\mathcal{O}_t, \mathcal{P}_t^x, \mathbf{x}_t, \mathbf{f}_t^x)$. Here, compared to state S_t , \mathbf{r}_t and \mathbf{f}_t are replaced by the decision \mathbf{x}_t and the corresponding eco-label violation vector \mathbf{f}_t^x , respectively, and the set of available paths $\mathcal{P}_t^x = \bigcup_{o \in \mathcal{O}_t} \mathcal{P}_t^{o,x}$ is updated by excluding all paths that are not feasible in the next stage any more. This exclusion is described for each order's paths $\mathcal{P}_t^{o,x}$ in Equation (7.9). In particular, according to the first case, we only include the selected path in the post-decision state if it involves loading at the train's current location. From this, once we decide to load an order onto the train at the current stop $t_p^1 = t$, we also fix the unloading terminal t_p^2 according to the selected path p . In the second case, we also only consider the selected path if there is just one path available for this order, i.e. the decision is made automatically because of missing alternatives. Otherwise, if none of the previous cases apply, according to the third case in Equation (7.9), we update the

paths such that we only keep those intermodal paths p' for which $t_{p'}^1 \geq t + 1$, simply, because paths with loading at earlier train stops are not accessible any more when the train approaches its next stop $t + 1$.

$$\mathcal{P}_t^{o,x} = \begin{cases} \{p\}, \text{ if } (x_t(p) = 1 \text{ and } t_p^1 = t) \\ \{p\}, \text{ if } |\mathcal{P}_t^o| = 1 \\ \{p' \mid p' \in \mathcal{P}_t^o : t_{p'}^1 \geq t + 1\}, \text{ else} \end{cases}, \quad \forall o \in \mathcal{O}_t, p \in \mathcal{P}_t^o \quad (7.9)$$

Stochastic information.

The stochastic information Ω in our problem relates to the arrival of new orders and their characteristics. We use $\hat{\omega}_{t+1} \in \Omega$ to describe a potential realization of this information at decision point $(t + 1)$, consisting of new orders $\tilde{\mathcal{O}}_{t+1}$ and corresponding new paths $\tilde{\mathcal{P}}_{t+1}$, i.e., $\hat{\omega}_{t+1} = (\tilde{\mathcal{O}}_{t+1}, \tilde{\mathcal{P}}_{t+1})$. The distribution functions used in this process are later specified in the experimental section.

Transition.

The transition generally describes how the system evolves over time from one state S_t in point t to a next state S_{t+1} in point $t + 1$. Using the stochastic information $\hat{\omega}_{t+1}$, we can transit from S_t^x to S_{t+1} using system model function $S^M(S_t^x, \hat{\omega}_{t+1})$ as described in Equation (7.10). Here, the set of orders is updated in Equation (7.11), the set of paths is updated in Equation (7.12), the routing vector is updated in Equation (7.13), and the eco-label violation vector is updated in Equation (7.14). Note that the default value for the routing and eco-label violation vector is 0.

$$S_{t+1} = S^M(S_t^x, \hat{\omega}_{t+1}) = (\mathcal{O}_{t+1}, \mathcal{P}_{t+1}, \mathbf{r}_{t+1}, \mathbf{f}_{t+1}) \quad (7.10)$$

where

$$\mathcal{O}_{t+1} = \mathcal{O}_t \cup \tilde{\mathcal{O}}_{t+1} \quad (7.11)$$

$$\mathcal{P}_{t+1} = \mathcal{P}_t^x \cup \tilde{\mathcal{P}}_{t+1} \quad (7.12)$$

$$\mathbf{r}_{t+1} = [x_t(p)]_{p \in \mathcal{P}_t^x} \cup [0]_{p \in \tilde{\mathcal{P}}_{t+1}} \quad (7.13)$$

$$\mathbf{f}_{t+1} = [f_t^x(o)]_{o \in \mathcal{O}_t} \cup [0]_{o \in \tilde{\mathcal{O}}_{t+1}} \quad (7.14)$$

Optimal policy.

We are searching for a policy $\pi \in \Pi$ describing a decision \mathbf{x}_t for each state S_t . Thereby, the set of all policies is denoted with Π and an optimal policy π^* minimizes the objective function from Equation (7.6) over all of the considered periods. Formally, such a decision can be calculated in our discrete problem by using the well-known Bellman Equation (Bellman; 1957). The equation considers for a decision \mathbf{x}_t in the current state S_t the immediate reward $R(\cdot)$ as well as the expected future reward of the post-decision state when following an optimal policy. We use $V_t(S_t^x)$ to denote the future reward of a post-decision state S_t^x . The optimal decision \mathbf{x}_t^* at decision point t can then be found by solving the following Bellman Equation:

$$\mathbf{x}_t^* = \arg \min_{\mathbf{x}_t \in \mathcal{X}(S_t)} (R(S_t, \mathbf{r}_t, \mathbf{x}_t, \mathbf{f}_t, \mathbf{f}_t^x) + \mathbb{E}(V_t(S_t^x))). \quad (7.15)$$

7.4 Solution approach

This section describes our proposed solution approach. Section 7.4.1 motivates the use of VFA with basis functions by highlighting the challenges of the multimodal problem with eco-labels. Section 7.4.2 describes the general structure of the VFA algorithm and Section 7.4.3 elaborates on our enhancement regarding the learning of weights of the basis functions. Section 7.4.4 describes the procedure for selecting the basis functions for the VFA.

7.4.1 Motivation

As many other stochastic dynamic transportation problems, we face the well-known curses of dimensionality when trying to solve the Bellman Equation. For our problem, the decision space is vast due to the different potential paths for the orders in the system. Furthermore, evaluating a decision is challenging as not only future requests and their reward are uncertain but the fulfillment of eco-labels of existing orders may also change based on future requests and decisions.

We address these issues as follows. For the complex decision problem at each stage, we formulate a mixed-integer linear program (MIP) that can be solved within reasonable computation time by state-of-the-art MIP-solvers. This MIP is used to make decisions

regarding the routing of the orders in every state. To evaluate decisions, we integrate the Bellman Equation in the MIP and approximate the unknown second term of Equation (7.15) via Value Function Approximation (VFA). A VFA repeatedly simulates trajectories of the problem, stores observed states and approximated values, and uses the updated values in the subsequent trajectory.

To enable embedding the VFA into the MIP and using standard solvers, our VFA relies on linear basis functions. Therefore, the states are represented by a set of meaningful features. The purpose of features is to aggregate the high-dimensional (post-decision) state space while allowing differentiation of states with different values. For our multi-objective problem, the ‘value’ of states depends on both costs and eco-label violations as well as their weighting parameter α . Some features may mainly reflect future costs as others may solely reflect different values of eco-level violations. As using a large number of features often obstructs learning of the VFA, we propose using different feature sets for different α -parameter values.

Another challenge when applying VFA to our problem is that the consequences of current decisions realize substantially later in the process. For example, loading goods on the train in an early state reduces valuable train capacity but also the relative emissions of requests loaded onto the train in the future. We therefore observe a trade-off between flexibility and consolidation. Furthermore, the number of eco-label violations may be reduced by future consolidation effects. As a VFA uses only approximated values in the (therefore suboptimal) decision making, the observed values in a trajectory are a *primal bound* of the potential values that could have been achieved in the same trajectory. ‘Classical’ VFAs usually start with an empty value function and therefore myopic decision making (e.g., Ulmer and Thomas; 2020) with a potentially very weak primal bound, especially for our problem due to the aforementioned reasons. That means that the observed and stored values are likely substantially different compared to the real values. This often leads to poor decision making especially in early trajectories and may even lead to no learning at all. We therefore propose a combination of the too pessimistic primal bound values with *dual bound* values. To this end, we solve the unique decision problem of the primal trajectory recursively ex-post when all information is known. The results are dual bound-values, potentially too optimistic compared to the expected values of the observed states. To balance the pessimism of the primal bounds with the optimism of the dual bounds, we update the VFA-values with a convex combination of both. We denote this strategy as *primal-dual VFA*. In the following, we will first discuss the general concept of VFAs with basis functions. Then, we will define our primal-dual VFA in detail. Finally, we will present the features we will use for different weights of the α -parameter.

Step 1: Choose initial values for weights θ_a^0 of all features $a \in \mathcal{A}$,
Step 2: for $n = 1, 2, \dots, N$ do
 Step 2a: Draw information $\hat{\omega}_1^n \in \Omega$ for initial state S_1^n .
 for $t = 1, 2, \dots, T-1$ do
 Step 2b: Find primal decision \mathbf{x}_t^n by solving MIP model (7.17) to (7.23)
 using weights θ_a^{n-1} .
 Step 2c: Store decision \mathbf{x}_t^n , post-decision state $S_t^{n,x}$, and accumulated
 reward.
 Step 2d: Draw information $\hat{\omega}_{t+1}^n \in \Omega$ and transform to next state:
 $S_{t+1}^n = S^M(\cdot)$.
 end
 Step 2e: Update weights θ_a^n for all features $a \in \mathcal{A}$ using the values from step
 2c.
end

Algorithm 1: Generic algorithm for VFA with basis functions.

7.4.2 VFA with basis functions

This section describes the general procedure of VFA with basis functions. The goal of the approach is to replace a post-decision state's S_t^x true value $V_t(S_t^x)$, which is intractable to be calculated for large-dimensional problems, by a 'good' approximation $\bar{V}_t(S_t)$. This approximation is calculated by using a set of features denoted with \mathcal{A} . Each feature $a \in \mathcal{A}$ is associated with a basis function $\phi_a(S_t^x)$, describing how the value of feature a is calculated for a post-decision state S_t^x , and a weight θ_a , describing its relative importance for the approximation. With this, the approximation of a post-decision state's value is calculated as follows:

$$V_t(S_t^x) \approx \bar{V}_t(S_t^x) = \sum_{a \in \mathcal{A}} \theta_a \cdot \phi_a(S_t^x). \quad (7.16)$$

In VFA with basis functions, the values of the weights are learned through a combination of simulation and forward programming over a large number of iterations. We use the superscript n to map values to iterations. Algorithm 1 depicts the general steps. Step 1 is to initialize the feature weights θ_a^0 , which is done by using 0 for all features in our experiments. This results in an initially myopic policy. The problem is then solved in N iterations under Step 2, where each iteration simulates a single trip of the train along its route for a sampled set of orders appearing at each terminal, i.e., in each iteration we compute one trajectory of the problem. Thereby, N is a sufficiently large iteration counter

at which the approximations converged sufficiently. It is parameterized by experiment. At each iteration $n = 1, 2, \dots, N$, we randomly draw an information $\hat{\omega}_1^n$ that yields the currently known orders for the initial state S_1^n (in which the train is at the first terminal), see Step 2a. From here, we solve the problem in a forward programming manner once for each decision point $t = 1, 2, \dots, T - 1$. In particular, we find a decision x_t^n in Step 2b by solving the MIP (7.17)-(7.23) with the latest values of the features' weights θ_a^{n-1} (the weights obtained after the previous iteration). The MIP is formally described at the end of this section. The decision and the value of the corresponding post decision state are stored in Step 2c as they are used later in the updating process. Then, in Step 2d, we draw an outcome of the random information $\hat{\omega}_{t+1}^n$ to obtain new orders and transform to the next state S_{t+1}^n using the transition function $S^M(\cdot)$ from Equation (7.10). Finally, after making the last decision in the last relevant decision point $T - 1$ (the train's penultimate stop), we update the weights of the features in Step 2e using the stored values from Step 2c. The value of $S_t^{n,x}$ can be calculated as the difference in accumulated reward in t and T . The update of the weights is described in detail in Section 7.4.3.

The MIP that is solved in Step 2b is principally a representation of the Bellman Equation (7.15) for a single decision point t using the basis functions to approximate the value of a post-decision state. The MIP is formulated as follows, where the iteration superscript n is dropped for reasons of readability. The constraints of the MIP resemble the Equations (7.2)-(7.5) that describe a decision in the sequential decision process.

$$\min \alpha \cdot R_t^C(\cdot) + (1 - \alpha) \cdot R_t^E(\cdot) + \sum_{a \in \mathcal{A}} \theta_a \cdot \phi_a(\cdot) \quad (7.17)$$

subject to

$$\sum_{p \in \mathcal{P}_t^o} x_t(p) = 1, \quad \forall o \in \mathcal{O}_t \quad (7.18)$$

$$l_t(t') = \sum_{o \in \mathcal{O}_t} \left(q_o \cdot \sum_{p \in \mathcal{P}_t^o: t' \in \mathcal{T}_p} x_t(p) \right) \leq L^{\max}, \quad \forall t' \in \mathcal{T} \quad (7.19)$$

$$e_t^x(p) = e_p^{truck} + q_o \cdot \sum_{t' \in \mathcal{T}_p \setminus \{t_p^2\}} e^{train}(l_t^x(t')), \quad \forall o \in \mathcal{O}_t, p \in \mathcal{P}_t^o \quad (7.20)$$

$$f_t^x(o) = \begin{cases} 1, & \text{if } \sum_{p \in \mathcal{P}_t^o} x_t(p) \cdot e_t^x(p) > \bar{e}_o \\ 0, & \text{else} \end{cases}, \quad \forall o \in \mathcal{O}_t \quad (7.21)$$

$$e_t^x(p), l_t^x(t') \geq 0, \quad \forall p \in \mathcal{P}_t, t' \in \mathcal{T} \quad (7.22)$$

$$x_t(p), f_t^x(o) \in \{0, 1\}, \quad \forall p \in \mathcal{P}_t, o \in \mathcal{O}_t \quad (7.23)$$

The first two terms of objective function (7.17) represent the reward function (7.6), where objectives costs (R_t^C) and eco-labels (R_t^E) are weighted by a parameter α . The third part of the objective describes the basis functions and reflects the reached post-decision state. They are formulated as a linear combination of the features $a \in \mathcal{A}$ outcome values $\phi_a(\cdot)$, weighted by θ_a . The features and their formulation are later introduced in Section 7.4.4. Note that feature weights θ_a are determined by our VFA algorithm and given as input to the MIP.

Constraint (7.18) states that each order has to use exactly one of its paths. Constraint (7.19) defines the load of the train at each terminal, which cannot exceed the train's capacity. Constraint (7.20) calculates the emissions per path p under a decision and is denoted by $e_t^x(p)$. Here, $e^{train}(l_t^x(t'))$ describes train's emissions as a non-linear function of the train's load. This is easily linearized through further binary decision variables that test for the relevant payload ranges (see Figure 7.1b), which is, however, not shown here in the model for reasons of comprehensibility. Constraint (7.21) sets the eco-label violation decision variable $f_t(o) = 1$ if an order o violates its eco-label, and $f_t(o) = 0$ otherwise. This non-linear constraint can be implemented by using a big-M formulation or an indicator constraint as is usually provided by state-of-the-art solvers. Constraints (7.22) and (7.23) state the domains of the decision variables.

7.4.3 Learning in primal-dual VFA

This section describes how the primal-dual VFA is embedded in the general VFA algorithm described in the previous section. In particular, in primal-dual VFA, the feature weights are updated after each iteration using two trajectories. In the primal trajectory, values of post-decision states are evaluated based on the (suboptimal) forward decisions as in 'classical VFA'. In the dual trajectory, values of post-decision states are evaluated recursively solving an ex-post optimization problem using the same stochastic information as in the primal trajectory. That is, a decision is made in each state assuming knowledge

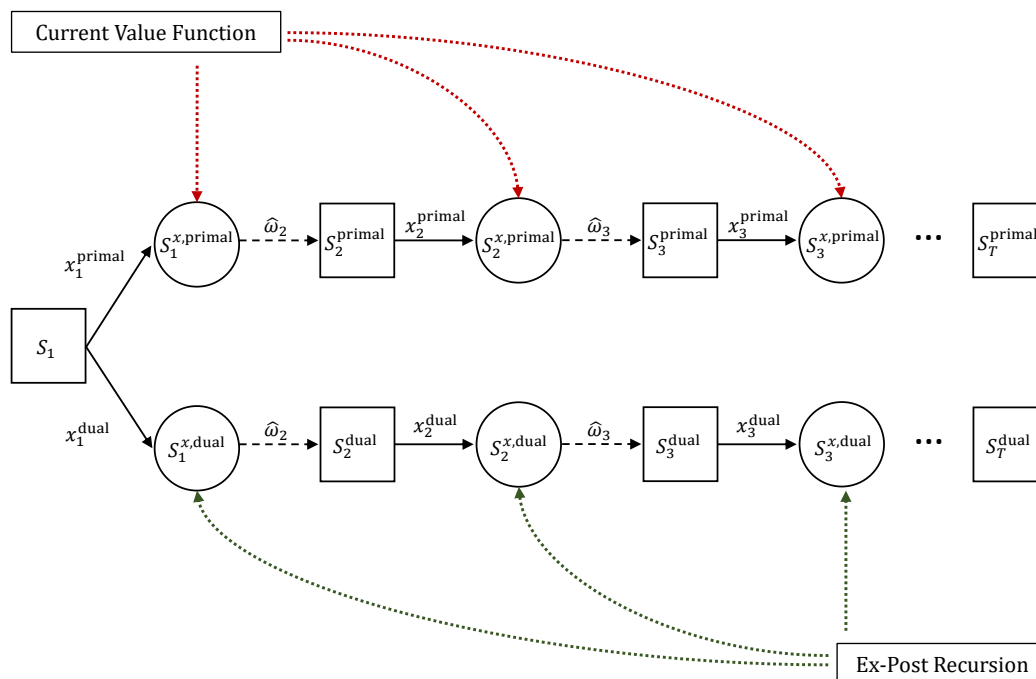


Figure 7.4: Illustration of the primal-dual VFA.

about future orders, resulting in a trajectory different from the primal trajectory. For the ex-post optimization, we solve a deterministic problem at the last decision point, considering *all* orders and paths of iteration n and break down the resulting optimal routings recursively to evaluate what the ‘perfect decision’ in each decision point $t \in \mathcal{T}$ would have been. In doing so, the dual trajectory constitutes a lower bound for the primal trajectory’s minimization problem and provides a valuable piece of information in the learning process. It allows us to pretend a fully deterministic setting for which it is much easier to calculate an optimal solution compared to the multidimensional stochastic setting. In our problem setting, the dual trajectory can be calculated within seconds using a standard solver but, still, it requires additional computational resources. However, as all calculations are done offline, the (short) additional calculation time can be neglected.

Figure 7.4 conceptually depicts the primal-dual VFA. Here, states are shown as rectangles, post-decision states as circles, solid black arcs represent the decision making between states and post-decision states, and dashed black arcs the arrival of stochastic information after the post-decision state. The upper part of the figure shows the primal trajectory: it starts at initial state S_1 and ends at final state S_T^{primal} by making decisions $\mathbf{x}_t^{\text{primal}}$ at points $t < T$ and by simulating information $\hat{\omega}_{t+1}$ after each decision. Here,

decisions are made using the MIP with the integrated current value function, which is depicted through the dotted arcs at the top of the figure. The lower part of the figure shows the dual trajectory: it also starts at initial state S_1 but ends at a final state S_T^{dual} . In the dual trajectory, a decision $\mathbf{x}_t^{\text{dual}}$ is made at each decision point and the same information $\hat{\omega}_{t+1}$ from the primal trajectory is used to transit to the next stage. Like in the primal trajectory, decisions are also made using the MIP but, now, the values from the recursive ex-post optimization are used for the value function. This is illustrated by the dotted arcs at the bottom of the figure.

Once the primal and dual trajectories are calculated, we update the weights of the features using the states and their respective values from both trajectories. The update of the weights θ_a is formally done by using a primal-dual learning parameter $0 \leq \beta \leq 1$. This parameter scales the relative importance of each trajectory: $\beta = 0$ means that only the primal trajectory is used to fit the weights, $\beta = 1$ means that only the dual trajectory is used to fit the weights, and $\beta \in (0, 1)$ describes combinations thereof. We use a linear regression model for the computation of the weights and integrate the relation expressed through β by weighting the trajectories accordingly. We use a preset value of $\beta = 0.5$ in our experiments but also show results for varying β -values in Section 7.5.

The general steps of the primal-dual VFA are shown in Algorithm 2. Just like the general VFA of Algorithm 1, the primal-dual VFA starts with an initial selection of the feature weights in Step 1. Then, the algorithm processes over N iterations and, for each iteration n , it computes the primal trajectory as well as the dual trajectory. We again use the superscript n to map values to iterations. The information $\hat{\omega}_t^n$ is drawn in Step 2 for all periods and is then used in both trajectories. In particular, the primal trajectory (Steps 3a to 3d) is computed just like in Algorithm 1 and the same general type of steps are also used to compute the dual trajectory (Steps 4a to 4d). In Step 4a, the initial state $S_1^{n,\text{dual}}$ is initialized by using information $\hat{\omega}_1^n$ as was used in the primal trajectory. Then, for each decision point t , a dual decision is found in Step 4b and it is stored together with the value of the post-decision state and the accumulated reward in Step 4c. For the decision making, there are two important differences compared to the primal trajectory: first, we solve the MIP without the basis functions and, second, we assume full knowledge about all information at each decision point. Then, Step 4d describes the transformation to the new state $S_{t+1}^{n,\text{dual}}$ by using the same information that was also used in the primal trajectory ($\hat{\omega}_{t+1}^n$). Note that this procedure results in the equivalent outcomes as applying ex-post recursion. Finally, Step 5 updates the weights by using decisions and values of the post-decision states of both trajectories that were stored in Step 3c (primal) and Step 4c (dual).

7.4.4 Feature selection

Our solution approach relies on features to aggregate the high dimensional state space. Thereby, features should summarize states of similar values and differentiate states of different values. The design of feature sets needs to be done with care for two reasons. First, too many features impede the learning process as learning many parameters is more difficult than learning just a few relevant ones. Second, the objective in our prob-

Step 1: Choose initial values for weights θ_a^0 of all features $a \in \mathcal{A}$.
for $n = 1, 2, \dots, N$ **do**

Step 2: Draw information $\hat{\omega}_t^n \in \Omega$ for all periods and for both trajectories.

Primal trajectory

Step 3a: Use information $\hat{\omega}_1^n \in \Omega$ for initial state $S_1^{n,\text{primal}}$.
for $t = 1, 2, \dots, T-1$ **do**

Step 3b: Find primal decision $x_t^{n,\text{primal}}$ by solving MIP model (7.17) to (7.23) using weights θ_a^{n-1} .
Step 3c: Store decision $x_t^{n,\text{primal}}$, post-decision state $S_t^{n,x,\text{primal}}$, and accumulated reward.
Step 3d: Use information $\hat{\omega}_{t+1}^n \in \Omega$ to transform to next state:
 $S_{t+1}^{n,\text{primal}} = S^M(\cdot)$.

end

Dual trajectory

Step 4a: Use information $\hat{\omega}_1^n \in \Omega$ for initial state $S_1^{n,\text{dual}}$.
for $t = 1, 2, \dots, T-1$ **do**

Step 4b: Find dual decision $x_t^{n,\text{dual}}$ by solving MIP model (7.17) to (7.23) without the basis functions and assuming that information $\cup_{t=1}^T \hat{\omega}_t^n$ is known.
Step 4c: Store decision $x_t^{n,\text{dual}}$, post-decision state $S_t^{n,x,\text{dual}}$, and accumulated reward.
Step 4d: Use information $\hat{\omega}_{t+1}^n \in \Omega$ to transform to next state:
 $S_{t+1}^{n,\text{dual}} = S^M(\cdot)$.

end

Step 5: Update weights θ_a^n for all features $a \in \mathcal{A}$ using the stored values from step 3c and 4c.

end

Algorithm 2: Algorithm for primal-dual VFA with basis functions.

Table 7.3: Feature sets used in our study.

nr.	name	description	calculation	VFA		
				EL	CO	All
1	A-orders RO	number of orders, with requested eco-label A, routed road-only	$\sum_{o \in \mathcal{O}_t: \lambda_o = A} \sum_{p \in \mathcal{P}_t^o: \mathcal{T}_p = \emptyset} r_t(p)$	x	-	x
2	B-orders RO	number of orders, with requested eco-label B, routed road-only	$\sum_{o \in \mathcal{O}_t: \lambda_o = B} \sum_{p \in \mathcal{P}_t^o: \mathcal{T}_p = \emptyset} r_t(p)$	x	-	x
3	C-orders RO	number of orders, with requested eco-label C, routed road-only	$\sum_{o \in \mathcal{O}_t: \lambda_o = C} \sum_{p \in \mathcal{P}_t^o: \mathcal{T}_p = \emptyset} r_t(p)$	x	-	x
4	A-orders IM	number of orders, with requested eco-label A, routed intermodally	$\sum_{o \in \mathcal{O}_t: \lambda_o = A} \sum_{p \in \mathcal{P}_t^o: \mathcal{T}_p \neq \emptyset} r_t(p)$	x	-	x
5	B-orders IM	number of orders, with requested eco-label B, routed intermodally	$\sum_{o \in \mathcal{O}_t: \lambda_o = B} \sum_{p \in \mathcal{P}_t^o: \mathcal{T}_p \neq \emptyset} r_t(p)$	x	-	x
6	C-orders IM	number of orders, with requested eco-label C, routed intermodally	$\sum_{o \in \mathcal{O}_t: \lambda_o = C} \sum_{p \in \mathcal{P}_t^o: \mathcal{T}_p \neq \emptyset} r_t(p)$	- ^a	-	- ^a
7	costly-orders RO	number of costly-orders routed road-only	$\sum_{o \in \mathcal{O}_t: a_o = 1} \sum_{p \in \mathcal{P}_t^o: \mathcal{T}_p = \emptyset} r_t(p)$	-	x	x
8	costly-orders IM	number of costly-orders routed intermodally	$\sum_{o \in \mathcal{O}_t: a_o = 1} \sum_{p \in \mathcal{P}_t^o: \mathcal{T}_p \neq \emptyset} r_t(p)$	-	x	x
9	costly-orders IM3	number of costly-orders routed intermodally until one of the last three terminals	$\sum_{o \in \mathcal{O}_t: a_o = 1} \sum_{p \in \mathcal{P}_t^o: t_p^2 \geq \mathcal{T} - 3} r_t(p)$	-	x	x
10	orders RO	number of orders routed road-only	$\sum_{p \in \mathcal{P}_t: \mathcal{T}_p = \emptyset} r_t(p)$	- ^a	x	- ^a
11	terminal	number of orders that are routed intermodally until each terminal	$\sum_{p \in \mathcal{P}_t: t_p^2 = t} r_t(p), \forall t \in \mathcal{T}$	x	x	x
12	cost-ratio	sum of an order's chosen path cost-ratio for orders routed intermodally	$\sum_{p \in \mathcal{P}_t: \mathcal{T}_p \neq \emptyset} c_p^r$	x	x	x
13	constant	constant to model the intercept	1	x	x	x

^a not considered as this information is already covered by other features.

lem is twofold and, with this, the same set of features may not be equally effective for both objectives as some features are only relevant for either costs or eco-label violations

whereas others may be relevant for both. In the following, we discuss factors that influence the two parts of the objective from which we then derive the features used in our study.

Some problem attributes are equally important to both objectives, e.g., a larger distance via truck corresponds to higher costs *and* higher emissions. Thus, the structure of the selected routing paths should be reflected in the features, such as whether an order is routed intermodally using the train, or not. Likewise, it is also important to capture the length of the pre- and post-carriage as they are always conducted by trucks. Features should also consider how long an order ‘blocks’ the capacity of the train in order to allow an intermodal routing for future orders that are not yet known when the decision is made for this considered order. Regarding the costs, we need to consider the relative costs for transporting orders via truck, resulting from factors like empty return trips, overtime, or own/rented trucks. We refer to orders whose direct truck transportation is above-average as ‘costly-orders’. Considering all these factors, we design three feature sets for our study: one focusing on eco-Labels (*VFA EL*), one focusing on cost (*VFA CO*), and a combination of both (*VFA All*). Table 7.3 shows a list of the features that are contained in these sets. The first column gives each feature a number, the second column states the abbreviated names of the features, the third column verbally describes the features, the fourth column states how to calculate the value of the features to integrate it in our MIP, and the last three columns indicate whether a feature is included in a feature set (marked by ‘x’), or not (marked by ‘-’).

The first six features in the table explicitly relate to the orders’ requested eco-labels λ_o . For this, we define A-, B-, and C-orders as orders requesting eco-labels A, B, or C, respectively. With this, Features 1 to 3 count the number of A-, B-, and C-orders that are routed directly using only the truck (road-only) and Features 4 to 6 the number of A-, B-, and C-orders that are routed intermodally using the train. Features 7 to 9 relate to the cost structure by counting the number of costly-orders that are routed either directly or intermodally. Here, Feature 9 puts a special emphasis on whether a costly-order is routed until one of the last three terminals, or not, as this comes along with using the train for a relatively long main-carriage compared to orders that use the train only for a few stops. Features 10 to 13 are relevant for both objectives. Feature 10 counts the number of orders that are routed road-only and Feature 11 counts the number of orders that are routed intermodally until each terminal. Feature 12 is the cost-ratio of an order’s chosen path and calculated by dividing the path’s total costs by the order’s road-only costs for a direct routing. This ratio also serves as an indicator for a paths relative length of the pre- and post-carriage. Finally, Feature 13 is a constant to model

the intercept. Notice that Feature 6 ('C-orders IM') is not used in any of the feature sets and Feature 10 is not included in *VFA EL* and *VFA All* as their information is already covered through other features. For example, Feature 10 is also expressed through the sum of Features 1 to 3.

All of the features are further differentiated between mustGo and mayGo orders, which is a common way of classifying orders in the transportation literature (e.g., Mes and Rivera; 2017). Thus, every feature (except for the constant) is included twice: once as mustGo and once as mayGo feature. A mustGo order is defined as an order for which an intermodal routing is not possible at future decision points, i.e., if we do not decide to route this order intermodally via terminal t (i.e., at the currently considered decision point) it has to be routed using the truck only (direct routing). In contrast, a mayGo order can also be routed intermodally at at least one of the future train stops. The differentiation between mustGo and mayGo orders is helpful for the algorithm to identify critical orders w.r.t. to their routing options. All features are linear formulations such that they can be directly integrated into the MIP model by using the calculation shown in Table 7.4.4.

7.5 Experimental study

This section presents the experiments that evaluate the proposed solution method as well as the trade-off between costs and eco-label violations in our stochastic and dynamic transportation problem. Section 7.5.1 describes the test data and the experimental set up. The results regarding different aspects of the solution method and the problem are discussed in Sections 7.5.2 to 7.5.4.

7.5.1 Test data and experimental design

We consider a train operating between Stockholm (Sweden) and Palermo (Italy) as depicted in Figure 7.5. The infrastructural data as well as the train's route are based on the Trans-European Transport Network and described in Appendix 7.7. Based on this setting, the number of stops (terminals) and decision points is $K = 16$. We model orders occurring around these stops as follows. An order's origin and destination location is a randomly chosen point within a 50 km radius around one of the train's stops. We consider orders that appear on relatively short notice whose origin location is around the train's current or next stop. As intermodal routings are more relevant for orders with relatively large direct distances, we assume that an order's destination is around a terminal that is

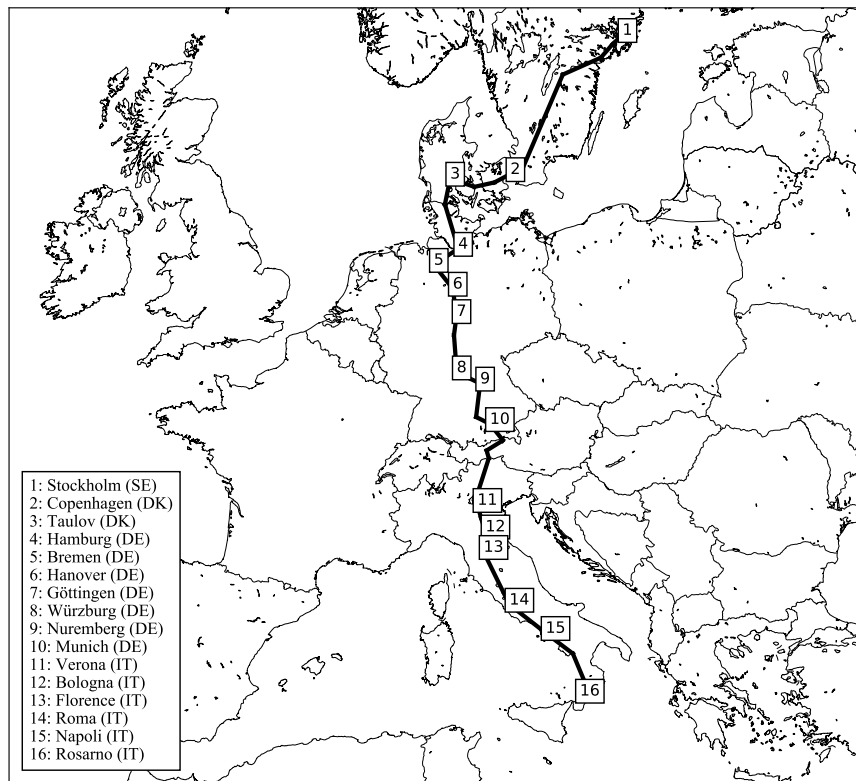


Figure 7.5: Rail service network considered in our experimental study.

at least 4 terminals ahead of the train's current stop. To reflect that the train operates regularly as a scheduled service, we assume a default load of 500 ton throughout the trip and that the number of orders appearing at the first stop is significantly larger compared to later stops. In particular, we consider the case that 20 orders are in expectation at the first stop and that a uniformly distributed random number between 3 to 10 new orders occur at each later stops. We assume orders of equal size ($q_o = 3$ FTL à 16 tons) with a randomly chosen eco-label A, B, or C, each with a probability of $1/3$. To reflect different cost structures among the orders, we select with equal probability if an order is considered to be a costly-order, or not, and assume twice as high costs for direct transportation for these orders, for example, due to empty travel. Cost rates for truck transportation are based on average values reported between European Union's NUTS2-level regions (Persyn et al.; 2020). For example, for routing an order from Copenhagen (Denmark) to Hamburg (Germany) we use a rate of 2.46 Euro per FTL-km and for routing the same order to Rome (Italy) we use a rate of 2.25 Euro per FTL-km. The train operates on a significantly lower cost rate of 0.32 Euro per FTL-km (Forkenbrock; 2001; Janic;

2007). Emissions are calculated using the EcoTransIT world emission estimation model (EcoTransIT World Initiative; 2020). For the trucks, we assume a fix emission rate of 70 gCO₂e per ton-km. For trains, we consider load-dependent emission rates that are linear between four load states at 500, 750, 1250, and 2000 tons that result in emission rates of 24.15, 18.78, 13.68, and 10.22 gCO₂e per ton-km, respectively, see Figure 7.1b. Finally, we assume for the train a total capacity of 26 orders (78 FTL), resulting in a total payload of 1,728 ton for a fully loaded train (including the default load). Note that, for reasons of simplicity, we use the load as single capacity restriction whereas the length of the train might also be relevant in practice (European Commissions; 2014).

We generally report results for three solution approaches (policies):

- *primal-dual VFA*: Our proposed VFA using one of the previously described feature sets (*VFA EL*, *VFA CO*, *VFA All*). For reasons of readability, we refer to this approach simply as ‘VFA’.
- *single stage*: A simple heuristic solving the problem just like VFA but ignoring any future impact, i.e., it solves the MIP decision problem in a point t by setting the weight of all features to 0.
- *ex-post*: A solution obtained from applying the same logic as for calculating the dual trajectory in the VFA algorithm. With this, it constitutes the lower bound for a considered realization.

We also considered rule-based decision policies, such as routing all orders with eco-label A or B via the train and all orders with eco-label C directly via truck, but preliminary tests showed an inferior performance even when compared to the single stage heuristic.

We evaluate results using the absolute costs (in tsd. Euro) and the eco-label’s violation level (in %). In this regard, the violation level reflects the percentage of orders that are *not* routed in accordance to their requested eco-label. We also report a lower bound gap (in %) reflecting the difference in the objective value between the considered approach (VFA or single stage) and the ex-post solution. The gap is calculates as follows:

$$\text{lower bound gap} = \frac{(\text{policy's objective value}) - (\text{ex-post's objective value})}{(\text{ex-post's objective value})}. \quad (7.24)$$

We report average results for 10 instance settings (each with a different random seed) in which we apply our approaches to 100 realizations. For the VFA learning, we conduct $N = 200$ iterations and set $\beta = 0.5$ as the default primal-dual learning parameter. Regarding the general fit of our feature sets, we perform an analysis of the coefficient of

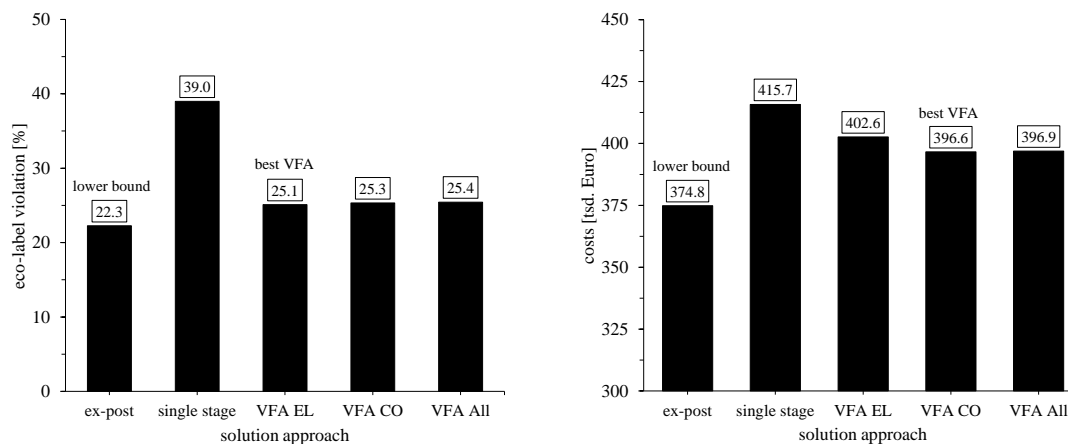
(a) Objective eco-label violations ($\alpha = 0$).(b) Objective costs ($\alpha = 1$).

Figure 7.6: Results for objective eco-label violations and costs.

determination that is described in Appendix 7.8. We solve all MIPs using IBM CPLEX Optimizer Version 12.9. The computation time per decision point in primal VFA (as well as for the single stage heuristic) is generally below one second and the computation time for the dual MIP solution is generally below three seconds.

7.5.2 The value of objective specific feature sets

We start by analyzing how different solution approaches perform when striving for a minimizing of costs and eco-label violations. Figures 7.6a and 7.6b shows the eco-label violations and total costs achieved when setting cost and eco-labels as objective, respectively, as achieved by the solution approaches single stage, ex-post (lower bound), *VFA EL*, *VFA CO*, and *VFA All*. It can be seen that the approaches perform differently for the two measures. The ex-post solution constitutes per definition the lower bound for the minimization problem but VFA solutions perform good as well, especially when compared to the single stage heuristic. The violation level is 25.1% under eco-label feature set *VFA EL*, which is slightly above the value of the ex-post solution (22.3%) but much lower than the value of the single stage heuristic (39.0%), see Figure 7.6a. This shows that the VFA-learning process is very helpful in obtaining good solutions for a stochastic dynamic setting, where information to calculate the ex-post solution is actually not available and its solution merely describes a theoretic benchmark. Similarly, according to the costs reported in Figure 7.6b, the average solution costs are 396.6 tsd. Euro using the cost-specific feature set *VFA CO* and, with this, 21.8 tsd. Euro higher than the

ex-post solution but 19.1 tsd. Euro lower than the single stage heuristic. Comparing the results of the three VFA-feature sets, we see only small differences when looking at the absolute performance measures. To analyze how the features contribute to obtaining best solutions, we report in Table 7.4 the percentage of data realizations in which the two objective-specific feature sets perform better, equal, or worse compared to the other solution approaches. The comparison is done with respect to the relevant performance measure, i.e., for objective eco-labels it is the number of orders that violate their eco-label and for objective costs it is the total costs of a solution. The results show that VFA-solutions obtained from an objective-specific feature set clearly outperform solutions of the single stage heuristic. In particular, *VFA EL* and *VFA CO* solutions are better than the single stage heuristic for 100% and 94.3% of the realizations, respectively. It can also be seen that *VFA EL* outperforms the other two VFA approaches as it performs better or equal for 75% of the realizations. Regarding feature set *VFA CO*, we also see that it outperforms the solutions under *VFA EL* in 71.8% of the realization but it shows a similar performance compared to solutions under feature set *VFA All*. All this indicates the importance of designing feature sets that take upon the factors influencing the objective.

To underpin these findings, we report in Figure 7.7a the lower bound gap of the three VFA approaches. Here, the three feature sets result in gaps between 13.4% and 14.8% for objective eco-labels and between 6.2% and 7.5% for objective costs. We see that using *VFA EL* under objective eco-labels results in remarkably lower gaps compared to both of the other two feature sets. Moreover, the gap is the highest using *VFA All*, indicating that using all features is not the best strategy in our multi-objective decision problem as the non-significant features impede the learning. For the objective costs, the gap is the same using sets *VFA CO* and *VFA All* but both sets outperform VFA solutions using *VFA EL*. Finally, Figure 7.7b depicts the pareto frontiers of our approaches demonstrat-

Table 7.4: Relative performance (in %) of feature sets VFA EL and VFA CO.

solution approach	VFA EL under objective eco-labels			VFA CO under objective costs		
	better	equal	worse	better	equal	worse
ex-post	0.0	8.9	91.1	0.0	0.0	100.0
single stage	100.0	0.0	0.0	94.3	0.0	5.7
VFA EL	-	-	-	71.9	0.2	27.9
VFA CO	40.5	33.1	26.5	-	-	-
VFA All	42.0	32.1	26.1	50.4	0.4	49.2

(a) Results under the pure eco-label ($\alpha = 0$) and costs ($\alpha = 1$) objective. (b) Results for varying weights of the two objectives (pareto frontier).

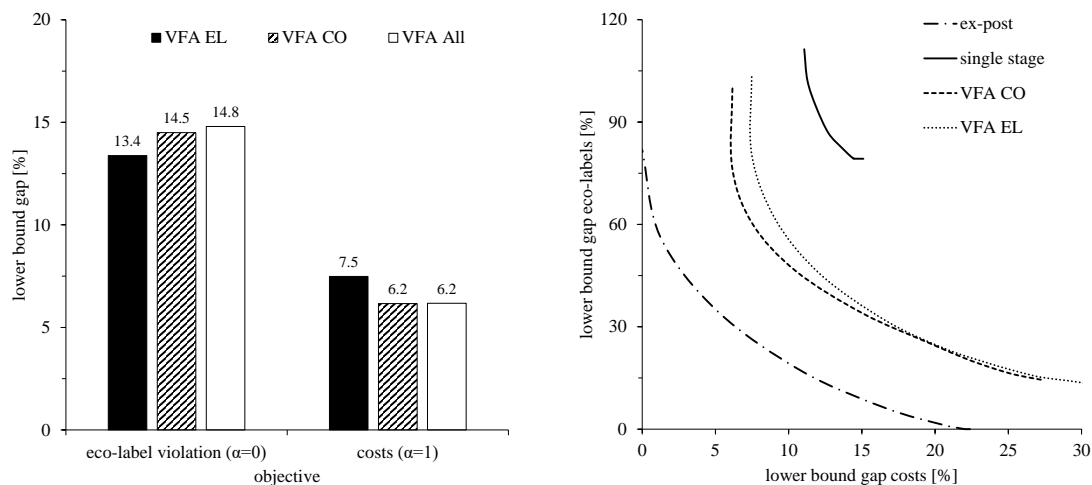
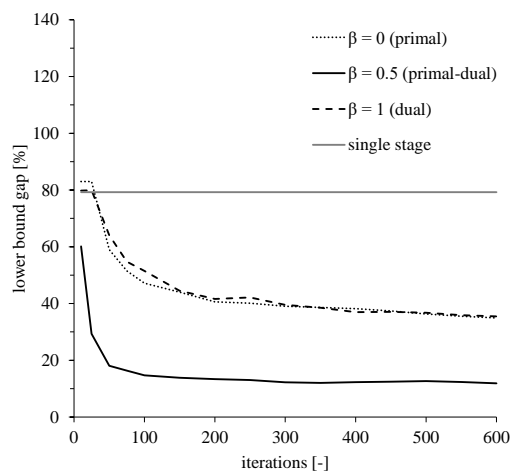
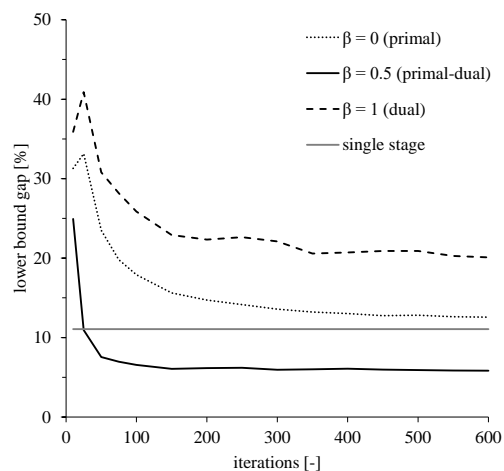


Figure 7.7: Results for the VFA feature sets for different weights of the two objectives.

ing the general trade-off between the two objectives. For the figure, we set parameter α to values between 0 and 1 representing different weightings for objectives eco-labels and costs. We scaled the axes differently for the purpose of presentation. In the figure, results with the lowest eco-label violations ($\alpha = 0$) correspond to low values on the vertical axis and results with the lowest costs ($\alpha = 1$) correspond to low values on the horizontal axis. For reasons of clarity, we do not show the pareto frontier for *VFA All*, which lies between the frontiers of the other two VFA approaches. The figure shows that the VFA solutions lie between the solutions obtained ex-post and under the single stage heuristic in all of the considered α -settings. Generally, less eco-label violations come along with an increase in the cost and vice versa. Thus, the figure clearly illustrates the trade-off between the two objectives that is particularly relevant for α values close to 0 or 1. For example, the VFA-curves are very steep at low values for the cost gap, indicating that a relatively small improvement in the cost gap corresponds to a large increase in the eco-label gap. Even the ex-post solutions show this strong trade-off. For example, pursuing a pure eco-label objective results in costs that are about 22% larger (horizontal intercept) compared to the pure cost objective. The pareto curves also show that *VFA CO* outperforms *VFA EL* for most of the settings as the same eco-label gap can be achieved with a lower cost gap. However, *VFA EL* and *VFA CO* are almost identical for settings strongly emphasizing the eco-label objective (the right part of the curves) and *VFA EL* outperforms *VFA CO* in the extreme case of $\alpha = 0$ as has been shown in the previous

(a) Learning curves of *VFA EL* for three β -settings under objective eco-labels.(b) Learning curves of *VFA CO* for three β -settings under objective costs.Figure 7.8: Learning curves with different settings of the primal-dual learning parameter β for *VFA EL* under objective eco-labels and for *VFA CO* under objective costs.

analysis. Overall, we conclude that it is important to design feature sets such that they are aligned to the influencing factors of the considered objective.

7.5.3 The value of primal-dual VFA

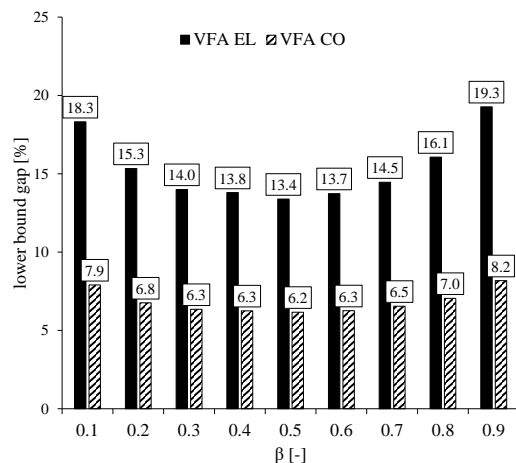
This section presents results regarding our primal-dual VFA. We start by showing the learning curves for objectives eco-labels (using feature set *VFA EL*) and costs (using feature set *VFA CO*) in Figures 7.8a and 7.8b, respectively. We show learning curves for three settings of our primal-dual learning parameter β : (i) $\beta = 0$ means that we only use the primal trajectory for updating our VFA, (ii) $\beta = 1$ means that we only use the dual trajectory for updating our VFA, and (iii) $\beta = 0.5$ means that both trajectories are used to the same extent for updating our VFA. The horizontal grey line corresponds to the single stage heuristic that does not involve learning at all. For the purpose of presentation, we show the lower bound gap after every 25th iteration. The horizontal axis depicts the number of iterations where more iterations refer to a longer learning process. The learning curves show the classical behaviour of a fast initial learning and a convergence at around $N = 200$ iterations for all considered β -settings. The primal-dual VFA ($\beta = 0.5$) clearly outperforms the two pure learning strategies ($\beta = 0$ and $\beta = 1$) in terms of performance and speed. That is, using the primal and the dual trajectories together in the estimation of the features weights improves the learning in VFA. For

the eco-label objective, all three β -settings outperform the single stage heuristic but the primal-dual VFA results in the lowest gap. This is different under the cost objective. Here, compared to single stage, only the primal-dual VFA results in a lower gap and both of the pure VFA approaches result in larger gaps. Thus, only by applying our novel primal-dual VFA we are able to produce results that outperform a non-anticipating heuristic. The results from Figure 7.8 also shows that objective-specific feature sets *VFA EL* and *VFA CO* show a quite different behaviour under the different learning strategies. According to that, the performance of the feature sets also correlates with how the different trajectories are weighted in the learning process, which points towards a future research direction.

To better understand the influence of the primal-dual learning parameter β , we show in Figure 7.9a the lower bound gap for both objectives and varying β -values between 0.1 and 0.9. The pure learning strategies ($\beta = 0$ and $\beta = 1$) are not reported in the figure as they result in much higher gaps, see Figure 7.8. The gaps in Figure 7.9a correspond to the objective of the respective feature set, e.g., gaps for *VFA EL* are reported for objective eco-labels and gaps for *VFA CO* are reported for objective costs. It can be seen that there is a ‘U-shape’ for both objectives. The lowest gaps are observed for $\beta = 0.5$ and they increase almost symmetrically towards lower and higher β -values. Thus, the particular chosen weighting of the two trajectories around $\beta = 0.5$ looks quite stable. Irregardless of this, it is clear that all of the combined learning strategies outperform the pure learning strategies depicted in Figure 7.8 (even the ones in which one of the trajectories is included through a low weight only).

One drawback of ‘classical’ VFA is that its performance generally decreases with an increasing level of stochasticity (e.g., Reddy et al.; 2020). This is because it gets more difficult for the algorithm to approximate the value function using the primal trajectories which get more *noisy* in more stochastic settings. We expect our primal-dual VFA to be a mean to make approximations more robust as the dual trajectory is generally less prone to increasing stochasticity. To show this, we compare the performance of the primal-dual VFA with the pure learning strategies and the single stage heuristic for varying levels of the stochastic information. For this, we use a variation parameter $\gamma \in [0, 1]$ that alters the orders’ eco-labels. Parameter γ describes the probability that an order’s eco-label is determined randomly using the distribution described in Section 7.5.1, whereas it is A otherwise. Thus, $\gamma = 0$ means that all orders request eco-label A, and $\gamma = 1$ means that each order’s eco-label is A, B, or C with an equal probability of $1/3$ (default setting). Figure 7.9b shows the results for the varied γ -values (horizontal axis). We report the lower bound gap under objective eco-labels (vertical axis) using feature set

(a) Results for *VFA EL* and *VFA CO* under objectives eco-labels and cost, respectively, for varying values of the primal-dual learning parameter β .



(b) Results for *VFA EL* under objective eco-labels for varying values of eco-label stochasticity parameter γ .

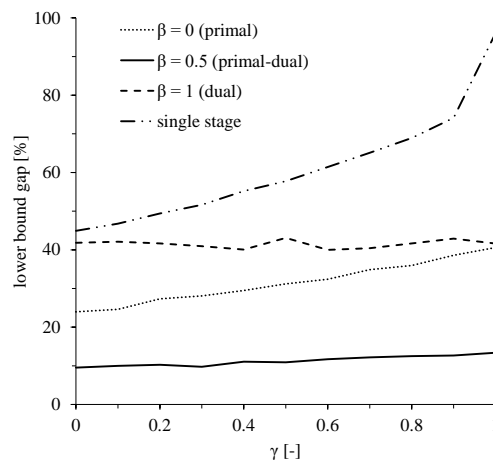


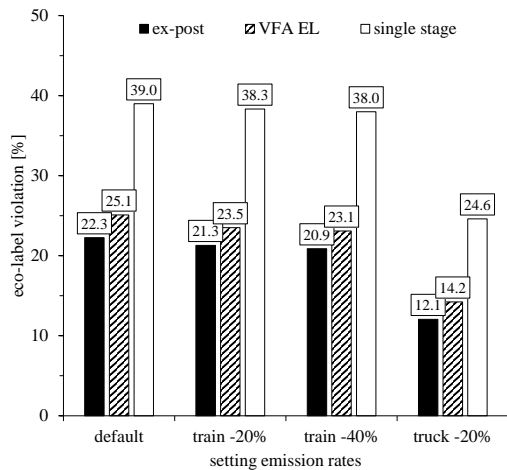
Figure 7.9: Results for varying the primal-dual parameter β and the eco-label stochasticity parameter γ .

VFA EL for the VFA approaches. It can be seen that our primal-dual VFA ($\beta = 0.5$) outperforms both of the pure learning strategies under all of the γ -settings, confirming its clear dominance in our problem setting. Furthermore, the results show that the single stage heuristic and the VFA approach with $\beta = 0$ (not considering the dual trajectory at all) clearly suffer from an increasing variability of the requested eco-labels as is revealed by an increasing lower bound gap. In contrast, the two strategies that consider the dual trajectory are quite robust against this variability. This shows that including the dual trajectory into VFA's learning makes the learning less prone for variations in the level of stochasticity. Nevertheless, the figure also demonstrates that the combination of the two trajectories ($\beta = 0.5$), our primal-dual VFA, leads to the lowest gaps and is therefore the best approach under all of the considered γ -settings.

7.5.4 Eco-label fulfillment under varied transport emission rates

In this final results section, we use the proposed primal-dual VFA to derive deeper insights on the fulfillment of eco-labels. More precisely, we quantify the levels of eco-label violations that are achievable under varied emission rates of trucks and trains. Such reductions can be achieved, for example, through technological advancements or through a greener electricity mix when using electric vehicles. In addition to the default setting

(a) Eco-label violations per solution approach using different settings for the modes' emission rates.



(b) Intermodal share per eco-label for two emission rate settings and two solution approaches.

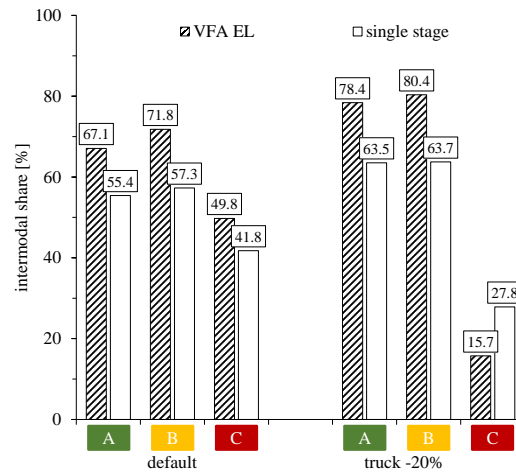


Figure 7.10: Eco-label violations and intermodal shares for varied emission rates of the transport modes (both under the eco-label objective).

described in Section 7.5.1, we consider three cases: (i) a reduction of the train's emission rate by 20%, (ii) a reduction of the train's emission rate by 40%, and (iii) a reduction of the truck's emission rate by 20%. Figure 7.10a shows the eco-label violations under the eco-label objective for the three settings and for solution approaches ex-post, *VFA EL*, and single stage. It can be seen all three approaches react in a similar way to the variations in the emission rates. In particular, the level of eco-label violations decreases by about 1-2% and 10-15% for the train and truck emission rate reduction settings, respectively. Thus, in our problem, reductions of truck emissions have a much higher impact on the eco-label violations compared to reductions of train emissions. It is also interesting to see that a reduction of truck emissions by 20% is required to let the single stage heuristic achieve levels of eco-label violations comparable to our *VFA* approach under the default setting. In other words, using a powerful solution method can improve results in a magnitude similar to technological advancements regarding truck emissions, in particular, if they replace simple planning procedures such as a single stage heuristic.

To better understand the corresponding structural changes of solutions, we depict the intermodal share per eco-label (i.e., the percentage of A-, B-, and C-orders that are routed intermodally) in Figure 7.10b for the default setting and the setting in which truck emissions are reduced by 20%. In this context, A-, B-, and C-orders refer to those

orders that respectively request the eco-labels A, B, and C for their shipping. Results are reported for the *VFA EL* approach and the single stage heuristic while the values from the ex-post solution are not shown as they behave similar to *VFA EL*. Although the overall intermodal share is not shown in the figure, it can be deduced that it is higher under the VFA approach compared to the single stage for both settings. In particular, it is on average about 11% higher in the default setting and about 8% higher in the truck reduction setting. This means that more orders are routed intermodally via the train under *VFA EL* and, with this, more orders can be routed in accordance to their eco-label resulting in less eco-label violations. However, looking at the intermodal share of the orders per requested eco-label, we can see that these results not directly follow from a high overall intermodal share, but, also, from decisions about *which* orders are routed intermodally. Under both settings, the intermodal share is higher for A- and B-orders than it is for C-orders. This is reasonable as these orders are more sensitive toward their total emissions and it is therefore beneficial to route them intermodally. However, what strikes out is that the intermodal share of C-orders is remarkably lower compared to A- and B-orders in the setting with reduced truck emissions. This can be explained by the fact that these orders can always be routed by truck in accordance to their eco-label if truck emissions are 20% below their default value. Routing some of these orders intermodally is then done only in order to fill up the train (and, thus, reduce its emission rate for accompanying orders) or due to lower overall costs. Either way, our primal-dual VFA successfully identifies which of these orders should be routed intermodally and which of them should not. In contrast, the single stage heuristics routes too many C-orders via the train which, ultimately, leads to a much higher intermodal share for these orders but also to more eco-label violations as shown in Figure 7.10a. This once again demonstrates the benefits from using VFA with features related to eco-labels as this allows the approach to learn the impact of the labels on the appropriate routing decisions.

7.6 Conclusion and outlook

In this paper, we have investigated the role of order-specific eco-labels in an intermodal stochastic and dynamic transportation problem. The eco-labels serve as an indicator for a customer's environmental cautiousness and constitute an upper bound on each order's allowed emissions. To solve this problem, we have proposed a value function approximation with basis functions, where we have enhanced the learning by considering two trajectories of the same iteration. In particular, we have used a primal trajectory

resulting from the ‘classical’ forward decisions and a dual trajectory resulting recursively from an ex-post optimization problem. There are several opportunities for future work.

In our paper, we have considered a single train operating on a fixed schedule and we have decided it was the task to decide about the routing of spontaneously appearing orders: either intermodally using the train or directly using trucks only. In the future, it might be interesting to extend the problem towards dimensions like multiple trains, additional modes for the main-carriage (e.g., barges), multiple periods, or uncertainty regarding the train schedule.

We have addressed a multi-objective problem considering the minimization of costs and the number of orders violating their requested eco-label. For this, we have designed feature sets that focus on those factors that influence eco-labels, costs, or both. Our experiments in an European rail corridor have shown that objective-specific feature sets outperform feature sets that do not relate to the weight of the two parts of the objective. Here we see the research opportunity of dynamically selecting features according to a (weighted) objective.

We have also demonstrated in the experiments that our primal-dual VFA improves the learning both in terms of quality and speed compared to VFAs that solely use either the primal trajectory or the dual trajectory. We have shown that this is because the combination of the two works as kind of exploration strategy as it evaluates yet another trajectory of the observed information. In the experiments, we have set an a priori relation to specify how to weight the two trajectories. For future work, it might be interesting to analyze the impact of a dynamic weighting of the two trajectories in the learning process (e.g., higher weight at the beginning, lower weight at the end).

Finally, as our primal-dual VFA is a general methodological contribution to approximate dynamic programming, it would be worth looking on how to apply it to problems not related to transportation.

Acknowledgments

The authors wish to thank Warren Powell and Justin Goodson for their valuable comments on learning with ex-post solutions. Arne Heinold’s work is funded by project 268276815 of the Deutsche Forschungsgemeinschaft (DFG, German Research Foundation). Marlin Ulmer’s work is funded by the Emmy Noether Programme of the DFG, project 444657906. This support is gratefully acknowledged.

7.7 Appendix A. Rail corridor data

Table 7.5 provides detailed information about the rail corridor considered in the experimental study.

Table 7.5: Rail corridor data used in the experiments.

id	country	city	latitude	longitude	NUTS2 code	km to next stop
1	Sweden	Stockholm	59.330709	18.057823	SE11	638.7
2	Denmark	Copenhagen	55.672019	12.565903	DK01	221.7
3	Denmark	Taulov	55.545105	9.615722	DK03	287.0
4	Germany	Hamburg	53.552812	10.007076	DE60	116.7
5	Germany	Bremen	53.082983	8.813076	DE50	122.2
6	Germany	Hanover	52.376319	9.741539	DE92	98.3
7	Germany	Göttingen	51.549884	9.925847	DE91	235.3
8	Germany	Würzburg	49.801296	9.936146	DE26	126.9
9	Germany	Nuremberg	49.446139	11.082447	DE25	200.6
10	Germany	Munich	48.140116	11.560487	DE21	435.6
11	Italy	Verona	45.427006	10.949910	ITH3	112.6
12	Italy	Bologna	44.506286	11.344115	ITH5	92.2
13	Italy	Florence	43.787270	11.251361	ITI1	260.3
14	Italy	Roma	41.892000	12.517239	ITI4	236.0
15	Italy	Napoli	40.853414	14.288077	ITF3	406.6
16	Italy	Rosarno	38.488598	15.970070	ITF6	-

7.8 Appendix B. Analyzing the fit of the feature sets

We report in Table 7.6 the coefficient of determination (R^2) resulting from a regression between the optimal value (calculated ex-post like the dual trajectory) and the value from the VFA approach in the final decision point T . This measure is considered as an indicator for the fit of a feature set, i.e., if it is generally suited to predict the value of a post-decision state. However, at the same time, it is also viewed of only having a limited use when it comes to predicting the actual performance of feature sets (Mes and Rivera; 2017). This means that the feature set with the highest R^2 does not necessarily lead to the best overall solution. The table shows values for both performance measures under both objectives. For objective eco-labels, the values for all feature sets and for both measures are high ($R^2=1$ means a perfect fit) and differences between VFA approaches are small. In contrast, for objective costs, differences between the sets are once again small, but R^2 is clearly higher for the (corresponding) measure costs than for measure eco-labels. This means that the objective costs does not work well for complying with eco-labels, whereas the objective eco-labels also leads to relatively good values for the measure costs. This observation is also in line with the finding from Figure 7.7b (pareto frontier) in which

the gaps for eco-labels are higher under the pure cost objective compared to the gaps for costs under the pure eco-label objective.

Table 7.6: Coefficient of determination (R^2) of the solution approaches under both objectives.

	<i>VFA EL</i>	<i>VFA CO</i>	<i>VFA All</i>
objective eco-labels			
eco-labels	0.8977	0.8968	0.8987
costs	0.9059	0.8978	0.9033
objective costs			
eco-labels	0.6530	0.6710	0.6728
costs	0.9761	0.9793	0.9815

Bibliography

- Archetti, C., Peirano, L. and Speranza, M. G. (2021). Optimization in multimodal freight transportation problems: A survey, *European Journal of Operational Research* (In Press).
- Bauer, J., Bektaş, T. and Crainic, T. G. (2010). Minimizing greenhouse gas emissions in intermodal freight transport: an application to rail service design, *Journal of the Operational Research Society* **61**(3): 530–542.
- Baykasoğlu, A. and Subulan, K. (2016). A multi-objective sustainable load planning model for intermodal transportation networks with a real-life application, *Transportation Research Part E: Logistics and Transportation Review* **95**: 207–247.
- Bellman, R. (1957). *Dynamic Programming*, Princeton University Press.
- Chen, K., Yang, Z. and Notteboom, T. (2014). The design of coastal shipping services subject to carbon emission reduction targets and state subsidy levels, *Transportation Research Part E: Logistics and Transportation Review* **61**: 192–211.
- Crainic, T. G. and Kim, K. H. (2007). Intermodal transportation, *Handbooks in Operations Research and Management Science* **14**: 467–537.
- Delbart, T., Molenbruch, Y., Braekers, K. and Caris, A. (2021). Uncertainty in intermodal and synchromodal transport: Review and future research directions, *Sustainability* **13**(7): 3980.
- Demir, E., Bektaş, T. and Laporte, G. (2011). A comparative analysis of several vehicle emission models for road freight transportation, *Transportation Research Part D: Transport and Environment* **16**(5): 347–357.
- Demir, E., Burgholzer, W., Hrušovský, M., Arıkan, E., Jammernegg, W. and Van Woensel, T. (2016). A green intermodal service network design problem with travel time uncertainty, *Transportation Research Part B: Methodological* **93**: 789–807.
- EcoTransIT World Initiative (2020). Ecological transport information tool for worldwide transports (update 2020). https://www.ecotransit.org/wordpress/wp-content/uploads/20210531_Methodology_Report_EcoTransIT_World.pdf (visited on 20.09.2021).
- European Commissions (2014). Core network corridors progress report of the European coordinators. <https://ec.europa.eu/transport/sites/default/files/infrastructure/tent>

- [ec/tentec-portal/site/brochures_images/CorridorsProgrReport_version1_2014.pdf](https://ec.tentec-portal/site/brochures_images/CorridorsProgrReport_version1_2014.pdf) (visited on 20.09.2021).
- European Environment Agency (2021). Greenhouse gas emissions from transport in Europe. <https://www.eea.europa.eu/data-and-maps/indicators/transport-emissions-of-greenhouse-gases-7/assessment> (visited on 20.09.2021).
- Forkenbrock, D. J. (2001). Comparison of external costs of rail and truck freight transportation, *Transportation Research Part A: Policy and Practice* **35**(4): 321–337.
- George, A. P. and Powell, W. B. (2006). Adaptive stepsizes for recursive estimation with applications in approximate dynamic programming, *Machine Learning* **65**(1): 167–198.
- George, A. P., Powell, W. B. and Kualkarni, S. R. (2008). Value function approximation using multiple aggregation for multiattribute resource management., *Journal of Machine Learning Research* **9**(10).
- Heinold, A. (2020). Comparing emission estimation models for rail freight transportation, *Transportation Research Part D: Transport and Environment* **86**: 102468.
- Heinold, A. and Meisel, F. (2018). Emission rates of intermodal rail/road and road-only transportation in Europe: A comprehensive simulation study, *Transportation Research Part D: Transport and Environment* **65**: 421–437.
- Heinold, A. and Meisel, F. (2019). Emission oriented vs. time oriented routing in the European intermodal rail/road freight transportation network, in C. Bierwirth, T. Kirschstein and D. Sackmann (eds), *Logistics Management*, Springer International Publishing, Cham, pp. 188–202.
- Heinold, A. and Meisel, F. (2020). Emission limits and emission allocation schemes in intermodal freight transportation, *Transportation Research Part E: Logistics and Transportation Review* **141**: 101963.
- Hrušovský, M., Demir, E., Jammerneegg, W. and Van Woensel, T. (2020). Real-time disruption management approach for intermodal freight transportation, *Journal of Cleaner Production* **280**: 124826.
- Janic, M. (2007). Modelling the full costs of an intermodal and road freight transport network, *Transportation Research Part D: Transport and Environment* **12**(1): 33–44.

- Jiang, D. R., Al-Kanj, L. and Powell, W. B. (2020). Optimistic monte carlo tree search with sampled information relaxation dual bounds, *Operations Research* **68**(6): 1678–1697.
- Jiang, D. R. and Powell, W. B. (2015). An approximate dynamic programming algorithm for monotone value functions, *Operations Research* **63**(6): 1489–1511.
- Jiang, J., Zhang, D., Meng, Q. and Liu, Y. (2020). Regional multimodal logistics network design considering demand uncertainty and CO2 emission reduction target: A system-optimization approach, *Journal of Cleaner Production* **248**: 119304.
- Lam, J. S. L. and Gu, Y. (2016). A market-oriented approach for intermodal network optimisation meeting cost, time and environmental requirements, *International Journal of Production Economics* **171**: 266–274.
- Li, L., Negenborn, R. R. and De Schutter, B. (2015). Intermodal freight transport planning—a receding horizon control approach, *Transportation Research Part C: Emerging Technologies* **60**: 77–95.
- Lorenzo-Toja, Y., Vázquez-Rowe, I., Amores, M. J., Termes-Rifé, M., Marín-Navarro, D., Moreira, M. T. and Feijoo, G. (2016). Benchmarking wastewater treatment plants under an eco-efficiency perspective, *Science of the Total Environment* **566**: 468–479.
- Mes, M. R. K. and Iacob, M.-E. (2016). Synchronodal transport planning at a logistics service provider, in H. Zijm, M. Klumpp, U. Clausen and M. t. Hompel (eds), *Logistics and Supply Chain Innovation: Bridging the Gap between Theory and Practice*, Springer International Publishing, Cham, pp. 23–36.
- Mes, M. R. K. and Rivera, A. P. (2017). Approximate dynamic programming by practical examples, in R. J. Boucherie and N. M. van Dijk (eds), *Markov Decision Processes in Practice*, Springer International Publishing, Cham, pp. 63–101.
- Miller, J., Nie, Y. M. and Liu, X. (2020). Hyperpath truck routing in an online freight exchange platform, *Transportation Science* **54**(6): 1676–1696.
- Persyn, D., Díaz-Lanchas, J. and Barbero, J. (2020). Estimating road transport costs between and within European Union regions, *Transport Policy* (In Press).
- Piecyk, M., Cullinane, S. and Edwards, J. (2012). Assessing the external impacts of freight transport, in A. McKinnon, M. Browne and A. Whiteing (eds), *Green logistics:*

- Improving the Environmental Sustainability of Logistics*, 2 edn, Kogan Page Limited London, chapter 2, pp. 31–50.
- Powell, W. B. (2009). What you should know about approximate dynamic programming, *Naval Research Logistics* **56**(3): 239–249.
- Powell, W. B. (2011). *Approximate Dynamic Programming: Solving the Curses of Dimensionality*, 2nd edn, John Wiley & Sons.
- Powell, W. B. (2021). *Reinforcement Learning and Stochastic Optimization*, John Wiley & Sons.
- Reddy, G. T., Reddy, M. P. K., Lakshmana, K., Kaluri, R., Rajput, D. S., Srivastava, G. and Baker, T. (2020). Analysis of dimensionality reduction techniques on big data, *IEEE Access* **8**: 54776–54788.
- Resat, H. G. and Turkay, M. (2019). A discrete-continuous optimization approach for the design and operation of synchromodal transportation networks, *Computers & Industrial Engineering* **130**: 512–525.
- Rivera, A. E. P. and Mes, M. R. (2017a). Anticipatory freight selection in intermodal long-haul round-trips, *Transportation Research Part E: Logistics and Transportation Review* **105**: 176–194.
- Rivera, A. E. P. and Mes, M. R. (2019). Integrated scheduling of drayage and long-haul operations in synchromodal transport, *Flexible Services and Manufacturing Journal* **31**(3): 763–806.
- Rivera, A. E. P. and Mes, M. R. K. (2017b). Scheduling drayage operations in synchromodal transport, in T. Bektaş, S. Coniglio, A. Martinez-Sykora and S. Voß (eds), *Computational Logistics*, Springer International Publishing, Cham, pp. 404–419.
- Rudi, A., Fröhling, M., Zimmer, K. and Schultmann, F. (2016). Freight transportation planning considering carbon emissions and in-transit holding costs: a capacitated multi-commodity network flow model, *EURO Journal on Transportation and Logistics* **5**(2): 123–160.
- Schaul, T., Zhang, S. and LeCun, Y. (2013). No more pesky learning rates, *International Conference on Machine Learning*, PMLR, pp. 343–351.

- Shar, I. E. and Jiang, D. (2020). Lookahead-bounded q-learning, in H. D. III and A. Singh (eds), *Proceedings of the 37th International Conference on Machine Learning*, Vol. 119 of *Proceedings of Machine Learning Research*, PMLR, pp. 8665–8675.
- Smith, L. N. (2017). Cyclical learning rates for training neural networks, *2017 IEEE Winter Conference on Applications of Computer Vision (WACV)*, pp. 464–472.
- Steadie Seifi, M., Dellaert, N. P., Nuijten, W., Van Woensel, T. and Raoufi, R. (2014). Multimodal freight transportation planning: A literature review, *European Journal of Operational Research* **233**(1): 1–15.
- Sun, Y. and Lang, M. (2015). Modeling the multicommodity multimodal routing problem with schedule-based services and carbon dioxide emission costs, *Mathematical Problems in Engineering* **2015**.
- Ulmer, M. and Savelsbergh, M. (2020). Workforce scheduling in the era of crowdsourced delivery, *Transportation Science* **54**(4): 1113–1133.
- Ulmer, M. W. (2020). Dynamic pricing and routing for same-day delivery, *Transportation Science* **54**(4): 1016–1033.
- Ulmer, M. W., Goodson, J. C., Mattfeld, D. C. and Hennig, M. (2019). Offline–online approximate dynamic programming for dynamic vehicle routing with stochastic requests, *Transportation Science* **53**(1): 185–202.
- Ulmer, M. W., Goodson, J. C., Mattfeld, D. C. and Thomas, B. W. (2020). On modeling stochastic dynamic vehicle routing problems, *EURO Journal on Transportation and Logistics* **9**(2): 100008.
- Ulmer, M. W., Mattfeld, D. C. and Köster, F. (2018). Budgeting time for dynamic vehicle routing with stochastic customer requests, *Transportation Science* **52**(1): 20–37.
- Ulmer, M. W. and Thomas, B. W. (2020). Meso-parametric value function approximation for dynamic customer acceptances in delivery routing, *European Journal of Operational Research* **285**(1): 183–195.
- van Heeswijk, W. J., Mes, M. R. and Schutten, J. M. (2019). The delivery dispatching problem with time windows for urban consolidation centers, *Transportation Science* **53**(1): 203–221.

- van Heeswijk, W., Mes, M., Schutten, J. and Zijm, W. (2018). Freight consolidation in intermodal networks with reloads, *Flexible Services and Manufacturing Journal* **30**(3): 452–485.
- Zhao, Y., Xue, Q. and Zhang, X. (2018). Stochastic empty container repositioning problem with CO2 emission considerations for an intermodal transportation system, *Sustainability* **10**(11): 4211.

Appendix

Appendix A

A Tutorial on Value Function Approximation for Stochastic Dynamic Transportation Problems

Publication status Submitted to *4OR - A Quarterly Journal of Operations Research* (29.09.2021). Currently under review (first round).

Arne Heinold

School of Economics and Business, Kiel University, Kiel, Germany

Abstract This paper provides an introductory tutorial on Value Function Approximation (VFA), a solution class from Approximate Dynamic Programming. VFA describes a heuristic way for solving sequential decision processes like a Markov Decision Process. Real-world problems in supply chain management (and beyond) containing dynamic and stochastic elements might be modeled as such processes, but large-scale instances are intractable to be solved to optimality by enumeration due to the curses of dimensionality. VFA can be a proper method for these cases and this tutorial is designed to ease its use in research, practice, and education. For this, the tutorial describes VFA in the context of stochastic and dynamic transportation and makes three main contributions. First, it gives a concise theoretical overview of VFA's fundamental concepts, outlines a generic VFA algorithm, and briefly discusses advanced topics of VFA. Second, the VFA algorithm is applied to the taxicab problem that describes an easy-to-understand transportation planning task. Detailed step-by-step results are presented for a small-scale instance, allowing readers to gain an intuition about VFA's main principles. Third, larger instances

are solved by enhancing the basic VFA algorithm demonstrating its general capability to approach more complex problems. The experiments are done with artificial instances and the respective Python scripts are part of an electronic appendix. Overall, the tutorial provides the necessary knowledge to apply VFA to a wide range of stochastic and dynamic settings and addresses likewise researchers, lecturers, tutors, students, and practitioners.

Keywords Tutorial, Reinforcement Learning, Approximate Dynamic Programming, Value Function Approximation, Markov Decision Process

A.1 Introduction

Supply Chain Management (SCM) generally describes the management of flow-related processes among suppliers, customers, and business partners (Christopher; 2010). Many of these processes are data-driven like inventory management and transportation planning. An increasing awareness among companies about it and improvements in data tools have facilitated the use of analytical tools to optimize supply chain, constituting the field of supply chain analytics (e.g., Souza; 2014; Hoberg; 2020). An important field in SCM is the transportation of passengers and goods. Here, recent technological advancements result in new business models and a mould-breaking variety of transportation possibilities, such as drone delivery, car/bike/ride sharing, autonomous driving, or crowd shipping (e.g., Behrend and Meisel; 2018, 2019). Many of these problems take place in dynamic (multi-period) environments and comprise at least one form of uncertainty, such as uncertain demand, uncertain vehicle capacities, or uncertain travel times (e.g., Schilde et al.; 2011; Ulmer; 2020; Ulmer et al.; 2019). The ever increasing amount of passengers and goods also needs to be transported in conjunction with high customer expectations. For instance, Rayle et al. (2016) show that short waiting times and fast travel times are among the top reasons why customers choose ridesourcing. In this business context, it is the goal of companies to find transport solutions, often within seconds, whilst taking into account that such transportation problems are usually computationally difficult to be solved to optimality within a reasonable computation time due to complex sets of restrictions (e.g., Secomandi and Margot; 2009; Maxwell et al.; 2010; Mes et al.; 2010; Schmid; 2012; Pironet; 2015; Cattaruzza et al.; 2017; Alnaggar et al.; 2020). Advanced data-driven solution methods are often used to deal with this and one of such is subject to this paper: Value Function Approximation (VFA).

VFA is generally applied to problems modeled as sequential decision processes and is one of the solution classes described in Approximate Dynamic Programming (ADP, Powell; 2011). It builds upon the same framework and concepts that are also used in the wide field of reinforcement learning (Sutton and Barto; 2018). While the focus of this paper is on transportation, it is noted that VFA can be generally applied to sequential decision processes as which many SCM problems - as well as problem not related to business at all - might be formulated. So far, introductory papers on VFA either focus on the underlying theory (e.g., Powell; 2009) or present intricate examples (e.g., Mes and Rivera; 2017), making its understanding difficult for first-time users. The goal of this tutorial is to close this gap.

This paper's tutorial makes three main contributions. First, it provides a concise theoretical background of the fundamental concepts used in VFA. The tutorial applies each theoretical concept right after it is introduced, allowing readers to experience the interplay between theory and application. Second, it demonstrates the method on a vanilla-type transportation planning problem. The well-known taxicab problem is used for this purpose and detailed step-by-step results are presented for a small-scale instance. Using such a readily accessible example from transportation planning, the tutorial aims at providing an insight into the methodology to ease its application. Third, it points towards advanced topics relevant to VFA applications by considering two simple enhancements of the basic VFA algorithm. The impact of the enhancements is demonstrated on a larger instance but even this instance has a definite form such that it is suited to gain an intuition. With these contributions, the tutorial aims at fulfilling two purposes: first, to be a starting point for readers interested in VFA coming from various fields and disciplines like business administration, computer science, and engineering, and, second, to support readers not familiar with algorithms and common operations research methods to apply VFA to their problem. Consequently, the tutorial might be likewise interesting for researchers, lecturers, tutors, students, and practitioners.

This tutorial can be worked through from end to end or it can be used to focus on some sections only. For this, the rest of this paper is organized as follows. Section A.2 provides a short review of transportation problems that apply VFA. This section also briefly explains VFA's fundamental principles and brings VFA into line with other solution classes. Section A.3 provides a description of the taxicab problem that is used throughout the tutorial. Section A.4 elaborates on the modeling framework and the optimal policy. In particular, Section A.4.1 introduces Markov Decision Processes (MDPs) in a formal and mathematical way, Section A.4.2 introduces the Bellman equation, and Section A.4.3 uses these concepts to describe the optimal policy for the taxicab problem.

Section A.5 introduces VFA. Here, Section A.5.1 motivates the need for VFA, Section A.5.2 depicts a basic VFA algorithm, Section A.5.3 introduces post-decision states (an important concept in VFA), and Section A.5.4 applies the basic VFA algorithm step-by-step to a small-scale instance. Section A.6 provides additional insights to VFA. For this, Section A.6.1 discusses an alternative updating function, Section A.6.2 enhances the basic algorithm with an exploration strategy, and Section A.6.3 shows results for tuning some VFA parameters and presents a runtime analysis. Section A.7 concludes this paper. All solution approaches are implemented in Python and the scripts are made publicly available, see Appendix A.

A.2 Solving stochastic and dynamic problems (in transportation)

This section generally provides an overview of how to model and solve stochastic and dynamic problems and reviews some exemplary VFA applications in transportation. In this context, dynamic refers to a setting that spans over multiple periods (multistage) of distinct points in time (discrete) and is stochastic in the sense that some problem elements are uncertain (Mes and Rivera; 2017). These problems can be modeled as sequential decision processes in which decisions are made after each period and the stochastic information is received afterwards. Markov Decision Processes (MDPs) provide a mathematical framework for a setting like this. For stochastic dynamic vehicle routing problems, which constitute an important and broad problem class in transportation, MDPs are the most common modeling theme (Ulmer et al.; 2020). Solving such problems is challenging as they usually cannot be solved to optimality within a reasonable computation time due to their large and complex dimensions. As a ‘broad umbrella for a modeling and algorithmic strategy for solving problems that are sometimes large and complex, and are usually (but not always) stochastic’ (Powell; 2009, p. 239), Approximate Dynamic Programming distinguishes between four broad decision policy classes: policy function approximations, lookahead policies, cost function approximations, and VFAs. The main idea of each class is depicted in Figure A.1 and shortly described in the following. For a comprehensive description it is referred to Powell (2011) and Powell and Meisel (2015).

In policy function approximation, decisions are made using a rule-based policy without actually formulating an optimization problem. For example, such policies in transportation might sound like ‘routing large orders via train and small orders via truck’ or ‘pick-up the customer that is closest to the vehicle’. Although this policy class might

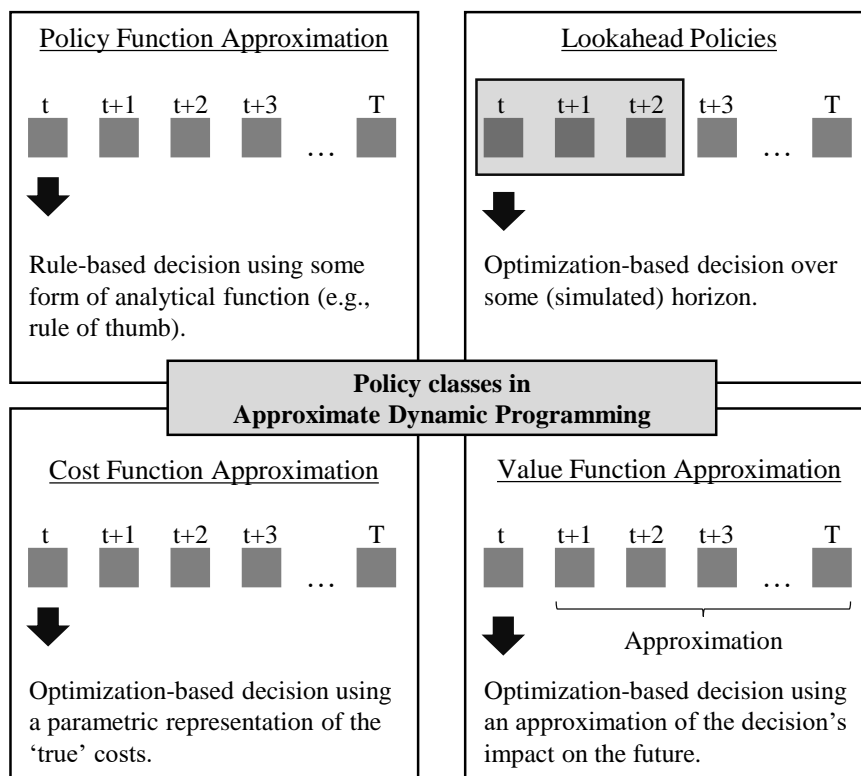


Figure A.1: Policy classes in Approximate Dynamic Programming (based on Powell and Meisel; 2015; Soeffker et al.; 2021).

appear at first sight to be ‘too simple’, it can be quite effective in real-world settings, particularly, if the factors influencing a problem’s objective can be easily identified and controlled when decisions are made. Cost function approximations also do not explicitly model ‘the future’. However, decisions are based on an optimization incorporating some kind of parametric representation of a decision’s ‘true’ costs. For example, the cost function might use penalties for ‘bad’ and incentives for ‘good’ aspects of a decision. In contrast, lookahead policies explicitly consider a decision’s impact on ‘the future’ by optimizing over some horizon (e.g., a few hours or a few days). Such a policy can lead to good decisions especially if decisions only affect nearby periods, have a limited impact on far-away periods, or good forecasts are available. In contrast to the previous three solution classes, VFA’s principal idea is as follows: make decisions by stepping forward in time over a large number of iterations and, after each iteration, evaluate decisions to improve decision quality for the next iteration. In order to step forward, time-dependent (sequentially appearing) information is used that can result from recurring simulation runs

or empirical observations. Eventually, a ‘good’ decision policy is learned that can then be applied to real-world settings. The paradigm of stepping forward raises completely new questions like how far ahead one should look. In this tutorial, some of these issues are discussed by presenting a detailed theoretical description of VFA and by describing its application to an easy-to-understand transportation problem. Generally speaking, modeling problems as sequential decision processes/MDPs and approaching them with algorithms that ‘learn’ from additional data like in VFA is also used in the communities of reinforcement learning and artificial intelligence (e.g., Sigaud and Buffet; 2013; Sutton and Barto; 2018). Powell and Meisel (2015) provide a concise tutorial on the modeling (and its language) of such problems in different scientific communities (control theory, dynamic programming, stochastic programming, and robust optimization).

The capability of VFA to solve large and complex stochastic dynamic problems has been demonstrated on various artificial and real-world instances from diverse fields, see, for example, Powell’s seminal book on ADP (Powell; 2011) and numerous publications resulting from research in Princeton’s CASTLE Lab (<https://castlelab.princeton.edu/>). The rest of this section reviews three exemplary transportation studies in which VFA has been shown to provide fast solutions of high quality. Simao et al. (2009) apply VFA to a large-scale fleet management problem for the task of assigning drivers to loads. Thereby, immediate rewards of the current period (e.g., that results from the assignment) are considered together with future rewards from richer operational issues (e.g., hours of service or returning drivers home). The authors show that VFA leads to solutions of high quality that match the performance of the company’s highly skilled dispatchers. Rivera and Mes (2017) apply the forward programming VFA approach in an intermodal long-haul round-trip problem. The authors consider the task of assigning orders either to (less costly) round-trips with a barge, or to (more costly) direct trips with a truck. Uncertainty about the number of orders shipped between the locations as well as about the orders’ characteristics (e.g., time windows) are key reasons why it is computationally intractable to solve large problem instances to optimality. For example, the computation time for small instances is about 800 seconds using an optimal solution strategy, whereas it is below 5 seconds using VFA. With respect to performance, the authors show that the VFA approach leads to optimality gaps of at most 11% for small instances and, compared to a single-period heuristic, to cost reductions of up to 25.5% for larger instances. Finally, Ulmer et al. (2018) apply VFA to a multi-period dynamic vehicle routing problem with stochastic customer requests. In the problem, requests arrive sequentially during the day and the task is to either integrate them in the current day’s routing (requiring an update of the vehicles current route) or to postpone them to the next day (constraining next

day’s routing possibilities). The authors compare their VFA approach with a benchmark heuristic and show that it improves the solution quality as well as it leads to more balanced acceptance decisions regarding the requests’ time and location.

A.3 The taxicab problem

This section presents the problem that is considered throughout the entire tutorial: a basic version of the taxicab problem (sometimes also referred to as nomadic trucker problem), see Powell (2011, p. 176) or Mes and Rivera (2017, p. 66). It describes the multiperiod problem of a single vehicle (taxi) faced with an uncertain demand. It is the task to find an optimal move for the vehicle in each period. This move determines the demand that is served in that period and consists of a starting point and an endpoint. Thereby, the vehicle’s starting point in a period is determined by its endpoint in the previous period. After the move of the vehicle (e.g., in the next period), the uncertain new information about the demand appears. Figure A.2 conceptually sketches the problem for five locations and three periods.

The rest of this section formally describes the problem such that the notations presented in the subsequent sections can be easily applied. A graph-based depiction of the problem is used in which $G(\mathcal{V}, \mathcal{E})$ describes the network. Vertices \mathcal{V} , also referred to as locations, are fully connected through arcs \mathcal{E} , i.e., $(v, v') \in \mathcal{E}, \forall v, v' \in \mathcal{V}$, and

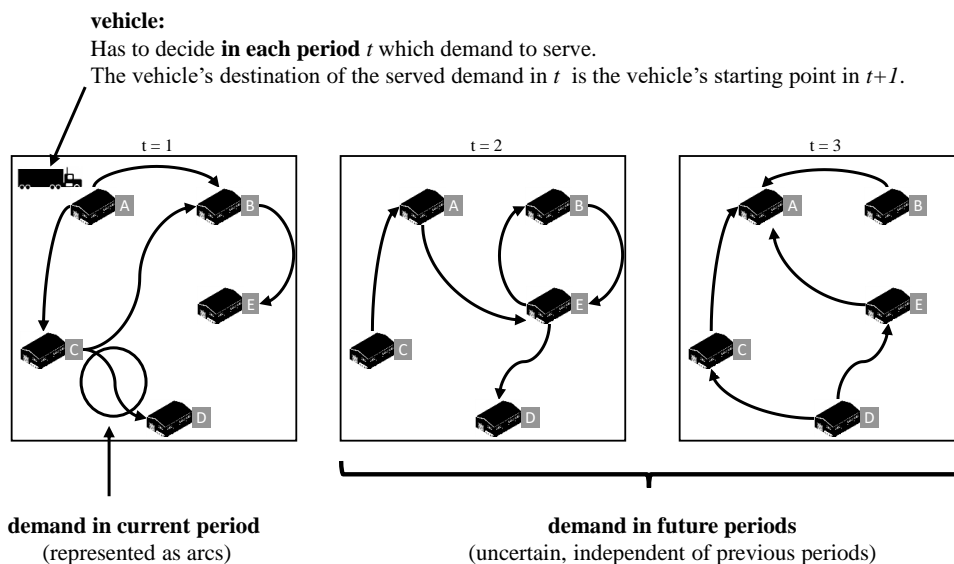


Figure A.2: Illustration of the taxicab problem with five locations and three periods.

the total number of locations is denoted with V . The planning problem spans over $\mathcal{T} = \{0, 1, 2, \dots, T\}$ periods. In each period $t \in \mathcal{T}$, p_{ijt} describes the probability of demand d_{ijt} between locations $i \in \mathcal{V}$ and $j \in \mathcal{V}$. Consequently, there is no demand ($d_{ijt} = 0$) between these locations with a probability of $(1 - p_{ijt})$. The demand is assumed to be uncertain and independent of previous periods, i.e., p_{ijt} is not affected by the vehicle's movement in periods $t' \neq t$. Considering the demand in network $G(\mathcal{V}, \mathcal{E})$, it is the task to select a move $x_t \in \mathcal{V}$ for the vehicle in each period. This move describes the vehicle's location at the end of period t , which then is its origin location $l_{t+1} \in \mathcal{V}$ at the beginning of the next period, i.e., $x_t = l_{t+1}$ and $l_t = x_{t-1}$. In other words, the vehicle has to be assigned to exactly one arc $(l_t, x_t) \in \mathcal{E}$ per period. If the vehicle moves from $l_t \in \mathcal{V}$ to $x_t \in \mathcal{V}$ in period $t \in \mathcal{T}$, it automatically serves demand $d_{l_t x_t t}$ and receives a contribution of $c_{l_t x_t t} = d_{l_t x_t t}$. If $x_t = l_t$, the vehicle remains at its current location. For the experiments in this tutorial, it is assumed that the origin location in the first period is known, the problem spans over a finite time horizon (e.g., T is known), and a stochastic distribution of the demand is known for all periods (including the initial period). In particular, artificial instances are used in which random numbers between $[0, 100]$ and $[0, 1]$ describe the demand (d_{ijt}) and its probability (p_{ijt}) between any two locations $i, j \in \mathcal{V}$ of a period $t \in \mathcal{T}$, respectively.

A.4 Modeling and optimal policy

This section introduces the modeling framework of VFA and elaborates on the optimal policy to solve such problems. For this, Sections A.4.1 and A.4.2 respectively describe MDPs and the Bellman equation in a formal and mathematical way using the notation often used in the operations research community (Powell; 2009, 2011). Section A.4.3 then describes the optimal policy for the taxicab problem. Table A.1 shows the relevant notation that is used throughout this tutorial.

A.4.1 Markov Decision Process

As shown in the short review in Section A.2, MPDs are a common modeling theme for stochastic and dynamic (transportation) problems that can then be approached with VFA. More generally, they are a special but important case of sequential decision processes. This section briefly introduces MDPs and, with this, it comprises all definitions required to apply VFA to sequential decision processes. A thorough introduction to MDPs can be found, for example, in Powell (2011, Chapter 3).

Table A.1: Relevant notation used in this study.

Name	Description
$C(S_t, x_t)$	contribution if decision x_t is taken in state S_t
$p(s' S_t, x_t)$	probability to transit to state s' if decision x_t is taken in state S_t
\mathcal{S}	set of all states
S_t	state in period t
$S^M(\cdot)$	transition function used to move from one state to another
$V_t(S_t)$	value of state S_t in period t
W_t	information in period t (usually stochastic)
$X^\pi(\cdot)$	decision function of policy $\pi \in \Pi$
X_t	set of all available decisions in period t
x_t	decision in period t ($x_t \in X_t$)
γ	discount factor
Π	set of available policies

MDPs describe sequential decision making problems in which uncertainty is considered. They essentially formulate the dynamics of moving between states over time. In this context, the term state refers to the properties or characteristics that are associated to this point in time, e.g., the weekday or the demand. The set \mathcal{S} describes all states of a process that spans over $\mathcal{T} = \{0, 2, \dots, T\}$ periods and $S_t \in \mathcal{S}$ denotes a state in period $t \in \mathcal{T}$. In a state S_t , the set X_t describes all possible decisions and the contribution of a decision $x_t \in X_t$ is denoted by $C(S_t, x_t)$. Note that, depending on the problem at hand, the terms action or move may be used instead of decision and the terms costs or value may be used instead of contribution. The next period's state S_{t+1} results from a

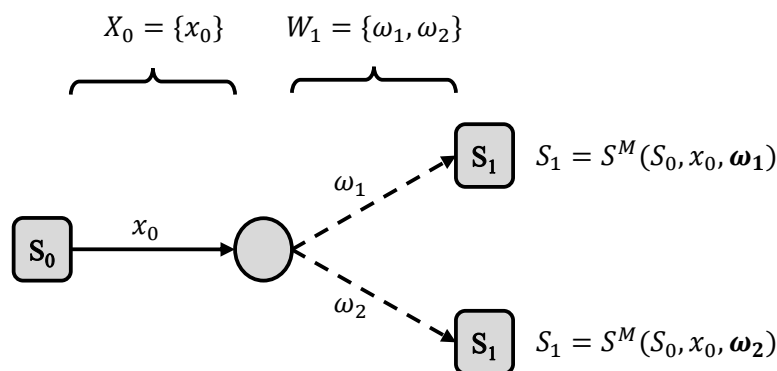


Figure A.3: Generic decision tree for the transition from state S_0 to next period's states S_1 . Squares are decision nodes, circles are outcome nodes, solid lines are decisions, and dashed lines are (uncertain) outcomes.

transition function $S^M(S_t, x_t, W_{t+1})$, i.e., $S_{t+1} = S^M(\cdot)$. The transition depends on the current state S_t , the decision x_t , and the (uncertain) information W_{t+1} . This transition process is also referred to as ‘model’, which is why S^M is attached with superscript ‘M’. Figure A.3 shows the generic decision tree for the transition from state S_0 to state S_1 , assuming one possible decision ($X_0 = \{x_0\}$) and two (uncertain) information outcomes ($W_1 = \{\omega_1, \omega_2\}$). A larger version of such a generic decision tree can be found in Powell (2011, p. 130).

Policies are used to describe sets of decisions in such sequential decision processes. More precisely, a policy comprises a decision in each state, i.e., a specific policy π can be seen as a function $X^\pi(S_t)$, referred to as decision function, that returns a decision x_t for the state S_t under policy π . An optimal policy π^* maximizes the expected contribution over all periods and is selected from the set of all possible policies Π . Formula (A.1) states the selection of such an optimal policy by looking at the expected contribution over all periods.

$$\pi^* = \sup_{\pi \in \Pi} \mathbb{E} \sum_{t=0}^T \gamma \cdot C(S_t, x_t) \quad (\text{A.1})$$

Discount factor γ is used to incorporate contributions from decisions in different points in time and the expectation \mathbb{E} is used because the contribution implicitly depends on uncertain information W_t . In particular, contribution $C(\cdot)$ in period t depends on the policy’s decision $x_t = X^\pi(S_t)$ as well as the current state S_t , which is calculated from the transition function, i.e., $S_t = S^M(S_{t-1}, x_{t-1}, W_t)$. For the experiments in this tutorial, the discount factor is set to $\gamma = 0.8$ in each period t . The optimal decisions $X^{\pi^*}(S_t)$ that are embedded in an optimal policy π^* can be calculated with the Bellman equation, which is described in the following section.

A.4.2 Bellman equation

The Bellman equation essentially calculates the value $V_t(S_t)$ of a state S_t in period t , assuming that decisions with the highest expected value are selected in each state (Bellman; 1957). More precisely, the value of a decision $x_t \in X_t$ in state S_t is calculated by (i) the decision’s immediate contribution $C(S_t, x_t)$ and (ii) the discounted value $V_{t+1}(S_{t+1})$ of next period’s state S_{t+1} . Formula (A.2) shows the Bellman equation in its expectation form, assuming that information W_t is known in period t and unknown for periods $t' > t$. Thus, the contribution $C(S_t, x_t)$ is deterministic and the value of future states $V_{t+1}(S_{t+1})$ is stochastic. This stochasticity results from transition function $S^M(\cdot)$ in which the current state S_t and decision x_t are deterministic and information W_{t+1} is uncertain. An

equivalent formulation of the Bellman equation uses the so-called one-step probability $p(s'|S_t, x_t)$, see Formula (A.3). The one-step probability describes the probability to transit to state s' , if decision x_t is taken in state S_t .

$$V_t(S_t) = \max_{x_t \in \bar{X}_t} (C(S_t, x_t) + \gamma \cdot \mathbb{E}\{V_{t+1}(S_{t+1})\}) \quad (\text{A.2})$$

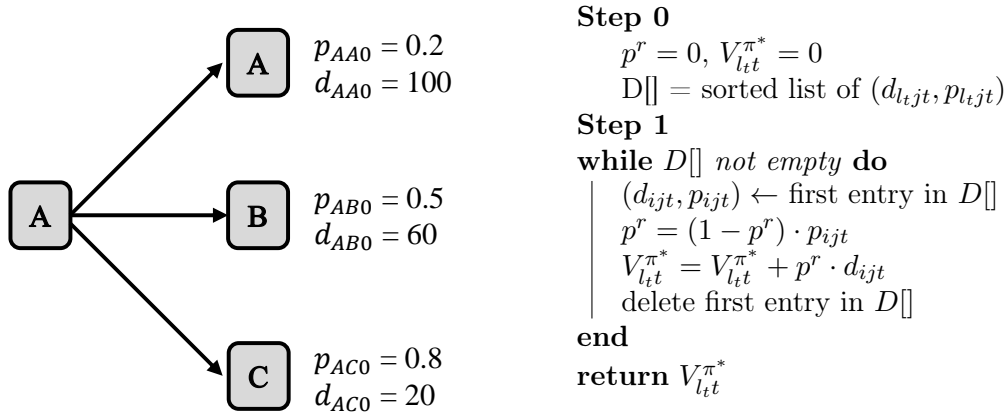
$$V_t(S_t) = \max_{x_t \in \bar{X}_t} \left(C(S_t, x_t) + \gamma \cdot \sum_{s' \in S} p(s'|S_t, x_t) V_{t+1}(s') \right) \quad (\text{A.3})$$

The Bellman equation is recursive, i.e., $V_t(\cdot)$ is calculated from $V_{t+1}(\cdot)$, which in turn is calculated from $V_{t+2}(\cdot)$, and so on. Backward dynamic programming can be used to find optimal solutions. For problem with finite time horizons, the expected value of states beyond T are simply set to 0, i.e., $\mathbb{E}\{V_{T+1}(S_{T+1})\} = 0$. Problems with infinite time horizons can, for example, be approached backwardly and dynamically by looking at the states' values they converge to. A generic backward dynamic algorithm for problems with a finite time horizon is provided in Appendix B.

A.4.3 Optimal policy for the taxicab problem

For the taxicab problem, a policy describes how the vehicle moves in each state and an optimal policy has the highest expected value among all available policies. The (expected)

- (a) Illustrative example with three nodes. (b) Expected value $V_{l_t}^{\pi^*}$ of the optimal policy π^* for being in l_t in period t .



Step 0

$$p^r = 0, V_{l_t}^{\pi^*} = 0$$

$D[]$ = sorted list of $(d_{l_t j_t}, p_{l_t j_t})$

Step 1

while $D[]$ *not empty* **do**

$(d_{i_j t}, p_{i_j t}) \leftarrow$ first entry in $D[]$

$$p^r = (1 - p^r) \cdot p_{i_j t}$$

$$V_{l_t}^{\pi^*} = V_{l_t}^{\pi^*} + p^r \cdot d_{i_j t}$$

 delete first entry in $D[]$

end

return $V_{l_t}^{\pi^*}$

Figure A.4: Illustrative example and algorithm for calculating the expected value of the optimal policy.

value of such optimal policy should not be confused with the (expected) value of a single optimal decision, which, for example, is often used in classical decision tree analyses. An illustrative example is used to demonstrate the differences. Figure A.4a shows the case of two periods (0 and 1) and three decisions (A, B, and C). The expected value of a *single decision* is calculated by multiplying a decision's demand (d_{ijt}) with its probability (p_{ijt}), resulting in values of 20, 30, and 16 for decisions A, B, and C, respectively. In contrast, the expected value of the optimal *decision policy* is calculated by considering the optimal decision under each possible demand-combination. In particular, the highest possible demand is considered with the corresponding probability, the second highest demand is considered with one minus the sum of all previously considered probabilities multiplied with its probability, and so on (Mes and Rivera; 2017). The algorithm in Figure A.4b describes this procedure in which 'rolling probability' p^r is used to calculate the expected value $V_{l_t}^{\pi^*}$ of optimal policy π^* for being in location l_t in period t . For the illustrative example from Figure A.4a, the value of the optimal policy is 50.4 (if demand in A, go to A; if no demand in A but demand in B, go to B; if no demand in A or B, go to C). For problems with $T > 1$, a decision's downstream value needs to be considered in addition to its immediate reward, i.e., the initialization of $D[]$ in Step 0 uses $(d_{l_t j t} + V_{j, t+1}^{\pi^*}, p_{l_t j t})$ for all periods $t < T$. It further requires a consideration of constellations in which the immediate reward is 0, i.e., $D[]$ includes $(d_{l_t j t} + V_{j, t+1}^{\pi^*}, p_{l_t j t})$ as well as $(0 + V_{j, t+1}^{\pi^*}, 1)$. The probability of '1' for values with no immediate reward lets the algorithm de facto terminate once such value is considered for the first time. Appendix C illustrates the optimal policy for an instance with three nodes and three periods. This instance is also used in the step-by-step application of VFA that is provided at the end of the next section.

A.5 Value Function Approximation

This section outlines VFA's main principles using the previously introduced notation. Section A.5.1 motivates the use of VFA by shortly discussing the three curses of dimensionality. Then, Section A.5.2 introduces a basic VFA algorithm and Section A.5.3 describes the concept of post-decision states. Section A.5.4 provides a step-by-step application of VFA to a small-scale instance of the taxicab problem. In this tutorial, the expected value of the initial state is used as the main measure for evaluating VFA's performance. Its value is calculated from a full backward investigation of the decision tree, applying the optimal policy to each location-period combination.

A.5.1 Motivation and VFA's main principles

Large MDPs are usually intractable to be solved recursively with the Bellman equation. Powell (2011) describes three reasons for this and refers to them as the three curses of dimensionality. The three dimensions are: the state space S_t , covering all sorts of information in a given period, the decision space X_t , covering all possible decisions in a given period, and, the outcome space W_t , covering all (stochastic) possibilities to transfer from one period to another. VFA is a heuristic applied to problems in which the optimal solution cannot be calculated within a reasonable computation time due to their 'high dimensionality', i.e., it provides a mean to deal with the three curses of dimensionality. Thereby, VFA algorithms follow two central principles (Powell; 2009): (i) they *step forward* in time and (ii) they *estimate* the expected value of (all) future states, which is also referred to as downstream value/costs, cost-to-go, or reward-to-go. The second principle is the source of VFA's name as it is of particular interest to find good functions for approximating states' future values. Traditionally, VFA algorithms follow a pure forward programming approach and select the decision that leads to the highest value in each period, considering both, the decision's immediate (deterministic) reward as well as its estimated reward-to-go. The paradigm of stepping forward in time makes it unnecessary to perform a full backward investigation of the decision tree, leading to a manageable computation time of the VFA algorithm.

A.5.2 Basic VFA algorithm

Following these main principles, it is essentially the task of VFA to find good approximations for the values of downstream states. This is done by approaching the problem in N iterations in which each iteration $n = \{1, \dots, N\}$ uses a sample $\omega^n \in \Omega$ of the uncertain information, i.e., $W_t \leftarrow \omega^n, \forall t = \{1, \dots, T\}$. In each iteration n , the algorithm steps forward in time and selects for state S_t^n the decision \hat{x}_t^n with the highest expected value \hat{v}_t^n , using Formulas (A.4) and (A.5), respectively. These formulations are similar to the Bellman equation but there is one main difference. While the contribution $C(S_t^n, x_t)$ is still deterministic and results from the decision, the expected downstream value $\mathbb{E}\{V_{t+1}(\cdot)\}$ is now replaced by its previous iteration's approximated but deterministic estimate $\bar{V}_{t+1}^{n-1}(\cdot)$.

$$\hat{x}_t = \arg \max_{x_t \in X_t} \left(\underbrace{C(S_t^n, x_t)}_{\text{deterministic}} + \gamma \cdot \underbrace{\bar{V}_{t+1}^{n-1}(S_{t+1}^n)}_{\text{approximated}} \right) \quad (\text{A.4})$$

Step 0
initialize:

 Choose an initial state S_0^1

 Choose an initial approximation for $\bar{V}_t^0(S_t)$ for all states S_t
Step 1
for $n = 1, 2, 3, \dots, N$ **do**
Step 1a

 choose a sample path $\omega^n \in \Omega$
for $t = 0, 1, 2, \dots, T$ **do**
Step 1b
 \hat{x}_t^n using Formula (A.4)

 \hat{v}_t^n using Formula (A.5)

Step 1c
 $\bar{V}_t^n(S_t) = U^V(\cdot)$ using \hat{v}_t^n
 $S_{t+1}^n = S^M(S_t^n, \hat{x}_t^n, W_{t+1})$
end
end

Algorithm 3: Basic VFA algorithm with a pure forward pass.

$$\hat{v}_t^n = \max_{x_t \in X_t} \left(\underbrace{C(S_t^n, x_t)}_{\text{deterministic}} + \gamma \cdot \underbrace{\bar{V}_{t+1}^{n-1}(S_{t+1}^n)}_{\text{approximated}} \right) \quad (\text{A.5})$$

This approximation, which is an estimation of the state's downstream value, is updated after each iteration using a so-called update function $U^V(\cdot)$, i.e., $\bar{V}_t^n(S_t^n) = U^V(\cdot)$. The update function is also referred to as approximation function and uses several parameters as inputs. This tutorial uses a simple (yet effective) updating function based on lookup-tables. Here, $\bar{V}_t^n(S_t^n)$ is estimated from its previous iteration's value $\bar{V}_t^{n-1}(S_t^n)$ as well as the value \hat{v}_t^n that results from decision \hat{x}_t^n , taken in state S_t^n for iteration n . The parameter α , also referred to as stepsize or learning rate, is used to weight these inputs, see Formula (A.6). For other variants of the update functions it is referred to George and Powell (2006), George et al. (2008), and Powell (2011, 2009).

$$\bar{V}_t^n(S_t^n) = U^V(\bar{V}_t^{n-1}(S_t^n), \hat{v}_t^n) = (1 - \alpha) \cdot \bar{V}_t^{n-1}(S_t^n) + \alpha \cdot \hat{v}_t^n \quad (\text{A.6})$$

Algorithm 3 describes a basic VFA algorithm with a pure forward pass (Powell; 2009).

In Step 0, the initial state and the initial approximations of the states' downstream values are chosen. Throughout this tutorial, initial states' approximations are set to $\bar{V}_t^0(S_t^0) = 0, \forall t \in \mathcal{T}$. Step 1 describes the forward programming of the algorithm. Step 1a chooses a sample path that could also be replaced by real-world observations, Step 1b calculates the optimal decision and its value with Formulas (A.4) and (A.5), respectively, and Step 1c updates the expected downstream values and uses transition function $S^M(\cdot)$ to select the state of the next period. The algorithm terminates after the preset number of iterations (N). Note that, in this algorithm, a full forward investigation over all periods T is done for each iteration. This might not be required for some problems, e.g., if there is a high discount factor, it might be reasonable to consider the value only of some future periods, resulting in a reduced computational demand per iteration.

A.5.3 Post-decision states

So far, states, decisions, and uncertain information have been stated as discrete sets, an intuitive and easy way to outline a problem. However, if the uncertain information is a (multidimensional) vector, which is usually the case for real-world applications, it is much harder to determine optimal solutions due to the sheer number of potential outcomes (and states). This is the reason why the concept of post-decision states is often used in the context of VFA (Ruszczynski; 2010; Powell; 2011). A post-decision state describes the status of a state right after a decision is taken but before receiving any new (uncertain) information W_{t+1} . In decision trees, decision nodes represent pre-decision states and outcome nodes represent post-decision states, see Figure A.3. More formal, a post-decision state S_t^x results from transition function $S^{M,x}(S_t, x_t)$, which, in contrast to transition function $S^M(\cdot)$ from Section A.4.1, only considers decision x_t and pre-decision state S_t . Thus, it does not consider uncertain information W_{t+1} and solely depends on deterministic inputs. Now, the idea is to estimate the downstream values of current period's post-decision states in place of downstream values of next period's pre-decision states. In particular, $\bar{V}_t^{x,n-1}(S_t^{x,n})$ replaces $\bar{V}_{t+1}^{n-1}(S_{t+1}^n)$ in Formulas (A.4) and (A.5) to determine the optimal decision \hat{x}_t^n and its value \hat{v}_t^n in state S_t^n for iteration n , respectively. By using current period's post-decision state $S_t^{x,n}$ instead of next period's pre-decision state S_{t+1}^n , it is unnecessary to fully evaluate the often large and multidimensional outcome and state space. The concept of post-decision states is also applied in the following example.

A.5.4 Step-by-step application

This section applies VFA to a small-scale instance with three locations (A, B, and C) and three periods (0, 1, and 2). The vehicle's starting point in period $t = 0$ is $l_0 = A$. Table A.2 shows the corresponding probability and demand for each location-period combination. The decision tree for this problem is shown in Appendix C. Applying the general definition of states to the taxicab problem already leads to a relatively large state space. More precisely, each demand-constellation depicts a new state, resulting in 2^3 combinations per period and per location. The concept of post-decision states is used to reduce the number of required approximations per (post-decision) state. In post-decision states, all random information is excluded, leading to one post-decision state S_t^x per location-period combination. This reduces the size of the problem and, with this, also the computational demand of the VFA algorithm. Note that, in this view, even our initial state is a kind of post-decision state although it does not result from a decision. The reason is that its demand is not known in our setup. If, for example, initial period's demand is known, the optimal decision simply results from the demand and the corresponding (estimated) downstream value. These estimates are calculated in the same way as described in the remainder of this section. In the following, states consistently refer to post-decision states and prefix 'post-decision' is omitted for reasons of readability.

Remember that the VFA algorithm draws a sample path of each period's demand at the beginning of each iteration. Table A.3 shows the realization of the samples (random numbers) that are used in VFA's first two iterations. For example, demand between locations A and B in period $t = 0$ is 0 for iteration $n = 1$ ($p_{AB0} = 0.62 < 0.63$) and 52 for iteration $n = 2$ ($p_{AB0} = 0.62 > 0.57$). The table shows that it is not required to

Table A.2: Probability and demand of the example.

i	j	$t = 0$		$t = 1$		$t = 2$	
		p_{ijt}	d_{ijt}	p_{ijt}	d_{ijt}	p_{ijt}	d_{ijt}
A	A	0.49	98	0.53	6	0.33	66
A	B	0.62	52	1.00	39	0.61	46
A	C	0.74	28	0.64	18	0.36	18
B	A	0.96	13	0.79	33	0.68	91
B	B	0.77	19	0.39	13	0.93	10
B	C	0.87	43	0.60	72	0.12	46
C	A	0.55	41	0.78	82	0.26	71
C	B	0.61	57	0.66	34	0.07	71
C	C	0.01	12	0.92	52	0.90	86

Table A.3: Sample realizations (random numbers) used in the first two VFA iterations.

i	j	n = 1			n = 2		
		t = 0	t = 1	t = 2	t = 0	t = 1	t = 2
A	A	0.78	-	-	0.69	-	0.38
A	B	0.63	-	-	0.57	-	0.7
A	C	0.42	-	-	0.11	-	0.37
B	A	-	-	-	-	0.4	-
B	B	-	-	-	-	0.65	-
B	C	-	-	-	-	0.62	-
C	A	-	0.93	0.24	-	-	-
C	B	-	0.41	0.72	-	-	-
C	C	-	0.90	0.28	-	-	-

draw sample realizations for all (post-decision) states, i.e., it is not necessary to span the whole outcome and state space. This is because random outcomes are only sampled for the visited states due to VFA's forward decisions. The following step-by-step application demonstrates this using a fixed stepsize of $\alpha = 0.02$.

Iteration 1

The initial state is described by the vehicle's location $l_t = A$ in period $t = 0$. The available decisions consist of moving to any of the three locations. The optimal decisions in periods 0, 1, and 2 are $\hat{x}_0^1 = C$, $\hat{x}_1^1 = C$, and $\hat{x}_2^1 = C$ and result from choosing the move with the highest (expected) value. Formulas (A.4) and (A.5) in Section A.5 generally state how to calculate the decision and its value, respectively. Formulas (A.7) to (A.9) apply them to the example problem. In the first iteration, the downstream value of all states is zero as this is their initial value, making the decision solely depending on the (sampled) demand. These samples are only required for states that are actually visited, which is why Table A.3 only reports those probabilities that are actually required by the algorithm. This forward approach investigates the value of three states (one per period) per iteration and, eventually, it does not require a full investigation of all states, which is required in the optimal backward dynamic approach.

$$\hat{v}_0^1 = \max\left\{\underbrace{\left(\underbrace{0 \cdot 98}_{\text{demand real.}} + \gamma \cdot \underbrace{0}_{\bar{V}_1^0(S_1^{x,0}|l_1=A)}\right)}_{\hat{x}_0^1=A}, \underbrace{(0 \cdot 52 + \gamma \cdot 0)}_{\hat{x}_0^1=B}, \underbrace{(1 \cdot 28 + \gamma \cdot 0)}_{\hat{x}_0^1=C}\right\} = 28 \quad (\text{A.7})$$

Table A.4: Approximation of the states' downstream values \bar{V}_t^n .

	$n = 1$			$n = 2$			$n = 500$		
	state's location			state's location			state's location		
	A	B	C	A	B	C	A	B	C
t = 0	0.56	-	-	1.59	-	-	144.84	-	-
t = 1	0	0	1.04	0	0.66	1.04	93.28	96.97	30.10
t = 2	0	0	1.72	0	0	1.72	23.80	66.79	72.35

$$\hat{v}_1^1 = \max\{(0 \cdot 82 + \gamma \cdot 0), (1 \cdot 34 + \gamma \cdot 0), (1 \cdot 52 + \gamma \cdot 0)\} = 52 \quad (\text{A.8})$$

$$\hat{v}_2^1 = \max\{(1 \cdot 71), (0 \cdot 71), (1 \cdot 86)\} = 86 \quad (\text{A.9})$$

The estimated downstream values are updated retrospectively after each move, i.e., for being in locations A, C, and C in periods 0, 1, and 2. The calculation is shown in Formulas (A.10) to (A.12) and these values are also shown in Table A.4. The general form of the update function is given by Formula (A.6) in Section A.6.

$$\bar{V}_0^1(S_0^{x,0} | l_0 = A) = (1 - \alpha) \cdot \underbrace{0}_{\bar{V}_0^0} + \alpha \cdot \underbrace{28}_{\hat{v}_0^1} = 0.56 \quad (\text{A.10})$$

$$\bar{V}_1^1(S_1^{x,0} | l_1 = C) = (1 - \alpha) \cdot 0 + \alpha \cdot 52 = 1.04 \quad (\text{A.11})$$

$$\bar{V}_2^1(S_2^{x,0} | l_2 = C) = (1 - \alpha) \cdot 0 + \alpha \cdot 86 = 1.72 \quad (\text{A.12})$$

Iteration 2

The optimal decisions in periods 0, 1, and 2 are $\hat{x}_0^2 = B$, $\hat{x}_1^2 = A$, and $\hat{x}_2^2 = A$ and result from choosing the move with the highest (expected) value, see Formulas (A.13) to (A.15). Decision \hat{x}_2^2 is not distinct as all moves result in the same value (0) and it is then assumed that the vehicle remains at its current location.

$$\hat{v}_0^2 = \max\{(0 \cdot 98 + \gamma \cdot 0), (1 \cdot 52 + \gamma \cdot 0), (1 \cdot 28 + \gamma \cdot 0.56)\} = 52 \quad (\text{A.13})$$

$$\hat{v}_1^2 = \max\{(1 \cdot 33 + \gamma \cdot 0), (0 \cdot 13 + \gamma \cdot 0), (0 \cdot 72 + \gamma \cdot 0)\} = 33 \quad (\text{A.14})$$

$$\hat{v}_2^2 = \max\{(0 \cdot 66), (0 \cdot 46), (0 \cdot 18)\} = 0 \quad (\text{A.15})$$

The estimated downstream values are updated retrospectively for being in locations A, B, and A in periods 0, 1, and 2 by Formulas (A.16) to (A.18), respectively. These values are also shown in Table A.4.

$$\bar{V}_0^2(S_0^1 | l_0 = A) = (1 - \alpha) \cdot 0.56 + \alpha \cdot 52 = 1.59 \quad (\text{A.16})$$

$$\bar{V}_1^2(S_1^1 | l_1 = B) = (1 - \alpha) \cdot 0 + \alpha \cdot 33 = 0.66 \quad (\text{A.17})$$

$$\bar{V}_2^2(S_2^1 | l_2 = A) = (1 - \alpha) \cdot 0 + \alpha \cdot 0 = 0 \quad (\text{A.18})$$

It can be seen that the approximation of the expected value of the initial state increases in the first two iterations and, with more iterations, it eventually converges to its optimum. For example, after 500 iterations, it is 144.84 (see Table A.4) and only 4.87 (3.25%) below its true value that is 149.71. A detailed description of using backward dynamic programming to calculate the true value for this problem is provided in Appendix C.

Figure A.5 shows how VFA's approximation of the initial state's downstream value \bar{V}_0^n (vertical axis) evolves over $N = 1,500$ iterations (horizontal axis) for three exemplary instances. The true values are depicted as horizontal lines. The smallest instance ($V=3$, $T=3$) is the example from the step-by-step calculation and the only one for which the initial state's estimate comes close to its true value. More precisely, it reaches this value (149.71) after about 500 iterations and varies around it afterwards. In contrast, both of the larger instances are still far off their true values even after 1,500 iterations which is very large considering the size of the instances. More realistically, only a fraction of the size of the state space is reasonable for real-world applications (Mes and Rivera; 2017). Therefore, the next section discusses VFA enhancements highlighting two common challenges in applying the algorithm. Together, the enhancements improve the performance for all three instances significantly.

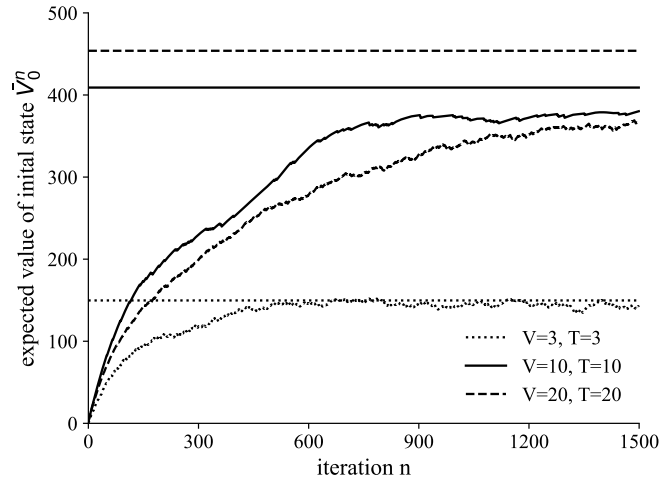


Figure A.5: Results for three instances using the basic VFA algorithm.

A.6 More about VFA

This section discusses additional topics of VFA. It starts by considering two enhancements to the basic VFA algorithm: Section A.6.1 considers an alternative way of calculating the stepsize and Section A.6.2 enhances the VFA algorithm by a greedy exploration strategy. It is shown that the collective application of both modifications to the considered problem enables the algorithm to approximate an initial state’s value that is close to its true value already after a low number of iterations. For the analyses, the instance with 10 nodes and 10 periods is used as its size allows a graphical depiction of the full (post-decision) state space that is helpful in understanding the enhancements. Finally, Section A.6.3 concludes with a discussion on tuning the newly introduced parameters and shows some results regarding the runtime.

A.6.1 Harmonic stepsize

The stepsize is a powerful parameter as it decides how estimates are updated after each iteration. So far, a fixed stepsize (FS) has been used with a rather low value of $\alpha = 0.02$, resulting in a well-balanced continual update of the estimates without any ‘jumps’ or the like as shown in Figure A.5. A harmonic stepsize (HS) can be used to assign a higher weight to earlier visits and limiting the impact of later visits (George and Powell; 2006; Powell; 2011). Formula (A.19) shows the variant of the HS that is used in this paper. Here, a is a constant parameter to adjust the convergence of the HS and $N_{S_t^{x,n}}$ describes

the number of visits, i.e., how often state $S_t^{x,n}$ has been visited after iteration n .

$$\alpha(N_{S_t^{x,n}}) = \frac{a}{a + N_{S_t^{x,n}}} \quad (\text{A.19})$$

Figure A.6 shows the initial state's value for the instance with 10 nodes and 10 periods. Here, the black solid line shows the so-far used VFA with a FS and parameter $\alpha = 0.02$ and the black dashed line shows the results for VFA with a HS and parameter $a = 10$. The blue lines are explained in the next section. The optimal value of 409.0 of this instance is once again demonstrated with a horizontal line. It can be seen that the results with the HS are volatile for a low number of iterations and converge later on. In particular, values at around 300 are obtained already after a few iterations but also remain at this level with more iterations. Thus, estimates with the HS converge to a value that is even below the estimates resulting from the FS (black solid line), showing that solely using a HS in our setting does not improve our VFA. This is because some states' downstream values have not been explored, i.e., some states have not been, or at least have not been often enough, visited in the algorithm. One reason for this is that initial estimates of the states are poor and another reason is that VFA's forward decisions have a general bias towards already visited states (this is particularly true here as the HS emphasizes early visits), because these states might already have a better value. Eventually, this can result in not exploring the optimal path as it is so-far the case for the considered instance. This issue is referred to as the 'exploration vs. exploitation' trade-off and further discussed in

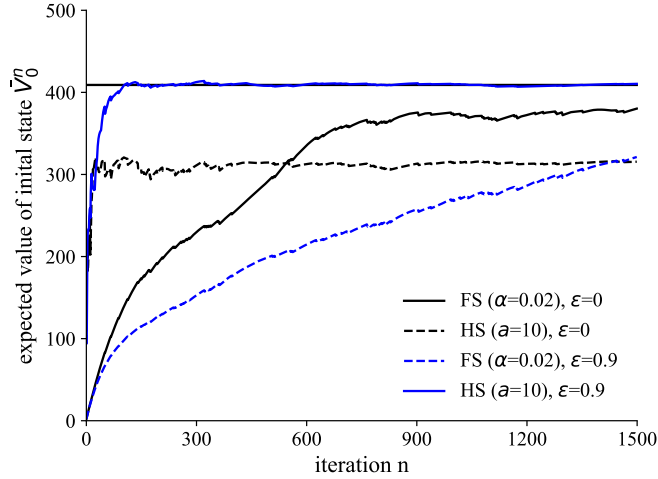


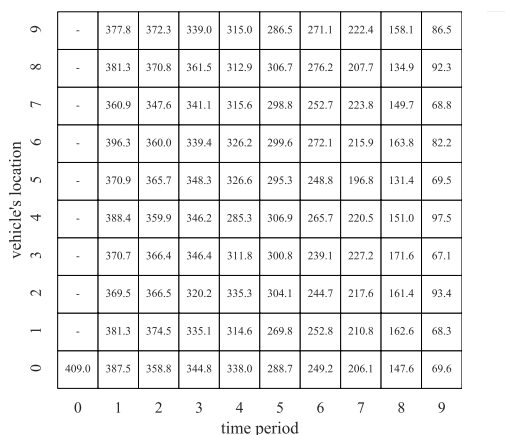
Figure A.6: Results using different stepsizes and a greedy exploration strategy (instance $V = T = 10$).

the following section.

A.6.2 Exploration strategy

The exploration of the state space is illustrated in Figure A.7. Here, the periods are depicted on the horizontal axis (0 to 9) and the vehicle’s potential locations on the vertical axis (0 to 9). In our setting, a state refers to the position of the vehicle in a period, i.e., the two axes span the problems full state space that is shown as a matrix. The values in the figure are the downstream values per state for the instance with 10 nodes and 10 periods. Figure A.7a shows the values obtained from backward programming (true values) and Figure A.7b the values from the VFA algorithm (approximated values) with a HS ($a = 10$) after $N = 1,500$ iterations. A comparison between the values shown in Figures A.7a and A.7b reveals that most states have a very poor estimate, while a few estimates in the last period are relatively close to the their actual values (e.g., the true value of 67.1 for being in period 9 in location 3 is estimated with 67.5). However, the VFA results are clearly unsatisfactory when looking at the initial state (shown at the bottom left corner of the matrix), reaching a value of only 315.5 that is far off its true value of 409.0. Furthermore, some states in Figure A.7b are still at their initial value of 0 after 1,500 iterations, indicating that these states have not been visited at all while processing the algorithm. For example, in period 1, the vehicle moves to location 6 in each of the 1,500 iterations, resulting in initial estimates of 0 for all other locations.

(a) Values from backward dynamic programming.



(b) VFA values: HS ($a = 10$).

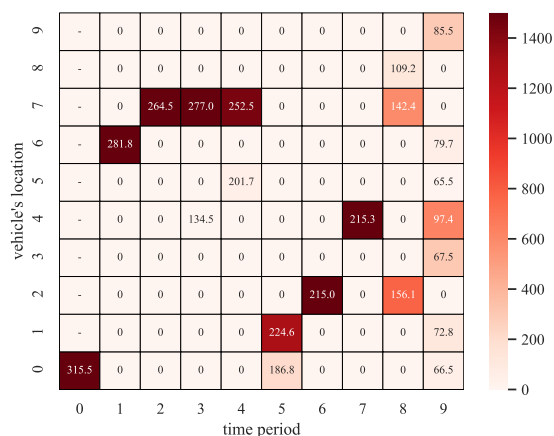


Figure A.7: Analyzing states’ downstream values under backward dynamic programming and VFA with a harmonic stepsize (instance $V = 10$, $T = 10$).

Thus, even with a considerably large number of iterations, the values of some states have not been explored as they are not visited by the algorithm and, eventually, this makes VFA missing the optimal path. To emphasize this, the color in Figure A.7b indicates the relative frequency of the number of visits per state. For example, being in location 0 in period 0 (bottom left corner) has a dark red color as it is the initial state and has been visited in all of the 1,500 iterations and, contrary, states with estimates of 0 have a light red color as they have not been visited at all. With this, it is easy to see that VFA with a HS leads to an unbalanced exploration of states, which, consequently, also leads to poor estimates of the states' downstream values.

To reduce this bias, VFA algorithms can be enhanced by methods that force the exploration of states, e.g., by randomly selecting decisions that lead to states with less promising downstream estimates. However, given preset limits on the total computation time or the number of iterations N , this constitutes a trade-off between *exploring* the value of more states and *exploiting* the value of states that appear to be more promising. A greedy-policy is used to demonstrate the idea of exploring more states. In particular, this strategy uses a parameter ϵ that describes the percentage in which a random move (\tilde{x}_t^n) is carried out instead of the move that appears to be more promising (\hat{x}_t^n). The value of the originating state is updated only if the random move \tilde{x}_t^n turns out to be better than \hat{x}_t^n . The algorithm for the greedy strategy is shown in Appendix B. Figure A.6 shows that this strategy with a high ϵ -value of 0.9 alone does not lead to better results, i.e., the blue dashed line from the greedy strategy is even below the lines resulting from the

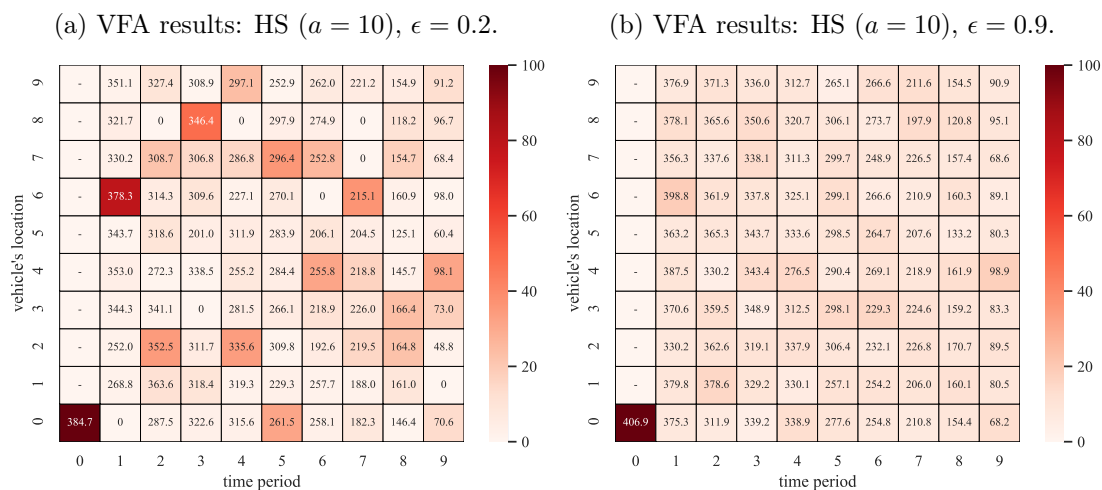


Figure A.8: Analyzing states' downstream values using an exploration strategy (instance $V = 10$, $T = 10$).

FS/HS algorithm without random moves. However, if it is applied in combination with a harmonic stepsize ($a = 10$, $\epsilon = 0.9$), good results are achieved after a small number of iterations (see blue solid line in the figure). Figures A.8a and A.8b illustrate how the greedy strategy explores more states by showing results for setting parameter ϵ to 0.2 and 0.9, respectively, in a VFA algorithm with a HS and $a = 10$. The setup of the figures is just like for Figure A.7b but, now, results are shown after already 100 iterations. For both strategies, the estimates for the states are much better compared to the non-greedy case in Figure A.7b, although, the algorithm is processed with such a low number of iterations. Furthermore, as expected, a higher ϵ -value leads to a more balanced number of visits per state, which is apparent as all states in Figure A.8b have a similar color. For VFA with a HS ($a = 10$) and a high emphasis on exploring new states ($\epsilon = 0.9$), the estimated value of the initial state after 100 iterations is 406.9 and very close to its true expected value of 409.0.

A.6.3 Parameter tuning and runtime analysis

The previous experiments have shown that the a -parameter, used in the updating function with a harmonic stepsize, and the ϵ -parameter, used in the greedy exploration strategy, are two integral ways for improving the performance of VFA algorithms. Figure

(a) Optimality gap using different HS- and greedy-parameter combinations. (b) Computation time saving from solving instances with VFA instead of backwardly and dynamically.

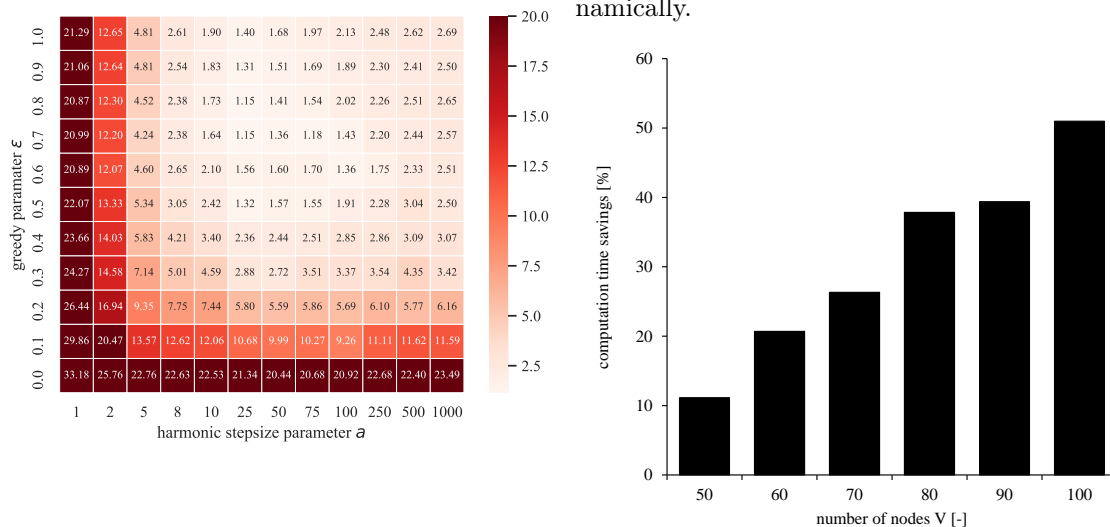


Figure A.9: Tuning VFA parameters and analyzing computation time savings.

A.9a illustrates how the tuning of these parameters impacts the performance. For this, the optimality gap of 10 random instances à 10 nodes and 10 periods ($V = T = 10$) are averaged and used as a performance measure. It can be seen that, for this problem type and size, the optimal combination of HS's a -parameter (x-axis) and greedy's ϵ -parameter (y-axis) is at about values of 25 and 0.8, respectively. Thus, a too-low or too-high value for either one of them is not optimal and the exact tuning requires a good understanding of the problem at hand often gained in preliminary experiments.

Finally, Figure A.9b shows the computation time saving (in %) for solving instances with VFA instead of solving them backwardly and dynamically. Results are shown as averages over 20 random instances for a varying number of nodes of $V = \{50, 60, \dots, 100\}$ in a setting with $T = 20$ periods. For VFA's computation time, the HS is used with $a = 25$, the greedy exploration strategy is used with $\epsilon = 0.8$, and the number of iterations N is dynamic as the algorithm is forced to iterate until the optimality gap drops below 5% (N is usually between 100 and 150). The figure shows that the computational performance of the VFA algorithm is better compared to the backward dynamic approach that is used to find the optimal policy. For example, for the largest instances with 100 nodes, the VFA solution is obtained on average twice as fast compared to the optimal solution approach. Clearly, this computation time savings are strongly affected by the problem size as well as the VFA implementation used to fit approximations. Nevertheless, they show the clear benefit of using VFA in settings in which it is computationally expensive to find the optimal solution.

A.7 Conclusion

This paper has provided a tutorial on value function approximation in stochastic and dynamic transportation. It has been designed to be a starting point for readers from various fields and disciplines and for readers with a diverse familiarity with algorithms and operations research methods. For this, the tutorial has covered the following contents.

First, it has discussed application cases of VFA in the context of stochastic and dynamic transportation. Problems of this kind might be modeled as sequential decision processes, for which the tutorial has explained relevant concepts, such as Markov Decision Processes and the Bellman equation. The description and discussion has been general to emphasize that VFA can be applied also to problems not related to transportation.

Second, the tutorial has followed a hands-on approach in which VFA has been applied to artificial instances of a variant of the well-known but easy-to-understand taxicab

problem. Results for the taxicab problem have been presented in two ways: (i) step-by-step results have been shown for a small-scale instance, making it possible to experience VFA's basic principles in action and to gain an understanding and intuition of them and (ii) comprehensive results have been shown for larger instances, demonstrating VFA's general capability of solving larger and more complex problems.

Third, the tutorial has covered two ways for enhancing the basic VFA algorithm to obtain improved results for the considered taxicab problem: a harmonic stepsize and a greedy exploration strategy. Results from these enhancements have been shown and discussed for a large but tangible problem instance.

Future introductory papers on VFA might present additional insights on how to fit approximations, using more advanced methods like hierarchical aggregation or basis functions. In addition to that, it might be interesting to apply VFA to problems in other fields, such as inventory problems or budgeting problems, and to use real-world data instead of (or in addition to) artificial instances.

Acknowledgments

The research leading to this tutorial received funding from the German Research Foundation (DFG) under reference 268276815.

A.8 Appendix A. Python scripts

The Python scripts with the implementations of the two solution approaches (backward dynamic programming, VFA) are available as additional files in the electronic appendix of this paper. These scripts can be used to reproduce results from the experimental study. All data and material is also available from the corresponding author on request.

A.9 Appendix B. Additional algorithms

This section describes two algorithms: first, Algorithm 4 provides a generic description of how to solve the Bellman equation backwardly and dynamically and, second, Algorithm 5 extends the general VFA algorithm (see Algorithm 3 in Section A.5) with a greedy exploration strategy.

Step 0

initialize:

$V(S_t) = 0$ for all states S_t

$t = T$

Step 1

while $t \geq 0$ **do**

foreach $S_t \in S$ **do**

solve:

$V(S_t)$ using Formulas (A.2) or (A.3)

end

$t = t - 1$;

end

Algorithm 4: Backward dynamic algorithm to solve the Bellman equation.

Step 0

initialize:

Choose an initial state S_0^1

Choose an initial approximation for $\bar{V}_t^0(S_t)$ for all states S_t

Step 1

for $n = 1, 2, 3, \dots, N$ **do**

Step 1a

choose a sample path $\omega^n \in \Omega$

for $t = 0, 1, 2, \dots, T$ **do**

Step 1b

if ϵ -step **then**

draw random move \tilde{x}_t^n

\tilde{v}_t^n for \tilde{x}_t^n using Formula (A.5)

if $\tilde{v}_t^n > \bar{V}_t^{n-1}(S_t)$ **then**

| $\bar{V}_t^n(S_t) = U^V(\cdot)$ using \tilde{v}_t^n

end

$S_{t+1}^n = S^M(S_t^n, \tilde{x}_t^n, W_{t+1})$

else

\hat{x}_t^n using Formula (A.4)

\hat{v}_t^n using Formula (A.5)

$\bar{V}_t^n(S_t) = U^V(\cdot)$ using \hat{v}_t^n

$S_{t+1}^n = S^M(S_t^n, \hat{x}_t^n, W_{t+1})$

end

end

end

Algorithm 5: VFA with a greedy strategy.

A.10 Appendix C. Optimal policy in a small-scale example

This section provides details on the optimal policy of the small-scale example used in Section A.5. Figure A.10 shows the decision tree. Notice that the decision tree consists of repetitive sub-problems. For example, being in $t = 2$ in node A appears three times in the decision tree: (i) if $x_0 = A$ and $x_1 = A$, (ii) if $x_0 = B$ and $x_1 = A$, and (iii) if $x_0 = C$ and $x_1 = A$. In backward dynamic programming, values of sub-problems are memoized once they are calculated for the first time, which reduces the total computation time. In the decision tree, values atop of the nodes correspond to expected values following an optimal policy. Such policy considers the immediate reward (resulting from the demand) as well as the downstream value (resulting from future periods). These values are calculated backwardly and dynamically, i.e., first values in $t = 2$ are calculated, then values in $t = 1$, and so on. As explained in Section A.4.3, the value of the optimal policy does not simply result from choosing the move with the highest expected value. Instead, it is calculated by considering the optimal decision under each possible demand-combination. The algorithm for this is provided in Figure A.4b and exemplarily applied to nodes A, B, and A of periods 2, 1, and 0 in Formulas (A.20)-(A.22), respectively.

$$\begin{aligned}
 V_2(S_2|l_2 = A) &= (0.33) \cdot 66 + \\
 &\quad ((1 - 0.33) \cdot 0.61) \cdot 46 + \\
 &\quad ((1 - 0.33 - (1 - 0.33) \cdot 0.61) \cdot 0.36) \cdot 18 = 42.27
 \end{aligned} \tag{A.20}$$

$$\begin{aligned}
 V_1(S_1|l_1 = B) &= \underbrace{(0.60)}_{p_0^r} \cdot (72 + \gamma \cdot 79.61) + \\
 &\quad \underbrace{((1 - p_0^r) \cdot 0.79)}_{p_1^r} \cdot (33 + \gamma \cdot 42.27) + \\
 &\quad \underbrace{((1 - p_0^r - p_1^r) \cdot 0.39)}_{p_2^r} \cdot (13 + \gamma \cdot 66.27) + \\
 &\quad (1 - p_0^r - p_1^r - p_2^r) \cdot (0 + \gamma \cdot 79.61) = 107.96
 \end{aligned} \tag{A.21}$$

$$\begin{aligned}
 V_0(S_0|l_0 = A) &= \underbrace{(0.49)}_{p_0^r} \cdot (98 + \gamma \cdot 92.01) + \\
 &\quad \underbrace{((1 - p_0^r) \cdot 0.62)}_{p_1^r} \cdot (52 + \gamma \cdot 107.96) + \\
 &\quad \underbrace{((1 - p_0^r - p_1^r) \cdot 0.74)}_{p_2^r} \cdot (28 + \gamma \cdot 115.15) + \\
 &\quad (1 - p_0^r - p_1^r - p_2^r) \cdot (0 + \gamma \cdot 115.15) = 149.71
 \end{aligned} \tag{A.22}$$

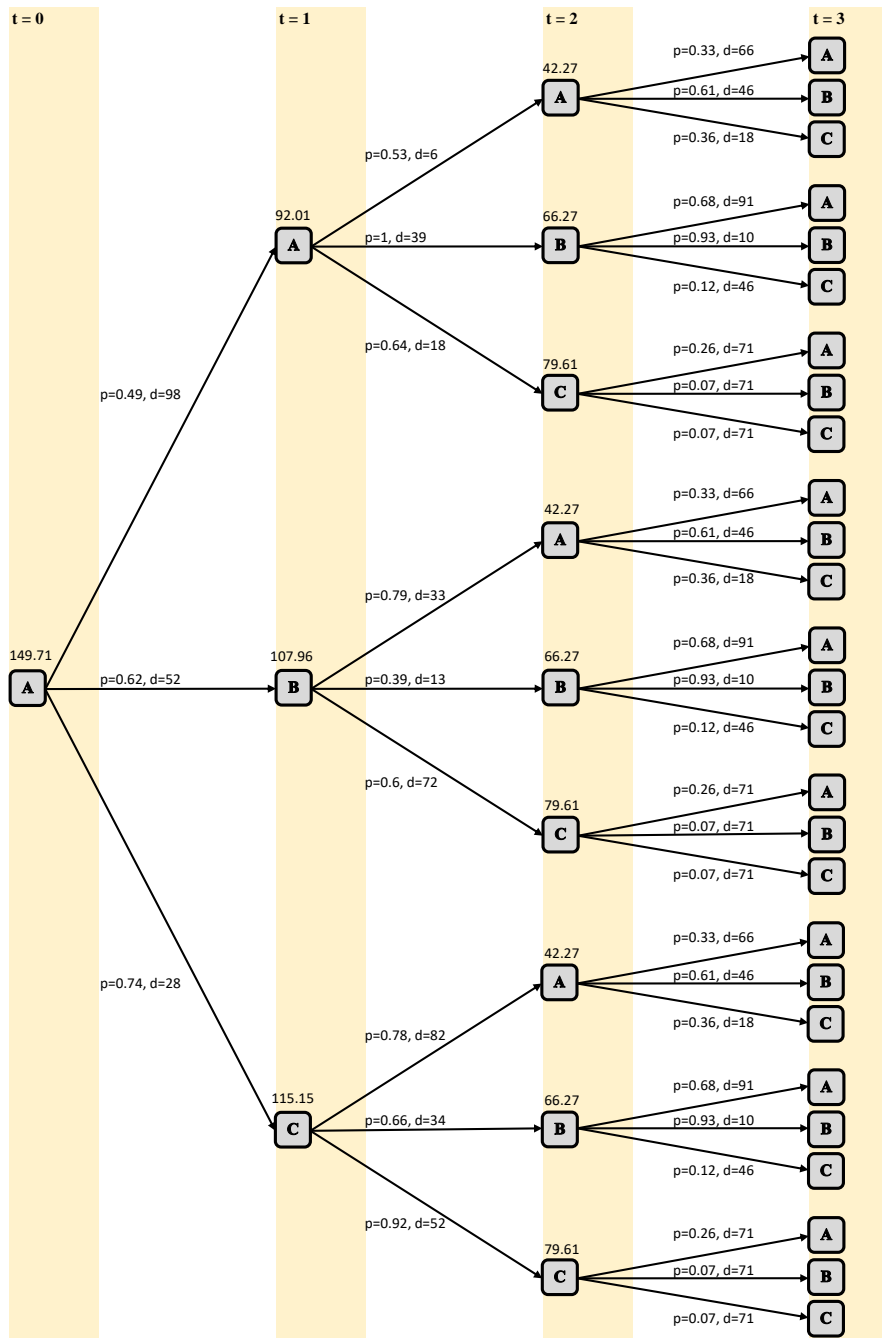


Figure A.10: Decision tree for the example problem. Values atop of the arcs are the demand and its probability and the values atop of the decision nodes are the discounted downstream value following an optimal policy.

Bibliography

- Alnaggar, A., Gzara, F. and Bookbinder, J. H. (2020). Distribution planning with random demand and recourse in a transshipment network, *EURO Journal on Transportation and Logistics* **9**(1): 100007.
- Behrend, M. and Meisel, F. (2018). The integration of item-sharing and crowdshipping: Can collaborative consumption be pushed by delivering through the crowd?, *Transportation Research Part B: Methodological* **111**: 227–243.
- Behrend, M. and Meisel, F. (2019). Heterogeneity of items in an integrated item-sharing and crowdshipping setting, in B. Fortz and M. Labbé (eds), *Operations Research Proceedings 2018*, Springer International Publishing, Cham, pp. 269–275.
- Bellman, R. (1957). *Dynamic Programming*, Princeton University Press.
- Cattaruzza, D., Absi, N., Feillet, D. and González-Feliu, J. (2017). Vehicle routing problems for city logistics, *EURO Journal on Transportation and Logistics* **6**(1): 51–79.
- Christopher, M. (2010). *Logistics and supply chain management*, Pearson Business.
- George, A. P. and Powell, W. B. (2006). Adaptive stepsizes for recursive estimation with applications in approximate dynamic programming, *Machine Learning* **65**(1): 167–198.
- George, A., Powell, W. B. and Kulkarni, S. R. (2008). Value function approximation using multiple aggregation for multiattribute resource management, *Journal of Machine Learning Research* **9**: 2079–2111.
- Hoberg, K. (2020). *Supply Chain and Big Data*, Springer International Publishing, Cham, pp. 1–5.
- Maxwell, M. S., Restrepo, M., Henderson, S. G. and Topaloglu, H. (2010). Approximate dynamic programming for ambulance redeployment, *INFORMS Journal on Computing* **22**(2): 266–281.
- Mes, M. R. K. and Rivera, A. P. (2017). Approximate dynamic programming by practical examples, in R. J. Boucherie and N. M. van Dijk (eds), *Markov Decision Processes in Practice*, Springer International Publishing, Cham, pp. 63–101.
- Mes, M., van der Heijden, M. and Schuur, P. (2010). Look-ahead strategies for dynamic pickup and delivery problems, *OR spectrum* **32**(2): 395–421.

- Pironet, T. (2015). Multi-period stochastic optimization problems in transportation management, *4OR* **13**: 113–114.
- Powell, W. B. (2009). What you should know about approximate dynamic programming, *Naval Research Logistics* **56**(3): 239–249.
- Powell, W. B. (2011). *Approximate Dynamic Programming: Solving the Curses of Dimensionality*, 2nd edn, John Wiley & Sons.
- Powell, W. B. and Meisel, S. (2015). Tutorial on stochastic optimization in energy—part i: Modeling and policies, *IEEE Transactions on Power Systems* **31**(2): 1459–1467.
- Rayle, L., Dai, D., Chan, N., Cervero, R. and Shaheen, S. (2016). Just a better taxi? A survey-based comparison of taxis, transit, and ridesourcing services in San Francisco, *Transport Policy* **45**: 168–178.
- Rivera, A. E. P. and Mes, M. R. (2017). Anticipatory freight selection in intermodal long-haul round-trips, *Transportation Research Part E: Logistics and Transportation Review* **105**: 176–194.
- Ruszczynski, A. (2010). Commentary: Post-decision states and separable approximations are powerful tools of approximate dynamic programming, *INFORMS Journal on Computing* **22**(1): 20–22.
- Schilde, M., Doerner, K. F. and Hartl, R. F. (2011). Metaheuristics for the dynamic stochastic dial-a-ride problem with expected return transports, *Computers & Operations Research* **38**(12): 1719–1730.
- Schmid, V. (2012). Solving the dynamic ambulance relocation and dispatching problem using approximate dynamic programming, *European Journal of Operational Research* **219**(3): 611–621.
- Secomandi, N. and Margot, F. (2009). Reoptimization approaches for the vehicle-routing problem with stochastic demands, *Operations Research* **57**(1): 214–230.
- Sigaud, O. and Buffet, O. (2013). *Markov Decision Processes in Artificial Intelligence*, John Wiley & Sons.
- Simao, H. P., Day, J., George, A. P., Gifford, T., Nienow, J. and Powell, W. B. (2009). An approximate dynamic programming algorithm for large-scale fleet management: A case application, *Transportation Science* **43**(2): 178–197.

- Soeffker, N., Ulmer, M. W. and Mattfeld, D. C. (2021). Stochastic dynamic vehicle routing in the light of prescriptive analytics: A review, *European Journal of Operational Research* (In Press).
- Souza, G. C. (2014). Supply chain analytics, *Business Horizons* **57**(5): 595–605.
- Sutton, R. S. and Barto, A. G. (2018). *Reinforcement Learning: An Introduction*, 2nd edn, MIT press.
- Ulmer, M. W. (2020). Dynamic pricing and routing for same-day delivery, *Transportation Science* **54**(4): 1016–1033.
- Ulmer, M. W., Goodson, J. C., Mattfeld, D. C. and Hennig, M. (2019). Offline–online approximate dynamic programming for dynamic vehicle routing with stochastic requests, *Transportation Science* **53**(1): 185–202.
- Ulmer, M. W., Goodson, J. C., Mattfeld, D. C. and Thomas, B. W. (2020). On modeling stochastic dynamic vehicle routing problems, *EURO Journal on Transportation and Logistics* **9**(2): 100008.
- Ulmer, M. W., Soeffker, N. and Mattfeld, D. C. (2018). Value function approximation for dynamic multi-period vehicle routing, *European Journal of Operational Research* **269**(3): 883–899.

Authors' Contribution Statements

This chapter describes the authors' contributions to the essays by using the established CRediT taxonomy (<https://casrai.org/credit/>). The taxonomy describes several roles that are typically used in the process of a collaborative scientific work. Not all of the roles are of significant importance to the essays (e.g., funding acquisition or resources) and only the following roles are used (in alphabetical order): conceptualization, data curation, investigation, methodology, software, supervision, validation, visualization, writing (original draft), and writing (review & editing). The name of the roles is self-explaining and a detailed explanation of them can be found on the CRediT website. If the same role applies to multiple authors, CRediT's suggestion to specify each author's degree of contribution as 'lead', 'equal', or 'supporting' is followed. The following pages comprise of the contribution statements for each distinct author-pairing.

Essays 1, 2, and 4

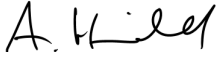
Roles

Arne Heinold and Frank Meisel are co-authors of Essays 1, 2, and 4. The same contribution to the roles applies to all three essays and is as follows:

role	Heinold	Meisel
Conceptualization	equal	equal
Data curation	lead	supporting
Investigation	lead	supporting
Methodology	lead	supporting
Software	lead	-
Supervision	-	lead
Validation	lead	-
Visualization	lead	-
Writing (original draft)	lead	supporting
Writing (review & editing)	lead	supporting

Confirmation

The authors confirm that above statement of contribution is accurate and true.

25.10.2021 
 Date _____ Arne Heinold

25.10.2021 
 Date _____ Frank Meisel

Essays 3 and 7

Roles

Arne Heinold is the single author of Essays 3 and 7 and serves as 'lead' in all roles.

Other

Careful proof readings were done for Essay 1 by Maximilian Krüger, Raziye Küçükcaraca, and Frank Meisel and for Essay 7 by Frederike Grabowski, Raziye Küçükcaraca, and Lara Perband. Their comments were of great help in improving the manuscripts. Marlin Ulmer provided some ideas towards the structure of Essay 7. He also motivated the author to submit it to a well-established B-journal where it was rejected after a thorough review process. The comments of the reviewers were of great help in preparing the manuscript for the submission at the *4OR* journal where it is currently under review.

Essay 5

Roles

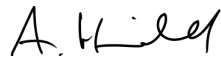
The research groups from Halle (Thomas Kirschstein, Martin Behnke, Christian Bierwirth) and Kiel (Arne Heinold, Frank Meisel) collaboratively worked on Essay 5. The authors' contribution to each role is as follows:

role	Kirschstein	Heinold	Behnke	Meisel	Bierwirth
Conceptualization	equal	equal	equal	equal	equal
Data curation	lead	lead	supporting	supporting	supporting
Investigation	equal	equal	equal	equal	equal
Methodology	equal	equal	equal	equal	equal
Software	lead	lead	supporting	supporting	supporting
Supervision	supporting	-	-	lead	lead
Validation	equal	equal	equal	equal	equal
Visualization	lead	supporting	supporting	supporting	supporting
Writing (original draft)	lead	supporting	supporting	lead	lead
Writing (review & editing)	lead	supporting	supporting	lead	lead


Confirmation

The authors confirm that above statement of contribution is accurate and true.

25.10.2021
 Date 
 Thomas Kirschstein

25.10.2021
 Date 
 Arne Heinold

25.10.2021
 Date 
 Martin Behnke

25.10.2021
 Date 
 Frank Meisel

25.10.2021
 Date 
 Christian Bierwirth

Essay 6

Roles

Arne Heinold and Frank Meisel from Kiel and Marlin Wolf Ulmer from Magdeburg collaboratively worked on Essay 6. The authors' contribution to each role is as follows:

role	Heinold	Meisel	Ulmer
Conceptualization	equal	equal	equal
Data curation	lead	supporting	supporting
Investigation	equal	equal	equal
Methodology	lead	supporting	lead
Software	lead	-	-
Supervision	-	lead	lead
Validation	lead	supporting	supporting
Visualization	lead	supporting	supporting
Writing (original draft)	lead	supporting	supporting

Other

The idea of the primal-dual VFA has been discussed with Warren B. Powell (Princeton University, USA) and Justin C. Goodson (Saint Louis University, USA). Their comments were helpful in preparing the manuscript. Marlin Ulmer's work is funded by the Emmy Noether Programme of the Deutsche Forschungsgemeinschaft (DFG, German Research Foundation), project 444657906.

Confirmation

The authors confirm that above statement of contribution is accurate and true.

25.10.2021

 Date Arne Heinold

25.10.2021

 Date Frank Meisel

25.10.2021

 Date Marlin Wolf Ulmer

Erklärung zum selbstständigen Verfassen der Arbeit

Ich erkläre hiermit, dass ich meine Doktorarbeit „Emission-oriented management of land-based freight transportation“ selbstständig und ohne fremde Hilfe angefertigt habe und als Autor bzw. Koautor maßgeblich zu den Fachartikeln beigetragen habe. Alle von anderen Autoren wörtlich übernommenen Stellen, wie auch die sich an die Gedanken anderer Autoren eng anlehenden Ausführungen der aufgeführten Beiträge, wurden besonders gekennzeichnet und die Quellen nach den mir angegebenen Richtlinien zitiert.

Kiel, 30.06.2022

Ort, Datum

Unterschrift (Arne Heinold)